HIV-1 induction of macrophage immune mediators

Cherrelle Dacon





St. Edmund Hall

Sir William Dunn School of Pathology

University of Oxford

Submitted in partial fulfilment of the requirements of the degree of Doctor of Philosophy

Trinity Term 2019

Dedicated to Karen, Cherish and Geraldine –

my rocks and daily motivation.

Abstract

Clinical studies convincingly associate increased monocyte migration and markers of myeloid cell activation with the pathogenesis of inflammatory conditions in HIV-1-infected individuals. However, the mechanisms by which myeloid cells contribute to HIV-1-associated inflammation are poorly understood. HIV-1 infection of human macrophages is believed to induce an innate immune response that includes IFN-I production. Previous studies also implicate the HIV-1 accessory protein Vpr as a potential modulator of pro-inflammatory antiviral responses to HIV-1 infection, but these reports are contradictory and require clarification.

To determine the immune mediators induced by HIV-1 and modulated by HIV-1 Vpr, I transduced human monocyte-derived macrophages with single-round pseudotyped viruses that were either competent or deleted for Vpr expression. Wide-scale soluble proteome analysis of conditioned media from the HIV-1-transduced human macrophages highlights that HIV-1 induces expression of a subset of pro-inflammatory factors, among which the interferon gamma-induced chemokine CXCL10/IP-10 is markedly enhanced. I find no evidence of enhanced primary monocyte migration towards either transduced MDM supernatants or recombinant soluble Env, a ligand for CCR5. Further analyses of macrophage supernatants using an IFN-reporter cell line and multiplex immunoassays show that HIV-1 Vpr expression downregulates IFN-α and IL-1β production. Together, these data support the idea MDMs elicit a modest innate response to HIV-1 of which the accessory protein Vpr is a negative regulator.

Acknowledgements

I am incredibly thankful to Professor Quentin Sattentau for his supervision, support and near-encyclopaedic knowledge of HIV infection. I am also grateful to Dr. Rebecca Russell for her supervision and superior molecular biology skills, and to Dr. Kenny Moore for his help and advice throughout my DPhil.

I would also like to thank past and present members of the Sattenatu lab; Lu Li Jovanoska and Scarlett Harris for their support and friendship, Dr. Niloofar Karaji for our tea breaks and late-night lab chats, and Amin Moghaddam for his advice on immunoassays.

Thank you to the Wellcome Trust DPhil in Infection, Immunology and Translational course directors for making IITM an incredibly supportive program. In particular, I would like to thank Professors Keith Gull, Helen Mc Shane and Christoph Tang for their support and advice during my DPhil. Thanks to our administrator Dawn Gibbons for her help throughout the course and her warm chats. Also thanks to Hannah Behrens, Marianne Clemence, Lucy Garner, Richard Morter and Layal Liverpool – the amazing IITM 2015 cohort!

I am grateful to many people for their help during my DPhil. In particular Professor William James for his enthusiasm on all things HIV-1/macrophage related and for his feedback at my transfer and confirmation assessments. Also, to Dr. Sally Cowley, Jane Vowles and Cathy Browne of the James Martin Stem Cell Facility for patiently teaching me stem-cell culture, and to Dr. Hazel Hall-Roberts for her help and advice. This project also benefitted from advice from Professor Jan Rehwinkle and my graduate advisor Professor David Greaves whose research group kindly shared their chemotaxis equipment with me. I'd also

like to thank the OMPI2 virus lab users for putting up with my near-constant occupation of Hood 2, and to everyone at the Sir William Dunn School of Pathology who has given me technical advice.

I am immeasurably thankful to the Rhodes Trust for my Rhodes Scholarship, without which I would not have been able to embark on this DPhil, and to St. Edmund Hall for my additional bursary funding.

Finally, a heartfelt thank you to my friends and family for their love and support, which I treasure.

Table of Contents

Abstract 2

Acknowledgements 3

Table of Contents 5

List of Abbreviations 10

Chapter 1: Introduction 16

1.1 The Human Immunodeficiency Virus 17

1.2 Origins of tissue-resident macrophages 24

1.3 Monocyte/macrophage involvement in HIV-1 infection 26

1.4 Macrophage activation in chronic HIV-1 infection 34

1.5 Role of monocytes/macrophages in the progression of HIV-1-associated inflammatory conditions 41

1.5.1 Association between monocyte/macrophage activation and CVD progression 41

1.5.2 Association between monocyte/macrophage activation and HAND progression 43

1.6 Effects of HIV-1 on leukocyte trafficking 45

1.7 Implications for future therapy 48

1.8 Scope of work 50

Chapter 2: Materials and methods 53

2.1 Cell culture 54

2.2 Isolation of $CD14^+$ blood monocytes 54

2.3 Differentiation of $CD14^+$ monocytes to blood monocyte-derived macrophages (MDMs) 55

2.4 Establishing human pluripotent stem cell (hPSC) pre-cursor cultures..... 55

2.5 Differentiation of hPSC pre-cursors to hPSC-derived macrophages (hPSC-DMs)..... 57

2.6 Optimisation of hPSC-derived macrophage transduction using HIV-1 NL4.3-eGFP pseudotyped virus..... 58

2.7 Analysis of cell surface marker expression..... 58

2.8 LPS activation of blood monocyte derived macrophages (MDMs)..... 60

2.9 Propagation of lentiviral vector and envelope expression plasmids in competent *E. coli*..... 60

2.10 Maxi-prep purification of plasmid DNA 61

2.11 Transient co-transfection of HEK 293Ts for HIV-1 NL4-3-eGFP vector production..... 62

2.12 Transient co-transfection of HEK 293Ts for VSV-G/SIV-Vpx virus like particle production 63

2.13 Concentration of HIV-1 NL4-3-eGFP vectors and VSV-G/SIV-Vpx virus-like particles ... 64

2.14 Quantification of BaL Env and VSV-G Env pseudotyped HIV-1 NL4-3-eGFP vector titres..... 64

2.15 Quantification of VSV-G Env pseudotyped SIV-Vpx virus like particles by SIV p27 ELISA..... 65

2.16 Quantification of HIV-1 NL4-3-eGFP vectors by HIV-1 p24 ELISA 65

2.17 Transduction of MDMs with single-cycle HIV-1-NL4.3-eGFP vectors 66

2.18 Proteome profiler analysis of soluble factors produced by HIV-1 NL4-3-eGFP transduced MDMs..... 67

2.19 Multiplex analysis of cytokine and chemokine expression by MDMs 68

2.20 Analysis of MDMs expression of CXCL10/IP-10 by ELISA 69

2.21 Optimising $CD14^+$ monocyte density for the xCELLigence migration assay 70

2.22 Optimising chemokine concentration for the xCELLigence migration assay with CD14+ monocytes..... 70

2.23 Optimising THP-1 monocytic cell line density for the xCELLigence migration assay 72

2.24 Optimising chemokine concentration for the xCELLigence migration assay with THP-1 monocytic cell line..... 72

2.25 Validation of the xCELLigence migration assay using 'checkerboard' analysis 73

2.26 ELISA analysis of chemokine diffusion across the xCELLigence CIM-16 membrane 74

2.27 CellTiter96 analysis of the effect of actin polymerisation inhibitors on CD14+ monocyte viability 74

2.28 Validation of the xCELLigence migration assay using inhibitors of actin polymerisation 75

2.29 Scanning electron microscopy of CIM-16 membrane 75

2.30 Expression of HIV-1 recombinant Env 76

2.31 Concentration and purification of HIV-1 recombinant Env 76

2.32 Analysis of HIV-1 recombinant Env endotoxin content 77

2.33 SDS-PAGE of recombinant envelope proteins 78

2.34 Measurement of recombinant HIV-1 Env binding to soluble CD4 (sCD4) 78

2.35 Measurement of recombinant HIV-1 Env binding to cell surface CD4 using CEM T-cell line..... 79

2.36 xCELLigence assay of the effects of HIV-1 Env on $CD14^+$ monocyte and THP-1 monocytic cell line migration..... 79

2.37 xCELLigence assay of the effects of transduced MDM supernatants on CD14$^+$ monocyte migration 80

2.38 Quantification of interferon activity of supernatants from transduced MDMs..... 80

2.39 Extraction of RNA from transduced or stimulated MDMs 81

2.40 Quantification of interferon stimulated gene (ISG) expression by qRT-PCR..... 82

2.41 Site-directed mutagenesis (SDM) of HIV-1 NL4.3-eGFP-Vpr$^+$ expression plasmids 83

2.42 Mini-prep purification and Sanger sequencing of mutagenized HIV-1 NL4.3-eGFP-Vpr$^+$ plasmids 85

Chapter 3: Establishing biologically relevant macrophage differentiation and transduction systems. 88

3.1 Introduction 89

3.2 Chapter rationale 93

3.3 Results 94

3.4 Discussion 129

3.5 Conclusion 134

Chapter 4: Analysis of macrophage immune mediators induced by HIV-1 and modulated by HIV-1 Vpr expression..... 136

4.1 Introduction 137

4.2 Chapter rationale 139

4.3 Results 140

4.4 Discussion 184

4.5 Conclusion 190

Chapter 5: Investigating primary monocyte migration towards supernatants of HIV-1-transduced MDMs and recombinant HIV-1 Env 191

5.1 Introduction 192

5.2 Chapter Rationale 197

5.3 Results 199

5.4 Discussion 247

5.5 Conclusion 253

Chapter 6: Discussion 254

6.1 Summary 255

6.2 Conclusions 256

6.3 Contributions to the field 257

Chapter 7: Appendix 263

7.1 Supplementary Tables 264

7.1 Conferences, symposiums and publications 294

References 295

List of Abbreviations

Ag	Antigen
Amp	Ampicillin
Amp^R	Ampicillin resistant
APC	Allophycocyanin
APOBEC3	Apolipoprotein B mRNA editing enzyme, catalytic polypeptide-like
AUC	Area under curve
BBB	Blood-brain barrier
BLT	Bone marrow, liver, thymus mouse model
BMP4	Bone morphogenic protein 4
BSA	Bovine serum albumin
C5aR	Complement component 5a receptor
cART	Combination antiretroviral therapy
CCR	C-C chemokine receptor
CCL	C-C chemokine ligand
CD11b	Cluster of differentiation molecule 11b
CD14	Cluster of differentiation molecule 14
CD163	Cluster of differentiation molecule 163
CD4	Cluster of differentiation molecule 4
CD4bs	CD4 binding site
CDK1	Cyclin dependent kinase 1
cDNA	Complementary DNA
CI	Cell index
CIM	Cell invasion and migration

CIMT	Carotid intima-media thickness
CMV	Cytomegalovirus
CNS	Central nervous system
CSF	Cerebrospinal fluid
CXCR	C-X-C chemokine receptor
CXCL	C-X-C motif chemokine ligand
CVD	Cardiovascular disease
$cXVivo_{15}$	$XVivo_{15}$ supplemented with 10% FCS
DMEM	Dulbecco's modified eagle media
DNA	Deoxyribonuclease acide
dNTP	Deoxynucleotide
EB	Embryoid body
EDTA	Ethylenediaminetetraacetic acid
eGFP	Enhanced green fluorescent protein
ELISA	Enzyme-linked immunosorbent assay
Env	HIV-1 envelope glycoprotein
ESCRT	Endosomal sorting complexes required for transport
FACS	Fluorescence-activated cell sorting
FCS	Fetal calf serum
FITC	Fluorescein isothiocyanate
fLuc	Firefly luciferase
FM	Factory media
fMLP	N-Formylmethionine-leucyl-phenylalanine
FPR	Formyl peptide receptor
GALT	Gut-associated lymphoid tissue

GDS	Global deficit score
gp120	Envelope glycoprotein 120
h	Hour
$hCD14^{+}$	Human CD14 positive
$hCD34^{+}$	Human CD34 positive
HEK	Human embryonic kidney
hESC	Human embryonic stem cell
HIV	Human immunodeficiency virus
hPSC	Human pluripotent stem cells
hPSC-MP	Human pluripotent stem cell macrophage precursor
HRP	Horseradish peroxidase
ID_{50}	50% infectious dose
IFI6	Interferon alpha inducible protein 6
IFN	Interferon
IHC	Immunohistochemistry
IL	Interleukin
IRF	Inteferon response factor
ISG	Interferon stimulated gene
ISH	In-situ hybridization
ISRE	Interferon-stimulated response element
Kan	Kanamycin
Kan^{R}	Kanamycin resistant
kb	Kilobase
LB	Luria-Bertani
LDL-R	Low density lipoprotein receptor

LPS	Lipopolysaccharide
LTR	Long terminal repeat
mAb	Monoclonal antibody
MCP	Monocyte chemoattractant protein
MI	Myocardial infarction
MIF	Macrophage migration inhibitory factor
MIG	Monokine induced by gamma interferon
min	Minute
MIP	Macrophage inflammatory protein
MoM	Myeloid-only-mouse model
Nef	Negative regulatory factor
NNRTI	Non-nucleoside reverse-transcriptase inhibitor
N/S	Non-obese diabetic/severe combined immunodeficiency mouse model
ORF	Open reading frame
P/S	Penicillin-Streptomycin
PAGE	Polyacrylamide gel electrophoresis
PBMC	Peripheral blood mononuclear cell
PBS	Phosphate buffered saline
PCR	Polymerase chain reaction
PE	Phycoerythrin
PEG	Polyethylene glycol
PEI	Polyethylenimine
PI	Protease inhibitor
PLWH	People living with HIV-infection
qRT-PCR	Quantitative reverse transcription polymerase chain reaction

RANTES	Regulated on activation, normal T Cell expressed and secreted
RNA	Ribonucleic acid
RT	Reverse transcriptase
RTCA-DP	Real-time cell analysis dual purpose
s	Seconds
SAMHD1	Sterile α-motif and HD domain–containing protein-1
SAPE	Streptavidin conjugated phycoerythrin
sCD4	Soluble CD4
SCF	Stem cell factor
SDM	Site-directed mutagenesis
SDS	Sodium dodecyl sulfate
SIV	Simian Immunodeficiency Virus
SOC	Super optimal broth with catabolite repression
T_A	Annealing temperature
T_m	Melting temperature
TBS	Tris-buffered saline
TC	Tissue culture
TE	Tris-EDTA
TLR	Toll-like receptor
TMB	Tetramethylbenzidine
TNF	Tumor necrosis factor
Trim5α	Tripartite motif 5-α
VEGF	Vascular endothelial growth factor
VLP	Virus-like particle
Vpr	Viral protein R

Vpx	Viral protein X
Vpu	Viral protein U
VSV-G	Vesicular stomatitis virus envelope glycoprotein
WB	Western blot
WT	Wild-type

Chapter 1:

Introduction

1.1 The Human Immunodeficiency Virus

The Human Immunodeficiency Virus (HIV) is a lentivirus of the retrovirus family with a genome that consists of two single-stranded RNA molecules enclosed within the core of each virus particle. There are two types of HIV: HIV-1 and HIV-2. Since HIV-1 is responsible for the global pandemic, I will from hereon only consider this virus. Simian immunodeficiency viruses (SIV) are related lentiviruses that cause disease in experimental infection of macaques – the SIV-macaque model for HIV-1 infection. The HIV-1 genome is approximately 9.2 kb and consists of open reading frames (ORF) for the 5' and 3' long terminal repeats (LTRs) which drive viral gene expression; the Gag, Pol, Env, Tat, and Rev proteins which are essential for viral replication; and for Nef, Vif, Vpu and Vpr which are accessory proteins (Figure 1). The HIV-1 proteins and their functions are reviewed in [1]. Briefly, the polyprotein Gag is the precursor for the structural capsid protein (CA/p24), matrix protein (MA/p17) and nucleoprotein (NC/p7) as well as the protein P6 which is involved in virus particle release. The polyprotein Pol is the precursor of the viral enzymes protease (PR), reverse transcriptase and RNase H (RT), and integrase (IN). The HIV-1 envelope glycoprotein (Env) is present on the surface of the virus as trimers of gp120/gp41 heterodimers in which the external domain gp120 is non-covalently associated with the gp41 subunit, which functions to anchor Env into the viral envelope. The Tat protein functions as a transcriptional activator for viral genes, while Rev regulates the export of viral mRNA. Nef enhances the infectivity of budding virus particles and is an important immune evasion molecule in vivo, Vpu is required to antagonise the tetherin restriction factor to allow virion release from infected cells [2], and Vif is critical to antagonise the

restriction factor family of APOBEC enzymes [3]. Vpr is packaged into nascent viral particles and mediates a range of effects including cell cycle arrest [4,5], enhanced viral infectivity [6], host cell proteome remodelling [7] and modulation of type-I interferon production (IFN-I) and associated pathways [8-11].

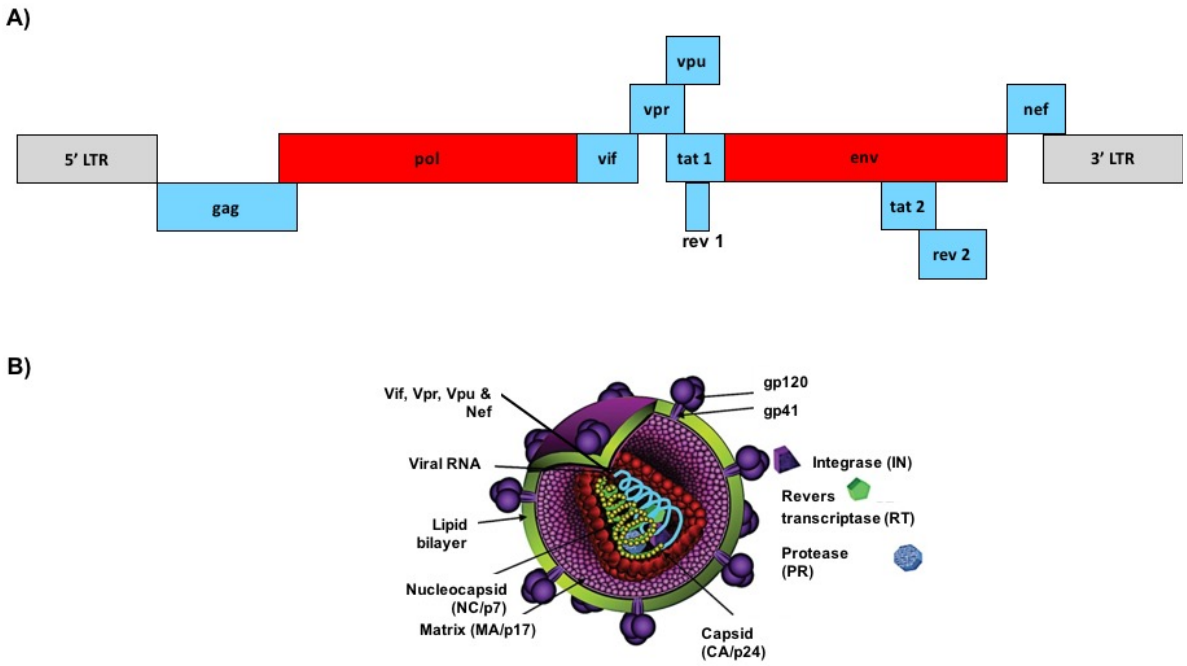


Figure 1: Schematic of the HIV genome and virus particle

Schematic of A) the ORFs encoded by the HIV-1 genome B) the localisation of viral proteins within the structure of a mature HIV-1 virion. Reproduced from Steckbeck et al [12].

While phylogenetic analyses estimate that HIV-1 was transmitted to human hosts from chimpanzees in central-west Africa circa 1920 [13], the virus (then termed HTLV-III or LAD) was first isolated from clinical tissue biopsies in the early 1980's [14-16]. The United Nations Joint Programme on HIV/AIDS (UNAIDS) estimates that approximately 75 million

infections have occurred worldwide since the start of the HIV epidemic [17], with HIV-1 subtype C accounting for approximately 48 % of these cases, followed by HIV-1 subtype A (12 %) and HIV-1 subtype B (11 %) [18].

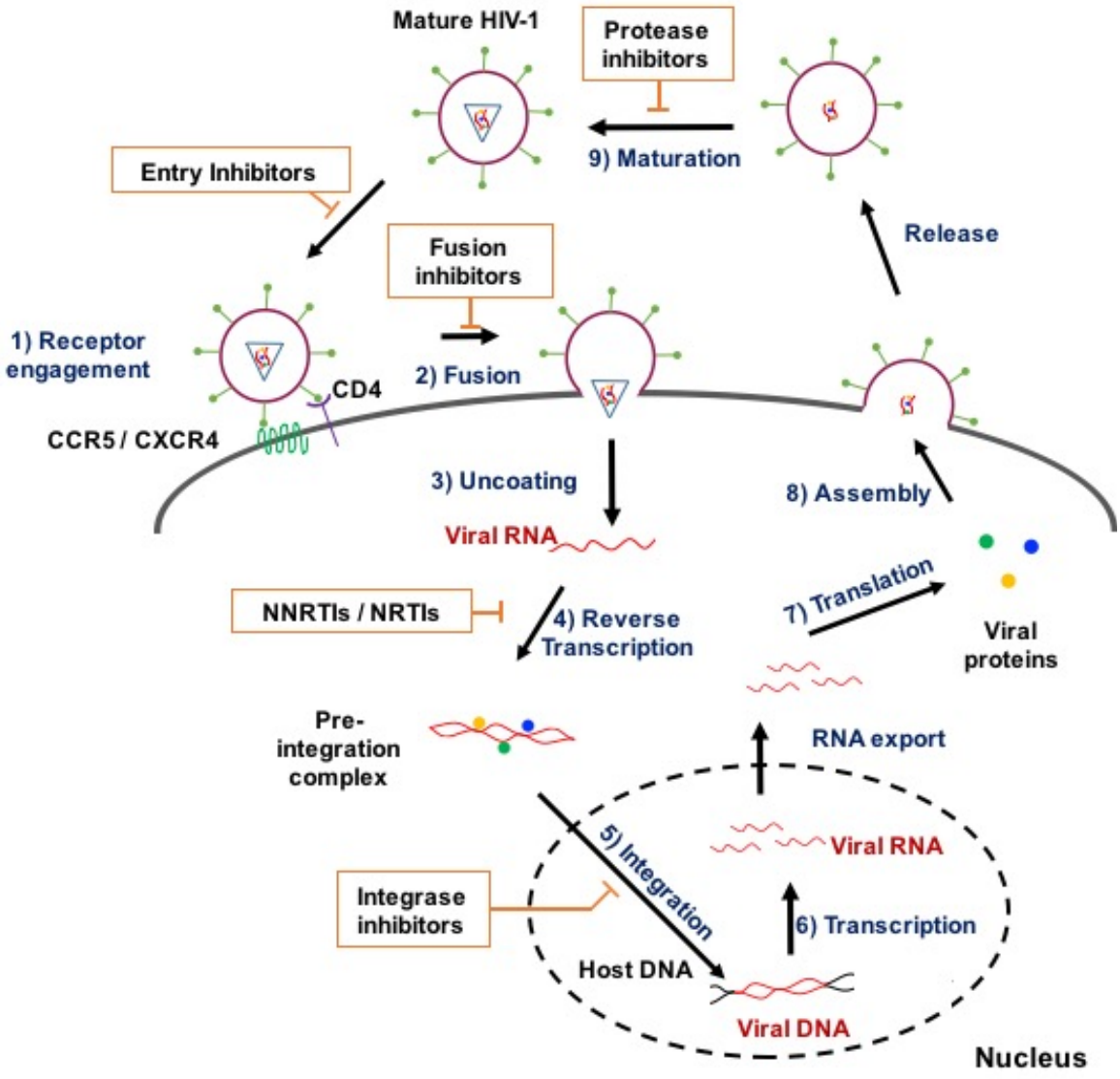


Figure 2: Schematic of the HIV replication cycle

As summarised in Figure 2, HIV-1 infection is initiated by binding of gp120 to the primary entry receptor CD4. Gp120 binding to CD4 induces a structural change that exposes the V3 loop and the CD4-induced (CD4i) region of gp120 for subsequent engagement with a co-receptor protein. For co-receptors, R5 tropic HIV-1 isolates utilise C-C chemokine receptor type 5 (CCR5), X4 tropic HIV-1 isolates utilise C-X-C chemokine receptor type 4 (CXCR4), and dual-tropic HIV-1 isolates can utilise either CCR5 or CXCR4. Co-receptor engagement triggers a further rearrangement of Env that activates gp41 and exposes its fusogenic domain. This final rearrangement event enables fusion of the target cell and viral membrane and thereby mediates viral entry [19]. HIV-1 entry can also occur when viral particles are engulfed by the host cell endocytic machinery [20,21]. Subsequent fusion of the viral envelope with either the plasma membrane or the endosomal membrane allows for translocation of the genomic RNA, RT, IN and other proteins within the capsid into the cytoplasm. Incoming viral RNA is then reverse transcribed by the RT enzyme to generate double-stranded viral cDNA which, in complex with the IN enzyme, other viral proteins and host proteins forms the pre-integration complex (PIC). The PIC then translocates to the nucleus, where the viral cDNA crosses a nuclear pore and is integrated into the host DNA by the IN enzyme [22]. If the cell is transcriptionally active, the host cell machinery transcribes integrated viral DNA to produce new viral mRNAs which serve as templates for the subsequent translation of new viral proteins, and new copies of genomic viral RNA. Newly produced viral RNA and proteins then translocate to the cell surface and are assembled into immature particles which bud off the host cell taking host cell membrane with them to form the viral envelope. Finally, cleavage of the Gag and Gag/Pol precursor

protein by PR generates a mature, infective HIV-1 particle and thereby completes the cycle of productive infection [23].

HIV-1 disease progression is reviewed by An and Winkler and represented in Figure 3. Briefly, the acute phase of HIV-1 infection lasts for 6-12 weeks post-transmission and is characterised by flu-like symptoms, and rapid HIV-1 replication which leads to high levels of HIV-1 RNA being detected in the plasma (viral load) and causes a rapid decline in $CD4^+$ T cell numbers. HIV-1 viral load peaks around 6 weeks post-transmission after which detectable HIV-1 RNA levels decline in response to antiviral innate IFN-I responses and adaptive immune responses. During this phase $CD4^+$ T-cell counts increase, but do not return to their pre-infection levels. In the absence of cART, HIV-1 continues to replicate at low levels during the clinical latency phase of infection. This chronic phase of HIV-1 infection can last from 7 - 10 years, during which HIV-1-infected individuals are usually asymptomatic and viral load stabilises to a steady level known as the virological set point.

HIV-1 infection is directly and indirectly cytopathic to $CD4^+$ T cells, and untreated HIV-1 infection leads to a progressive decline in $CD4^+$ T cell count and immune function (Figure 3). Productive infection of $CD4^+$ T cells induces caspase-3 dependent apoptosis; a form of programmed cell death that is not accompanied by the release of inflammatory factors from dying cells [24]. However, only a small proportion (approximately 5%) of HIV-1 infected, dying T cells undergo this non-inflammatory form of cell death. In contrast, in-vitro experiments suggest that the vast majority of HIV-1-infected T cell death is triggered by pyroptosis downstream of IFN-γ-inducible protein 16 (IFI6) sensing of incomplete viral DNA transcripts which accumulate in the cytosol of abortively infected $CD4^+$ T cells [25-27].

Signalling events downstream of IFI6 activation lead to IFN-I production and the activation of caspase-3 and the inflammasome-activated caspase 1. In turn, caspase-1 activation induces pyroptosis, a form of programmed cell death that is accompanied by the release of cytoplasmic contents and inflammatory cytokines into the extracellular space and the production of IL-1β [24]. In this way, HIV-1-induced pyroptotic cell death not only drives $CD4^+$ T cell decline, but also contributes to immune activation and inflammation.

Over time, $CD4^+$ depletion and macrophage dysfunction [28] results in state of immunocompromise that predisposes individuals to susceptibility to opportunistic infections and some cancers such as Kaposi's sarcoma, part of the eventual development of Acquired Immunodeficiency Syndrome (AIDS), the onset of which is usually accompanied by an increase in HIV-1 RNA. AIDS was first described in 1981 [29] and since its emergence, HIV/AIDS has represented one of the most fatal pandemics in history with 32 million deaths reported worldwide [17].

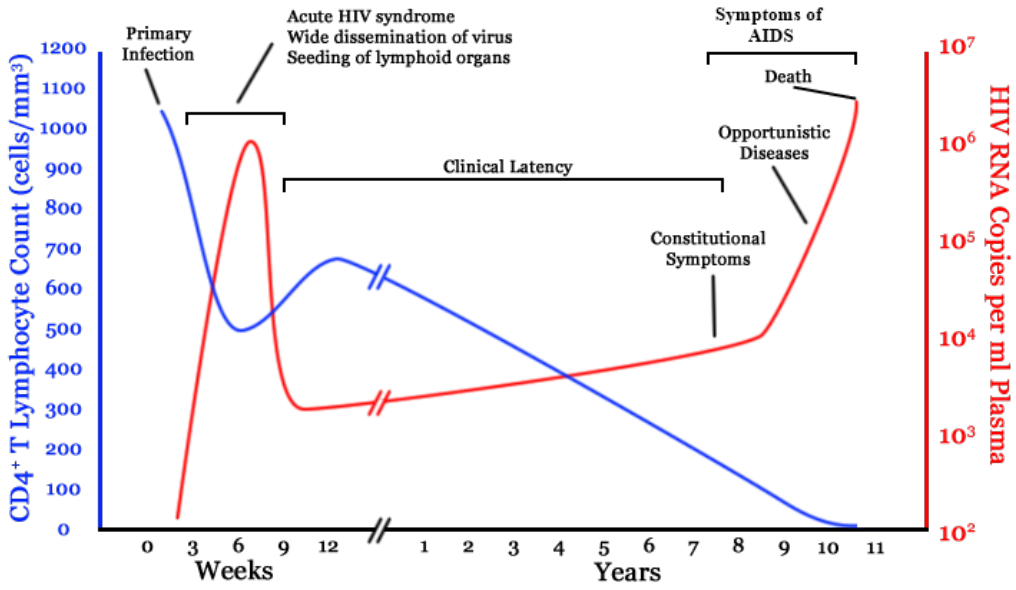


Figure 3: Timeline of HIV-1 disease progression in the absence of cART

Schematic representation of the changes in plasma HIV-1 RNA levels and CD4+ T cell count during the progression of untreated HIV-1 infection. Reproduced from An and Winkler [30].

Currently, 37.9 million individuals are infected with HIV-1 worldwide of which 62 % have access to combination antiretroviral therapy (cART) [17]. The major classes of antiretrovirals function by blocking crucial steps of the HIV-1 replication cycle including viral entry, viral envelope fusion with the host cell membrane, reverse transcription of viral RNA, integration of viral cDNA and maturation of nascent viral particles [31] (represented in Figure 2). Where available, routine use of cART in the clinical management of HIV-1 infection has considerably reduced AIDS-related morbidity and mortality, and increased the lifespan of HIV-1 infected individuals. In high-income countries for example, it is estimated that initiating cART at 20 and 35 years of age improves overall life expectancy of HIV-1 positive individuals by 43.3 and 32.2 years respectively. Lifespan is increased to a lesser

extent in low income countries, with enrolment on cART at 20 and 35 years of age providing an additional 28.3 and 25.6 years of life respectively [32]. Nonetheless, mounting clinical evidence demonstrates HIV-1-infected individuals bear an increased risk of developing non-AIDS morbidities despite effective cART suppression of viral replication [33-35]. The biological mechanisms underlying these observations are complex and are likely to represent the intersection of multiple factors including HIV-1-associated immune senescence [36], HIV-1-induced chronic immune activation and inflammation [33,37], as well as exposure to generalised risk factors associated with ageing due to the increased lifespan of cART treated individuals. In the context of chronic immune activation and inflammation, the contribution of monocytes/macrophages to the pathogenesis of non-AIDS morbidities is currently under scrutiny as these cells are both targets of HIV-1 infection and key mediators of the inflammatory response.

1.2 Origins of tissue-resident macrophages

Macrophages are antigen-presenting cells (APCs) of myeloid lineage which carry out pathogen sensing and clearance functions as part of the innate immune system. Macrophages are also involved in maintaining tissue homeostasis and can be found in almost all tissue compartments. Macrophages were long believed to derive solely from hematopoietic stem cells via bone-marrow precursor cells and peripheral blood monocyte intermediates. However, recent studies have overturned this dogma and instead show that tissue-resident macrophages can arise from two distinct populations of pre-cursor cells. Monocyte-derived macrophages (MDMs) derive from infiltrating, peripheral monocytes

and contribute to the maintenance of the macrophage pool, particularly during inflammation [38,39]. In contrast, most self-renewing tissue-resident macrophage populations arise from embryonic yolk sac and/or foetal liver-derived progenitor cells without a monocyte intermediate [40,41]. Relatedly, murine studies have demonstrated that the development of tissue-resident macrophages from embryonic progenitor cells is dependent on the transcription factor Myb, whereas MDMs follow a Myb-dependent development pathway [42]. While macrophages can originate from either embryonic progenitors or peripheral monocytes, under steady-state conditions peripheral monocytes contribute minimally to the tissue-resident macrophage pool and the ontogenic lineage of macrophages is tissue-specific [43]. For example, while the gut is initially colonised by foetal yolk sac and foetal liver-derived macrophages, these are gradually replaced and maintained by MDM throughout adult life [44]. Using murine models, Hoeffel et al have also shown that yolk sac-derived progenitor cells are capable of colonising the foetal liver and giving rise to Myb-expressing monocyte intermediate cells, which in turn differentiate into tissue-resident macrophages [45]. In contrast, microglia of the CNS [42,46], Kupffer cells of the liver [42] and alveolar macrophages [42] are self-renewing and mostly derive from embryonic precursors without a monocyte intermediate stage. Furthermore, these mature tissue-resident macrophages may themselves proliferate in response to inflammation or tissue damage and, together with infiltrating MDMs, contribute to increasing the tissue-resident macrophage pool when there is a need for greater macrophage turnover [47].

1.3 Evidence for monocyte/macrophage involvement in HIV-1 infection

While $CD4^+$ T-cells have long been established as the primary targets of HIV-1, the significance of monocytes and macrophages as cellular targets of infection remains under debate. Although monocytes express the HIV-1 entry receptor CD4 and co-receptor CCR5, it is unclear whether they are fully or partially refractory to HIV-1 infection. Numerous studies have demonstrated the presence of HIV-1 DNA or RNA in monocytes of HIV-1 infected individuals (summarised in Table 1). In contrast, others have demonstrated that monocytes do not support productive HIV-1 infection [48-52] and failed to detect viral DNA in moocytes preparations from HIV-1 infected patients [53]. Furthermore, it is suggested that detection of HIV-1 in monocyte isolations may be due to contamination with HIV-1-infected $CD4^+$ T-cells (reviewed in [54]).

Establishing evidence for productive HIV-1 infection of monocytes/macrophages is further complicated by the ability of myeloid cells to capture and harbour HIV-1 particles and infected cell debris without necessarily becoming infected [55,56]. However, evidence for the permissiveness of macrophages to HIV-1 infection is more conclusive than for monocyte infection. Macrophages express moderate levels of CD4 and CCR5, and are susceptible to infection by R5-tropic or dual tropic HIV-1 (SOURCE). Clinical studies have demonstrated the presence of HIV-1 DNA, RNA or p24 antigen in microglia of the CNS, Kupffer cells of the liver, alveolar, intestinal and testicular macrophages suggesting that tissue-resident macrophages are targets of HIV-1 infection (summarised in Table 1). While the level of productive infection in macrophages varies between donors and HIV-1 strains [57,58], quantification of HIV-1 DNA from rectal tissue biopsies suggest that up to 4 % of

HIV-1 infected cells are of myeloid origin [59]. Furthermore, numerous studies have convincingly demonstrated that macrophages remain infected with HIV-1 even in the presence of virological suppression by cART (summarised in Table 1) suggesting a potemtial role of macrophages as a viral reservoir.

In addition to the clinical studies summarised in Table 1, in vivo experiments using humanised mouse models and non-human primate models have demonstrated that macrophages can sustain HIV infection and replication in the absence of T cells. For example, Honeycutt et al generated a myeloid-only mouse (MoM) model by transplanting NOD/SCID mice with human $CD34^+$ ($hCD34^+$) stem cells and reconstituting the mice with human myeloid and B cells [53]. As a result, the MoM model is populated with human myeloid cells but murine and human T cell populations are completely absent. Following infection with the CCR5-tropic HIV-1 isolates, sustained levels of HIV-1 viral RNA are detectable in the plasma of MoM confirming that myeloid cells are capable of supporting HIV-1 infection and replication independently of T cells. Consistent with the human clinical studies summarised in Table 1, $hCD68^+$ cells isolated from the liver, lung and spleen tissue, as well as bone marrow of HIV-1-infected MoM were all found to contain HIV-1 RNA, confirming that human tissue-resident macrophages support HIV-1 infection and replication.

Macrophages are capable of sustaining productive HIV-1 infection and releasing infectious HIV-1 virions. Fow virometric analysis of the cellular proteins present on HIV-1 isolated from the plasma of infected individuals confirms that macrophage-derived virions specifically incorporate the class B scavenger receptor molecule CD36 into the viral

membrane. In contrast, T cell-derived virions incorporate CD27 molecules in their viral membranes [60,61]. Experiments using the bone marrow/liver/thymus (BLT) mouse model have also been used to demonstrate productive infection of macrophages. In this mouse model human fetal liver-derived $CD34^+$ hematopoietic stem cells are intravenously introduced to immunodeficient NS mice after the mice were surgically transplanted with human fetal liver and thymus tissue fragments. As a result, the BLT mice are populated with human lymphoid and myeloid cell populations [62]. HIV-1 infection and replication can be established in the MoM model when macrophages isolated from HIV-1 infected BLT mice are depleted of T cells and intravenously transferred to uninfected MoMs [53]. Together, these studies confirm that macrophages are productively infected by HIV-1.

Overall, these findings convincingly demonstrate the involvement of macrophages in the pathogenesis of HIV-1 infection both as target cells and sources of cell-free virus. Given that monocytes/macrophages are relatively resistant to the cytopathic effects of HIV-1 infection (reviewed in [63]) and $CD8^+$ T-cell mediated killing [64], these findings also highlight the role of monocytes/macrophages as a potential long-lived HIV-1 reservoir during suppressive cART [54].

Table 1: Evidence for *in vivo* HIV-1 infection of monocytes / macrophages

Reference	Total study participants	Participants enrolled on cART? / Length of time on cART	Participants for which virological suppression (viral load <50 copies / mL) was achieved	Source of monocytes / macrophages	Participants with HIV-1 positive monocytes/ macrophages	Evidence of HIV-1 infection
Lambotte et al [65]	n = 5	n = 5, 14-18 months	n= 5	Peripheral monocytes	n = 3	HIV-1 DNA and/or RNA detected by PCR
Calcaterra et al [66]	n = 11	n = 11, 18-32 months	n = 7	Peripheral monocytes	n = 9	Total HIV-1 DNA detected by PCR
Sonza et al [67]	n = 10	n = 10, n/a	n = 10	Peripheral monocytes	n = 10	Integrated HIV-1 DNA detected by PCR
Zhu et al [68]	n = 7	n = 7, 36-50 months	n = 7 but intermittent	Peripheral monocytes	n = 7	HIV-1 DNA and/or RNA detected by PCR
Crowe et al [69]	n = 10	n = 10, n/a	n = 10	Peripheral monocytes	n = 4	HIV-1 RNA in culture supernatant detected by PCR

Reference	Total study participants	Participants enrolled on cART? / Length of time on cART	Participants for which virological suppression (viral load <50 copies / mL) was achieved	Source of monocytes / macrophages	Participants with HIV-1 positive monocytes/ macrophages	Evidence of HIV-1 infection
Delobel et al [70]	n = 3	n = 3, 7 years	n = 3	Peripheral monocytes	n = 3	HIV-1 DNA detected by PCR
Ellery et al [71]	n = 17	n = 17, n/a	n = 5	Peripheral monocytes	n = 16	HIV-1 DNA detected by PCR
Gibellini et al [72]	n = 34	n = 34, 24 months	n = 34	Peripheral monocytes	n = 12	HIV DNA detected by PCR
Valcour et al [73]	n = 27	n = 26, > 48 weeks	n = 26	Peripheral monocytes	n = 4	HIV-1 DNA detected by PCR
Ndhlovu et al [74]	n = 12	n = 12, 2 - 24 years	n = 12	Peripheral monocytes	n = 12	HIV-1 DNA detected by PCR
Hansen et al [75]	n = 6	n = 6, n/a	n = 6	Peripheral monocytes and alveolar macrophages	n = 6	HIV-1 DNA detected by digital droplet PCR
Cattin et	n = 12	n = 12,	n = 12	Peripheral	n = 4	HIV-1 DNA detected by PCR

Reference	Total study participants	Participants enrolled on cART? / Length of time on cART	Participants for which virological suppression (viral load <50 copies / mL) was achieved	Source of monocytes / macrophages	Participants with HIV-1 positive monocytes/ macrophages	Evidence of HIV-1 infection
al [76]		4 months – 16 years		monocytes		
Deleage et al [77]	n =9	n/a	n = 7	$CD163^+$ macrophages in seminal vesicles	n/a	HIV-1 p24 and/or HIV-1 RNA detected by *in situ* hybridization (ISH) and immunohistochemistry (IHC)
Wang et al [78]	n = 9	n/a	n /a	$CD68^+$ multinucleated giant cells in lung and colon tissue	n = 2	HIV-1 p24 antigen detected by IHC
Yukl et al [59]	n = 7	n = 7, > 6 months	n = 7	$CD13^+CD45^+CD3^-$ myeloid cells in rectal tissue	n = 7	HIV-1 DNA detected by PCR
Cribbs et al [79]	n = 23	n = 23, n/a	n = 18	Alveolar macrophages	n = 16	HIV-1 DNA and/or RNA detected by PCR
Lamers et al [80]	n = 1	n =1, n/a	n/a	$CD68^+CD163^+$ macrophages in CNS tissue	n = 1	HIV-1 RNA detected by ISH

Reference	Total study participants	Participants enrolled on cART? / Length of time on cART	Participants for which virological suppression (viral load <50 copies / mL) was achieved	Source of monocytes / macrophages	Participants with HIV-1 positive monocytes/ macrophages	Evidence of HIV-1 infection
Lamers et al [81]	n = 1	n/a	n/a	Macrophages in meningeal vessels and CNS tissue	n = 1	HIV-1 p24 antigen detected by IHC
Rose et al [82]	n = 7	n = 7, n/a	n = 7	$CD68^+CD163^+$ macrophages in lymph node and CNS	n/a	HIV-1 DNA and/or RNA detected by ISH
Tso et al [83]	n = 2	n = 2, 2 – 12 years	n = 1	$CD68^+$ macrophages in CNS	n = 2	HIV-1 DNA and/or RNA detected by ISH
Kandathil et al [84]	n = 8	n = 8, 1 – 12 years	n = 8	Liver macrophages	n = 8	HIV-1 DNA detected by PCR
Ko et al [85]	n = 16	n = 16, n/a	n = 16	$CD68^+$ CNS or $CD206^+$ perivascular macrophages	n = 16	HIV-1 DNA and/or RNA detected by ISH
Ganor et al [86]	n = 20	n = 20, 3 – 22 years	n = 20	Iba-1^+ or $CD68^+$ macrophages in	n = 3	HIV-1 DNA detected by ISH HIV-1 virions and proteins

Reference	Total study participants	Participants enrolled on cART? / Length of time on cART	Participants for which virological suppression (viral load <50 copies / mL) was achieved	Source of monocytes / macrophages	Participants with HIV-1 positive monocytes/ macrophages	Evidence of HIV-1 infection
				urethral tissue		visualised by microscopy

IHC, immunohistochemistry; ISH, *in situ* hybridisation

1.4 Macrophage activation in chronic HIV-1 infection

In addition to being target cells of HIV-1 [53,87,88], macrophages carry out a variety of functions that are crucial to maintaining tissue homeostasis, and form a highly plastic cell population which can be activated along a spectrum of phenotypes (summarised in Figure 4). In particular, macrophages are key mediators of the innate immune response and activate inflammatory processes in response to stimuli in their microenvironment.

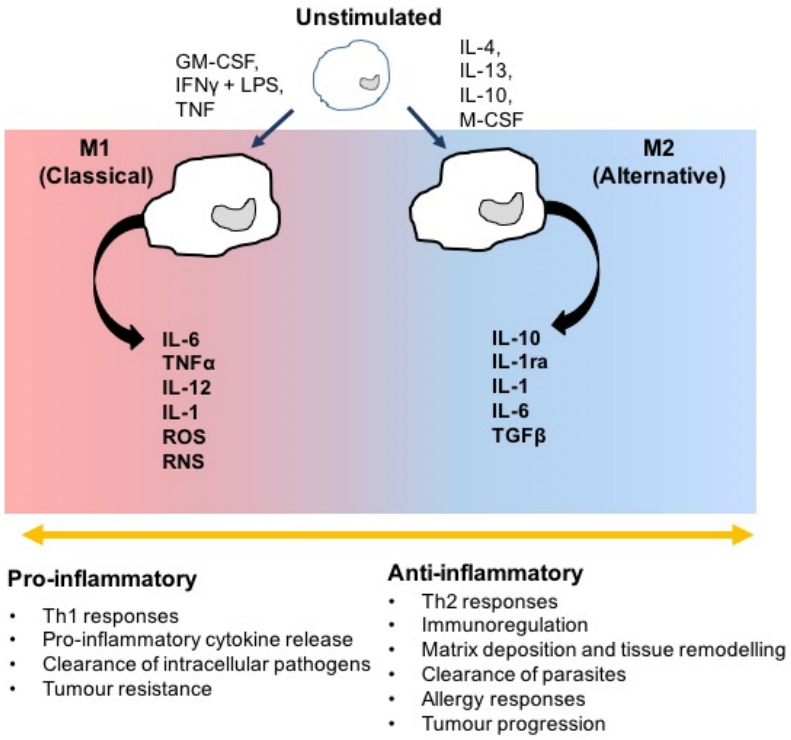


Figure 4: The M1/M2 paradigm of macrophage activation in response to environmental stimuli

Stimulation by cytokines and microbial products triggers the polarization of macrophages along a spectrum of inflammatory phenotypes. Stimulation by GM-CSF, TNF or IFNγ and LPS triggers M1 polarization while IL-4, IL-13, IL-10 or MCSF stimulate M2 polarization. Reviewed in [89,90].

Macrophages are thought to form a component of the long-lived HIV-1 viral reservoir [91-93] since, as mentioned above, they are relatively resistant to the cytopathic effects of HIV-1 infection [63], and also to $CD8^+$ T-cell-mediated cell killing [64]. These characteristics bear implications not only for HIV-1 eradication strategies, but also for the pathogenesis of HIV-1-associated chronic inflammation. Clayton et al recently demonstrated that inefficient killing of HIV-1-infected MDMs by $CD8^+$ T-cells allows for the formation of prolonged synapses between MDMs and $CD8^+$ T-cells, leading to sustained antigenic stimulation of the latter. As a result of the prolonged synapse time, $CD8^+$ T-cells were stimulated to produce enhanced levels of IFN-γ which in turn induced MDM production of pro-inflammatory chemokines. Furthermore, the level of pro-inflammatory chemokines produced by MDMs was sufficient to drive migration of monocytes and $CD4^+$ T-cells [64]. In this way, inefficient clearance and prolonged activation of HIV-1 infected macrophages may enhance leukocyte migration to tissues and contribute to the pathogenesis of inflammatory conditions in people living with HIV infection (PLWH).

The onset of immune activation as determined by classic inflammatory markers occurs alongside early phases of viral expansion as part of the innate immune response to HIV-1 infection as depicted in Figure 5 [94].

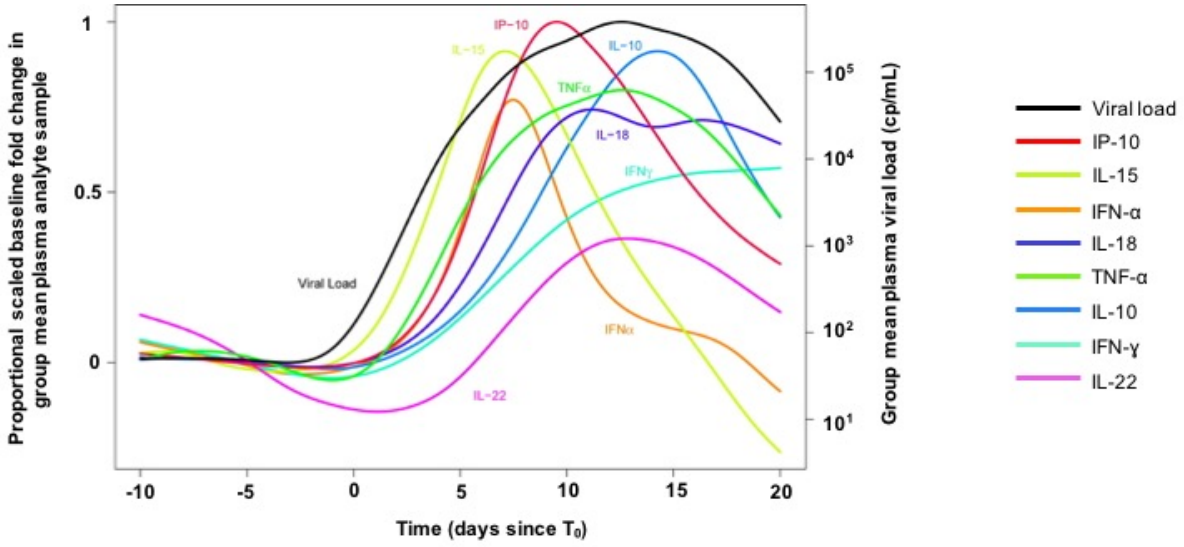


Figure 5: Timeline of the systemic cytokine cascade initiated during the acute phase of HIV-1 infection

Elevation of acute phase proteins is accompanied by successive waves of cytokine release during acute HIV-1 infection. The figure represents the mean change in plasma levels of cytokines during acute infection scaled relative to their respective baseline levels. Values for mean change are aligned to T_0, the time-point at which viral load was detected at 100 copies/mL. Reproduced from Stacey et al [94].

However, a striking feature of HIV-1 infection is the persistence of immune activation beyond the acute phase. In particular, monocyte/macrophage-associated markers of immune activation and systemic inflammation such as IL-6 [95-98], sCD14 [95,99-102], LPS [96], hsCRP [97,100,103-105], oxLDL [98], D-dimer[106], MCP-1 [102,107] and sCD163 [96,98,101,102] are elevated in PLWH. Although cART reduces the level of

monocyte/macrophage activation markers detected in the systemic circulation, therapy does not return these inflammatory markers to the levels observed in the general population [100]. These observations suggest that HIV-1 infection promotes a biological environment in which monocytes/macrophages may be activated to a chronic pro-inflammatory state.

Monocyte/macrophage engagement with infected T-cells, cell-free virus, viral proteins, chemokines, cytokines and translocated microbial products have all been proposed to contribute to cell activation and chronic inflammation as a consequence of HIV-1 infection. Although the pathways by which these stimuli direct monocytes/macrophages towards a pro-inflammatory phenotype are not well defined, they are likely to be interrelated and are summarised in Figure 6.

For example, several types of pattern recognition receptors (PRR) are involved in the recognition of HIV-1 PAMPs which include viral proteins, the incoming viral single-stranded RNA (ssRNA) genome and newly synthesised HIV-1 reverse transcripts. In the cytosol, the dsRNA helicase RIG-I senses HIV-1 genomic RNA and the cGAS-cGAMP-STING signalling complex detects double-stranded viral cDNA products of reverse transcription [108]. Additionally, endosomal TLR7/8 detect ssRNA, guanosine and deoxyguanosine[109],[110] . Viral sensing leads to activation of interferon regulatory factors (IRF), signal transduction via the NFKB, MAPK1 and AP-1 pathways, as well as downstream induction of IFN-I [110,111]. In turn, these signalling events culminate in the production of pro-inflammatory cytokines/chemokines and ISG expression [112,113]. HIV-1 proteins (e.g Nef, gp41, Tat and

gp120) also engage cell surface PRRs and activate cell-signalling pathways that have been linked to downstream pro-inflammatory events [114-117]. Cell surface expressed TLR2/4 may recognise HIV-1 Tat leading to TNF-α and IL-10 expression and [118] and exposure to HIV-1 Tat has also been shown to enhance expression of ICAM-1, VCAM-1, MCP-1/CCL2 and TNF-α in the CNS [119].

In addition to direct infection and sensing of viral PAMPs, cell-to-cell interactions also contribute to immune activation during HIV-1 infection. As previously described, prolonged synapse formation between $CD8^+$ T-cells and HIV-1-infected macrophages establishes a pro-inflammatory feedback loop in which enhanced IFN-γ expression by synapsed $CD8^+$ T-cells induces the downstream production of pro-inflammatory chemokines by macrophages [64]. Additionally, macrophages preferentially phagocytose infected T-cells [87] and viral spread between T-cells and macrophages is facilitated via an HIV-1-mediated cell-cell interaction known as a virological synapse [88]. However, it is not known to what extent interactions through the virological synapse affect monocyte/macrophage activation and pro-inflammatory phenotype.

Depletion of $CD4^+$ T cells in the gut associated lymphoid tissue (GALT) occurs in the early stages of infection as a result of viral replication, resulting the in the loss of barrier Th17 helper cells and inflammatory tissue damage. HIV-1 infection also appears to promote the proliferation of pathogenic gut bacteria that are associated with immune activation, whilst reducing the relative abundance of beneficial commensals, thereby altering the homeostatic balance within the gut to a pro-inflammatory environment [120]. As the $CD4^+$ T-cell population is not fully restored by cART, the structural integrity of the intestinal

epithelium is diminished over time, allowing for translocation of microbial products into the systemic circulation [120]. Furthermore, sCD14 (a marker of microbial translocation and immune activation) remains elevated despite cART suggesting a significant role for microbial translocation in chronic immune activation [95,121].

Lastly, increased co-pathogen burden also contributes to chronic immune activation. For example, HIV-1-induced immunosuppression facilitates the reactivation of cytomegalovirus (CMV) for which co-infection is associated with HIV-1 disease progression. Notably, CMV IgG antibody levels are correlated with elevated markers of immune activation in HIV-1 infected individuals [122,123]

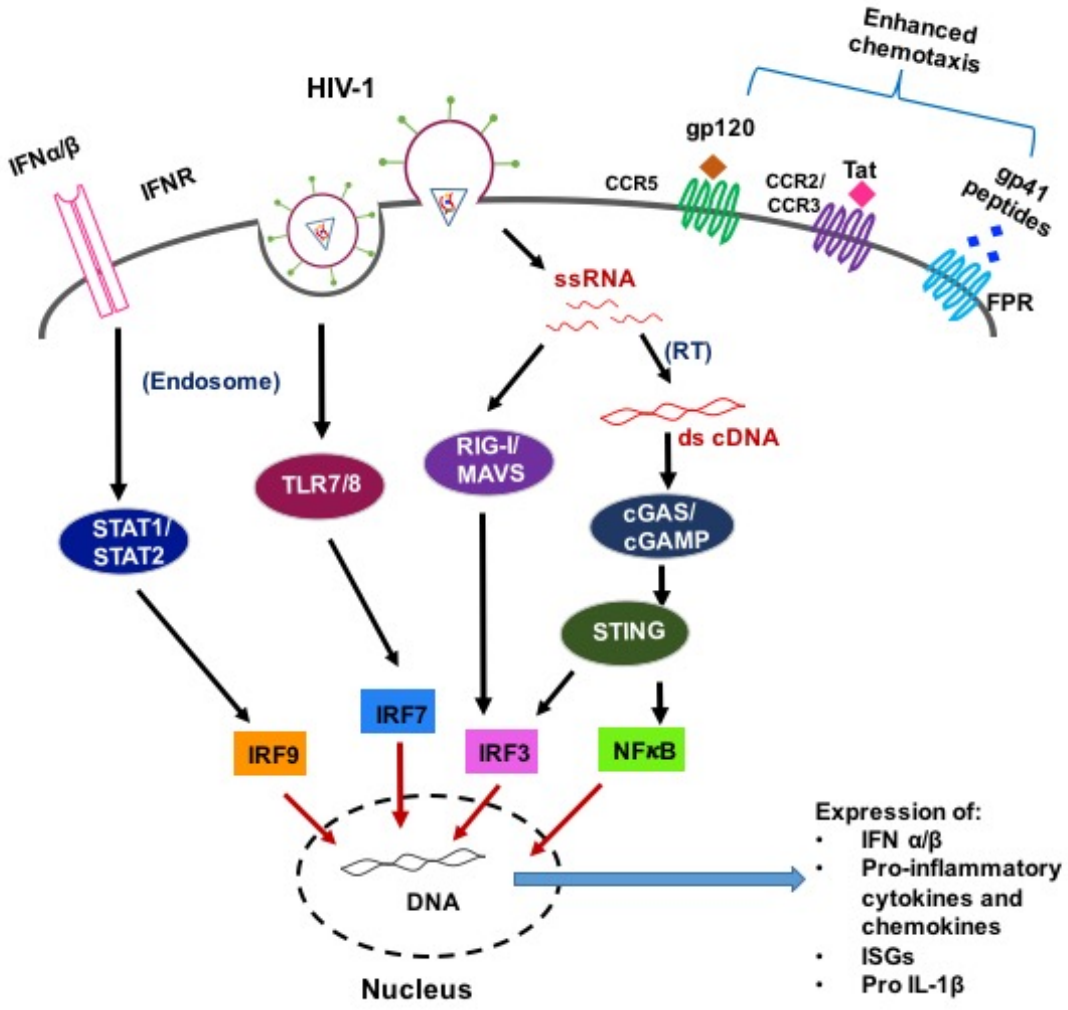


Figure 6: Summary of the stimuli and signalling pathways implicated in monocyte/ macrophage activation during HIV-1 infection

Direct HIV-1 infection, endocytic uptake of HIV-1 particles, cytokine engagement of cell surface receptors, intracellular sensing of pathogen nucleic acids and HIV-1 protein engagement of chemokine receptors activates signalling pathways and transcription factors that induce downstream pro-inflammatory effects [112,113,116,118,124-127]. The signalling pathways activated by phagocytosis of infected T-cells, spread of HIV-1 across the virological synapse and gp41 peptide engagement of formyl peptide receptors have not yet been defined [87,88,128-131].

1.5 Role of monocytes/macrophages in the progression of HIV-1-associated inflammatory conditions

In spite of the success of cART in reducing AIDS-related morbidity and mortality, PLWH bear an excess risk of developing chronic inflammatory conditions in comparison to their uninfected counterparts [97,132]. Clinical studies increasingly implicate macrophages in the pathogenesis of HIV-1-associated inflammatory disorders, the most prevalent of which are cardiovascular disease (CVD) [121,133,134] and HIV-1-associated-neurocognitive disorders (HAND) [135-137]. While evidence for *in vitro* and *in vivo* infection of MDMs by HIV-1 has been well established [91], it is unclear to what extent these HIV-1-infected macrophages contribute to the pathogenesis of HIV-1-associated inflammatory disease.

1.5.1 Association between monocyte/macrophage activation and CVD progression

The predominant HIV-1-associated inflammatory condition is CVD for which HIV-1-infected individuals bear a 1.5 – 2-fold risk in comparison to their uninfected counterparts [138,139]. Furthermore, clinical studies reveal that elevated markers of monocyte/macrophage activation often correlate with the progression of CVD in HIV-1 positive individuals (summarised in Table 2).

Table 2: Elevated markers of monocyte/macrophage activation and their association with CVD in HIV-1 infection

Marker	Associations with cardiovascular disease in HIV infection
sCD14	Mortality [37,121,140], CVD event [37], CIMT [141], atherosclerotic plaque formation [102]
IL-6	Mortality [37,140], CVD event[37,142]
hsCRP	Mortality [37,140], CVD event [142,143]
oxLDL	CIMT [144] , MI [105]
D-dimer	Mortality[37,140], CVD event[37,142]
LPS	CIMT [141]
MCP-1	Atherosclerotic plaque formation [102,145]
sCD163	Increased Framingham cardiovascular risk score, atherosclerotic plaque formation[96,102]

Cardiovascular disease (CVD), Carotid intima media thickness (CIMT), Myocardial infarction (MI)

These observations are likely to be linked to the central role of monocytes/macrophages in the pathogenesis of atherosclerosis - a CVD at the intersection of lipid metabolism and chronic inflammation. Therefore, it has been proposed that chronic activation of monocytes/macrophages during HIV-1 infection mediates the increased risk of CVD observed in HIV-1-infected individuals. Clinical studies also suggest that the pathogenesis of atherosclerotic disease in HIV-1-positive individuals differs from that of uninfected

individuals, as HIV-1 infection is associated with a phenotype of up-regulated monocyte/macrophage activation that facilitates the formation of non-calcified atherosclerotic lesions in the absence of traditional risk factors for CVD [96,102,146].

There is also ongoing debate as to whether cART itself significantly contributes to CVD risk in HIV-1 positive patients. The non-nucleoside reverse transcriptase inhibitor (NNRTI) Efavirenz promotes leukocyte adhesion to endothelial cells, and the protease inhibitor (PI) Ritonavir disrupts cholesterol metabolism and accumulation in macrophages [132]. These effects may enhance atherogenesis by promoting monocyte extravasation into the arterial intima and subsequent foam cell formation. However, newer therapies do not appear to have significant adverse effects on metabolism [147]. Furthermore, the decline in viral load achieved through adherence to therapy contributes to a net reduction in markers of immune activation and CVD risk among patients [132]. Therefore, cART more likely has a net positive effect on reducing the risk of developing HIV-1-associated CVD.

1.5.2 Association between monocyte/macrophage activation and HAND progression

While the advent of cART has reduced the incidence of HIV-1-associated dementia and opportunistic infections of the CNS such as cryptococcal meningitis and toxoplasmosis [148], it is estimated that 40-70% of HIV-1-infected individuals continue to develop conditions along the spectrum of HAND [137,149]. Neurocognitive decline in HAND-affected individuals most commonly manifests as sensory neuropathies, impaired motor speed and impaired memory [148,149]. Additionally, clinical evidence of decreased

neurocognitive function in HIV-1-infected individuals despite enrolment on cART supports the hypothesis that HIV-1 replication in the CNS may not be completely controlled by cART, possibly because some antiretroviral drugs may not effectively penetrate the blood-brain barrier.

HIV-1 RNA is detectable in the cerebrospinal fluid (CSF) of HIV-1-infected individuals as early as 8 days post-transmission [150], and early studies suggested that levels of CSF HIV-1 RNA were predictive of neurocognitive decline [151,152]. Together, these findings suggest that the CNS viral reservoir is established early on in HIV-1 infection. Metabolic markers of inflammation are also elevated in CNS tissues of HIV-1-infected individuals within the first month of infection [150,153]. Microglia and perivascular macrophages are believed to contribute significantly to the formation of this viral reservoir as HIV-1 DNA, RNA and p24 antigen are often detected in macrophage-lineage cells isolated from CNS tissue samples of HIV-1-infected individuals on suppressive cART (summarised in Table 1). Furthermore, numerous clinical studies have also revealed associations between the progression of HAND and markers of monocyte/macrophage activation (summarised in Table 3). For these reasons, it is hypothesised that HIV-1 infection of macrophage-lineage cells and ongoing macrophage activation in the CNS significantly contribute to the progression of neuro-inflammation and HAND.

Table 3: Elevated CSF markers of monocyte/macrophage activation and their association with HAND progression

Marker	Associated neurocognitive disorders in HIV-1 infection
CD163 (mRNA)	HIV-1 encephalitis [154,155]
sCD163 (plasma)	GDS impairment and minor neurocognitive disorder [156]
CCL2/MCP-1	HIV-1 encephalitis and concomitant CMV encephalitis [157], cerebral metabolite profiles associated with HAND [158,159]
CXCL10/IP-10	AIDS dementia complex [160], cerebral metabolite profiles associated with HAND [158]
Neopterin	HIV-1 dementia, cryptococcal meningitis, concomitant CMV encephalitis [161]
sCD14	Impaired neurocognitive testing [162]
Osteopontin	Cognitive impairment [163], HIV-1 associated dementia [164]

GDS, global deficit score

1.6 Effects of HIV-1 on leukocyte trafficking

In addition to chronic monocyte/macrophage activation, an increased propensity to migrate to sites of active viral replication and inflammation is a central aspect to monocyte/macrophage involvement in the progression of HIV-1-associated inflammatory conditions.

In the context of neuro-inflammation, *in vitro* experiments demonstrate that upregulated surface TNF-α expression on HIV-1-infected macrophages induces activation of astrocytes and consequent CCL2/MCP-1 release through contact-dependent engagement of their cell surface TNF-α receptors [165]. Increased CCR2 expression on monocytes during HIV-1 infection enhances their migration across blood-brain barrier (BBB) models towards CCL2/MCP-1 [166]. Furthermore, $CD14^{+}CD16^{+}$ monocyte infiltration into the CNS is preferentially enhanced during HIV-1 infection [135,136,167] and appears to be driven by increased levels of CCL2/MCP-1 [119,166] and CXCL12 [168]. These observation bear implications not only for the dissemination of HIV-1 in the CNS and establishment of a long-lived viral reservoir, but also strongly implicate monocyte trafficking in the pathogenesis of the neuro-inflammation that drives HAND [137].

Expression of HIV-1 viral proteins may also drive pro-inflammatory changes in monocyte/macrophage activation which promote enhanced leukocyte trafficking. For example, expression of HIV-1 Nef by infected macrophages leads to increased production of the CC-chemokines MIP-1α and MIP-1β which, in turn, stimulate lymphocyte chemotaxis towards the infected macrophages [169].

The function of CXCR4 and CCR5 as co-receptors for HIV-1 accounts for their involvement in HIV-1-induced leukocyte trafficking, as viral gp120 binds these chemokine receptors to facilitate viral entry into cells bearing the receptors. As a result, HIV-1 infection can indirectly contribute to immune cell trafficking when viral proteins provide chemotactic signals. For example, macrophage-tropic gp120 engages CCR5 on immature dendritic cells (DC), initiating a kinase cascade that induces chemotaxis by mediating phosphorylation of

leukocyte specific protein (LSP)-1 and its subsequent association with actin [170,171]. Gp120 has also been implicated in the induction of monocyte migration across the blood brain barrier (BBB) [117]. Additionally, both gp160 and gp120 versions of Env are reported to be capable of inducing both CCR5 [172,173] and CXCR4 [173,174] -dependent migration and G-protein coupled receptor (GPCR) activation in $CD8^+$ and $CD4^+$ T-cells. Although the chemotactic effects of gp120 on T-cells and DCs is well reported, its effects on monocyte activation and migration warrants further study.

Chemokine mimicry by viral proteins can also occur without engaging the canonical CXCR4 and CCR5 co-receptors. For example, cleavage of the gp41 ectodomain by epithelium expressed serine proteases generates chemotactic peptides that induce migration of monocytes through engagement of formyl peptide receptors [128-131]. The effects of HIV-1 Tat protein on leukocyte migration have also been widely reported and appear to be mediated through a variety of mechanisms. The Tat protein bears a cysteine rich (Cys-Cys-Phe) sequence that is structurally homologous with numerous β-chemokines. Tat may therefore be capable of inducing human monocyte/macrophage chemotaxis through engagement of CCR2 and CCR3 [124,125]. Tat also mimics the effects of vascular endothelial growth factor (VEGF) by binding to the VEGF receptor [175], thereby promoting enhanced migration and extravasation of monocytes/macrophages. Exposure to Tat also activates monocytes/macrophages, leading to enhanced TNF-α, VCAM-1 and ICAM-1 and β-1 integrin expression [119,176,177] and the production of pro-inflammatory cytokines and chemokines including MCP-1/CCL2 [119,178-180]. Together, these factors enhance monocyte/macrophage migration into the CNS tissues. Mechanistically, Tat is

multifunctional, capable of inducing responses that are normally elicited downstream of IFN activation [126], engaging the TLR4-CD14-MD2 complex [118], and relieving IκB repression of NFκB activity by competitively binding to the p65/RelA domain [127]. These events lead to transcription of NFκB- and IFN-inducible genes and the production of pro-inflammatory mediators which are capable of inducing T-cell and monocyte/macrophage chemotaxis [115,126,127].

It should be noted that most investigations into the effect of recombinant HIV-1 proteins on monocyte/macrophage activation have not included measures to control for contaminating immunoreactive factors that may originate from producer cells or during purification (e.g. bacterial endotoxin), and their possible confounding effects on cell signalling and chemotaxis. Nonetheless, on the occasions where endotoxin-free recombinant proteins have been used for functional assays, both Tat and gp120 have been reported to enhance T-cell and monocyte migration [174,176,177]. Additionally, monocytes/macrophages and DC have been shown to exhibit upregulated pro-inflammatory cytokine release in response to endotoxin-free Tat [115].

1.7 Implications for future therapy

As described in section 1.5.1, there is ongoing debate as to whether cART itself significantly contributes to inflammatory disease risk in HIV-1-positive patients. However, newer therapies do not appear to have significant adverse effects on metabolism [147]. Furthermore, the decline in viral load achieved through adherence to therapy contributes to a net reduction in markers of immune activation and CVD risk among patients [132].

Monocyte/macrophage extravasation and activation represent key events that are both upregulated during HIV-1 infection and central to the progression of CVD and HAND. For example, percentages of inflammatory ($CD14^{-}CD16^{++}$) and patrolling ($CD14^{+}CD16^{++}$) monocytes are increased in treatment-naïve HIV-1 patients compared to healthy individuals, and levels of inflammatory and patrolling monocytes in HIV-1-infected patients are similar to those observed in healthy individuals with cardiovascular pathology [181]. Furthermore, blocking monocyte/macrophage trafficking decreases HIV-1-associated cardiovascular pathology and the abundance of activated CD163 macrophages in cardiac tissue [182].

To date no therapies have been developed to specifically target chronic monocyte/macrophage activation for the purpose of diminishing HIV-1-associated inflammation. However, treatment with Maraviroc (an anti-CCR5 agonist that functions by blocking interaction between R5 HIV-1 gp120 and CCR5 receptors expressed on T-cells and macrophages) has been shown to decrease macrophage expression of the activation marker CD163 in cardiac tissue and to prevent diastolic dysfunction in an SIV-macaque model of HIV-1 infection [183]**.** Further evidence for the anti-inflammatory potential of Maraviroc therapy is demonstrated in its ability to decrease chemotaxis of monocytes/macrophages in vivo [184]**.** Another class of drugs that shows promise for ameliorating persistent monocyte/macrophage activation and inflammation are statins. Statins are HMG-CoA reductase inhibitors which have been traditionally used to lower CVD risk by inhibiting hepatic cholesterol production and increasing the uptake of plasma low density lipoprotein cholesterol into hepatic cells [185]. While statin therapy effectively

reduces lipid indices in HIV-1-infected individuals [186], there is mounting evidence that statins also possess immunodulatory properties which make them useful anti-inflammatory therapeutics. Ex vivo experiments demonstrate that treatment with the statins Simvastatin and/or Atorvastatin reduces: I) monocyte production of MCP-1/CCL2 following LPS activation; II) monocyte migration towards MCP-1/CCL2; and III) the numbers of pro-inflammatory $CD16^{+}$ monocytes in the myeloid cell pool – a monocyte subset which is often associated with the progression of HAND [187]. In addition to this evidence, a study of cART-enrolled patients reported a significant decrease in expression of the activation marker D-dimer, and the pro-inflammatory cytokines IL-8 and IL-12 after treatment with the statin Rosuvastatin [185,188]. Together with their known safety and efficacy for reducing CVD risk in uninfected individuals, these findings suggest that statins may be useful for reducing the progression of HAND and CVD in PLWH. It is clear therefore, that therapeutic management of HIV-1-associated inflammation will require a targeted approach towards identifying crucial steps in the mechanisms of monocyte/macrophage activation and trafficking that can be exploited for the development of anti-inflammatory therapies adjunctive to cART.

1.8 Scope of work

Given the clinical evidence that implicates macrophages in the pathogenesis of HIV-1-associated inflammatory conditions, I hypothesised that MDM sensing of HIV-1 PAMPs during viral replication induces an innate immune response which results in the production of immune modulators and chemotactic factors which are relevant to the pathogenesis of

HIV-1-associated inflammation. Additionally, I hypothesised that chemokine mimicry by HIV-1 Env via monocyte-expressed CCR5 may contribute HIV-1-associated inflammation by enhancing monocyte migration.

To address these hypotheses, the work detailed in this thesis centred on three main research questions:

I. What is the profile of pro-inflammatory immune mediators induced by HIV-1 transduction of MDMs?

II. Does HIV-1 Vpr modulate the profile of immune mediators expressed by HIV-1-transduced MDMs?

III. Do uninfected monocytes exhibit enhanced migration towards HIV-1 Env or factors expressed by HIV-1-transduced MDMs?

In my studies I chose to work with single cycle pseudotyped viruses as this obviates the confounding variables implicit in a multi-cycle spreading infection. In Chapter 3, I first generated and validated a panel of eGFP-tagged, single-round HIV-1 pseudotyped viruses that either encoded or were deleted for *vpr*. I then optimised an HIV-1 transduction system for maximum biological relevance, and applied an HS/FCS differentiation protocol to reduce MDM and hPSC-DM restriction of HIV-1. Following on from this work, in Chapter 4, I transduced MDMs with the NL4.3-Vpr^{+} and NL4.3-ΔVpr pseudotyped viruses and used a wide-scale, semi-quantitative immunoassay to probe changes in the expression profile of immune mediators in response to HIV-1-transduction and Vpr expression. I then used complementary quantitative Luminex assays and ELISAs to validate my initial findings of Vpr-mediated modulation of pro-inflammatory cytokine/chemokine expression. Lastly, I

investigated the effect of Vpr on the production of IFN-I and the expression of ISGs involved in MDM responses to HIV-1. In Chapter 3 I also detail the work carried out to optimise a site-directed mutagenesis approach for generating Vpr-mutated HIV-1-NL4.3 expression plasmids for future study of the mechanisms by which Vpr exerted effects on cytokine/chemokine expression and IFN-I production. Finally, in Chapter 5, I established a real-time electrical cell impedance based assay to measure the migration of primary human $CD14^+$ monocytes and validated the assay's ability to detect directional monocyte migration towards a range of chemokines. I then applied the assay to investigate primary human $CD14^+$ monocyte migration towards HIV-1 envelope glycoproteins and conditioned supernatants from HIV-1-transduced MDMs.

Together, the work presented in this thesis provides evidence that HIV-1 induces MDM production of chemotactic factors and also demonstrates that HIV-1 Vpr downregulates soluble IFN-I production by MDMs.

Chapter 2:

Materials and methods

2.1 Cell culture

The THP-1 monocytic cell line was maintained in RPMI-1640 medium (Gibco) supplemented with 10 % FCS (Gibco) and 1 % penicillin-streptomycin (P/S, Gibco) at 37°C and 5 % CO_2. The Human Embryonic Kidney (HEK) 293F cell line was maintained in 293 freestyle expression medium (Gibco) at 37°C and 5 % CO_2 with continuous shaking. The HEK293-Dual-mTLR4 (NF/IL-8) reporter cell line (Invivogen) line was maintained in DMEM (Gibco) supplemented with 10 % FCS, 1 % P/S, 100 µg/mL of Hygromycin B Gold (Invivogen) and 50 µg/mL of Zeocin (Invivogen) at 37°C and 5 % CO_2. The 293T cell line, HeLa-based TZM-bl luciferase reporter cell line and HEK293-ISRE-fLuc reporter cell lines were maintained at 37°C and 5 % CO_2 in DMEM (Sigma) supplemented with 1% P/S (Gibco) and 10 % FCS (Gibco). TZM-bl reporter cells were lifted with 10 mM EDTA at room temperature (RT) for 1 h. The HEK293T cell line and HEK293-ISRE-fLuc cells were lifted with 0.25% trypsin-EDTA (Gibco) for 5 min at 37°C. All cell lines were pelleted by centrifuging at 229 *x g* (1600 rpm) and 4°C for 5 min prior to re-suspension in cDMEM.

2.2 Isolation of $CD14^+$ blood monocytes

Peripheral blood mononuclear cells (PBMCs) were isolated from HIV-seronegative donors' leukocyte cones by Ficoll-Histopaque (Sigma) density gradient centrifugation. $CD14^+$ monocytes were negatively selected using the Human Pan Monocyte Isolation Kit (Miltenyi Biotec): thawed PBMCs were washed with RPMI-1640 medium and re-suspended in human IgG-based Fc Receptor blocking reagent. PBMCs were mixed with the kit-supplied cocktail of biotin-conjugated monoclonal antibodies (mAbs) against antigens not expressed on human monocytes, and incubated for 5 min at 4°C. The suspension was then incubated

with anti-biotin microbeads for 10 min at 4°C. The antibody-labelled cell mixture was applied to a magnetic column and the eluate (enriched for $CD14^+$ monocytes) was collected.

2.3 Differentiation of $CD14^+$ monocytes to blood monocyte-derived macrophages (MDMs)

Negatively isolated $CD14^+$ monocytes were maintained in X-$vivo_{15}$ (Lonza) supplemented with 1 % heat inactivated human AB serum (Sigma) for 3 days. The culture medium was then changed to X-$vivo_{15}$ supplemented with 10 % FCS (cX-$vivo_{15}$) and the cells were incubated for a further 4 days for a total of 7 days differentiation.

2.4 Establishing human pluripotent stem cell (hPSC) pre-cursor cultures

The hPSC lines used in this study were obtained from the James Martin Stem Cell Facility at the Sir William Dunn School of Pathology and are summarised in Table 4.

Table 4: Human induced pluripotent stem cell lines

hPSC line	Acronym
SFC-180-01-01	hPSC 180
SFC-840-03-03	hPSC 840
SFC-841-03-01	hPSC 841
SFC-854-03-02	hPSC 854
SFC-856-03-04	hPSC 856

6-well TC plates were coated by incubating with 5 % matrigel (v/v, Sigma) in KnockOut DMEM (Gibco) at 37°C for 1 h. hPSCs were thawed into 5 mL PBS and centrifuged at 400 *x g* (2 113 rpm) and 15°C for 5 min. The hPSC pellets were re-suspended in 2 mL of TeSR-E8-ROCKi medium (TeSR-E8 medium (StemCell Technologies) supplemented with 5 µM of Y-27632 ROCK inhibitor (AbCam Biochemicals)), plated into a well of the matrigel-coated TC plate and maintained at 37°C and 5 % CO_2 until confluent. hPSC cultures were split by aspirating medium off of confluent wells, washing successively with 1 mL PBS and 1mL of 0.5 mM EDTA v/v in PBS, and then incubating with 1 mL of 0.5 mM EDTA-PBS for 5 min at 37°C. The lifted hPSCs were gently washed off the surface of the TC plate with TeSR-E8 medium, and split 3-fold by plating into matrigel-coated wells of a 6-well TC plate.

AggreWell 800 plates (StemCell Technologies) were prepared by adding 500 µL of anti-adherence rinsing solution (StemCell Technologies) to the wells to be seeded with hPSCs and centrifuging at 3000 *x g* (5 876 rpm) to remove air bubbles. Wells were washed twice with 1 mL PBS and 1 mL of TeSR-E8-ROCKi medium was added per well of the AggreWell plate. Medium was aspirated from confluent hPSC cultures and the cells were washed with 1 mL PBS, then incubated with 1 mL of pre-warmed TrypLE for 5 min at 37°C. The lifted cells were gently washed off the surface of the TC plate with 1 mL PBS and the cell suspension was diluted 1:9 with PBS. The cells were centrifuged at 15°C and 400 *x g* (2 113 rpm) for 5 min, and the cell pellet was re-suspended in TeSR-E8-ROCKi medium. Approximately 4 x 10^6 cells were added to the prepared wells of the AggreWell 800 plate and evenly distributed among the wells by centrifuging the plate at 4°C and 100 *x g* (1 056 rpm) for 3 min.

For embryoid body development, 1 mL of the AggreWell culture medium was replaced with pre-warmed embryoid body (EB) medium (mTeSR (StemCell Technologies) supplemented with 50 ng/mL BMP4 (Invitrogen), 50 ng/mL VEGF (Peprotech) and 20 ng/mL SCF (Miltenyi). Two successive 1 mL medium changes were carried out for a 75 % medium change overall. The 75 % medium change was repeated daily for 3 days after which the EBs were transferred to wells of a low-binding 6-well TC plate using a 5 mL serological pipette. Daily 75 % medium changes were continued for a total of 7 days culture in EB medium. The EB culture was collected using a 5 mL pipette, filtered using a 40 µm cell strainer and the captured EBs were flushed into a 50 mL centrifuge tube using factory medium (X-Vivo$_{15}$ supplemented with 1 % Glutamax (Gibco), 1 % P/S (Gibco), 0.1 % beta-mercaptoethanol (Gibco), 100 ng/mL M-CSF (Invitrogen) and 25 ng/mL IL-3 (Invitrogen)). EBs were transferred to a 175 cm^2 TC flask and maintained in factory medium without disturbing for 7 days at 37°C and 5 % CO_2. Afterwards, 10 mL of pre-warmed factory medium was added to the hPSC factories on a weekly basis.

2.5 Differentiation of hPSC pre-cursors to hPSC-derived macrophages (hPSC-DMs)

Supernatant from the hPSC factories was collected using a 25 mL pipette and gently passed through a 40 µm cell strainer to remove cell debris and inadvertently captured EBs. hPSC precursor cells in the filtrate were pelleted by centrifuging at 400 *x g* (2113 rpm) and 4°C for 5 min. Cells were re-suspended in the appropriate differentiation medium and plated at a density of 2.5 x 10^5 cells per well of a 24-well plate. hPSC macrophage precursor cells were differentiated to hPSC-DMs by 7 days culture in X-vivo$_{15}$ supplemented with 1 %

GlutaMax 1 % P/S and 100 ng/mL M-CSF with a 50 % medium change at day 3. Alternatively, hPSC macrophage precursor cells were differentiated by culture in X-vivo$_{15}$ supplemented with 1 % heat inactivated human AB serum for 3 days. The culture medium was then changed to cX-vivo$_{15}$ and the cells were incubated for a further 4 days.

2.6 Optimisation of hPSC-derived macrophage transduction using HIV-1 NL4.3-eGFP pseudotyped virus

For optimisation of the hPSC-DM transduction protocol, approximately 2.5 x 10^5 hPSC-DMs were treated with 10 ng/well of VSV-G Env/SIV-Vpx VLPs, inoculated with HIV-1$_{BaL}$ pseudotyped vectors at 0-0.5 MOI, and incubated at 37°C and 5 % CO_2 for 3 h followed by a medium change to 2 mL of pre-warmed cX-vivo$_{15}$. To determine transduction efficiency, the hPSC-DMs were lifted by gentle scraping after a 5 minute incubation with 0.25 % trypsin-EDTA at 37°C and pelleted by centrifuging at 358 *x g* (2000 rpm) and 4°C for 2 min. MDMs were fixed with 4 % formaldehyde v/v in PBS and the proportion of cells successfully transduced was determined by measuring eGFP expression by flow cytometry using FACSCalibur. Data were analysed using FlowJo Software and GraphPad Prism.

2.7 Analysis of cell surface marker expression

Cells were pre-incubated with 10 µg/mL human IgG at room temperature for 10 min for Fc receptor blocking. Cells were then stained as required with the antibodies outlined in Table 5 and made up to a total volume of 100 µL with FACS buffer. Antibody staining was carried out at 4°C in the dark for 1 h, except for αCCR2-FITC and REA(S)-FITC isotype staining which were carried out in the dark and at RT for 10 min as per manufacturer's instructions.

Stained cells were washed twice by centrifuging at 358 *x g* (2000 rpm) for 3 min and re-suspended in 200 µL of FACS buffer (1 % BSA v/v (Sigma) and 0.01 % sodium azide w/v (Sigma) in phosphate buffered saline (PBS, Sigma). Finally, the monocytes were re-suspended in 100 µL FACS buffer and data were acquired using the BD FACSCalibur (BD Biosciences, USA). Data were analyzed using FlowJo version 10.2 (Tree Star Inc, USA) and GraphPad Prism version 7 (GraphPad Software, USA).

Table 5: Antibodies used for flow cytometry analysis of cell surface marker expression.

Antibody	Dilution	Isotype	Dilution
αCD4-APC (BD Biosciences)	1:50	Mouse IgG1-APC (Biolegend)	1:50
αCD11b-APC (Biolegend)	1:20	Mouse IgG1-APC (Biolegend)	1:50
αCD14-PE (eBiosciences)	1:20	Mouse IgG_{2A}-PE (BD Biosciences)	1:50
αCD163-PE (eBiosciences)	1:20	Mouse IgG1-PE (Miltenyi)	1:50
αCCR2-FITC (Miltenyi)	1:10	REA(S)-FITC (Miltenyi)	1:10
αCCR5-PE (Biolegend)	1:50	Rat IgG_{2A}-PE (Biolegend)	1:50
αC5aR-PE (Biolegend)	1:100	Mouse IgG_{2A}-PE (Biolegend)	1:50
αFPR1-PE (R&D Biosystems)	1:100	Mouse IgG_{2A}-PE (Biolegend)	1:50

2.8 LPS activation of blood monocyte derived macrophages (MDMs)

MDMs were incubated in cX-$vivo_{15}$ supplemented with *Salmonella minnesota* R595 ultrapure lipopolysaccharide (LPS, Invivogen) at 1 µg/mL for 18 h. After incubation, the macrophage supernatants were harvested and centrifuged at 4500 *x g* (7087 rpm) and 4°C for 10 min to clear cell debris. Cleared supernatants were stored at -80°C until further use.

2.9 Propagation of lentiviral vector and envelope expression plasmids in competent *E. coli*

Expression plasmids for HIV-1 NL4.3-eGFP-ΔVpr, HIV-1 NL4.3-eGFP-Vpr^+ and SIV-Vpx were used to transform the competent *E. coli* strain Stbl3 (Invitrogen) which is derived from *E. coli* HB101 and has the following genotype: F^-*mcr*B *mrr hsd*S20 *(r*B^-*, m*B^-*) rec*A13 *sup*E44 *ara*14 *gal*K2 *lac*Y1 *pro*A2 *rps*L20 *(*Str^R*) xyl5* λ^-*leu mtl1*. Expression plasmids for pcDNA, HIV-1

Vpr, VSV-G *env* or HIV-1 BaL *env* were used to transform the *E. coli* strain DH5α (Invitrogen) which has the following genotype: *F*⁻ *ϕ*80d*lac*ZΔM15 *Δ(lac*ZYA-*arg*F*) U*169 *end*A1 *rec*A1 *hsd*R17 *(r_K^- m_K^+) deo*R *thi*1 *pho*A *sup*E44 *λ*⁻*gyr*A96 *rel*A1.

Competent cells were transformed by adding 1 µL of plasmid DNA to 50 µL of freshly thawed competent cells, incubating on ice for 30 min and heat shocking at 42°C for 45 seconds, followed by 5 min incubation on ice. 700 µL of Luria-Bertani (LB) broth was added to the transformed cells and the cell suspension was incubated at 37°C and 5 % CO_2 with continuous shaking at 3 *x g* (180 rpm) for 45 min. For transformations with the HIV-1 NL4.3-eGFP, SIV-Vpx, VSV-G *env* and HIV-1_{BaL} *env* expression plasmids, 300 µL of the culture was spread onto LB agar plates supplemented with 100 µg/mL ampicillin (Amp). For transformations with the HIV-1 Vpr expression plasmid, 300 µL of the culture was spread onto LB agar plates supplemented with 50 µg/mL kanamycin (Kan). The plates were cultured overnight at 37°C and 5 %, and a single Amp^R or Kan^R colony was selected and used to inoculate 2 mL LB broth supplemented with either 100 µg/mL Amp or 50 µg/mL Kan as required. The starter culture was expanded by incubating for 2 h at 37°C and 5 % with continuous shaking at 3 *x g* (180 rpm). For long-term storage, starter cultures were frozen at -80°C in the presence of 50 % (v/v) glycerol.

2.10 Maxi-prep purification of plasmid DNA

250 mL of LB broth supplemented with 100 ng/mL Amp was inoculated with starter culture (0.1 % v/v) and incubated overnight at 37°C and 5 % CO_2 with continuous shaking at 3 *x g* (180 rpm). The cells were harvested by centrifugation at 4600 *x g* (7165 rpm) for 15 min

and subsequent plasmid DNA preparations were performed using the PureLink HiPure Plasmid Maxi-Prep kit (Invitrogen). The pelleted cells were first re-suspended in 10 mL of Resuspension Buffer supplemented with RNAse A (0.56 % v/v). 10 mL of Lysis Buffer was added to the cell suspension and incubated at RT for 5 min, followed by 10 mL of Precipitation Buffer and the lysate was mixed by inversion to obtain a homogenous mixture. The precipitate was pelleted by centrifuging at 4600 *x g* (7165 rpm) for 20 min at RT. The HiPure Maxi Column was prepared by washing with 30 mL Equilibration Buffer, and the cleared supernatant was applied to the column and allowed to drain through by gravity flow, after which the column-bound plasmid DNA was washed with 60 mL Wash Buffer. The plasmid DNA was eluted with 15 mL Elution Buffer, and precipitated by mixing with 10.5 mL of 100 % isopropanol (Sigma) followed by centrifuging at 4600 *x g* (7165 rpm) for 1 h at 4°C. The DNA pellet was washed by re-suspending in 5 mL 70 % ethanol and centrifuging at 4600 *x g* (7165 rpm) for 10 min at 4°C. The purified DNA pellet was air dried and then re-suspended in 500 µL of Tris-EDTA (TE) Buffer. The concentration of purified plasmid DNA was quantified using a NanoDrop 2000c spectrophotometer (Thermo Fisher).

2.11 Transient co-transfection of HEK 293Ts for HIV-1 NL4-3-eGFP vector production

$5x10^6$ HEK293T cells were seeded into 100 mm tissue-culture (TC) dishes (Corning) in 5 mL cDMEM and incubated overnight at 37°C and 5 % CO_2 to achieve 70-80 % confluency. Cells were co-transfected with 20 µg of either NL4.3eGFP-ΔEnv-ΔVpr or NL4.3-eGFP-ΔEnv-Vpr^+ expression plasmid and 5 µg of a BaL *env* expression plasmid in 5 mL DMEM supplemented with 0.2 µM polyethylenimine (PEI, Sigma). Delta-Env virus-like particles were produced by

co-transfecting the HEK 293Ts with 20 µg of either NL4.3eGFP-ΔEnv-ΔVpr or NL4.3-eGFP-ΔEnv-Vpr$^+$ expression plasmid and 5 µg of pcDNA plasmid in 5 mL DMEM supplemented with 0.2 µM PEI. For co-transfections, the PEI/DMEM mixture was added dropwise to DMEM supplemented with plasmid DNA while vortexing to ensure proper mixing. After a 20 min incubation at RT to allow for DNA-PEI complexing, 5 mL of transfection mix was added to the HEK 293Ts and the cells were incubated for 4 h at 37°C and 5 % CO_2, after which the mix was replaced with 5 ml cDMEM and the HEK 293Ts were incubated for 48 h.

2.12 Transient co-transfection of HEK 293Ts for VSV-G/SIV-Vpx virus-like particle production

5x10^6 HEK293T cells were seeded into 100 mm TC dishes (Corning) in 5 mL cDMEM and incubated overnight at 37°C and 5 % CO_2 in order to achieve a confluency of 70-80 %. Cells were co-transfected with 20 µg of Δ*env*/pSIV3$^+$ plasmid and 5 µg of VSV-G *env* expression plasmid in 5 mL DMEM supplemented with 0.2 µM polyethylenimine (PEI, Sigma). The PEI/DMEM mixture was added dropwise to DMEM supplemented with Δ*env*/pSIV3$^+$ and VSV-G *env* plasmid DNA while vortexing to ensure proper mixing. After a 20 min incubation at RT to allow for DNA-PEI complexing, 5 mL of transfection mix was added to the HEK 293Ts and the cells were incubated for 4 h at 37°C and 5 % CO_2, after which the mix was replaced with 5 ml cDMEM and the HEK 293Ts were incubated for 48 h.

2.13 Concentration of HIV-1 NL4-3-eGFP vectors and VSV-G/SIV-Vpx virus-like particles

Transfected HEK 293T culture supernatants were harvested 48 h post-transfection and filtered with a 0.45 µm syringe filter (VWR). The filtrate was concentrated with a PEG-6000 based concentrating reagent (50 % polyethylene glycol 6000 (Sigma) w/v in H_2O, 4 M NaCl (Sigma) w/v in H_2O, and PBS) at a ratio of 2 volumes filtrate : 1 volume concentrating reagent at 4°C for 1.5 h with mixing by inversion at 30 min intervals. Pseudotyped virus was pelleted by centrifuging the mixture at 4500 *x g* (7087 rpm) for 45 min at 4°C, re-suspended in a total of 2 mL cDMEM and stored at -80°C.

2.14 Quantification of BaL Env and VSV-G Env pseudotyped HIV-1 NL4-3-eGFP vector titres

HIV-1_{BaL} *env* or VSV-G *env* pseudotyped vector stock was thawed on ice, diluted 1:3 in cDMEM, and serially diluted 11 x 3-fold in quadruplicate wells of a 96 well flat-bottomed TC plate. TZM-bl reporter cells suspended in cDMEM were plated at a density of 1 x 10^4 cells per well of diluted vector stock. Control wells were prepared by plating 1 x 10^4 cells per well in the absence of vector. The inoculated TZM-bl cells were incubated at 37°C and 5.0 % CO_2. After 48 h, the TZM-bl cells were washed with 100 µL PBS (Sigma) and treated with 100 µL of 1X Reporter Lysis Buffer (Promega) with a freeze-thaw cycle at -80°C to ensure complete cell lysis. 50 µL of Bright-Glo reagent (Promega) was added 1:1 to TZM-bl lysate and incubated for 2 min at RT. Luminescence was then measured with 1000 ms integration time using the SpectraMaxM5 plate reader (Molecular Devices, CA, USA). Analyses of luminescence readings were carried out using Microsoft Excel (version 15.32) and

infectious dose 50% (ID_{50}) was calculated using the National Institutes of Health ID-50 program [189].

2.15 Quantification of VSV-G Env pseudotyped SIV-Vpx virus like particles by SIV p27 ELISA

VSV-G Env pseudotyped SIV-Vpx virus like particles (VSV-G Env/SIV-Vpx VLPs) were quantified using the RETROtek SIV p27 antigen ELISA (ZeptoMetrix) according to manufacturer's instructions except that the SIV p27 antibody coated microplates were incubated with standards and VSV-G Env/SIV-Vpx VLP samples for 2 h at 37°C. Absorbance was measured at 450 nm using the SpectraMaxM5 plate reader (Molecular Devices, CA, USA) and analysis of absorbance readings was carried out using Microsoft Excel and GraphPad Prism (version 7).

2.16 Quantification of HIV-1 NL4-3-eGFP vectors by HIV-1 p24 ELISA

HIV-1 NL4-3-eGFP vectors were inactivated by incubating with 5% empigen detergent (Sigma) at 56°C for 1 h. ELISA plates (Greiner) were coated overnight at RT with 100 µg/mL anti-HIV-1-p24 capture antibody (Aalto Bio Reagents). Plates were washed and blocked with 200 µL blocking buffer (BB) per well (2 % BSA (Sigma) v/v in TBS, pH 7.5) for 30 min at RT. All wash steps were carried out three times using 200 µL wash buffer (WB) per well (0.05 % Tween (ThermoFisher) v/v in Tris Buffered Saline (Sigma), pH 7.5) unless otherwise specified. Serial dilutions of samples and standards were prepared in TBS/E/S buffer (10 % FCS v/v and 0.5 % empigen (Sigma) v/v in TBS). The blocked plates were washed and incubated with 100 µL of either inactivated vector or recombinant HIV-1 p24 standards

(Aalto Bio Reagents) for 2 h at 37°C with gentle agitation. After incubation with samples and standards, the plates were washed 6 times with WBand incubated with biotinylated anti-HIV-1-p24 antibody (Aalto Bio Reagents) diluted 1/1000 in TMT/SS buffer (2 % BSA v/v and 20 % FCS v/v in TBS). Plates were washed 6 times with WB and incubated with 100 µL of 0.1 µg/mL streptavidin-horseradish peroxidase (HRP) conjugate (Bio-Rad) for 1 h at RT. Plates were developed with TMB-ELISA substrate (Thermo Scientific) 10 min in the dark, after which the developing reaction was stopped with 0.5 M sulphuric acid (Sigma). Absorbance was measured at 450 nm and 570 nm using the SpectraMaxM5 plate reader (Molecular Devices, CA, USA) and absorbance readings were processed using Microsoft Excel (version 15.32) and GraphPad Prism (version 7).

2.17 Transduction of MDMs with single-cycle HIV-1-NL4.3-eGFP vectors

For optimisation of the MDM transduction protocol, either HIV-1_{BaL} pseudotyped vectors at 0-0.25 MOI or VSV-G pseudotyped vectors at 0-0.025 MOI were added to 1 x 10^6 MDMs in a 24-well plate. cX-$Vivo_{15}$ was supplemented with 0-50 ng/well of VSV-G Env/SIV-Vpx VLPs and 5.0 µg/mL of polybrene (Sigma) where appropriate. MDMs were inoculated by centrifuging (i.e. 'spinoculated') at 1200 *x g* (3660 rpm) and 37°C for 30 min followed by incubation at 37°C and 5 % CO_2 for 2.5 h. Alternatively, MDMs were incubated with pseudotyped virus at 37°C and 5 % CO_2 for 3 h to inoculate without centrifuging.

For transduction experiments, 1x10^6 MDMs were cultured in a 24-well plate and inoculated with pseudotyped virus in the presence of 10 ng of VSV-G Env/SIV-Vpx VLPs in cX-$vivo_{15}$.

After 3 h incubation at 37°C and 5 % CO_2, the transduction medium was replaced with 2 mL pre-warmed cX-Vivo$_{15}$. MDM supernatants were harvested at 24, 72 and 96 h post-transduction, centrifuged at 4500 *x g* (7087 rpm) and 4°C for 10 min to clear cell debris and cleared supernatants were stored at -80°C until further use. To determine transduction efficiency, the MDMs were lifted by gentle scraping after a 5 min incubation with 0.25 % trypsin-EDTA at 37°C and pelleted by centrifuging at 358 *x g* (2000 rpm) and 4°C for 2 min. MDMs were fixed with 4 % formaldehyde v/v in PBS and the proportion of cells successfully transduced was determined by measuring eGFP expression by flow cytometry using FACSCalibur. Data were analysed using FlowJo Software and GraphPad Prism (version 7).

2.18 Proteome profiler analysis of soluble factors produced by HIV-1 NL4-3-eGFP transduced MDMs

Soluble factors expressed by HIV-1 NL4-3-eGFP transduced MDMs were measured using the 102-plex Human XL Cytokine Array Kit (R&D Systems, Biotechne). Each array membrane was blocked by incubating with 2 mL of the supplied array buffer-6 for 1 h on a rocking platform shaker at 4°C. Cleared MDM supernatants were thawed on ice and diluted 1:2 in array buffer-6. The blocked array membranes were then incubated with 1.5 mL of diluted supernatant for 18 h at 4°C on a rocking platform shaker. Afterwards, each membrane was washed 3 times in 25 mL of the supplied washing buffer for 10 min on a rocking platform shaker at 4°C. Washed membranes were incubated in the supplied biotinylated detection antibody cocktail diluted 1:50, for 1 h at 4°C with rocking. Membranes were developed by incubating with 2 mL of the streptavidin conjugated infrared dye IRDye 800CW-Streptavidin

(LICOR) diluted 1:2000 in array buffer-6 for 30 min at RT on a rocking platform shaker. Membranes were washed as previously described and imaged using the Odyssey Imager (LICOR). Pixel density intensities were determined using the LICOR Image Studio Lite software (version 5.2.5). Fold-change analyses were carried using Microsoft Excel and heat maps were generated using GraphPad Prism. Wilcoxon's matched-pairs signed-rank tests were computed using the ConsensusPathDB tool [190] to determine enriched gene sets and pathways based on the proteome profiler dataset.

2.19 Multiplex analysis of cytokine and chemokine expression by MDMs

Concentrations of IL-6, IL-10, IL-12 p70, TNF- α, IFN-γ, IFN-α, IL-1β, I-TAC (CXCL11), MCP-3 (CCL7), MIF, MIG (CXCL9), MIP-1α (CCL3) and MIP-1β (CCL4) expressed by MDMs were measured using custom ProcartaPlex multiplex immunoassays (ThermoFisher). A 4-fold serial dilution of the supplied antigen standard was prepared in cX-vivo$_{15}$ and cleared MDM supernatants were thawed on ice and diluted 1:1 in the manufacturer's dilution buffer. The supplied antibody-coupled magnetic beads were diluted with WB and 100 µL of beads were added to each well of a flat bottomed 96-well plate and washed. All wash steps were carried out using 150 µL of manufacturer's WB. The washed beads were incubated in duplicate with diluted supernatants, antigen standards or cX-vivo$_{15}$ only (for blank wells) for 2 h at RT with shaking at 22 *x g* (500 rpm). The plate was then incubated overnight at 4°C with shaking, after which the plate was shaken for an additional 30 min at RT and washed twice. The beads were then incubated with 25 µL of the kit-supplied biotinylated detection antibody for 30 min at RT with shaking. The assay plate was washed twice and

developed by incubating samples with 50 µL of the supplied streptavidin-conjugated phycoerythrin (SAPE) solution for 5 min at RT with shaking. The concentration of target analytes in each sample was interpolated from the standard curves of PE median fluorescence intensity that were generated using the supplied antigen standards. All data acquisition and analyses were carried out using the Bio-Plex 200 system and BioRad software.

2.20 Analysis of MDMs expression of CXCL10/IP-10 by ELISA

Concentrations of CXCL10/IP-10 expressed by HIV-1 NL4-3-eGFP transduced MDMs were measured using the human CXCL10/IP-10 DuoSet ELISA (R&D Systems). ELISA plates were coated by incubating overnight at RT with 100 µL per well of the supplied capture antibody. The plate was washed before blocking with reagent diluent (1 % BSA w/v in PBS) at RT for 1 h. For all wash steps, 200 µL of wash buffer (0.05 % Tween-20 v/v in PBS) was added to each well of the ELISA plate and then aspirated using an automatic plate washer. Serial dilutions of cleared MDM supernatants and the recombinant CXCL10/IP-10 standard were prepared using reagent diluent. 100 µL of diluted supernatants, standards or cX-vivo$_{15}$ (for blank wells) were added to plates in duplicate and was incubated for 2 h at RT, after which the plate was washed 3 times. The supplied biotinylated detection antibody was diluted using reagent diluent and the plates were incubated with 100 µL detection antibody for 2 h at RT. The plates were washed and developed for 20 min at RT with 100 µL of streptavidin-HRP. The developing reaction was stopped with 50 µL of 2 M H_2SO_4. Absorbance was measured at 450 nm and 570 nm using the SpectraMaxM5 plate reader

and analyses of absorbance readings were carried out using Microsoft Excel and GraphPad Prism.

2.21 Optimising $CD14^+$ monocyte density for the xCELLigence migration assay

Suspensions of $CD14^+$ monocytes ranging from 1.0 x 10^5 – 8.0 x 10^5 cells/mL were prepared in X-$Vivo_{15}$ media (Lonza) and pre-warmed to 37°C. 160 µl of vehicle (X-$Vivo_{15}$) and 5 nM CCL2/MCP-1 were loaded into wells of the bottom chamber of the CIM-16 plate. The CIM-16 plate was assembled and 50 µl of X-$Vivo_{15}$ media was added to each of the wells of the top chamber. The plate was then incubated at 37°C for 30 min to allow for equilibration of the medium temperature between the top and bottom chambers. Afterwards, the CIM-16 plate was docked into the xCELLigence RTCA-DP system (ACEA Biosciences, USA) and background cell index readings for each well were collected over a 15 s time period. 50 µL of each monocyte suspension were then added to wells of the top chamber. Immediately after addition of the monocytes to the top chamber, the CIM-16 plate was docked into the xCELLigence system and rested at 37°C for 5 min to allow for settling of the monocytes. After this period, cell index was measured at 15 s intervals over a total time-frame of 3 h.

2.22 Optimising chemokine concentration for the xCELLigence migration assay with CD14+ monocytes

Recombinant human CCL2/MCP-1 (R&D Systems) and human CCL5/RANTES (R&D Systems) were serially diluted from 1.25 – 10 nM in X-$Vivo_{15}$ media and pre-warmed to 37°C. Recombinant human fMLP (Sigma) and human C5a (R&D Systems) were serially diluted

from 0.625 – 40 nM in X-Vivo$_{15}$ media pre-warmed to 37°C. 160 µL of vehicle medium and each concentration of CCL2/MCP-1, CCL5/RANTES, fMLP and C5a were loaded into wells of the bottom chamber of the CIM-16 plate. The CIM-16 plate was assembled and 50 µL of X-Vivo$_{15}$ medium was added to each of the wells of the top chamber. The plate was then incubated at 37°C for 30 min to allow for equilibration of the media temperature between the top and bottom chambers. Afterwards, the CIM-16 plate was docked into the xCELLigence system and background cell index readings for each well were collected over a 15 s interval. 4 x 10^5 monocytes were then added to each well of the top chamber. Immediately after addition of the monocytes to the top chamber, the CIM-16 plate was docked into the xCELLigence system and rested at 37°C for 5 min to allow for settling of the monocytes. After this period, cell index was measured at 15 s intervals for a total time-frame of 3 h.

2.23 Optimising THP-1 monocytic cell line density for the xCELLigence migration assay

Suspensions of THP-1 cells ranging from 1.0 x 10^5 – 8.0 x 10^5 cells/mL were prepared in X-Vivo$_{15}$ media pre-warmed to 37°C. 160 µL of vehicle (X-Vivo$_{15}$) and 5 nM CCL2/MCP-1 were loaded into wells of the bottom chamber of the CIM-16 plate. The CIM-16 plate was assembled and allowed to equilibrate as previously described. After background cell index reading was measured, 50 µL of each THP-1 cell suspension were added to wells of the top chamber. Immediately after addition of the THP-1 cells to the top chamber, the CIM-16 plate was docked into the xCELLigence system and rested at 37°C for 5 min to allow for settling of the cells. After this period, cell index was measured at 15 s intervals over a total time-frame of 3 h.

2.24 Optimising chemokine concentration for the xCELLigence migration assay with THP-1 monocytic cell line

The chemoattractants CCL2/MCP-1 and CCL5/RANTES were serially diluted from 1.25 – 10 nM in X-Vivo$_{15}$ medium pre-warmed to 37°C. 160 µL of either vehicle (X-Vivo$_{15}$) or each concentration of the chemokines were loaded into wells of the bottom chamber of the CIM-16 plate. The CIM-16 plate was then assembled and 50 µL of X-Vivo$_{15}$ medium was added to each of the wells of the top chamber. The CIM-16 plate was assembled and allowed to equilibrate as previously described. After collecting the background cell index measurement, 4 x 10^5 THP-1 cells were added to each well of the top chamber. Immediately after addition of the monocytes to the top chamber, the CIM-16 plate was docked into the xCELLigence system and rested at 37°C for 5 min to allow for settling of the

monocytes. After this period, cell index was measured at 15 s intervals for a total time-frame of 3 h.

2.25 Validation of the xCELLigence migration assay using 'checkerboard' analysis

The CIM-16 plate was assembled as previously described and 5 nM CCL2/MCP-1 was added to either the top chamber, the bottom chamber or to both as outlined in Table 6. 5 nM CCL2/MCP-1 was added to only the bottom chamber to establish a positive chemokine concentration gradient across the CIM-16 membrane. To establish an equimolar (zero gradient) chemokine concentration, either 5 nM CCL2/MCP-1 or X-Vivo$_{15}$ media was added to both the bottom and top chambers. To establish a negative chemokine concentration gradient, cells were re-suspended in 5 nM CCL2/MCP-1 prior to being added to wells of the top chamber of the CIM-16 plate. Cell index readings were collected at 15 s intervals for a total time-frame of 3 h.

Table 6: CIM-16 plate set-up for checkerboard analysis of monocyte migration.

	Zero gradient	Zero gradient	Positive gradient	Negative gradient
Top chamber	-	+	-	+
Bottom chamber	-	+	+	-

'+' indicates the addition of CCL2/ MCP-1 to the wells and '-' indicates the addition of X-Vivo$_{15}$ only to the wells

2.26 ELISA analysis of chemokine diffusion across the xCELLigence CIM-16 membrane

160 µL of either 5 nM CCL2/MCP-1 or 5 nM CCL5/RANTES were added to wells of the bottom chamber. The CIM-16 plate was assembled as previously described and 100 µL of X-Vivo$_{15}$ medium only was added to wells of the top chamber. The plate was incubated at 37°C and 5 % CO_2 and the media in the top wells was harvested at 0, 5, 15, 30, 45, 60, 90 and 120 min time-points. Each media harvest was analysed using the Human MCP-1/CCL2 ELISA Max assay (Biolegend) or Human CCL5/RANTES ELISA Max assay (Biolegend) to determine the change in concentration of the respective chemokine in the top wells of the CIM-16 plate with time. The ELISA assays were carried out according to manufacturer's instructions and absorbance was measured at 450 nm and 570 nm using the SpectraMaxM5 plate reader. Analyses of absorbance readings were carried out using Microsoft Excel and GraphPad Prism.

2.27 CellTiter96 analysis of the effect of actin polymerisation inhibitors on CD14+ monocyte viability

1 x 10^6 freshly isolated monocytes were seeded into wells of a 96-well plate. The monocytes were pelleted by centrifuging at 229 *x g* (1600 rpm) for 5 min and were re-suspended in either 100 µL of X-Vivo$_{10}$ only or 100 µL of X-Vivo$_{10}$ supplemented with cytochalsinD (1 - 25 µg/mL), latrunculin (0.2 – 5 µg/mL), jasplakinolide (0.04 – 1 µg/mL) or pertussis toxin (0.01 – 1 µg/mL). Monocytes were incubated in the presence of the compounds for 2 h at 37°C and 5 % CO_2. After incubation, 20 µL of CellTiter96 reagent was added to each well, and the plate was incubated for a further 1 h. Absorbance was measured at 490 nm using the SpectraMaxM5 plate reader (Molecular Devices, CA, USA)

and analyses of absorbance readings were carried out using Microsoft Excel (version 15.32) and GraphPad Prism.

2.28 Validation of the xCELLigence migration assay using inhibitors of actin polymerisation

CytochalsinD (1 - 25 µg/mL), latrunculin (0.2 – 5 µg/mL), jasplakinolide (0.04 – 1 µg/mL) and pertussis toxin (0.01 – 1 µg/mL) were prepared in X-Vivo$_{15}$ media. The CIM-16 plate was assembled as previously described with either 160 µL of X-Vivo$_{15}$ media or 5 nM CCL2/MCP-1 loaded into the bottom wells. Freshly isolated monocytes were re-suspended to 8 x 10^6 cells/mL of each concentration of inhibitor. After measuring the background cell index signal, 50 µL of the cell suspensions (~4 x 10^5 monocytes) were added to each well of the upper chamber and cell index readings were collected at 15 s intervals for a total time-course of 3 h.

2.29 Scanning electron microscopy of CIM-16 membrane

The CIM-16 plate was assembled as previously described with either 160 µL of X-Vivo$_{15}$ media or 5 nM CCL2/MCP-1 loaded into the bottom wells of the CIM-16 plate. After measuring the background cell index signal, 4 x 10^5 monocytes were added to each well of the upper chamber and allowed to migrate towards 5 nM of CCL2/MCP-1 for 2 h. Immediately upon completion of the assay, the microporous membrane of the CIM-16 plate was fixed by replacing the media in the top and bottom chambers with 2.5 % glutaraldehyde (Sigma) v/v in PBS. The plate was incubated overnight at 4°C. Further

sample preparation and imaging was carried out by Dr. Errin Johnson at the Sir William Dunn School Bio-Imaging Facility.

2.30 Expression of HIV-1 recombinant Env

Soluble HIV-1 Env gp120 wild-type (WT), gp120 CD4bs mutant and gp140 trimer, all derived from the BG505 clone, were expressed by transient transfection of 293F cells [191]. The CD4bs Env variant bears a D368R mutation in the CD4 binding loop of gp120 that ablates binding between the envelope glycoprotein and CD4 [192]. The 293F transfection reagent was prepared by mixing 125 µg of the appropriate *env* expression plasmid in 10 mL OptiMem media (Gibco) and 375 µg PEI Max (Sigma) in 10 mL OptiMem media, for a total volume of 20 mL. To produce the recombinant HIV-1 Env glycoproteins, 20 mL of the 293F transfection reagent was added to $1x10^6$ 293F cells per mL in 400 mL Freestyle 293 Expression medium (Gibco), and the cells were maintained at 37°C and 5 % CO_2 with continuous shaking for 5 days. The culture supernatant was harvested 5 days post-transfection and centrifuged at 202 *x g* (1500 rpm) for 10 min at 20°C to remove cell debris.

2.31 Concentration and purification of HIV-1 recombinant Env

Cleared 293F supernatants were vacuum filtered, and HIV-1 Env proteins were purified overnight at 4°C using a 2G12-sepharose column. Column-bound proteins were eluted using 3 M $MgCl_2$ and stored at 4°C until further use. The eluates were purified by dialysis against 1X endotoxin-free PBS for 2 h at 4°C using SnakeSkin dialysis tubing (ThermoFisher Scientific). After this initial round of dialysis, the 1X endotoxin-free PBS was replaced and a

second round of dialysis was carried out overnight at 4°C. The dialysed protein preparations were concentrated by centrifuging at 4000 *x g* for 5 min at RT in 30 KDa Amicon Ultra-15 Centrifugal Filter Units (Merck Millipore). The concentrated proteins were then filter sterilised using 0.45 µm syringe filters (VWR) under aseptic conditions. The filter sterilised proteins were transferred to 35 kDa Slide-A-Lyzer dialysis casettes (ThermoFischer Scientific) and subjected to a final round of dialysis against 1X endotoxin-free PBS under aseptic conditions for 2 h. The purified proteins were stored at 4°C until further use.

2.32 Analysis of HIV-1 recombinant Env endotoxin content

The HEK293-Dual-mTLR4 (NF/IL8) reporter cell line (Invivogen) was used to assess the endotoxin content of purified HIV-1 recombinant Env preparations. HEK293-Dual-mTLR4 (NF/IL8) reporter cells were dissociated by incubating with 1X PBS at 4°C for 5 min. The dissociated cells were added to a flat-bottom 96-well plate at a density of 5 x 10^4 cells per well and then pelleted by centrifuging at 229 *x g* (1600 rpm) for 5 min. The cells were then re-suspended in 200 µL of the sample to be analysed (in cDMEM supplemented with 100 µg/mL normocin, Invivogen) and incubated overnight at 37°C and 5% CO_2. After incubation, the supernatants were cleared of cell debris by centrifuging at 229 *x g* (1600 rpm) for 5 min. The level of IL-8 production induced by each sample was quantified using the IL-8 Human Uncoated ELISA Kit (Invitrogen) according to manufacturer's instructions. Absorbance was measured at 490 nm and 570 nm using the SpectraMaxM5 plate reader

(Molecular Devices, CA, USA) and analyses of absorbance readings were carried out using Microsoft Excel (version 15.32) and GraphPad Prism (version 7).

2.33 SDS-PAGE of recombinant envelope proteins

5 µg each of the recombinant gp120 wild-type, gp120 CD4bs mutant and gp140 trimer proteins were heat-denatured at 95°C for 5 min. Samples were separated on a reducing and denaturing NuPAGE Bis-Tris gel (Invitrogen) by electrophoresis for 1.5 h at 150 V. The gel was developed using Simply Blue Safe Stain (Invitrogen) according to the manufacturer's instructions and analysed using Adobe Photoshop software (version 11.0.2).

2.34 Measurement of recombinant HIV-1 Env binding to soluble CD4 (sCD4)

96-well ELISA plates (Cellstar) were coated overnight at 4°C in 0.5 µg/mL of either recombinant gp120 WT, gp120 CD4bs mutant, gp140 trimer or PBS (negative control). After coating, plates were blocked with 2 % BSA (Sigma) / Tween-20 (ThermoFisher) for 1 h at RT. The coated wells were incubated with biotinylated versions of anti-gp120 mAb (2G12) at 2 ng/mL - 2 µg/mL, a mAb to the gp120 CD4 binding site (VRCO1) at 1 ng/mL - 1 µg/mL or soluble biotinylated CD4 at 1 ng/mL - 2 µg/mL for 2 h at RT. The plates were further incubated with a streptavidin-horseradish peroxidase (HRP) conjugate (Thermo Scientific) at 1:4000 dilution for 1 h at RT. The ELISA plates were developed by adding 50 µL of TMB-ELISA substrate (Thermo Scientific) to each well and incubating for 10 min in the dark. The developing reaction was stopped with 50 µL of 2 M H_2SO_4, and absorbance was measured at 450 nm using the SpectraMaxM5 plate reader (Molecular Devices, CA, USA)

and analyses of absorbance readings were carried out using Microsoft Excel (version 15.32) and GraphPad Prism.

2.35 Measurement of recombinant HIV-1 Env binding to cell surface CD4 using CEM T-cell line

96-well TC plates (Cell Star) were seeded with $1x10^5$ CEM cells per well. The CEM cells were then incubated with 1 ng/mL - 10 µg/mL of either recombinant WT gp120, gp120 CD4bs mutant or gp140 trimer in cRPMI at 37°C for 1 h. After incubation with the Env glycoproteins, CEM cells were washed with cRPMI, re-suspended in 2 µg/mL biotinylated 2G12 mAb and incubated for 1 h at 37°C and 5.0 % CO_2. 2G12-untreated controls were re-suspended in cRPMI only. The CEM cells were re-suspended in Alexa Fluor 647 conjugated streptavidin (Life Technologies) diluted 1:5000 in FACS buffer, and incubated for 1 h at RT in the dark. Alexa Fluor 647-untreated controls were re-suspended in FACS buffer only and incubated under the same conditions. CEM cells were fixed in 4 % formaldehyde and Alexa Fluor 647 intensity was measured using FACSCalibur (BD Biosciences, UK). Data were analysed using FlowJo Software and GraphPad Prism.

2.36 xCELLigence assay of the effects of HIV-1 Env on $CD14^+$ monocyte and THP-1 monocytic cell line migration

The CIM-16 plate was assembled as previously described with either 160 µL of vehicle, 5 nM CCL2/MCP-1, 5 nM CCL5/RANTES, and the wild-type, CD4bs mutant or gp140 trimer variants of HIV-1 Env loaded into wells of the bottom chamber of the CIM-16 plate. After measuring background CI readings for each well, either $4x10^5$ $CD14^+$ monocytes or $4x10^5$ THP-1 cells were added to each well of the top chamber. Immediately after addition of the

cells to the top chamber, the CIM-16 plate was docked into the xCELLigence RTCA-DP system and rested at 37°C for 5 min to allow for settling of the monocytes. After this period, cell index was measured at 15 s intervals for a total time period of 2 h.

2.37 xCELLigence assay of the effects of transduced MDM supernatants on $CD14^+$ monocyte migration

The CIM-16 plate was assembled with 160 µL of vehicle, 5 nM CCL2/MCP-1 and cleared supernatants from MDMs transduced with HIV-NL4.3-eGFP based vectors loaded into wells of the bottom chamber. After measuring background CI readings for each well, $4x10^5$ autologous $CD14^+$ monocytes were added to each well of the top chamber. Immediately after addition of the monocytes to the top chamber, the CIM-16 plate was docked into the xCELLigence RTCA-DP system and rested at 37°C for 5 min to allow for settling of the monocytes. After this period, cell index was measured at 15 s intervals for a total time period of 2 h. Summary data for the chemotaxis assays are reported as mean ± SEM of *n* replicates. Area under the curve and 'maximum-minimum' migration analyses were carried out using GraphPad Prism. Statistical analyses for chemotaxis assays were also performed on GraphPad Prism.

2.38 Quantification of interferon activity of supernatants from transduced MDMs

Serial dilutions of cleared MDM supernatants and recombinant human IFN-2α (PBL Assay Science) or human IFN-*β* standard (R&D Systems) were prepared in cDMEM. 2.5 x 10^4 HEK293-3C11-ISRE-fLuc cells were plated per well of a flat-bottomed TC plate and 50 µL of either supernatant, IFN-α or IFN-*β* standard was separately added to the wells in duplicate.

The HEK293-3C11-ISRE-fLuc reporter cells were incubated with the supernatants or IFN standards for 24 h at 37°C and 5 % CO_2 after which the cDMEM was aspirated and the cells were washed. The cells were then treated with 100 µL of 1X Reporter Lysis Buffer and a single freeze thaw cycle was carried out at -80°C to ensure complete cell lysis. The cell lysate was mixed with 1:1 with Bright-Glo reagent and incubated for 2 min at RT. Luminescence was measured at 1000 ms integration time using a SpectraMaxM5 plate reader, and interferon activity in the MDM supernatants was interpolated from standard curves of *Luminescence vs IFN activity* using the GraphPad Prism software.

2.39 Extraction of RNA from transduced or stimulated MDMs

Total RNA was isolated from transduced or stimulated MDMs using the RNeasy Mini Kit (Qiagen). Approximately $2x10^6$ MDMs were lysed with 700 µL of lysis buffer consisting of 1 volume β-mercaptoethanol (Sigma): 5 volumes buffer RLT (Qiagen). For extractions, cell lysate was loaded onto a QIAshredder spin column (Qiagen) and homogenised by centrifuging at 18000 *x g* for 2 min at 4°C. Homogenised lysate was mixed with 70% ethanol at a 1:1 volume ratio, loaded onto a RNeasy spin column and centrifuged at 8000g for 20 s at 4°C. Successive washes of the spin column membrane were carried out using buffer RW1 and then buffer RPE with centrifuging at 8000 *x g* for 20 s at 4°C at each wash step. A final column wash was carried out with buffer RPE by centrifuging at 8000 *x g* for 2 min at 4°C. The column was then dried by centrifuging at 18000 *x g* for 2 min at 4°C. Membrane bound RNA was eluted by adding 50 µL of RNAse free water to the spin column

and centrifuging at 8000 *x g* for 1 min at 4°C. The elution step was repeated to obtain a total of 100 µL RNA.

2.40 Quantification of interferon stimulated gene (ISG) expression by qRT-PCR

First strand cDNA was synthesised using SuperScript II reverse transcriptase (Invitrogen). Each reaction contained 5 ng total RNA, 1 µL of 500 µg/mL Oligo(dT)$_{12\text{-}18}$ random primers (Invitrogen) and 1 µL of 10 mM dNTPs made up to a total volume of 12 µL with nuclease free water (ThermoFisher). The reaction mixture was first incubated at 65°C for 5 min, then supplemented with 4 µL of 5X First-Strand Buffer (Invitrogen) and 2 µL of 0.1 M dithithreitol, and further incubated at 42°C for 2 min. cDNA synthesis was carried out by adding 1 µL (200 units) of SuperScript II reverse transcriptase to the reaction mixture and incubating for 50 min at 42°C, followed by a final inactivation step at 70°C for 15 min.

To quantify expression of interferon stimulated genes (ISGs), cDNA was amplified using the StepOnePlus real-time PCR system (Applied Biosystems). Each qRT-PCR reaction contained 1.5 µL cDNA template, 0.75 µL of gene-specific TaqMan Assay mix (ThermoFisher) as detailed in Table 7, 7.5 µL TaqMan Fast Advanced Mastermix (ThermoFisher) and 5.25 µL of nuclease free water. The qRT-PCR program consisted of an initial incubation step at 50°C for 2 min and a polymerase activation step at 95°C for 2 min, followed by 40 cycles of denaturation at 95°C for 1 min and annealing/extension at 60°C for 20 s. ISG expression data were normalized to GAPDH expression and analyzed by the ΔΔCT relative quantification method using Microsoft Excel. The TaqMan gene expression assays used to quantify ISG expression in this study are listed in Table 7.

Table 7: TaqMan Assays used to quantify interferon stimulated gene expression by qRT-PCR

Gene	**TaqMan Assay ID**
CXCL10	Hs00171042_m1
DDX58 (RIG-I)	Hs01061436_m1
GAPDH	Hs02758991_g1
IFI44L	Hs00915292_m1
IFIH1	Hs00223420_m1
IFIT1	Hs03027069_s1
ISG15	Hs00192713_m1
MX2	Hs01550808_m1

2.41 Site-directed mutagenesis (SDM) of HIV-1 NL4.3-eGFP-Vpr$^+$ expression plasmids

The HIV-1 NL4.3-eGFP-Vpr$^+$ expression plasmid gifted by Jan Rehwinkel was obtained through the NIH AIDS Reagent Program from Zhang et al. [193], the primers used for site-directed mutagenesis PCR are detailed in Table 8 and PCR was carried out using a Veriti 96-well thermal cycler (Applied Biosystems).

The H71R mutagenesis primer pair was designed using the NEBaseChanger software (New England Biolabs) following the guidelines of the Q5 Site-Directed Mutagenesis kit (New England Biolabs) and synthesised by Sigma. For optimisation of H71R mutagenesis conditions, reactions contained 5-100 ng of HIV-1 NL4.3-eGFP-Vpr$^+$ template plasmid, 0.5 units Phusion Polymerase (New England Biolabs), 0.5 µM forward and reverse primer, 200 µM dNTPs (Invitrogen), 3 % (v/v) DMSO and were made up to a total volume of 25 µL with

nuclease free water (Thermo Fisher Scientific). The PCR cycles were initiated at 98°C for 3 min to denature template DNA, followed by 25 amplification cycles each of which consisted of denaturation at 98°C for 10 seconds, annealing at 60-70°C for 30 seconds and extension at 72°C for 15 min (approximately 1 minute per 1 kb). PCR cycles were completed with a final extension step at 72°C for 15 min.

The Q65R, K27, S28 and K27/S28 mutagenesis primer pairs were designed using the QuikChange Primer Design Program (Agilent Technologies), modified according to the guidelines of the Liu and Naismith [194] and synthesised by Sigma. For optimisation of Q65R, K27, S28 and K27/S28 mutagenesis conditions, reactions contained 5-25 ng of HIV-1 NL4.3-eGFP-Vpr^{+} template plasmid, 0.5 units Phusion Polymerase, 0.5 µM forward and reverse primer, 200 µM dNTPs, 3 % (v/v) DMSO and were made up to a total volume of 25 µL with nuclease free water. The PCR cycles were initiated at 95°C for 5 min to denature template DNA, followed by 15 amplification cycles each of which consisted of denaturation at 95°C for 1 minute, annealing at 60-70°C for 1 minute and extension at 72°C for 15 min (approximately 1 minute per 1 kb). PCR cycles were completed with a second annealing step at 40-60°C for 1 minute and a final extension step at 72°C for 30 min. 5 µL of PCR product was visualised on a 1 % agarose gel by electrophoresis at 110V for 45 min and compared to a 1 kb HyperLadder (Bioline). 10 µL of the PCR products that gave an intense band $\geq$10 kb was digested with 20 units DpnI (New England Biolabs) for 2 h at 37°C.

NEB 5-alpha competent *E. coli* (New England Biolabs) were used for SDM transformations, and has the following genotype: *fhu*A2 Δ(*arg*F^{-}*lacZ*)U169 *pho*A *gln*V44 Φ80 Δ(*lacZ*)M15 *gyr*A96 *rec*A1 *rel*A1 *end*A1 *thi*-1 *hsd*R17. For SDM transformations, 5 µL of the DpnI digest

product was added to 50 µL of freshly thawed NEB 5-alpha competent *E. coli*, incubated on ice for 30 min and heat shocked at 42°C for 45 seconds followed by 5 min incubation on ice. 950 µL of SOC was added to the transformed cells and the suspension was incubated at 37°C and 5 % CO_2 with continuous shaking at 3 *x g* (180 rpm) for 1 h. 300 µL of the culture was spread onto an LB agar plate supplemented with 100 µg/mL Amp and cultured overnight at 37°C and 5 %. The following day a single Amp^R colony was selected and used to inoculate 2 mL LB broth supplemented with 100 µg/mL Amp. The starter culture was expanded by incubating for 2 h at 37°C and 5 % CO_2 with continuous shaking at 3 *x g* (180 rpm). For long-term storage, starter cultures were frozen at -80°C in the presence of 50 % (v/v) glycerol.

2.42 Mini-prep purification and Sanger sequencing of mutagenized HIV-1 NL4.3-eGFP-Vpr^+ plasmids

2 mL of LB broth supplemented with 100 ng/mL Amp was inoculated with a single Amp^R colony and incubated overnight at 37°C and 5 % CO_2 with continuous shaking at 3 *x g* (180 rpm). The cells were pelleted at 4600 *x g* (7165 rpm) for 15 min and re-suspended in 200 µL of Resuspension Buffer supplemented with RNAse A (0.56 % v/v, Invitrogen). 200 µL of Lysis Buffer (Invitrogen) was added to the cell suspension and incubated at RT for 5 min, followed by 150 µL of Precipitation Buffer and the lysate was mixed by inversion to obtain a homogenous mixture. The precipitate was incubated on ice for 5 min and pelleted by centrifuging at 15 142 *x g* (13 000 rpm) for 10 min at RT. The cleared supernatant was mixed with 500 µL of 96 % isopropanol and centrifuged at 15 142 *x g* (13 000 rpm) for 10 min at 4°C. The DNA pellet was washed by re-suspending in 350 µL of 70 % ethanol and

centrifuging at 15 142 *x g* (13 000 rpm) for 3 min at 4°C. The purified DNA pellet was air dried and then re-suspended in 50 µL of Tris-EDTA (TE) Buffer. The concentration of purified plasmid DNA was quantified using a NanoDrop 2000c spectrophotometer.

The HIV-1 Vpr ORF sequencing primer pair (5'CTAGGTGTGAATATCAAGCAGG3' and 5'GGAGATGCCTAAGGCTTTTGT3') was designed using the Serial Cloner software (version 2.6.1) and synthesised by Sigma. Sequencing primers diluted to 3.2 pmol/µL and purified plasmid DNA diluted to 100 ng/µL were submitted to SourceBioscience for Sanger DNA sequencing. DNA sequence chromatograms were analysed using 4Peaks software (version 1.8) and mutations were verified by sequence alignment using the Serial Cloner software. Successfully mutated plasmids were transformed into Stbl3 competent cell line for long-term maintenance as described in section 2.9.

Table 8: Primers used for site-directed mutagenesis PCR

Primer name	**Primer sequence**	**T_m** (°C)	**Tm_{pp}** (°C)	**Tm_{no}** (°C)	**Mutation induced in Vpr ORF**
H71R_Fwd	5'AACTGCTGTTTATCC***<u>G</u>***TTTCAGAATTGGGTGT3'	74.1	n/a	n/a	H71R
H71R_Rev	5'GTTGCAGAATTCTTATTATGGCTTCCACTCC3'	71.4	n/a	n/a	
Q65R_Fwd	*5'AAGAATTCTG****<u>AG</u>****ACAACTGCTG*TTTATCCATTTCAGAATTGGGTGTCGACAT3'	82.4	60.1	72.1	Q65R
Q65R_Rev	*5'CAGCAGTTGT****<u>CT</u>****CAGAATTCTT*ATTATGGCTTCCACTCCTGCCCAAGTATCC3'	83.4	60.1	74.8	
K27_Fwd	*5'AGAGGAACTT****<u>T</u>***A*GAGTGAAG*CTGTTAGACATTTTCCTAGGATATGGCTCC3'	78.3	51.7	68.6	Nonsense mutation
K27_Rev	*5'CTTCACTCT****<u>A</u>****AAGTTCCTCT*AAAAGCTCTAGTGTCCATTCATTGTATGGC3'	77.7	51.7	69.8	
S28_Fwd	*5'GAACTTAAG****<u>T</u>****G****<u>A</u>****GAAGCTGTT*AGACATTTTCCTAGGATATGGCTCCATAAC3'	77.2	54.5	69.8	Nonsense mutation
S28_Rev	*5'AACAGCTTC****<u>T</u>****C****<u>A</u>****CTTAAGTTC*CTCTAAAAGCTCTAGTGTCCATTCATTGTA3'	77.2	54.5	65.2	
K27/S28_Fwd	*5'GAGGAACTT****<u>T</u>***AG***<u>T</u>****G****<u>A</u>****GAAGCTGT*TAGACATTTTCCTAGGATATGGCTCCATAAC3'	78.8	59.6	67.8	Double nonsense mutation
K27/S28_Rev	*5'ACAGCTTC****<u>T</u>****C****<u>A</u>****CT****<u>A</u>****AAGTTCCTC*TAAAAGCTCTAGTGTCCATTCATTGTATGGC3'	79.8	58.8	69.5	

Primer-primer overlapping sequences are italicized, and the mutagenic bases are in bold and underlined. 'ORF' denotes open reading frame, 'Fwd' indicates the forward primer of the primer pair, 'Rev' indicates the reverse primer of the primer pair, 'Tm' denotes the melting temperature calculated from the entire primer sequence, 'Tm_{pp}' denotes the melting temperature calculated from the primer-primer overlap sequence and 'Tm_{no}' denotes the melting temperature calculated from the non-overlapping primer sequence.

Chapter 3:

Establishing biologically relevant macrophage differentiation and transduction systems.

3.1 Introduction

As a lentivirus, HIV-1 is capable of productively infecting terminally differentiated macrophages despite their terminally differentiated state. This is because HIV-1 does not require the nuclear envelope breakdown that accompanies mitosis to facilitate the translocation of the viral genome into the nucleus for integration [195]. Instead, HIV-1 nuclear import of the PIC is facilitated by a cell-cycle independent mechanism that has not yet been completely defined [196,197]. Productive infection of target cells with replication competent HIV-1 culminates in the assembly and release of infectious progeny virus particles which can go on to seed a subsequent round of infection (Figure 2). In contrast, single-cycle HIV-1 vectors are defective in one or more viral proteins that function after viral assembly and which are necessary to facilitate proper assembly of progeny HIV-1 particles. For example, HIV-1 expression plasmids are commonly engineered to bear inactivating mutations in the *env* ORF. Transient co-transfection of producer cells (e.g. HEK293Ts) with an *env*-deficient HIV-1 expression plasmid and a complementary *env* expression plasmid, generates recombinant infectious vectors. When cells of interest are transduced with these vectors, expression of the *env*-deficient viral genome occurs within the infected cell but the replication cycle culminates in the production of defective, non-infectious virions which are not capable of spreading infection to a second round of cells. For this reason, I used single-cycle lentiviral systems in this study to minimize any potential confounding effects of multiple rounds of infection.

Despite the ability of lentiviruses to infect non-dividing cells, HIV-1 infection of macrophages is relatively inefficient in comparison to infection of $CD4^+$ T-cells. A challenge

to investigating responses of macrophages to HIV-1 *in vitro* is the expression of host restriction factors which act at different steps of HIV-1 replication to limit productive HIV-1 infection. For example, Apolipoprotein B Editing Complex (APOBEC3) proteins act on products of reverse transcription to induce guanosine-to-adenosine hypermutations that either de-stabilise the HIV-1 reverse transcripts, leading to their degradation before integration, or lead to integration of defective HIV-1 provirus [3,198]. The cell surface protein BST-2/CD317 (Tetherin) also restricts productive infection by tethering virions to the plasma membrane thereby blocking the release of nascent HIV-1 particles [2,199]. In addition to these factors, macrophages express the sterile α-motif and HD domain–containing protein-1 (SAMHD1) which hydrolyses deoxynucleotide-triphosphates (dNTPs) to deoxynucleosides and inorganic triphosphate. SAMHD1 activity decreases the concentration of cytosolic dNTPs to levels that are insufficient to sustain reverse transcription, thereby restricting HIV-1 infection [200]. HIV-2 and certain strains of SIV express the lentiviral accessory protein Vpx, which targets SAMHD1 for proteosomal degradation and downregulates its activity [201,202]. As a result of SAMHD1 downregulation by Vpx, the cytosolic pool of dNTPs available for reverse transcription of viral RNA is increased, and productive HIV-1 infection is enhanced [200]. However, HIV-1 does not express Vpx and therefore cannot counteract SAMHD1 activity by a Vpx-dependent mechanism.

Various experimental manipulations can be used to increase the efficiency of HIV-1 infection and transduction of MDMs. These include enhancing the entry efficiency of HIV-1 vectors by pseudotyping with VSV-G Env [203,204], using centrifugal inoculation to

enhance viral binding and entry into target cells [205,206], enhancing virus adsorption on target cell membranes with cationic polymers such as polybrene [207], and downregulating SAMHD1 restriction of HIV-1 either by delivering SIV Vpx to target cells in VLPs [201,202] or by using factors such as FCS to promoting CDK1-mediated deactivation of SAMHD1 activity [208]. Other authors have suggested that HIV-1 evades immune sensing and does not induce an IFN response in A549 lung epithelial cells, THP-1 monocytic cells and normal human dermal fibroblasts (NHDFs) [209,210]. I sought to further investigate the question of whether or not HIV-1 fully evades immune sensing and whether HIV-1 is able toi induce the production of immune mediators in macrophages.

MDMs are widely used to investigate macrophage responses to HIV-1. However, recent studies have highlighted human induced pluripotent stem cell-derived macrophages (hPSC-DMs) as an alternative *in vitro* model. hPSCs are derived by reprogramming adult cells to a pluripotent state by transduction of the transcription factors Oct4, Sox2, C-myc, and Klf41 [211-213]. Human and murine PSCs are capable of long-term self-renewal, and resemble embryonic stem cells (ESCs) in terms of morphology, gene expression and their ability to differentiate into cell types of different lineages under defined culture conditions [212,213]. Furthermore, recent work by Buchrieser et al. has demonstrated that the transcriptional regulation of hPSC-DM development recapitulates that of yolk-sac-derived tissue-resident macrophage populations [214]. For these reasons, there is growing interest in the use of hPSC-DMs as an *in vitro* model for studying the cellular mechanisms of tissue-resident macrophage-mediated pathologies. For example, hPSC-DMs have been used to investigate the cellular mechanisms of tissue-resident macrophage-mediated

pathologies [215], macrophage responses to zika and dengue viruses [216,217] and can be differentiated to tissue-resident macrophage-like populations that are relevant to the pathogenesis of HIV-1 infection [218,219]. Lastly, hPSC-DMs are permissive to transduction with HIV-1 pseudotyped viruses and have been used as a model to study mechanisms of HIV-1 entry in MDMs [220]. Together with their amenability to genetic manipulation, these characteristics highlight the potential utility of hPSC-DMs as *in vitro* models for interrogating the molecular mechanisms of macrophage responses to HIV-1 infection [220].

3.2 Chapter rationale

Given the clinical evidence that implicates macrophages in the pathogenesis of HIV-1-associated inflammatory conditions, I hypothesise that sensing of HIV-1 PAMPs by MDMs induces an innate immune response which results in the production of immune modulators which are relevant to to the pathogenesis of HIV-1-associated inflammation. While primary MDMs are widely used to study interactions between macrophages and HIV-1, hPSC-DMs recapitulate the ontogeny of yolk-sac-derived macrophage populations and therefore may provide a more relevant model for investigating tissue-resident macrophage responses to HIV-1. Having chosen to use a single-cycle pseudotyped virus approach to macrophage transduction to avoid multi-cycle spreading infection and the complication of interpreting data from such systems, I set about establishing and optimising pseudotyped virus production and transduction protocols for use with both primary MDMs and hPSC-DMs. Therefore, through the work I present in this chapter, I aimed to:

I. Optimise systems for isolation and differentiation of MDM
II. Establish and validate a panel of single-cycle eGFP-tagged NL4.3 pseudotyped viruses for transduction of MDMs and hPSC-DMs
III. Optimise an MDM transduction protocol to include minimal activating factors
IV. Establish embryoid body cultures for the long-term production of human induced pluripotent stem cell derived macrophage precursors (hPSC-MPs) and hPSC-DMs
V. Characterise MDM, hPSC-MP and hPSC-DM morphology and cell surface marker expression profile
VI. Optimise conditions for hPSC-DM transduction

3.3 Results

3.3.1 Characterisation of primary human blood-derived MDMs

SAMHD1 restriction of HIV-1 is a key contributor to the low permissivity of MDMs to HIV-1 infection [201,202]. Notably, Mlcochova et al. recently reported that a transition to a G1-like cell cycle phase upon MDM differentiation in the presence of FCS facilitates upregulation of cyclin-dependent kinase 1 (CDK1) activity [208]. CDK1 phosphorylation of SAMHD1 at the critical T592 residue downregulates its antiviral activity [221], although it is unclear whether this phosphorylation event mediates downregulation of HIV-1 restriction by specifically disrupting SAMHD1's hydrolase activity [222]. Nonetheless, MDMs that have transitioned to the G1-like state exhibit downregulated SAMHD1 antiviral activity and enhanced susceptibility to HIV-1.

In light of this finding, I attempted to generate MDMs that were relatively more permissive to HIV-1 transduction by differentiating negatively isolated $CD14^+$ monocytes in X-$Vivo_{15}$ media supplemented with human serum (HS) for 3 days followed by media supplemented with 10% FCS for a further 4 days (denoted as HS/FCS). This approach was a modification of our research group's previously established macrophage differentiation protocol by which negatively isolated $CD14^+$ monocytes were differentiated in X-$Vivo_{15}$ supplemented with 1% HS for a total of 7 to 10 days. I confirmed the purity of monocyte isolations by measuring $CD14^+$ expression by flow cytometry, and validated the phenotype of MDMs that were differentiated using the modified HS/FCS protocol by characterising the morphology, expression of myeloid cell markers and LPS responses of differentiated MDMs.

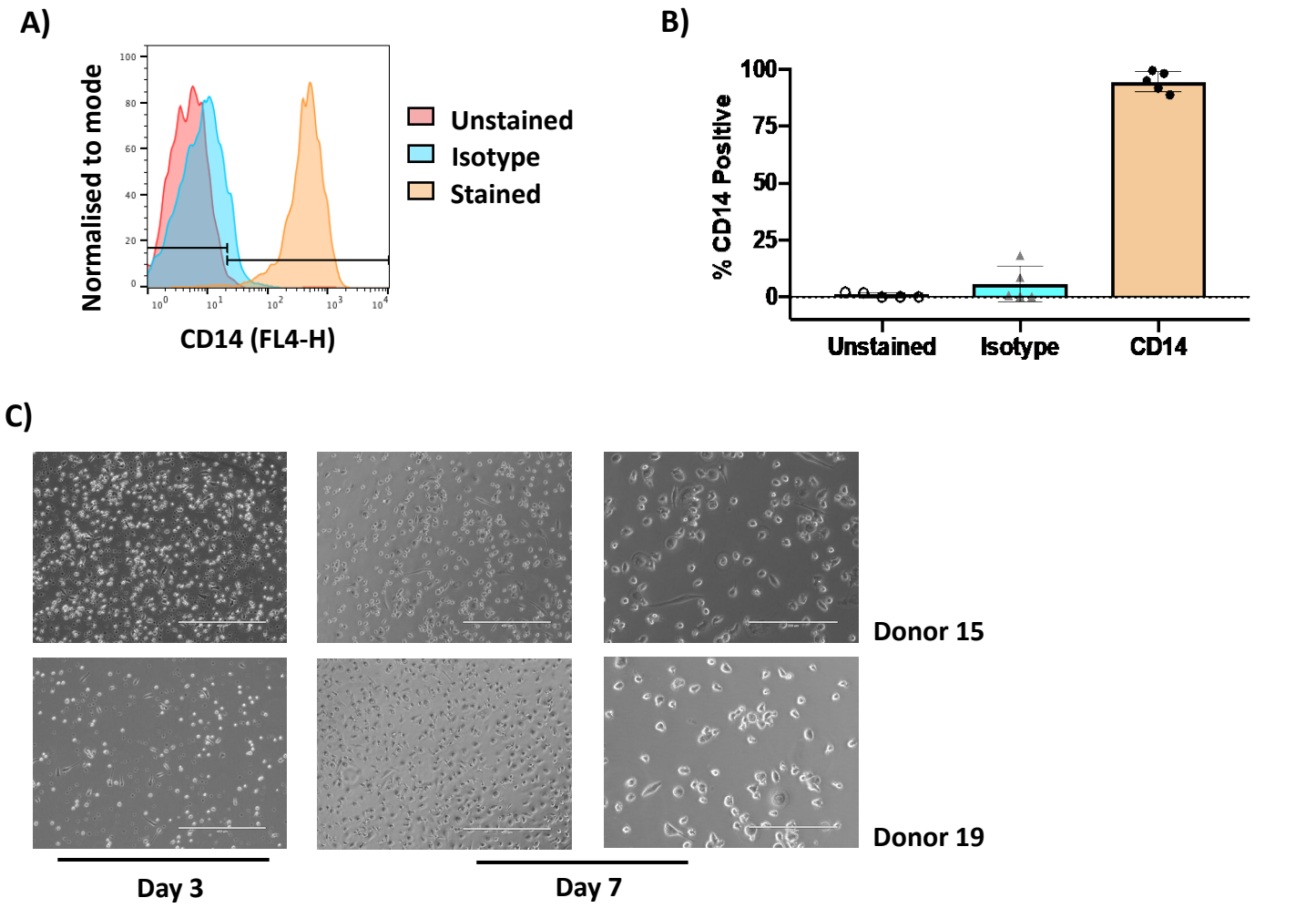


Figure 7: Characterisation of primary human monocyte derived macrophages (MDMs)

Figure 7: ***A) Representative histogram of CD14 expression (n = 1) for monocytes isolated by negative enrichment from PBMCs B) Purity of monocytes isolated by negative enrichment from PBMCs. Error bars indicate mean %CD14$^+$ ± SD for 5 independent donors. C) MDM morphology was assessed by light microscopy after 3 days culture in X-vivo$_{15}$ supplemented with 1 % HS (scale bar = 400 µm), and after a media change to X-Vivo$_{15}$ supplemented with 10 % FCS and a further 4 days differentiation (scale bars = 400 µm and 200 µm). Images are shown for two representative donors. D) MDM expression of the myeloid lineage cell surface markers CD14, CD163 and CD11b, the HIV-1 receptor CD4 and HIV-1 co-receptor CCR5 was assessed by flow cytometry. Error bars indicate mean of median fluorescence intensity (M.F.I.) ± SD for 5 independent donors. *p<0.05 and n.s. denotes 'not significant' for paired t-test comparison of mean MFI versus the isotype control. E) MDMs were treated with 1 µg/mL LPS for 18 h and the concentrations of IL-6, IL-10, IL-12 p70 and TNF-α produced as a result of LPS stimulation was determined by multiplex immunoassay. Error bars indicate mean with SD of 2 technical replicates for 2 independent donors.***

Negative isolation routinely enriched for a cell population that was at least 90% CD14$^+$ (Figure 7B). I also assessed the morphology of the HS/FCS-differentiated MDMs by light microscopy and observed a mixture of the characteristic elongated spindle and rounded 'fried egg' morphology of MDMs in culture (Figure 7B). I also investigated MDM expression of the HIV-1 receptor CD4, HIV-1 co-receptor CCR5, and the myeloid lineage cell surface markers CD14, CD163 and CD11b by flow cytometry (Figure 7B). The macrophage markers CD14 ($p = 0.03$) and CD11b ($p = 0.02$) were significantly expressed over the relative isotype staining, however CD163 expression varied greatly across donors and overall was not significantly different to the isotype control ($p = 0.08$). While MDMs appreciably expressed the HIV-1 co-receptor CCR5 ($p = 0.02$), expression of the primary receptor CD4 was very low and did not not reach significance ($p = 0.2$).

To characterise the inflammatory response of MDMs generated by HS/FCS differentiation, MDMs were stimulated with 1 μg / mL LPS for 18 h and the resulting production of IL-6, IL-10, IL-12 p70 and TNF-α was measured by multiplex immunoassay. This panel of cytokines was selected for investigation as they are known to be expressed by macrophages as part of the inflammatory response and are inducible by LPS stimulation of Toll-like receptor 4 (TLR4). In particular, LPS stimulation of classically-activated / M1-like macrophages induces expression of IL-6, TNF-α and IL-12 p70, while LPS stimulation of alternatively-activated / M2-like macrophages induces expression of the anti-inflammatory cytokine IL-10 [223-225]. Our protocol does not bias differentiation into either M1 or M2 pathways, and so we consider our MDM to represent most closely an 'M0' phenotype, although some morphological heterogeneity is clearly evident in the cultures.

The levels of IL-6, IL-10, IL-12 p70 and TNF-α produced by LPS-stimulated MDMs are summarised in Figure 7C. Although the magnitude of responses differed between donors, LPS stimulation most notably induced TNF-α and IL-6 production by MDMs. IL-10 production was induced to a lesser extent and IL-12 p70 production was negligible. Overall, these results confirm that MDMs derived using the modified protocol exhibit characteristic macrophage morphology, myeloid cell markers, expression of HIV-1 receptors and LPS-induced TNF-α and IL-6 production.

3.3.2 Generation of single-cycle HIV-1-NL4.3eGFP pseudotyped virus

Two overarching aims of my study were: i) to characterise HIV-1 induction of MDM-expressed mediators of inflammation and; ii) to investigate the effect of the HIV-1

accessory protein Vpr on the expression profile of these mediators. Given that lentiviral vectors stably integrate into the host genome to maintain transgene expression and are routinely used to transduce non-dividing cells, I sought to establish a single-cycle HIV-1 vector system for transducing MDMs using eGFP-tagged constructs based on the HIV-1 NL4.3 clone.

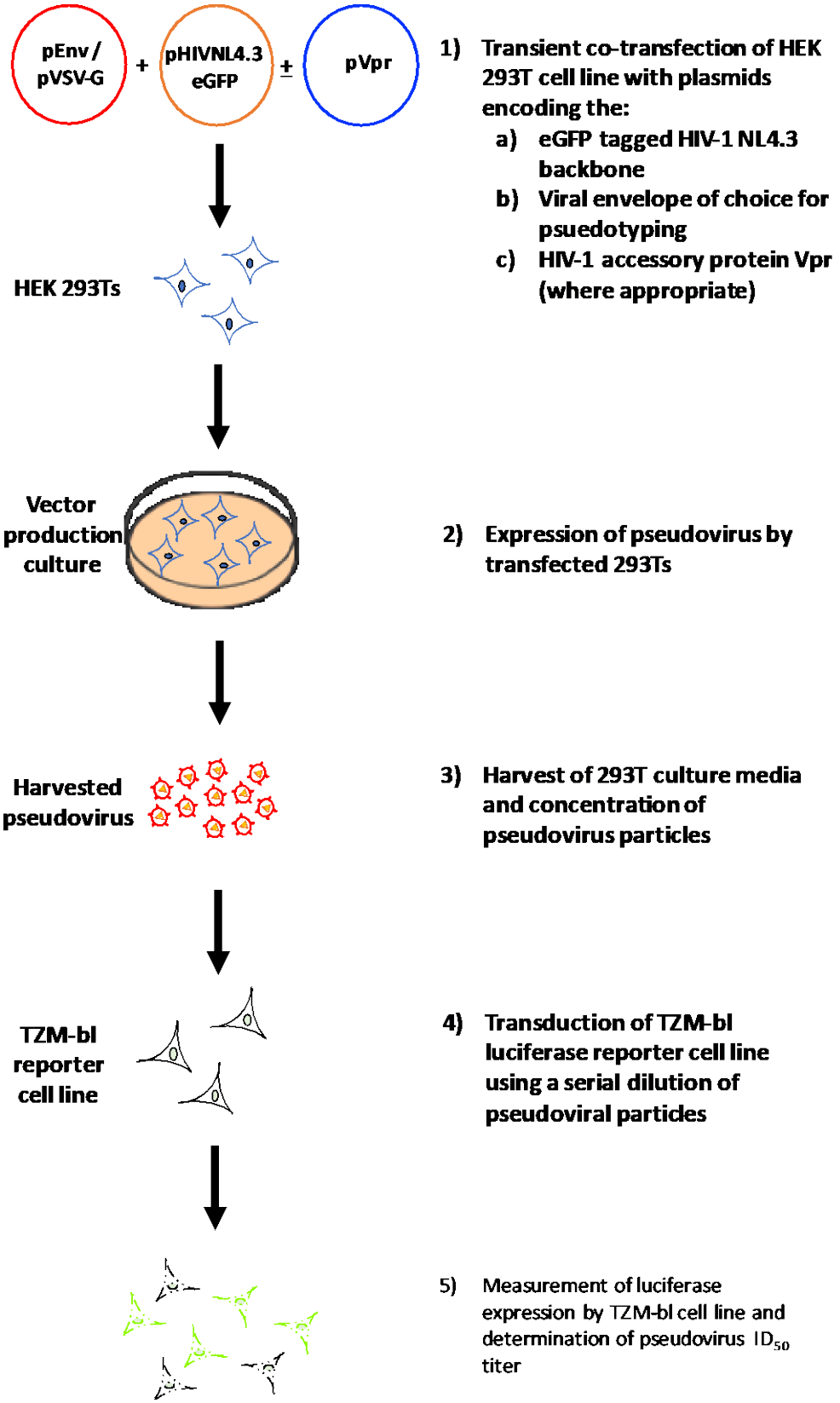


Figure 8: Schematic of HIV-1-NL4.3-eGFP vector production and titration

As discussed in section 3.3.1, macrophages express HIV-1 restriction factors and as a result, exhibit low permissisivity to HIV-1-infection and transduction. In the past, reserachers have used a variety of experimental manipulations that to circumvent this challenge. The most common of these approaches is increasing HIV-1 vector entry efficiency and breadth of tropism by pseudotyping with the vesicular stomatitis virus envelope glycoprotein (VSV-G) which utilises the ubiquitously expressed low density lipoprotein receptor (LDL-R) to mediate viral entry [226]. Although VSV-G pseudotyping provides advantages of increased transduction efficiency and particle stability, the mechanism of VSV-G pseudotyped virus entry differs from that of viral particles bearing HIV-1-derived Env. VSV-G facilitates viral entry by pH-dependent, clathrin-mediated endocytosis [203,204] whereas HIV-1-derived Env facilitates viral entry via a pH-independent, receptor-mediated mechanism [21,227,228]. This difference in mechanism of viral entry was of concern for this study as it is unclear whether transduction by VSV-G pseudotyped viruses appropriately recapitulates the cellular activation events that occur in response to physiological infection. Therefore, I investigated the responses of MDMs in response to transduction by both VSV-G and HIV-1_{BaL} Env pseudotyped HIV-1 vectors. As summarised in Figure 8, I generated pseudotyped viruses by transient co-transfection of HEK293Ts with HIV-1-NL4.3-ΔVpr expression plasmids and either VSV-G Env or HIV-1_{BaL} Env expression plasmids. The 50% tissue culture Infectious Dose (ID_{50}) of VSV-G and HIV-1_{BaL} Env pseudotyped viruses were determined using the TZM-bl reporter cell-line; a HeLa cell derivative that was engineered to express CD4 and CCR5, and to express the firefly luciferase (fLuc) reporter gene under the

transcriptional control of the HIV-1 long-terminal repeat (LTR) promoter [229,230]. As a result, inoculated TZM-bls express fLuc in proportion to the number of cells that have been successfully transduced with HIV-1 pseudotyped virus, and quantification of the fLuc activity in the lysate of transduced TZM-bls provides an accurate estimation of the infectious dose of pseudotyped virus stocks.

Control 'Delta Env' (ΔEnv) vectors were generated by transient co-transfection of HEK293Ts with HIV-1-NL4.3-ΔVpr expression plasmids and a pcDNA control plasmid (Clontech). The pseudoyped viruses generated as a result of these transfections do not incorporate viral Env and are unable to engage with the cell surface receptors that facilitate viral entry into either MDMs or the TZM-bl reporter cell line. Therefore, I quantified the ΔEnv vectors by ELISA measurement of their HIV-1 p24 antigen (Ag) content. Unexpectedly, the HIV-1 p24 Ag content of HIV-1_{BaL} Env/NL4.3-ΔVpr pseudotyped viruses was significantly lower than that of ΔEnv/NL4.3-ΔVpr pseudotyped viruses (Figure 9C). HIV-1 p24 Ag determination by ELISA measures the total p24 Ag content of a sample, which may include both mature, infectious pseudotyped virus particles as well as defective, non-infectious pseudotyped virus particles. In contrast, TC ID_{50} provides an accurate estimation of the infectious dose of pseudotyped virus stocks. Therefore, I also determined the TC ID_{50} of the ΔEnv vectors by interpolating the HIV p24 Ag values against that of HIV-1_{BaL} Env pseudotyped viruses for which both the ID_{50} and p24 Ag content had been determined. To account for variation in p24 Ag content, all subsequent transductions were carried out at standard MOIs based on the TC ID_{50} of the pseudotyped virus preparations.

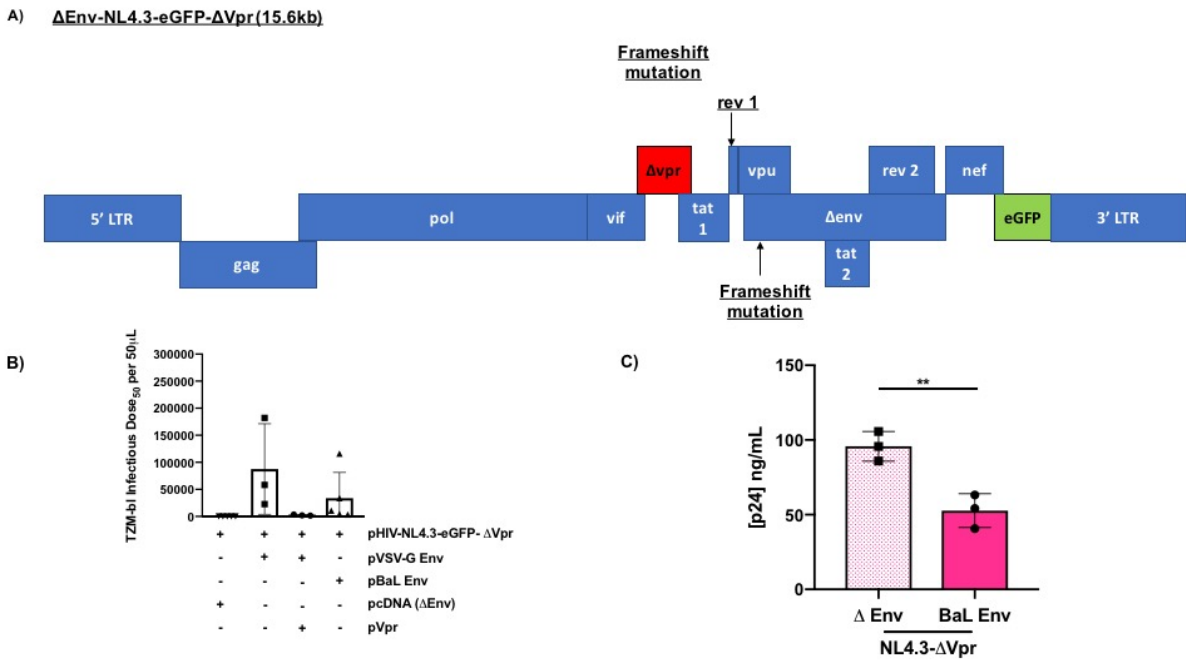


Figure 9: Optimisation of single cycle HIV-NL4.3eGFP-ΔVpr vector production

A) Enhanced green fluorescent protein (eGFP)-tagged reporter vectors were derived from the HIV-1 clone NL4-3. The HIV-1-NL4.3-eGFP-ΔVpr expression vector carries frameshift mutations in both the Env and Vpr open reading frames, and resulting vectors express a truncated, non-functional form of both the Vpr and Env protein. B) Mean with SD for 3 representative preparations of vector. Co-transfection of expression plasmids encoding the NL4.3eGFP backbone, and either the VSV-G envelope or HIV-1 BaL envelope (CCR5 tropic) in the absence of the expression plasmid encoding the HIV-1Vpr accessory protein resulted in the production of vectors that appreciably transduced the TZM-bl reporter cell line. However, co-transfection of the Vpr plasmid resulted in vectors that were not capable of efficiently transducing the reporter cell line. C) HIV-1 p24 Ag content was determined by ELISA for both Delta Env and HIV-1_{BaL} Env versions of NL4.3-ΔVpr pseudotyped viruses. Error bars indicate mean [p24] ± S.D. for 3 representative vector preparations. The dataset was analysed by Shapiro-Wilk normality testing and one way ANOVA with Sidak's post-test comparison. **p < 0.01 and n.s. denotes 'not significant'.

As VSV-G pseudotyping is known to generate particles of high stability and transduction efficiency [231], I focussed the initial attempts at vector production on generating VSV-G pseudotyped viruses. As shown in Figure 9B, co-transfection of separate expression plasmids encoding the HIV-1-NL4.3-eGFP-ΔVpr backbone and VSV-G *env* generated vectors of appreciable titres that were capable of efficiently transducing the TZM-bl reporter cell line. As with the VSV-G pseudotyped virus, co-transfection of expression plasmids encoding the HIV-1-NL4.3-eGFP-ΔVpr backbone and HIV-1_{BaL} *env* generated pseudotyped virus of appreciable titres. Also shown in Figure 9B, the matched ∆Env vectors did not induce detectable luciferase activity as they were not capable of transducing the TZM-bl cell line, thereby confirming their suitability as control vectors.

Given my interest in investigating the effect of HIV-1 Vpr on MDM responses to HIV-1, I next attempted to generate isogenic HIV-1-NL4.3-eGFP-Vpr^+ pseudotyped virus by co-transfecting HEK293Ts with separate plasmids encoding the HIV-1-NL4.3-eGFP-ΔVpr backbone, VSV-G and HIV-1 Vpr. However, the resulting pseudotyped virus stocks were not capable of transducing the TZM-bl reporter cell line. On the whole, attempts at generating viable HIV-1-NL4.3-eGFP-Vpr^+ pseudotyped virus by this approach were unsuccessful.

3.3.3 Optimisation of MDM transduction using VSV-G/HIV-1-NL4.3-eGFP pseudotyped virus

Previous studies have increased lentiviral vector transduction efficiency by inoculating target cells at a high multiplicity of infection (MOI), with the assistance of centrifugal inoculation ('spinoculation') [205,206], by inoculating target cells in the presence of

chemical enhancers of transduction such as polybrene [207] and/or by treating target cells with VSV-G/SIV-Vpx VLPs containing Vpx which downregulates the HIV-1 restriction factor SAMHD1 [201,202]. To address concerns that these manipulations would introduce confounding factors to my studies of HIV-1-induced macrophage activation, I sought to establish a 'minimal' protocol that would utilise reduced amounts of VSV-G/SIV-Vpx VLPs, and eliminate the requirement of polybrene and spinoculation for MDM transduction.

I used VSV-G/HIV-1-NL4.3-eGFP-ΔVpr pseudotyped viruses for initial attempts at optimising the MDM transduction protocol as VSV-G pseudotyped viral particles are known to provide good transduction efficiency [231]. To optimise the MOI and determine the minimal amount of SIV Vpx VLPs necessary for MDM transduction by VSV-G/HIV-1-NL4.3-eGFP-ΔVpr pseudotyped virus, I transduced MDMs at an MOI range of 0-0.025 in cX-Vivo$_{15}$ supplemented with 0-50 ng per well of SIV-Vpx VLPs. Additionally, to determine whether spinoculation was required to efficiently transduce MDMs with VSV-G/HIV-1-NL4.3-eGFP-ΔVpr pseudotyped virus, transductions were carried out either in the absence or presence of centrifugal inoculation ('spinoculation').

As shown in Figure 10, MDMs that were not inoculated with pseudotyped virus (MOI=0) did not express eGFP across any of the conditions investigated, confirming that eGFP expression was a specific read-out for MDMs that had been successfully transduced by VSV-G/HIV-1-NL4.3 pseudotyped virus. For transductions carried out in the absence of spinoculation, MDM eGFP expression was negligible at 24 h post-transduction for all MOIs and VSV-G/SIV-Vpx amounts tested. However, eGFP expression was detectable 72 and 96 h post-transduction without spinoculation, and efficiencies were increased 96 h

post-transduction in comparison to the 72 h time-point. In contrast, when transductions were carried out with the assistance of spinoculation, higher transduction efficiencies were achieved and MDM eGFP expression was detectable at an earlier time-point of 24 h post-transduction for all conditions tested. Therefore, although spinoculation enhanced the efficiency of transductions, this step was not required for successful transduction of MDMs with VSV-G Env/HIV-1-NL4.3-eGFP-ΔVpr pseudotyped virus.

The efficiency of MDM transductions and infections can also be enhanced by treating MDMs with SIV Vpx which downregulates SAMHD1 antiviral activity. However, SIV-Vpx is not a physiologically expressed protein during HIV-1 infection and other studies have raised concerns that SIV Vpx treatment enhances MDM recognition of viral PAMPs [209]. For this reason, I sought to determine the minimal amount of SIV-Vpx that was necessary to facilitate MDM transduction. To do this, I transduced MDMs in the presence of 0 - 50 ng per well of VSV-G/SIV-Vpx VLPs and analysed the effect of SIV-Vpx on transduction efficiency. Successful transduction in the absence of SIV-Vpx treatment was observed only in one case, at 96 h after transductions in which MDMs had been inoculated at 0.025 MOI with the assistance of spinoculation. For all other conditions investigated, it was clear that SIV-Vpx was required to facilitate MDM transduction as eGFP expression was undetectable in the absence of SIV-Vpx treatment. As shown in Figure 10A, in the absence of spinoculation MDMs treated with 10 ng of VSV-G/SIV-Vpx per well exhibited unexpectedly high transduction efficiencies (49.4, 46.8, 37.5 and 16.6 % eGFP positive cells at MOI of 0.001, 0.005, 0.025 with FCS, and 0.025 without FCS respectively) at the 96 h time-point. This observation was particularly striking as similar magnitudes of transduction efficiencies

were not obtained when MDMs were treated with greater amounts of VSV-G/SIV-Vpx VLPs. I believe this result is an anomaly as there is no biological explanation for the high transduction efficiencies observed for these conditions. Nonetheless, over the SIV-Vpx range tested in my experimental set-up, 10 ng per well was the minimal amount of VSV-G/SIV-Vpx VLPs that was needed to facilitate MDM transductions. Therefore, it was decided that future VSV-G Env/HIV-1-NL4.3-eGFP-ΔVpr pseudotyped virus transductions would include supplementation with 10 ng per well of VSV-G Env/SIV-Vpx.

To validate whether the modified MDM differentiation protocol described in section 3.3.1 enhanced pseudotyped virus transduction efficiency, I differentiated MDMs for 7 days in X-vivo$_{15}$ supplemented with 1 % HS only and inoculated these MDMs at 0.025 MOI (denoted as 'no FCS'). I compared the resulting transduction efficiencies at 24, 72 and 96 h post-transduction to that of MDMs that were differentiated by HS/FCS and transduced at the same MOI. For transductions carried out in the absence of spinoculation, both groups of MDMs expressed negligible levels of eGFP at 24 h post-transduction (Figure 10A). At 72 h, transduction efficiency was enhanced for MDMs differentiated by the modified protocol (5.3, 10.2 and 9.2% eGFP positive cells at 10, 25, 50 ng of VSV-G/SIV-Vpx treatment per well respectively) when compared to 1% HS-differentiated MDMs (0.5, 2.6 and 8.4% eGFP positive cells at 10, 25, 50 ng of VSV-G/SIV-Vpx treatment per well respectively). At 96 h, a similar trend of enhanced transduction efficiency was observed for MDMs differentiated by the modified protocol (37.4, 8.8 and 10.2 % eGFP positive cells at 10, 25, 50 ng of VSV-G/SIV-Vpx treatment per well respectively) when compared to 1 % HS-differentiated MDMs (16.6, 5.3 and 2.7 % eGFP positive cells at 10, 25, 50 ng of VSV-G /SIV-Vpx treatment

per well respectively). In contrast, when transductions were carried out with the assistance of spinoculation, the trend of enhanced transduction efficiency for MDMs differentiated by the modified protocol was apparent at all time-points analysed. At 24 h post-transduction, eGFP expression by MDMs differentiated by the modified protocol (19.9, 16.9 and 20.4 % eGFP positive cells at 10, 25, 50 ng of VSV-G/SIV-Vpx treatment per well respectively) was much higher than that of 1 % HS-differentiated MDMs (2.0, 1.5 and 3.7 % eGFP positive cells at 10, 25, 50 ng of VSV-G Env/SIV-Vpx treatment per well respectively). As shown in Figure 10, at 72 h transduction efficiency was similarly enhanced for MDMs differentiated by the modified protocol (30.5, 38.3, 39.7 % eGFP positive cells at 10, 25, 50 ng of VSV-G/SIV-Vpx treatment per well respectively) when compared to 1 % HS-differentiated MDMs (23.4, 18.6 and 24.2 % eGFP positive cells at 10, 25, 50 ng of VSV-G/SIV-Vpx treatment per well respectively). Similarly, at 96 h post-transduction MDMs differentiated by the modified protocol showed enhanced transduction efficiency (14.5, 27.8, 16.9, 17.5 % eGFP positive cells at 0, 10, 25, 50 ng of VSV-G/SIV-Vpx treatment per well respectively) when compared to 1 % HS-differentiated MDMs (1.4, 7.0, 13.2 and 10.2 % eGFP positive cells at 0, 10, 25, 50 ng of VSV-G/SIV-Vpx treatment per well respectively). Therefore, although the small sample size (n=2 independent donors) precluded statistical analysis of eGFP expression by transduced MDMs, a trend of enhanced transduction efficiency was observed for MDMs that were differentiated using HS/FCS in comparison to differentiation in 1 % HS only. Furthermore, this trend was observed regardless of whether transductions were carried out in the absence or presence of spinoculation. These observations support previously published reports that inclusion of FCS in the MDM differentiation protocol

enhances permissivity to transduction with VSV-G pseudotyped virus [208], and it was decided that future VSV-G/HIV-1-NL4.3-eGFP-ΔVpr pseudotyped virus transductions would utilise MDMs differentiated by the modified protocol. All optimised conditions for VSV-G/HIV-1-NL4.3-eGFP transductions are summarised in Table 9.

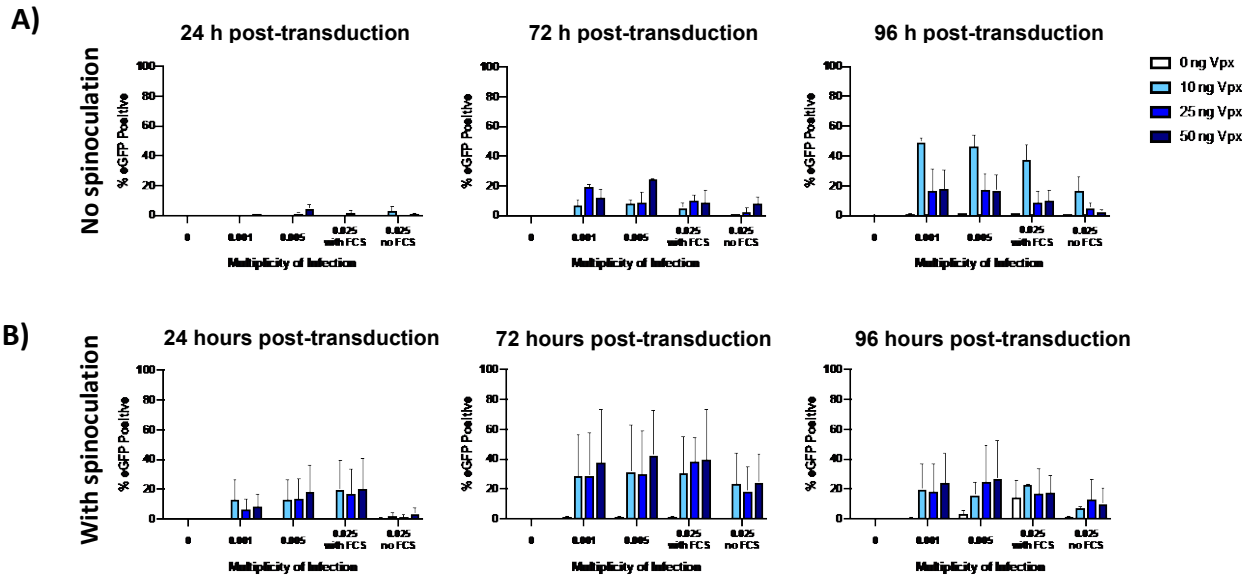


Figure 10: Optimisation of transduction protocol using VSV-G Env-NL4.3eGFP-ΔVpr pseudotyped virus

Approximately 1 x 10^6 $CD14^+$ monocytes were plated per well of a 24-well plate and differentiated by 3 days culture in X-vivo$_{15}$ supplemented with 1 % HS, followed by 4 days culture in X-vivo$_{15}$ supplemented with 10 % FCS (denoted as 'with FCS') or by culture in X-vivo$_{15}$ supplemented with 1% HS for 7 days (denoted as 'no FCS'). Differentiated MDMs were inoculated with VSV-G/HIV-NL4.3-eGFP-ΔVpr pseudotyped virus at 0 – 0.025 MOI and supplemented with 0-50 ng of SIV-Vpx virus-like particles per well. Transductions were carried out either A) without spinoculation by incubating incoculated MDMs at 37°C for 3 h; or B) with spinoculation at 1200g for 30 min and 2.5 h incubation at 37°C. Transduction efficiency was determined by flow cytometry measurement of eGFP expression by MDMs at 24, 72 and 96 h post-transduction. Error bars indicate mean with range for 2 independent donors.

3.3.4 Optimisation of MDM transduction using HIV-1$_{BaL}$ Env/HIV-1-NL4.3- ΔVpr pseudotyped virus

As discussed in section 3.3.2, the VSV-G-mediated mechanism of pseudotyped virus entry differs from that of viral particles bearing HIV-1-derived Env. It was unclear whether transduction by VSV-G pseudotyped viruses would induce different cellular activation events than those which occur in response to physiological infection and in turn, whether this would affect the profile of immune mediators expressed by MDMs transduced with VSV-G pseudotyped viruses. To establish a transduction system that more closely recapitulated the events occurring in physiological infection, I next sought to optimise a 'minimal' transduction protocol using HIV-1$_{BaL}$ Env pseudotyped viruses.

Having confirmed that MDMs differentiated by 3 days culture in X-vivo$_{15}$ supplemented with 1 % HS, followed by 4 days culture in X-vivo$_{15}$ were more permissive to transduction by HIV-NL4.3-eGFP pseudotyped virus (section 3.3.3), all MDMs used for optimisation of HIV-1$_{BaL}$ Env pseudotyped virus tranductions were differentiated by this protocol.

To optimise MOI and determine the minimal amount of SIV Vpx VLPs necessary for MDM transduction by HIV-1$_{BaL}$ Env/HIV-1-NL4.3-eGFP-ΔVpr pseudotyped virus, I transduced MDMs at an MOI range of 0-0.25 in cX-Vivo$_{15}$ supplemented with 0-50 ng per well of SIV-Vpx VLPs. Additionally, to determine whether spinoculation was required to efficiently transduce MDMs with HIV-1$_{BaL}$ Env/HIV-1-NL4.3-eGFP-ΔVpr pseudotyped virus, transductions were carried out either in the absence or presence of spinoculation as previously described.

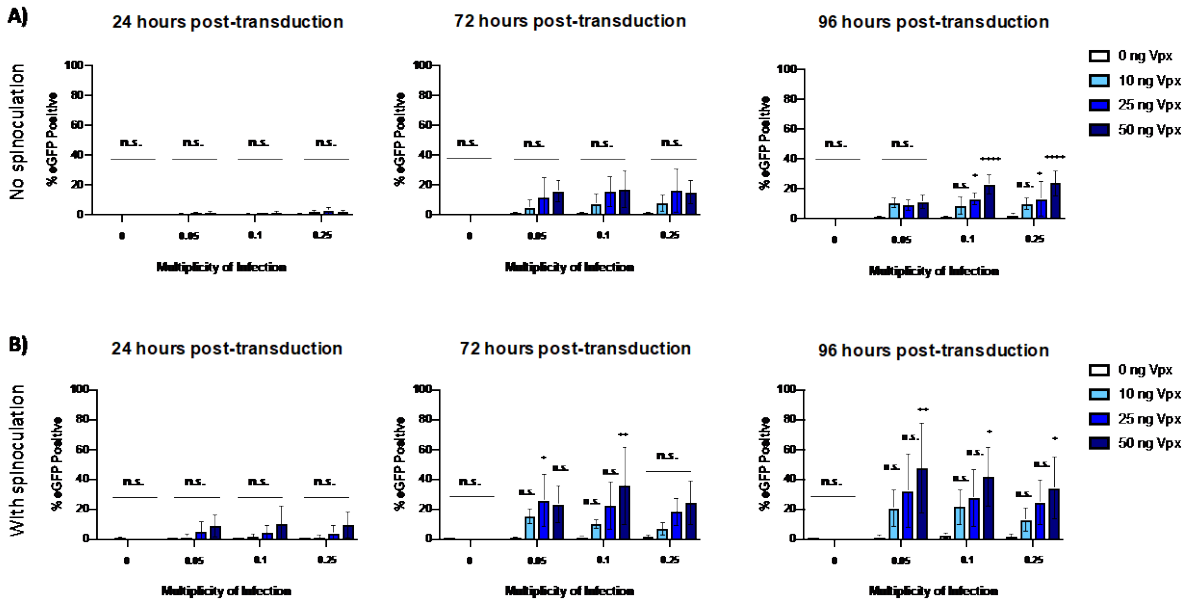


Figure 11: Optimisation of transduction protocol using HIV-1_{BaL} Env-NL4.3-eGFP-ΔVpr pseudotyped virus

Approximately 1 x 10^6 $CD14^+$ monocytes were plated per well of a 24-well plate and differentiated by 3 days culture in X-$vivo_{15}$ supplemented with 1 % HS, followed by 4 days culture in X-$vivo_{15}$ supplemented with 10 % FCS (denoted as 'with FCS') or by culture in X-$vivo_{15}$ supplemented with 1% HS for 7 days (denoted as 'no FCS'). Differentiated MDMs were inoculated with HIV-1_{BaL} Env/HIV-NL4.3-eGFP-ΔVpr pseudotyped virus at 0 – 0.25 MOI and supplemented with 0-50 ng of SIV-Vpx virus-like particles per well. Transductions were carried out either A) without spinoculation by incubating incoculated MDMs at 37°C for 3 h; or B) with spinoculation at 1200g for 30 min and 2.5 h incubation at 37°C. Transduction efficiency was determined by flow cytometry measurement of eGFP expression by MDMs at 24, 72 and 96 h post-transduction. Error bars indicate mean with SD for 3 independent donors and the effects of SIV-Vpx VLP treatment on transduction efficiency were statistically assessed by two-way ANOVA with Tukey's post-test comparison and *p < 0.05, **p<0.01, ****p<0.0001 and n.s. denotes 'not significant'.

As shown in Figure 11A and Figure 11B, eGFP expression by transduced MDMs was significantly enhanced over the control, un-inoculated (MOI = 0) MDMs for which eGFP expression was not detected, confirming that eGFP expression was a specific read-out for successful transduction by HIV-1_{BaL} Env/HIV-1-NL4.3-eGFP-ΔVpr pseudotyped virus.

Transductions carried out in the absence of spinoculation are summarised in Figure 11A. MDM eGFP expression was negligible at 24 h post-transduction, except for MDMs transduced at 0.25 MOI for which transduction efficiencies were low and ranged from 1.9 % to 2.6 %. eGFP expression increased over time and was detectable across all MOIs tested at both 72 h post-transduction. At 72 h there appeared to be a trend of enhanced transduction efficiency as SIV-Vpx VLP treatment was increased from 0 ng - 50 ng per well within each of the MOI groups, but this was not statistically significant. At the 96 h time-point for MDMs inoculated at 0.05 MOI, transduction efficiency was significantly enhanced over the untreated condition only in the presence of 50 ng SIV-Vpx VLP treatment ($p = 0.05$). For MDMs inoculated at 0.1 MOI, transduction efficiency was enhanced for MDMs treated with 25 ng ($p = 0.04$) and 50 ng SIV-Vpx VLP ($p< 0.001$) when compared to the untreated condition. For MDMs inoculated at 0.25 MOI, transduction efficiency was enhanced for MDMs treated with 25 ng ($p = 0.03$) and 50 ng SIV-Vpx VLP ($p< 0.001$) when compared to the untreated condition. Overall, these results show that in the absence of spinoculation transductions were most efficient at 0.25 MOI with 50 ng per well SIV-Vpx VLP supplementation. However, a minimum of 10 ng per well SIV-Vpx VLP was required to facilitate successful MDM transduction.

The efficiencies of transductions carried out with spinoculation are summarised in Figure 11B. At the 24 h time-point transduction efficiencies ranged from 1.3 % – 10.2 %. However, statistical analyses indicate that increasing either SIV-Vpx VLP treatment or MOI had no apparent effect on the efficiency of transductions measured at 24 h post-transduction. Notably, the transduction efficiencies observed at this time-point were higher than those observed for the respective transductions carried out in the absence of spinoculation, suggesting that spinoculation enhanced transduction efficiency.

At 72 h post-transduction, eGFP expression was detectable across all MOIs tested. For MDMs inoculated at 0.05 MOI, eGFP expression was enhanced over the untreated condition when transductions were carried out with SIV-Vpx VLP treatment of 25 ng per well ($p = 0.03$) and 50 ng per well ($p = 0.05$), but not 10 ng per well ($p = 0.3$). For MDMs inoculated at 0.1 MOI, eGFP expression was enhanced over the untreated condition when transductions were carried out with SIV-Vpx VLP treatment of 50 ng per well ($p = 0.002$), but not for 10 ng per well ($p = 0.7$) or 10 ng per well ($p = 0.08$) treatment. For MDMs inoculated at 0.25 MOI, eGFP expression was enhanced over the untreated condition only when transductions were carried out with SIV-Vpx VLP treatment of 50 ng per well ($p = 0.05$).

At 96 h post-transduction, eGFP expression was detectable across all MOIs tested. For MDMs inoculated at 0.05 MOI, eGFP expression was enhanced over the untreated condition when transductions were carried out with SIV-Vpx VLP treatment of 50 ng per well ($p = 0.02$), but not for 10 ng per well ($p = 0.4$) or 50 ng per well ($p = 0.06$). Similarly, for MDMs inoculated at 0.1 MOI, eGFP expression was enhanced over the untreated condition

when transductions were carried out with SIV-Vpx VLP treatment of 50 ng per well ($p = 0.01$), but not for 10 ng per well ($p = 0.4$) or 10 ng per well ($p = 0.2$) treatment. For MDMs inoculated at 0.25 MOI, eGFP expression was also enhanced over the untreated condition only when transductions were carried out with SIV-Vpx VLP treatment of 50 ng per well ($p = 0.04$) but not for 10 ng per well ($p = 0.8$) or 10 ng per well ($p = 0.2$) treatment.

In summary, regardless of the MOI at which MDMs were inoculated, the time elapsed post-transduction or whether transductions were carried out with the assistance of spinoculation, eGFP expression ranged only from 0 % - 2.6 % in MDMs that were inoculated without SIV-Vpx VLP treatment. Together, these results confirmed that SIV-Vpx VLP treatment was a requirement for efficient MDM transduction by HIV-1_{BaL} Env/HIV-1-NL4.3-eGFP-ΔVpr pseudotyped virus. Although the trend of enhanced transduction efficiency in response to increasing SIV-Vpx VLP treatment was not statistically significant, 10 ng SIV-Vpx VLP per was found to be sufficient to facilitate MDM transduction. Furthermore, although transduction efficiencies were strikingly enhanced with spinoculation, results in Figure 11A confirm that this step was not required to efficiently transduce MDMs and could be excluded from the 'minimal' protocol for HIV-1_{BaL} Env/HIV-1-NL4.3-eGFP transductions. Given the exclusion of spinoculation and restriction of SIV-Vpx VLPs to 10 ng per well, it was decided that the highest MOI tested (0.25) would be used for future inoculations to ensure reliable transduction of MDMs. All optimised conditions for HIV-1_{BaL} Env/HIV-1-NL4.3-eGFP transductions of MDMs are summarised in Table 9.

Table 9: Optimised conditions for MDM transductions

Factor	Original Protocol	Minimal Protocol
Amount of SIV-Vpx VLP	25 ng per well	10 ng per well
Polybrene treatment	5 µg/mL	None
MDM Inoculation	1200 *x g*, 37°C, 45 mins	No spinoculation
Incubation post-inoculation	37°C, 2 h	37°C, 3 h

3.3.5 Production and characterisation of human induced pluripotent stem cell macrophage precursors (hPSC-MPs)

Since most in-vitro models of HIV-1 macrophage infection are based on MDMs, my initial experiments to optimise the HIV-1-NL4.3-eGFP transduction protocol utilised MDMs as target cells. However, MDMs do not fully recapitulate the biology, origin and development of tissue resident macrophages as macrophages derived from infiltrating monocytes have been shown to be developmentally and transcriptionally distinct from self-renewing tissue-resident macrophages which arise from the foetal yolk sac [41]. In light of these findings, it would be important to attempt to evaluate the contribution of HIV-1-infected macrophages to the pathogenesis of HIV-1-associated inflammation using a macrophage model that is more relevant to tissue-resident macrophage biology.

To determine the utility of a human induced pluripotent stem cell-derived macrophage model, I first established a system for continuous production of hPSC-MPs following a well-established and defined protocol [232,233]. The workflow for directed differentiation of hPSCs to generate hPSC-MP factories, and subsequent differentiation of hPSC-MPs to hPSC-DMs is summarised in Figure 12.

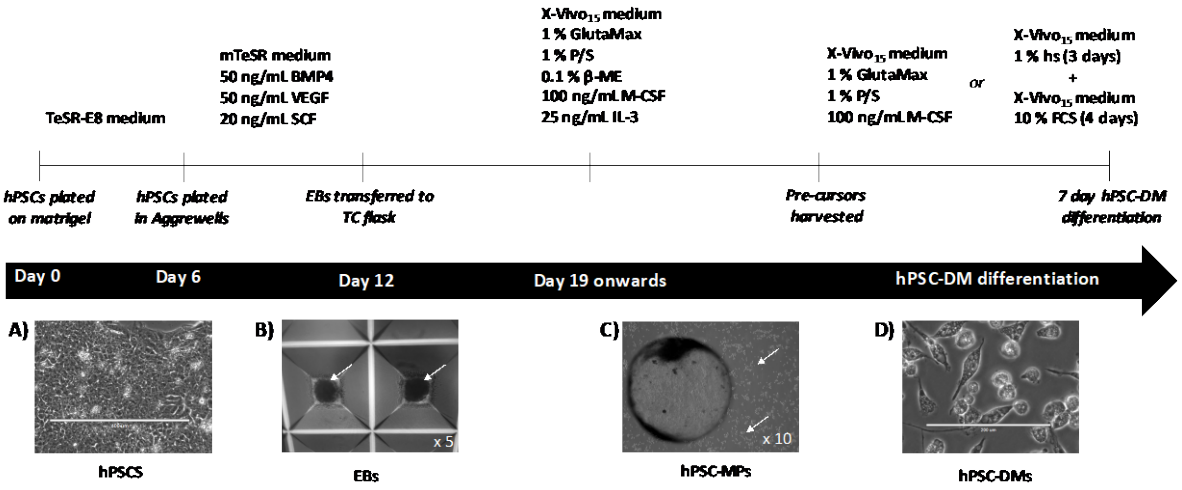


Figure 12: Schematic of directed human induced pluripotent stem cell macrophage precursor (hPSC-MP) culture and differentiation of hPSC-derived macrophages (hPSC-DMs)

A) hPSCs were plated into matrigel-coated wells of TC plates and expanded by 6 days culture in TeSR-E8 medium with a 2-fold split on day 3. B) On day 6, hPSCs were lifted, approximately 4 x 10^6 cells were evenly distributed among the microwells of an AggreWell by centrifugation at 100 x g for 3 min, and embryoid bodies were directed towards hematopoeitic differentiation by 7 days culture in the presence of 50 ng/mL BMP4, 50 ng/mL VEGF and 20 ng/mL SCF. C) On Day 12, EBs were transferred to a tissue culture flask and maintained undisturbed for 7 days in the presence of 100 ng/mL M-CSF and 25 ng/mL IL-3 to establish hPSC-MP factories. From day 19 onwards, the factories were provided with fresh medium on a weekly basis. After 4-6 weeks, the EBs were cystic in shape and continuously produced hPSC-MPs (indicated by white arrows) which were harvested from the culture supernatant. D) hPSC-MPs were differentiated to hPSC-DMs by 7 days culture in the presence of X-vivo15 supplemented with 100 ng/mL M-CSF or by 3 days culture in X-vivo15 supplemented with 1% HS followed by a media change to X-Vivo15 supplemented with 10% FCS and a further 4 days differentiation.

hPSCs obtained from the James Martin Stem Cell Facility were cultured to 90% confluency on matrigel; a mouse-sarcoma derived matrix that contains proteins and growth factors which support PSC proliferation and maintain the stem cell phenotype (Figure 12A) [234]. The hPSCs were dissociated into a single-cell suspension, and seeded into the microwells of an AggreWell 800 plate by centrifugation. By evenly distributing hPSCs among the microwells, allowing them to aggregate and to grow until they were limited by the size of the microwells, this method promoted the spontaneous formation of homogenously sized, spherical embryoid bodies (EBs) (Figure 12B).

From day 6 – 12, I cultured the EBs in the presence of bone morphogenic protein 4 (BMP4), vascular endothelial growth factor (VEGF) and stem cell factor (SCF). Together, these growth factors supported continued EB development by mimicking physiological signalling pathways and inducing patterns of gene transcription that are activated in developing mammalian embryos, and which are necessary to give rise to the ectoderm, mesoderm and endoderm layers. As demonstrated by Pick et al. using a human ES cell (hESC) differentiation system [235], BMP4 induces the transcription of the gene MIXL1 which is crucial to the development of the hematopoietic mesoderm layer. These authors also showed that VEGF drives the development of hematopoietic progenitor cells from EBs, and that culture of EBs in the presence of SCF increases the overall yield of hematopoietic cells [235].

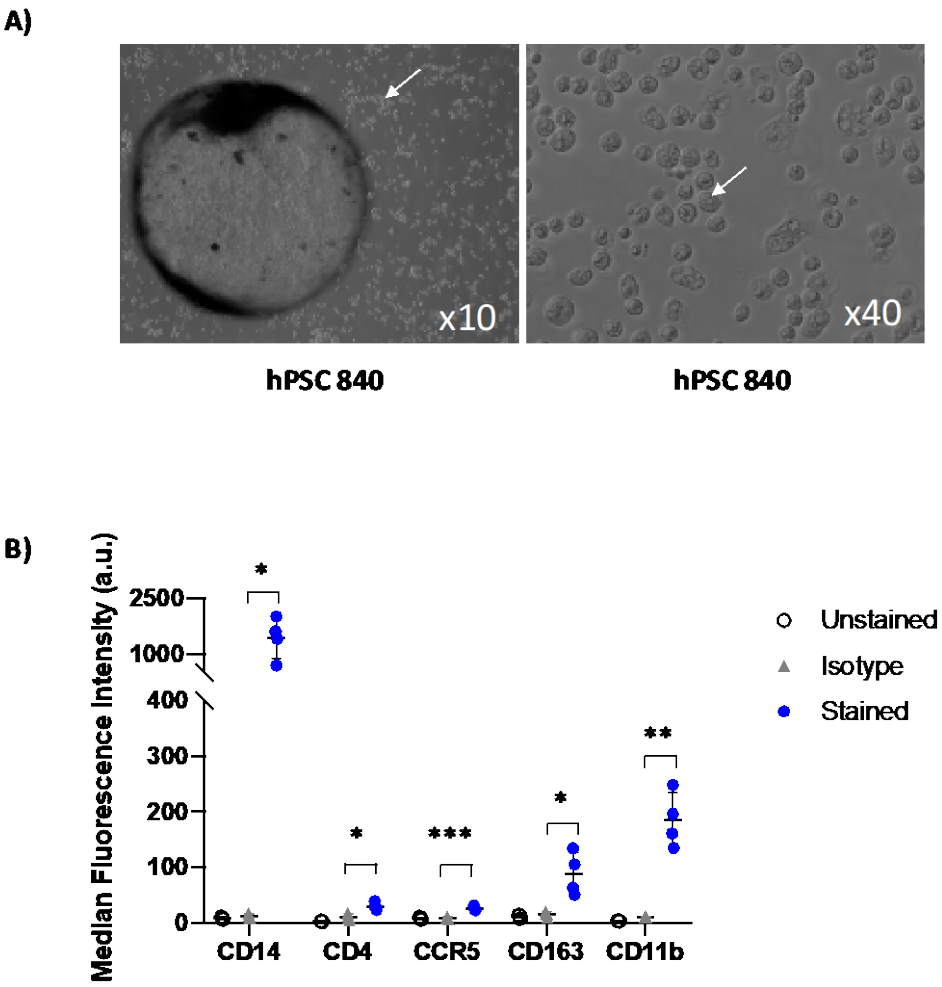


Figure 13: Characterisation of hPSC macrophage precursors (hPSC-MPs)

A) Morphology of hPSC macrophage pre-cursors was assessed by light microscopy and representative images show EBs in culture and producing hPSC-MPs (indicated by white arrows) 4-6 weeks after being transferred to tissue culture flasks. Images of the hPSC-MP cultures show one representative hPSC line at x10 and x40 magnification. B) hPSC-MP expression of the myeloid lineage cell surface markers CD14, CD163 and CD11b, the HIV-1 receptor CD4 and HIV-1 co-receptor CCR5 was assessed by flow cytometry. The dataset was analysed by Shapiro-Wilk normality testing and error bars indicate mean of M.F.I. ± SD for 4 independent hPSC lines. *p<0.05, **p<0.01, ***p<0.001 and n.s. denotes 'not significant' for paired t-test comparison of mean M.F.I. versus the isotype control.

After 7 days culture (cumulative day 12) in the presence of the growth factors, I harvested the EBs and transferred them to a TC flask where they were maintained undisturbed in factory medium (FM) containing M-CSF and IL-3 for a further 7 days to stimulate myeloid differentiation. During this period, the majority of EBs increased in size and began to take on a balloon-like cystic appearance. Although a small number of EBs remained floating in the culture medium, the majority became attached to the bottom of the TC flask by a layer of outgrowth cells which sprouted from the bottom of the EBs.

From day 19 onwards, the EBs cultures were supplemented with additional fresh factory medium on a weekly basis to support myeloid differentiation and establish the hPSC-MP factories. As shown in Figure 13A, within 4-6 weeks the cystic EBs began to continuously produce hPSC-MPs which were visible as large, round cells with a large cytoplasmic volume and some degree of membrane ruffling. To validate the myeloid lineage of the hPSC-MPs, I harvested the cells from the culture supernatants and analysed cell surface expression of CD14, CD163 and CD11b. As shown in Figure 13B, flow cytometry analysis indicated that hPSC-MPs expressed high levels of CD14 ($p = 0.01$), CD11b ($p = 0.006$) and CD163 ($p = 0.03$). The HIV-1 receptor CD4 ($p = 0.04$) and co-receptor CCR5 ($p = 0.006$) were also expressed, but at low levels. These data confirmed that I had established a system for continuously producing hPSC-MPs which exhibited a monocyte-like morphology and expressed high levels of the myeloid lineage marker CD14, but low expression of the HIV-1 receptor CD4 and HIV-1 co-receptor CCR5 which corroborated with previously published accounts of hPSC-MP culture [233].

3.3.6 Directed differentiation and characterisation of hPSC-derived macrophages (hPSC-DMs)

To examine the potential of using an hPSC-DM model for investigating the inflammatory responses of tissue resident-like macrophages, I generated hPSC-DMs according to a well-established protocol [232,233] that utilises M-CSF to stimulate differentiation. I also generated hPSC-DMs according to the modified protocol that was used in section 3.3.1 to differentiate MDMs, and which utilises a combination of HS and FCS to facilitate differentiation; the latter of which has been reported to enhance permissivity to HIV-1-transduction [208]. I then compared the morphologies and patterns of hPSC-DM cell surface marker expression that resulted from each differentiation method.

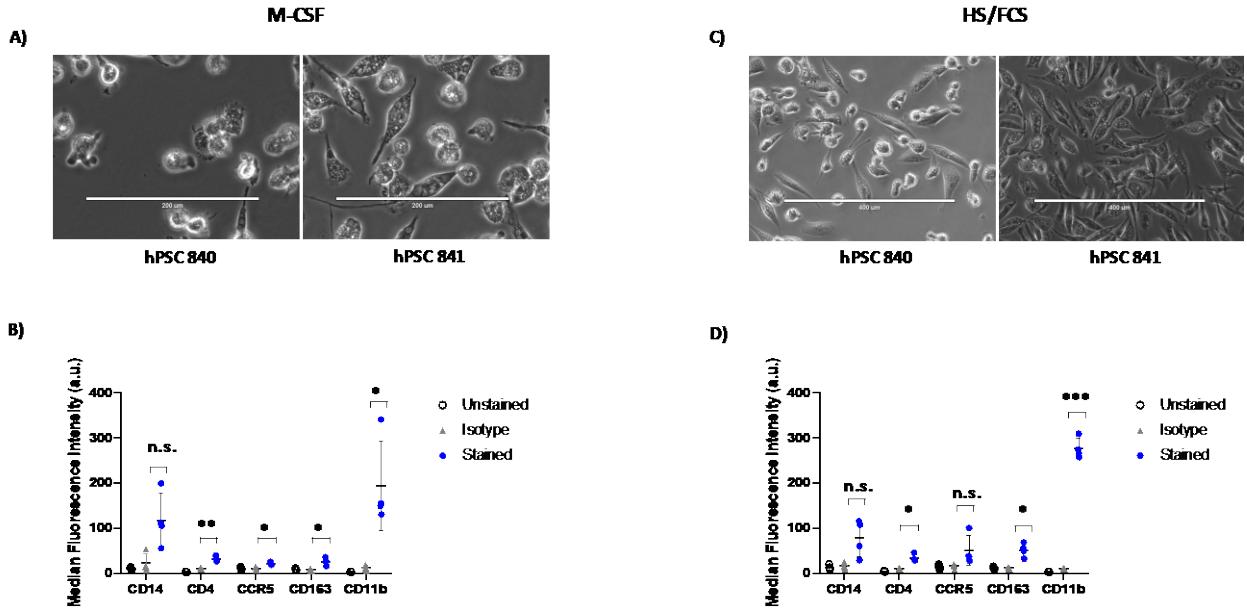


Figure 14: Characterisation of hPSC-DMs

Morphology of hPSC-DMs was assessed by light microscopy and representative images show A) hPSC-DMs differentiated by 7 days culture in the presence of X-vivo$_{15}$ supplemented with 100 ng/mL M-CSF (scale bar = 200 µm) and C) hPSC-DMs differentiated by 3 days culture in X-vivo$_{15}$ supplemented with 1% HS followed by a media change to X-Vivo$_{15}$ supplemented with 10% FCS and a further 4 days differentiation (scale bars = 400 µm). Two representative hPSC lines are shown for each hPSC-DM differentiation protocol. Expression of the myeloid lineage cell surface markers CD14, CD163 and CD11b, the HIV-1 receptor CD4 and HIV-1 co-receptor CCR5 was assessed by flow cytometry for B) hPSC-DMs differentiated by 7 days culture in the presence of X-vivo$_{15}$ supplemented with 100 ng/mL M-CSF; and D) hPSC-DMs differentiated by 3 days culture in X-vivo$_{15}$ supplemented with 1% HS followed by a media change to X-Vivo$_{15}$ supplemented with 10% FCS and a further 4 days differentiation. The dataset was analysed by Shapiro-Wilk normality testing and error bars indicate mean of M.F.I. $\pm$ SD for 4 independent hPSC lines. For each marker, the mean M.F.I was statistically assessed versus the isotype control by paired t-tests and differences in M.F.I. between HS/FCS differentiated hPSC-DMs and M-CSF differentiated hPSC-DMs were assessed by multiple

comparison t-tests with Holm-Sidak post-test correction of p-values. *p<0.05, **p<0.01, ***p<0.001 and n.s. denotes 'not significant'.

Regardless of the method employed, hPSC-DM differentiation generated a population of adherent cells with a mixture of elongated, spindle-like morphology and round, 'fried-egg' morphology (Figure 14A and Figure 14C). Flow cytometry analysis of myeloid lineage markers in Figure 14B indicate low CD163 expression ($p = 0.03$), high CD11b expression ($p = 0.04$) and a trend towards high CD14 expression ($p = 0.07$) by M-CSF-differentiated hPSC-DMs. Additionally, M-CSF-differentiated hPSC-DMs expressed low levels of the HIV-1 receptor CD4 ($p = 0.005$) and co-receptor CCR5 ($p = 0.01$). Similarly, flow cytometry analysis of the HS/FCS differentiated hPSC-DMs in Figure 14D confirmed CD163 expression ($p = 0.01$), high levels of CD11b expression ($p = 0.002$) and a trend towards high CD14 expression ($p = 0.05$). HS/FCS-differentiated hPSC-DMs expressed low levels of CD4 ($p = 0.01$) and CCR5 ($p = 0.1$). CD163 and CCR5 expression by HS/FCS-differentiated hPSC-DMs appeared to be greater than that observed for M-CSF-differentiated hPSC-DMs, but this observation was not statistically significant (Holm-Sidak adjusted $p = 0.1$ and $p = 0.4$ respectively). Furthermore, there was no significant difference in the expression of CD14, CD4 and CD11b when the two hPSC-DM groups were compared (Holm-Sidak adjusted $p = 0.5$, $p = 0.6$ and $p = 0.4$ respectively).

These data confirmed that morphologically similar hPSC-DMs could be differentiated from hPSC-MPs using either M-CSF or a combination of 1 % HS and 10 % FCS. Furthermore, although expression of CD163 and CCR5 appeared to be increased in hPSC-DMs differentiated by HS/FCS, these observations were not statistically significant. Therefore,

the hPSC-DM method employed had no differential effect on expression of myeloid markers, nor on expression of CD4 and CCR5.

*3.3.7 Optimisation of hPSC-DM transduction using HIV-1$_{BaL}$ Env/HIV-1-NL4.3-eGFP-**ΔVpr** pseudotyped virus*

As I was interested in using hPSC-DMs as a model for investigating the inflammatory responses of HIV-1-transduced tissue resident-like macrophages, I next sought to optimise a protocol for transducing hPSC-DMs with HIV-1$_{BaL}$ / HIV-1-NL4.3eGFP-ΔVpr pseudotyped virus. Given that differentiation of MDMs in HS/FCS enhances efficiency of HIV-1 transduction, it was unclear whether the hPSC-DM differentiation method would affect the efficiency of transduction with HIV-1$_{BaL}$ / HIV-1-NL4.3eGFP-ΔVpr pseudotyped virus. Therefore, I differentiated hPSC-DMs by both methods described in section 3.3.6, transduced the hPSC-DMs with HIV-1$_{BaL}$ / HIV-1-NL4.3eGFP-ΔVpr pseudotyped virus at 0 – 0.5 MOI and compared the effect of each differentiation protocol and MOI on the efficiency of transduction.

Having confirmed in section 3.3.4 that MDMs could be efficiently transduced by HIV-1$_{BaL}$ Env pseudotyped virus in the absence of spinoculation and with a minimum of 10 ng SIV-Vpx VLP per well, all transduction optimisation experiments detailed in this section were carried out according to the 'minimal' protocol outlined in Table 9.

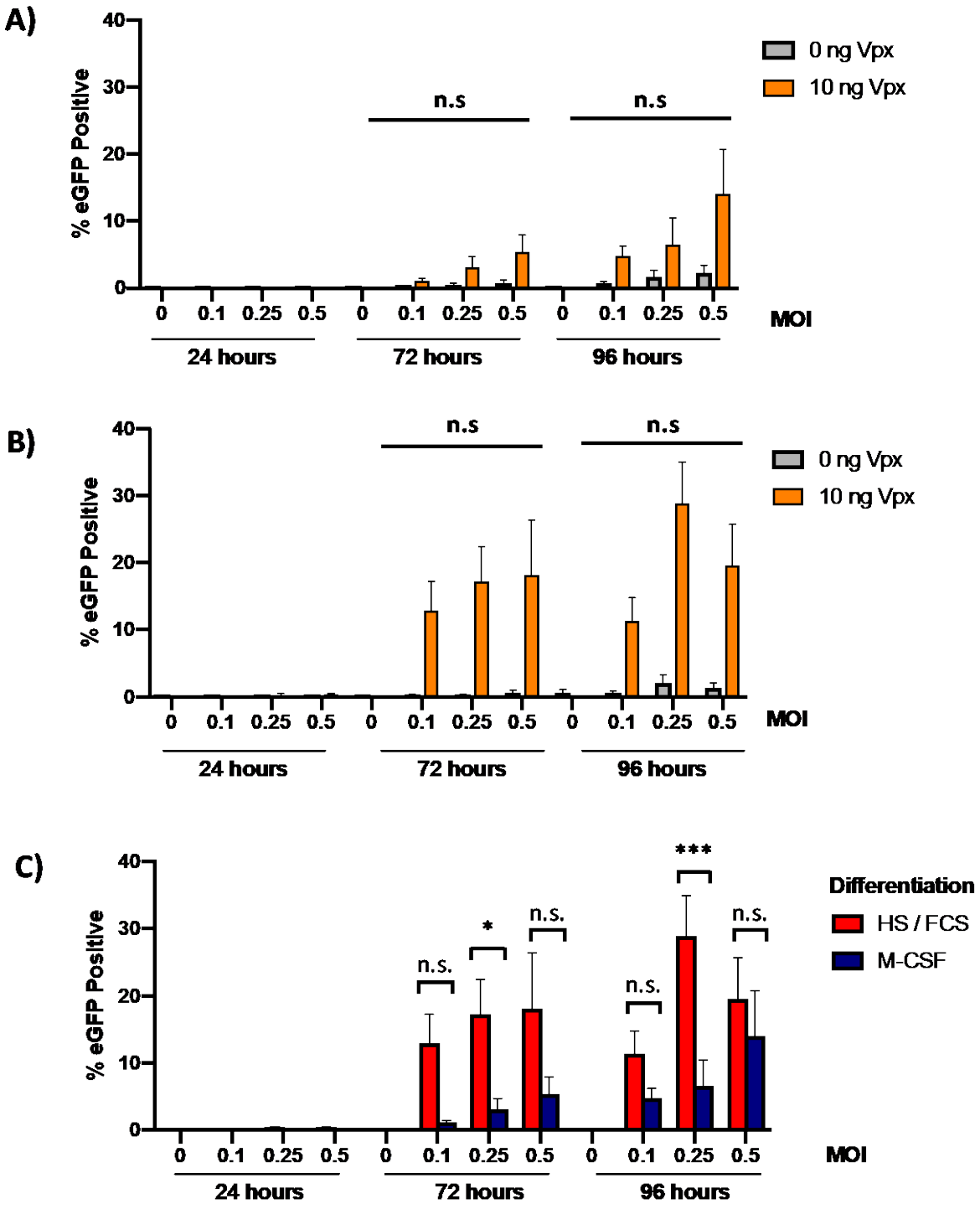


Figure 15: Optimisation of hPSC-DM transduction using HIV-1BaL Env-NL4.3-eGFP-ΔVpr pseudotyped virus

Approximately 2.5 x 10^5 hPSC macrophage precursors were plated per well of a 24-well TC plate and differentiated to hPSC-DMs by (A) 7 days culture in the presence of X-vivo$_{15}$ supplemented with 100 ng/mL M-CSF; or B) 3 days culture in X-vivo$_{15}$ supplemented with 1 % HS followed by a media change to X-Vivo$_{15}$ supplemented with 10 % FCS and a further 4 days differentiation. Differentiated hPSC-DMs were inoculated with HIV-1$_{BaL}$ Env/HIV-NL4.3-eGFP-ΔVpr pseudotyped virus at 0 – 0.5 MOI either in the presence or absence of supplementation with 10ng of SIV-Vpx virus-like particles per well, and incubated 37°C for 3 h followed by a media change to cX-Vivo$_{15}$. Transduction efficiency was determined by flow cytometry measurement of eGFP expression by MDMs at 24, 72 and 96 h post-transduction. The dataset was analysed by Shapiro-Wilk normality testing and error bars indicate S.E.M. with mean for 4 independent hPSC lines. The effects of MOI and differentiation methods on transduction efficiency were statistically assessed by two-way ANOVA with Tukey's post-test comparison.

I transduced hPSC-DMs at an MOI range of 0 – 0.5 either in the presence or absence of 10 ng per well of SIV-Vpx VLPs. As expected, eGFP expression was only detected for hPSC-DMs that were inoculated and transduced, whereas eGFP expression was not detected for un-inoculated hPSC-DMs (Figure 15A and B) confirming that eGFP expression was a specific read-out for successful hPSC-DM transduction by HIV-1$_{BaL}$ Env/HIV-1-NL4.3-eGFP-ΔVpr pseudotyped virus. Regardless of the hPSC-DM differentiation method used, eGFP expression was largely undetectable when transductions were carried out without SIV-Vpx VLP co-treatment, indicating that downregulation of SAMHD1 activity by SIV-Vpx was necessary for efficient transduction of hPSC-DMs.

Transduction efficiencies for M-CSF differentiated hPSC-DMs are summarised in Figure 15A. hPSC-DM eGFP expression was neither detectable at 24 h nor at 72 h post-transduction except for MDMs transduced at 0.25 and 0.5 MOI for which the mean

transduction efficiencies were 3.1 % and 5.4 % respectively. At 96 h post-transduction, eGFP expression increased and was detectable across all MOIs tested. A non-significant trend in increasing transduction efficiency with MOI was observed at 96 h with hPSC-DMs inoculated at MOIs of 0.1, 0.25 and 0.5 being 4.8 %, 6.5 % and 14 % eGFP positive respectively.

Transduction efficiencies for HS/FCS-differentiated hPSC-DMs are summarised in Figure 15B. eGFP expression by HS/FCS-differentiated hPSC-DMs was undetectable at 24 h. However, eGFP expression increased from 72 h and 96 h post-transduction and was detectable across all MOIs tested at these time points. At 72 h post-transduction, eGFP expression appeared to increase in response to increasing MOI from 0.1 – 0.5, however this trend did not approach statistical significance. At 72 h post-transduction, HS/FCS-differentiated hPSC-DMs inoculated at MOIs of 0.1, 0.25 and 0.5 were 12.9 %, 17.2 % and 18.1 % eGFP positive respectively, whereas the M-CSF-differentiated hPSC-DMs were 1.2%, 3.1 % and 5.4 % at the same MOIs. These differences suggest an enhanced transduction efficiency for HS/FCS-differentiated hPSC-DMs at 72 h post-transduction. A similar trend of enhanced transduction efficiency was observed at 96 h post-transduction at which HS/FCS-differentiated hPSC-DMs inoculated at MOIs of 0.1, 0.25 and 0.5 were 11.4 %, 28.9 % and 19.6 % eGFP positive respectively. In comparison, M-CSF-differentiated hPSC-DMs were 4.8 %, 6.5 % and 14 % eGFP positive at the same MOIs. However, it is unclear whether HS/FCS differentiation truly enhanced transduction efficiency as statistical comparison of the transduction efficiencies in Figure 15C highlights that this trend only approached significance for the hPSC-DMs that were inoculated at 0.25 MOI.

Together, these results confirm that hPSCs are permissive to transduction by HIV-1_{BaL} Env/NL4.3-ΔVpr pseudotyped virus without the assistance of polybrene treatment or spinoculation, and suggest that hPSC-DM differentiation with HS/FCS may enhance transduction efficiency. These data also suggest that HS/FCS-differentiation of hPSC-DMs is not sufficient to overcome the requirement for SIV-Vpx treatment for efficient transduction of hPSC-DMs. However, further analysis of the effect of HS/FCS differentiation SAMHD1 phosphorylation at T592 in hPSC-DMs would be required to confirm that the HS/FCS differentiation protocol enhances hPSC-DM transduction efficiency by downregulating SAMHD1 activity.

3.3.8 Validation of single-cycle HIV-1-NL4.3eGFP-Vpr$^+$ pseudotyped virus

A major aim of this study was to investigate the effect of HIV-1 Vpr on macrophage responses to HIV-1 by comparing the profile of soluble immune mediators expressed by macrophages transduced with NL4.3-eGFP-ΔVpr and NL4.3-eGFP-Vpr$^+$ pseudotyped viruses. As discussed in section 3.3.2, I first attempted to generate HIV-1-NL4.3-eGFP-Vpr$^+$ pseudotyped virus for this purpose by co-transfecting HEK293Ts with separate plasmids encoding the HIV-1-NL4.3-eGFP-ΔVpr backbone, HIV-1 Vpr and either VSV-G or HIV-1_{BaL} Env. However, all attempts at generating viable HIV-1-NL4.3-eGFP-Vpr$^+$ pseudotyped virus by this approach were unsuccessful as the resulting pseudotyped virus stocks were not capable of transducing the TZM-bl reporter cell line (Figure 9).

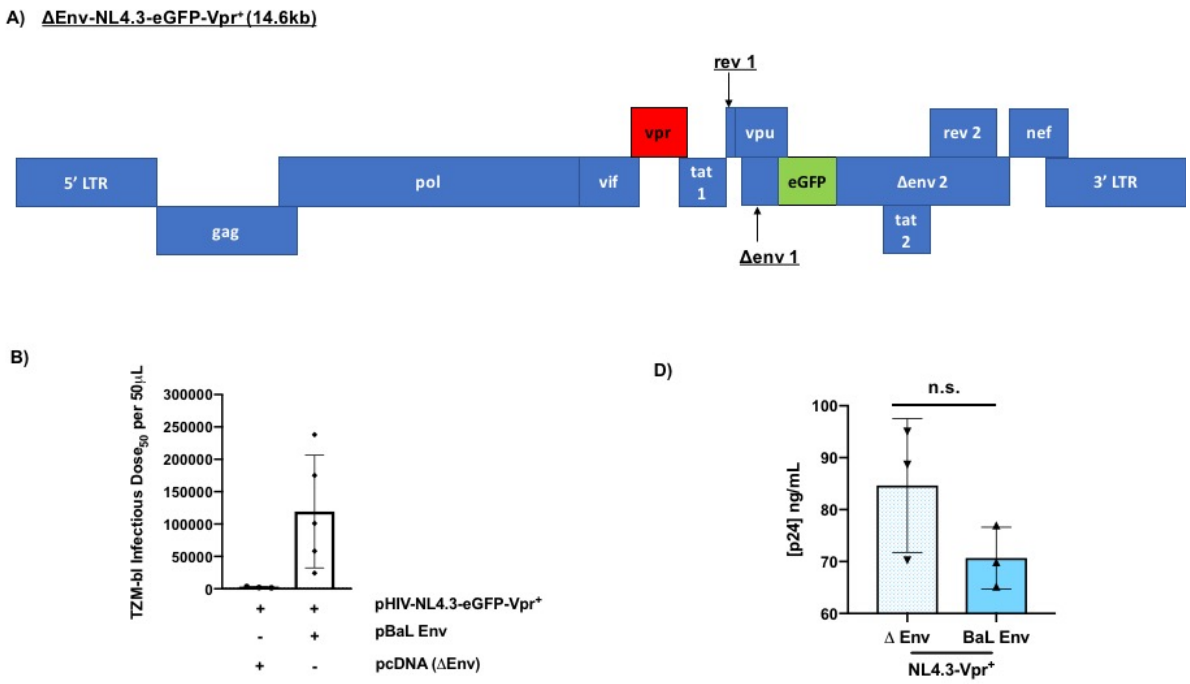


Figure 16: Optimisation of single cycle HIV-1-NL4.3-eGFP-Vpr$^+$ pseudotyped virus production

A) Enhanced green fluorescent protein (eGFP)-tagged reporter vectors were derived from the HIV-1 clone NL4-3. The HIV-1-NL4.3-eGFP-Vpr+ expression vector, the eGFP sequence has been inserted into the env open reading frame and resulting vectors express a truncated env-eGFP fusion protein with a non-functional env domain. B) Co-transfection of expression plasmids encoding the NL4.3eGFP-Vpr$^+$ backbone with HIV-1 BaL envelope (CCR5 tropic) resulted in the production of vectors that appreciably transduced the TZM-bl reporter cell line. Error bars represent mean$\pm$ S.D. for 3 representative preparations of vector. C) HIV-1 p24 Ag content was determined by ELISA for both Delta Env and HIV-1$_{BaL}$ Env versions of NL4.3-Vpr$^+$pseudotyped viruses. Error bars indicate mean [p24] $\pm$ S.D. for 3 representative vector preparations. The dataset was analysed by Shapiro-Wilk normality testing and one way ANOVA with Sidak's post-test comparison. **p < 0.01 and n.s. denotes 'not significant'.

To address this issue, I obtained an alternative HIV-1-NL4.3-eGFP expression plasmid (represented in Figure 16A) in which the Vpr ORF was not mutated and the eGFP sequence had been inserted into the *env* ORF. As a result, pseudotyped viruses produced using this plasmid express a truncated Env-eGFP fusion protein with a non-functional Env domain, and are competent for HIV-1 Vpr expression [193]. I generated pseudotyped virus stocks by co-transfecting HEK293Ts with expression plasmids encoding the HIV-1-NL4.3-eGFP-Vpr$^+$ backbone and HIV-1_{BaL} Env, and determined the ID_{50} of the resulting pseudotyped virus stocks using the TZM-bl reporter cell line. As shown in Figure 16B, using the HIV-1-NL4.3-eGFP-Vpr$^+$ backbone I was able to generate vectors of appreciable titres that were capable of efficiently transducing the TZM-bl reporter cell line and therefore suitable for macrophage transductions. ΔEnv / NL4.3-eGFP-Vpr$^+$ pseudotyped virus stocks were generated by transient co-transfection of HEK293Ts with HIV-1-NL4.3-eGFP-Vpr$^+$ expression plasmids and a pcDNA control plasmid. The resulting ΔEnv / NL4.3-eGFP-Vpr$^+$ pseudotyped viruses were not capable of transducing the TZM-bl reporter cell line (Figure 16B) and there was no significant difference in HIV-1 p24 Ag content of the Delta Env and HIV-1_{BaL} Env versions of the NL4.3-Vpr$^+$ pseudotyped virus (Figure 16C). Together, these results confirm their suitability as matched control pseudotyped virus. In the subsequent chapters of this thesis, I will detail the work done using these NL4.3-eGFP-Vpr$^+$ pseudotyped viruses together with the previously described NL4.3-eGFP-ΔVpr pseudotyped viruses to assess the effect of HIV-1 Vpr expression on the secreted proteome of HIV-1-transduced MDMs.

3.4 Discussion

The low permissivity of myeloid cells to *in vitro* HIV-1 infection and transduction presents a challenge to investigating HIV-1-induced immune responses in macrophages. MDM differentiation in the presence of FCS was recently shown by Mlcochova et al to facilitate HIV-1 infection and transduction by promoting CDK1-mediated deactivation of SAMHD1 antiviral activity [208]. Therefore, the MDMs used in this study were differentiated by culture for 3 days in medium supplemented with 1 % HS followed by a further 4 days culture in medium supplemented with 10 % FCS. Notably, the differentiation protocol used in this study exposed MDMs to FCS for fewer days than the protocol employed by Mlcochova et al in which MDM were differentiated by 3 days culture in medium supplemented with M-CSF and 10% FCS followed by a further 4 days culture in medium supplemented with 10 % FCS. However, in their report, Mlcochova et al confirm that expression of cell surface markers of macrophage polarisation was not dependent on the inclusion of FCS in the MDM protocol. Furthermore, MDMs in my study exhibited typical macrophage morphology, LPS-induced IL-6 and TNF-α production [223-225], and similar CD163 and CD14 expression as that observed by Mlcochova et al. Therefore, it was unlikely that the modified protocol used in this study affected MDM phenotype.

A limitation of pseudotyped virus production was the inability to generate isogenic NL4.3-eGFP-Vpr^{+} pseudotyped virus by transient co-transfection of HEK293Ts with expression plasmids for the HIV-1 NL4.3-eGFP-ΔVpr backbone, HIV-1 Vpr, and either VSV-G *env* or HIV-1_{BaL} *env*. Instead, I utilised an alternative NL4.3-eGFP backbone in which the Vpr ORF was not mutated and for which co-transfection of pHIV-1 Vpr was not required to

produce NL4.3-eGFP-Vpr^{+} pseudotyped virus. HIV-1 particle release is mediated by direct interactions between the C-terminal p6 domain of Gag and the cellular endosomal sorting complex required for transport (ESCRT) machinery [236]. Notably, HIV-1 Vpr is incorporated into progeny virus particles via direct interaction between the same p6 domain of the Gag polyprotein [237,238]. Therefore, it is possible that over-incorporation of HIV-1 Vpr due to expression from an extrinsic *vpr* plasmid may have negatively affected Gag function and thereby inhibited the assembly and/or release of infectious, mature pseudotyped virus. It is unlikely that HIV-1 Vpr has a negative effect on the HIV-1 LTR promoter as HIV-1 Vpr is highly conserved across different primate lentiviruses and an early study by Agostini et al suggests that expression of HIV-1 Vpr enhances HIV-1 LTR transcriptional activity [239]. However, HIV-1 Vpr is known to suppress the transcriptional activity of the cytomegalovirus (CMV) promoter [240]. Therefore, suppression of the CMV promoter present in the HIV-1_{BaL} *env* expression plasmid may explain why co-transfection with the *vpr* plasmid markedly diminished production of infectious pseudotyped virus.

Another challenge to pseudotyped virus production was batch-to-batch variation in the pseudotyped virus TC ID_{50} titres. Decreased efficiency of transient transfection may occur due to a variety of factors including poor viability of producer cells, sub-optimal producer cell density, incubation of producer cells in serum-supplemented media during transfection, prolonged time elapsed between transfection and supernatant harvest, and variations in the PEI : DNA ratio [241-243]. However, I routinely passaged HEK293T producer cells at 2 day intervals to maintain the cells at exponential growth phase and carried out transfections using FCS- and P/S-free media. Furthermore, the same co-

transfection protocol was used to produce each batch of pseudotyped virus and I collected HEK293T supernatants at 48 h post-transfection, which is within the recommended time-frame for pseudotyped virus harvesting. It is therefore unclear which factors contributed to the observed batch-to-batch variation in pseudotyped virus titers. However, to account for variation in the ID_{50} titres, MDMs were inoculated at standardized multiplicities of infection for transduction experiments.

Enhancing the permissivity of MDMs to HIV-1 by HS/FCS differentiation enabled me to eliminate the requirement for polybrene treatment and spinoculation for efficient transduction of MDMs using both VSV-G Env and HIV-1_{BaL} Env pseudotyped virus. In contrast to other studies, my experimental approach also emphasized the use of a low MOI for transductions. Under these minimal transduction conditions, it was not possible to efficiently transduce MDMs without SIV Vpx supplementation. The requirement of Vpx supplementation for efficient MDM transduction is a limitation of this study as Vpx is not expressed during normal HIV-1 infection. Furthermore, other authors have suggested that Vpx not only downregulates SAMHD1 activity, but may also enhance MDM recognition of viral PAMPs and thereby confound studies of innate responses to HIV-1 [209]. To reduce any potential confounding effects of SIV Vpx on macrophage activation, a minimal amount of SIV Vpx VLPs was used for all transduction experiments. Nevertheless, I cannot rule out that Vpx may have influenced some of the findings I report in later chapters.

This chapter details the application of a feeder and serum-free protocol [233] to generate hPSC-MPs and differentiated these precursor cells to hPSC-DMs using M-CSF. In agreement with previous reports [216,219,233] my analyses of myeloid lineage marker expression

confirmed CD14, CD11b and CD163 expression by the hPSC-MPs and hPSC-DMs generated in this study. The low CD4 and moderate CCR5 expression by hPSC-MPs and hPSC-DMs observed in my study has also been previously reported [233] and does not appear to inhibit HIV-1 transduction of hPSC-DMs.

In addition to the traditional M-CSF directed differentiation of hPSC-DMs, I also differentiated hPSC-DMs using HS/FCS and characterised the resulting phenotype. I found that HS/FCS differentiated hPSC-DMs were similar to M-CSF differentiated hPSC-DMs in terms of morphology and cell surface marker expression. However, HS/FCS-derived hPSC-DMs showed a trend of enhanced permissivity to HIV-1_{BaL} / NL4.3 transduction. Furthermore, in contrast to previous studies of HIV-1 transduction of hPSCs [220,233], I was able to efficiently transduce HS/FCS differentiated hPSC-DMs using HIV-1_{BaL} pseudotyped virus and without the assistance of polybrene treatment or spinoculation. These observations suggest that FCS-differentiation may induce CDK1-mediated downregulation of SAMHD1 antiviral activity in hPSC-DMs as has been previously reported with MDMs [208]. Thus the use of FCS and its effects on SAMHD1 must also be taken into account in this study.

Other authors have demonstrated that hPSC-DMs develop independently of regulation by the transcription factor MYB and therefore recapitulate an embryonic ontogeny similar to that of tissue-resident-like macrophages [214]. Furthermore, Mlcochova et al have confirmed that, similar to FCS-differentiated MDMs, populations of murine tissue-resident macrophages are maintained in a G1-like phase of the cell cycle and exhibit enhanced permissivity to transduction with VSV-G-pseudotyped HIV-1 [208]. Therefore, an

interesting but unanswered question that arises, is whether differentiating hPSC-DMs using HS/FCS instead of M-CSF enhances their relevance as a model for investigating tissue-resident macrophage responses to HIV-1. In order to resolve this question, it will be necessary to conduct further studies to confirm whether the G1-like state and SAMHD1 inactivation induced in FCS-differentiated MDMs is recapitulated in the HS/FCS-differentiated hPSC-DMs.

3.5 Conclusion

Through the work presented in this chapter, I established and validated a panel of single-cycle eGFP-tagged HIV-1 NL4.3 pseudotyped viruses that will be used to investigate the pro-inflammatory responses of macrophages to HIV-1. This panel features pseudotyped viruses that are either competent or deficient for HIV-1 Vpr expression and therefore will also be used to investigate how macrophage responses to HIV-1 are modulated by expression of the accessory protein.

To circumvent macrophage restriction of HIV-1, I applied a HS/FCS differentiation protocol to generate MDMs from $CD14^+$ monocytes. I show that these MDMs exhibit characteristic macrophage morphology, myeloid marker expression, CD4 and CCR5 expression, and LPS-induced inflammatory responses. Using both VSV-G and HIV-1_{BaL} Env pseudotyped viruses, I confirmed that HS/FCS differentiated MDMs are permissive to HIV-1 NL4.3-eGFP transduction, can be transduced without the assistance of polybrene or spinoculation, and require reduced SIV Vpx supplementation to facilitate efficient transduction.

In order to extend investigations of HIV-1 NL4.3-induced macrophage responses to a tissue-resident macrophage relevant model, I applied a feeder and serum-free protocol to establish a culture system for long-term production of hPSC-MPs, and differentiated these precursor cells to hPSC-DMs. As with MDMs, I confirmed that these hPSC-DMs exhibit characteristic macrophage morphology and expression profiles for myeloid markers, CD4 and CCR5. Using HIV-1_{BaL} Env pseudotyped viruses, I also confirmed that hPSC-DMs are conducive to HIV-1 NL4.3-eGFP transduction in the absence of spinoculation and polybrene treatment, but require SIV Vpx supplementation to facilitate efficient transduction. Lastly,

my experiments provide initial evidence to suggest that HS/FCS-differentiated hPSC-DMs exhibit enhanced permissivity to HIV-1 in comparison to M-CSF differentiated hPSC-DMs.

Chapter 4:

Analysis of macrophage immune mediators induced by HIV-1 and modulated by HIV-1 Vpr expression

4.1 Introduction

An HIV-1 accessory factor that is currently under intense scrutiny is Vpr. The *vpr* open reading frame is conserved in all human and primate immunodeficiency viruses, and encodes the Vpr protein of 96 amino acids that is encapsidated at relatively high copy number into the viral particle [244]. Amongst its functions, Vpr is reported to cause cell-cycle arrest, target enzymes involved in DNA repair pathways, modulate host cell apoptosis, influence nuclear import, and promote macrophage infection [245-247]. Current interest in the role of macrophages as HIV-1 tissue reservoirs [248] and as mediators of inflammation even under antiretroviral therapy [121,133,134] makes the role of Vpr in these cells of particular importance. Vpr expression facilitates HIV-1 replication in macrophages [249,250] and DC [251], with generally less striking effects in T cells [251,252].

Recognition of HIV-1 by the innate immune system induces the expression of cytokines and other soluble mediators of inflammation early on in HIV-1 infection [94]. The synthesis of type-I interferons (IFN-α /IFN-β) in response to viral infection is well documented [253-255] and plays a role in promoting inflammation in this context. Newly synthesised IFN-α /IFN-β signal through a common heterodimeric IFN receptor to activate signal transduction pathways that culminate in the transcriptional activation of genes that possess an interferon stimulated response element (ISRE) [256,257]. The products of these genes include cytokines, chemokines and proteins such as MxA, ISG15 and OAS which are integral components of antiviral pathways [9]. In this way, production of type-I IFNs not only contributes to protective antiviral mechanisms, but also leads to the induction of

pro-inflammatory cytokines, chemokines and other important mediators of the innate immune response.

One facet of Vpr function is the modulation of immune pathways associated with IFN-stimulated gene expression. In particular, Vpr was reported to promote release of pro-inflammatory cytokines IL-8 [258] and TNFα [259], with implications for viral replication and pathogenesis. Vpr was recently proposed to downmodulate type-I interferon (IFN-I) responses [11,260] via regulation of the DNA metabolism complex SLX4 [5]. However, others have found conflicting results. Zahoor et al expressed Vpr from an adenoviral vector and observed enhanced IFN-I signatures in MDMs [10] and myeloid-derived DCs [8]. Similarly, Vermeire et al reported that HIV-1-expressed Vpr amplified IFN-I responses in $CD4^+$ T cells [9]. Thus, the picture that emerges is complex and does not allow us to assign a clear role for Vpr function.

4.2 Chapter rationale

Previous studies have attempted to elucidate the immunomodulatory effects of HIV-1 Vpr by analysing transcriptomic changes in response to HIV-1 Vpr expression in MDM [10,261], monocyte-derived DC [8,261] and $CD4^+$ T-cells [9]. However, the effect of HIV-1 Vpr on MDM-expressed mediators of the immune response has not been thoroughly characterised at the protein level and it is unclear whether Vpr expression also affects the production of immune mediators that are post-transcriptionally modulated (e.g. IL-1β and IL-18). To address this gap in the literature, I aimed to:

I. Investigate the effect of HIV-1 Vpr expression on MDM transduction efficiency
II. Compare the profile of inflammatory factors expressed by MDMs after transduction with HIV-1 NL4.3-eGFP-ΔVpr and HIV-1 NL4.3-eGFP-Vpr^+ pseudotyped viruses
III. Investigate the effect of HIV-1 transduction and Vpr expression on activation of MDM immune signalling pathways
IV. Characterise the effect of HIV-1 Vpr on IFN-I production and ISG expression by MDMs
V. Establish a panel of Vpr-mutated HIV-1 NL4.3-eGFP expression plasmids for mechanistic study of Vpr modulation of MDM immune responses

4.3 Results

Having established MDM differentiation and transduction protocols through the work presented in Chapter 3, I next sought to I) characterise HIV-1 induction of MDM-expressed mediators of inflammation, and II) investigate the effect of the HIV-1 accessory protein Vpr on the expression profile of these mediators. The workflow for MDM transductions and subsequent analyses is summarised in Figure 17.

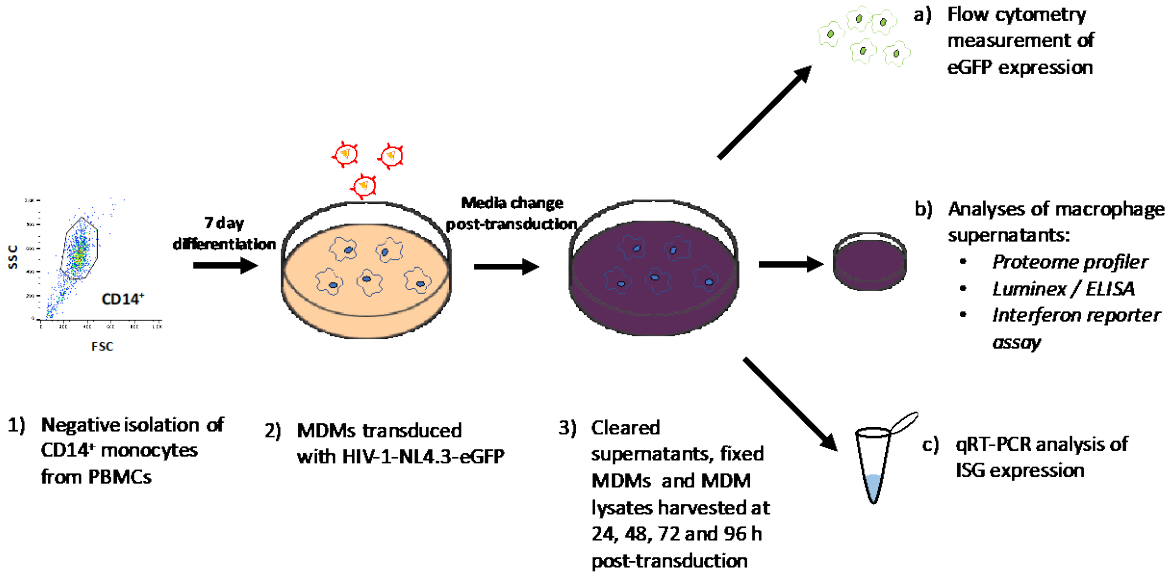


Figure 17: Schematic of workflow for MDM transductions and subsequent analyses

4.3.1 Pilot analysis of MDM responses to transduction using VSV-G/HIV-1-NL4.3-ΔVpr pseudotyped virus

I first conducted a pilot analysis of responses by MDMs transduced with eGFP-tagged VSV-G/HIV-1 NL4.3-ΔVpr pseudotyped virus. Transduction efficiencies were quantified by flow cytometry measurement of eGFP expression in MDMs at early (24 h) and late (72 h and 96

h) time-points and are fully detailed in Table 14. As summarised in Figure 18, eGFP expression was not detected at any of the time-points for the un-inoculated MDMs ('no vector') or the control transductions (ΔEnv). In contrast, eGFP expression was detectable at all time-points for the VSV-G/HIV-1 NL4.3-transduced MDMs and there was notable donor-to-donor variation in transduction efficiencies. eGFP expression by VSV-G/HIV-1 NL4.3 transduced MDMs was significant at 72 h post-transduction (p=0.017) and 96 h post-transduction (p<0.001) but not at 24 h post transduction (0.153) when analysed against the respective ΔEnv control transductions.

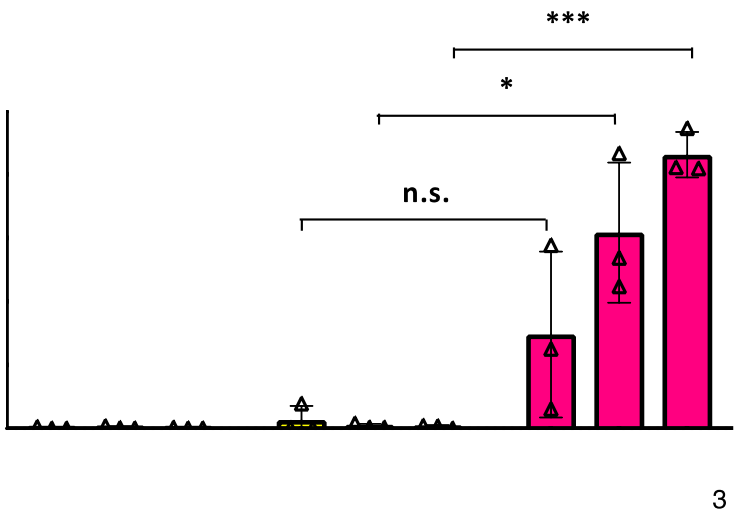


Figure 18: Efficiency of MDM transduction with VSV-G/HIV-1 NL4.3-ΔVpr pseudotyped virus

MDMs were inoculated with VSV-G/HIV-1 NL4.3-ΔVpr and Delta Env/HIV-1 NL4.3-ΔVpr pseudotyped virus at an MOI of 0.025, or were cultured in cX-Vivo$_{15}$ only for the 'no vector' condition. Transduction efficiencies were determined by flow cytometry measurement of eGFP expression at 24, 72 and 96 h post transduction. Data represent transduction efficiencies for 3 independent donors and error bars show mean ± S.D. eGFP

expression by HIV-1-transduced MDMs was statistically assessed using the Holm-Sidak method. *p<0.05, ***p<0.001 and n.s. denotes not significant (p>0.05).

Having confirmed eGFP expression by the MDMs transduced with VSV-G pseudotyped virus (and thereby confirmed successful transduction), I next used a membrane-based immunoassay (Proteome Profiler) to semi-quantitatively measure the expression of total of 102 factors in the supernatants of MDMs. Heat maps generated from Proteome Profiler analyses of MDM supernatants 72 h post transduction show that the expression profiles of interleukins (Figure 19 A), immune modulators (Figure 19 B), chemokines (Figure 19 C), and growth factors and colony stimulating factors (Figure 19 D) were different in each of the 3 independent donors analysed highlighting the large extent of donor-to-donor variability at the protein level for responses to HIV-1 transduction.

VSV-G/HIV-1 NL4.3-ΔVpr vs ΔEnv/HIV-1 NL4.3-ΔVpr fold change values (detailed in Table 15) revealed modest responses to VSV-G/HIV-1 NL4.3-ΔVpr transduction with only a subset of the total 102 factors investigated being differentially expressed 72 h post-transduction. CXCL10/IP-10 was most strikingly upregulated, being expressed at fold changes of 35.9, 15.9 and 36.7 by Donor 15, Donor 17 and Donor 19 respectively. The only other factors upregulated across all three donors were MIF (fold change of 4.2, 1.7 and 2.5 for Donor 15, Donor 17 and Donor 19 respectively) and adiponectin (fold change of 1.6, 1.7 and 6.2 for Donor 15, Donor 17 and Donor 19 respectively). However, HIV-1-induced upregulation of MIF and adiponectin was less striking than observed for CXCL10/IP-10.

HIV-1 transduction induced modest expression of the other factors analysed. Fold change $\geq$ 1.5 was observed across two donors for IL-3, CXCL9/MIG, SHBG, CCL17/TARC and vitamin D BP. Otherwise, fold change $\geq$ 1.5 was observed in one donor only for angiopoietin-1, BAFF, CD40 ligand, cripto-1, Dkk-1, emmprin, GM-CSF, ICAM-1, IFN-γ, IGFBP-2, IGFBP-3, IL-1β, IL-6, IL-13, IL-16, IL-31, IL-34, CXCL11/I-TAC, CCL2/MCP-1, CCL7/MCP-3, M-CSF, CCL20/MIP-3α, CCL19/MIP-3β, ST2, TFF3, TfR, Thrmobospondin-1, TNF-α and VEGF. VSV-G /HIV-1 NL4.3-ΔVpr transduction downregulated expression (fold change < 1) across all 3 donors for Leptin, LIF, lipocalin-2, CCL3/MIP-1α, CCL4/MIP-1β, MMP-9, osteopontin, PDGF-AA/AB, PDGF-BB, RAGE, CCL5/RANTES, CXCL12/SDF-1α, TGF-α and uPAR.

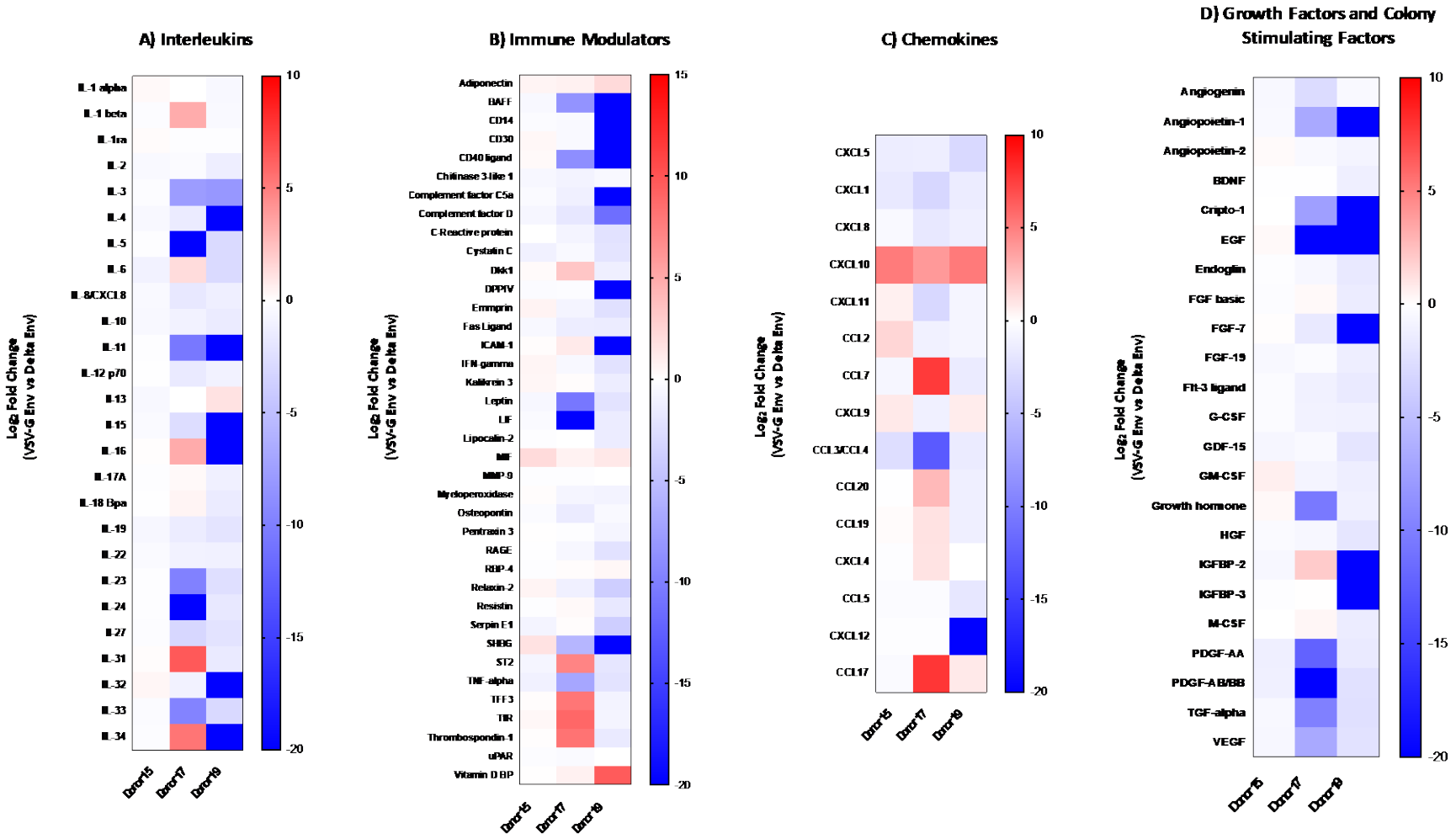


Figure 19: Proteome Profiler analysis of the MDM secreted proteome 72 h post-transduction with VSV-G/HIV-1 NL4.3- ΔVpr pseudotyped virus

Figure 19: Proteome Profiler analysis of the MDM secreted proteome 72 h post-transduction with VSV-G/HIV-1 NL4.3-ΔVpr pseudotyped virus

Cleared supernatants were harvested from MDM cultures 72 h post-transduction with either VSV-G/HIV-1 NL4.3-ΔVpr pseudotyped virus and proteome profiler arrays were used to analyse the expression of a total of 102 inflammatory factors. Expression data for the soluble factors are represented in functional groups of (A) interleukins (B) immune modulators, (C) chemokines and, (D) growth factors and colony stimulating factors. The level of each analyte present in the supernatants was semi-quantitatively detected as pixel density values. The heat maps represent log_2-fold change of the expression levels for analytes produced by VSV-G/HIV-1 NL4.3-ΔVpr transductions versus analyte expression levels for the Delta Env/HIV-1 NL4.3-ΔVpr transductions. Data represent 2 technical replicates for each pixel density reading and 3 independent donors were analysed.

Heat map plots did not highlight major trends in analyte expression across the functional groupings investigated. Therefore, I next tested the hypothesis that HIV-1 transduction activates biological pathways of relevance to the immune response using a gene set enrichment approach. Gene set enrichment was interrogated using the ConsensusPath DB network which analyses biological pathway interactions and the expression of functionally related gene clusters against multiple annotation databases using the paired Wilcoxon signed-ranked statistical analysis [262].

As summarized in Table 10, analyses revealed enrichment of the PI3K-Akt signalling pathway as well as pathways relevant to cytokine, interleukin and GPCR signalling for both Donor 15 and Donor 19. Activation of the MAPK signalling pathway was also identified based on the responses of Donor 15. There was no significant pathway enrichment determined based on the responses of Donor 17.

Overall, these analyses highlight significant donor-to-donor variation in responses to VSV-G/HIV-1 NL4.3-ΔVpr transduction. The results also confirm MIF and CXCL10/IP-10 as two inflammatory factors that show conserved upregulation across multiple donors, and reveal a marked CXCL10/IP-10 response to HIV-1.

Table 10: Gene set enrichment analysis of soluble factors expressed 72 h post VSV-G/HIV-1 NL4.3-ΔVpr transductions

	Annotation database	Term	Overlap	p-value	q-value
Donor 15	Reactome	Signalling by interleukins	32/254	0.000091	0.00393
		Immune system	56/1840	0.000216	0.00393
		Cytokine signalling in immune system	41/458	0.000921	0.05095
	INOH	GPCR signalling	33/262	0.000514	0.00393
	KEGG	PI3K-Akt Signalling pathways	23/352	0.000181	0.00393
		Pathways in cancer	25/526	0.00043	0.00393
		MAPK signalling pathway	19/295	0.00079	0.00553
Donor 17	*No significant pathway enrichment*				
Donor 19	Reactome	Immune System	43/1840	<0.00001	<0.00001
		Cytokine signalling in immune system	30/458	<0.00001	0.00004
		Signalling by interleukins	25/254	<0.00001	0.00004
		Signal transduction	37/2643	<0.00001	0.00009
	INOH	GPCR signalling	25/262	<0.00001	0.00004
		JaK STAT pathway and regulation	15/310	0.00061	0.0046
	KEGG	Cytokine-cytokine receptor interaction	8/35	<0.00001	0.00008
		Rheumatoid arthritis	17/90	0.000015	0.0002
		PI3K-Akt Signalling pathways	18/352	0.000015	0.0002

	Annotation database	Term	Overlap	p-value	q-value
		Pathways in cancer	19/526	0.00003	0.0003
		MAPK signalling pathway	15/295	0.00006	0.0006

Cleared supernatants were harvested from MDM cultures 72 h post-transduction with VSV-G/HIV-1 NL4.3-ΔVpr and Delta Env/HIV-1 NL4.3-ΔVpr vectors, and proteome profiler arrays were used to quantify the expression levels of a total of 102 inflammatory factors. Gene set pathway enrichment of analyte expression by VSV-G/HIV-1 NL4.3-ΔVpr vs Delta Env/HIV-1 NL4.3-ΔVpr transduced MDMs was carried out by paired Wilcoxon signed-rank testing using the ConsensusPath DB tool. Expression values from Delta Env/HIV-1 NL4.3-ΔVpr transduced MDMs were used as the control dataset for gene set enrichment analysis. Proteome profiler data from 3 independent donors were analysed. 'Overlap' denotes the number of genes that were determined to be differentially expressed in proportion to the total number of genes defined by the annotated gene set. p-values corrected for multiple testing using the false discovery rate method are represented as q-values. KEGG, Kyoto Encyclopedia of Genes and Genomes; INOH, Integrating Network Objects with Hierarchies.

4.3.2 Investigating the effect of HIV-1 Vpr expression on MDM transduction efficiency

The analyses presented in section 4.3.1 revealed that VSV-G/HIV-1 NL4.3 transduction of MDMs induced moderate expression of a subset of inflammatory factors and activated immune signalling pathways. However, an overarching goal of this study was to investigate HIV-1-induction of MDM immune responses under the most physiologically relevant conditions possible. Therefore, for all subsequent MDM transductions and analyses I used HIV-1_{BaL} Env pseudotyped viruses as these particles more appropriately model the CD4 and CCR5-dependent mechanism of virus entry that occurs in normal HIV-1 infection.

Early studies reported that HIV-1 Vpr expression is necessary for HIV-1 replication in MDMs [6,249,250], but not in $CD4^+$ T-cells [9,252] or myeloid-derived DCs [9]. To interrogate this, I transduced MDMs at an MOI of 0.25 with Vpr^+ or ΔVpr versions of HIV-1_{BaL} Env/HIV-1 NL4.3 pseudotyped virus. Control transductions were carried out either with ∆Env versions of the pseudotyped virus at the same MOI, or were mock-transduced with cX-$Vivo_{15}$ medium alone. Transduction efficiencies were quantified by flow cytometry measurement of eGFP expression by MDMs at early (24 h) and late (48 h, 72 h and 96 h) time-points and are fully detailed in Table 16 and Table 17. MDM harvests were carried out at 24 h, 72 h and 96 h post-transduction for initial experiments. However, a 48 h time-point was included for later experiments. Therefore, flow cytometry data is only available for 3 independent donors at the 48 h time-point.

As shown in Figure 20, only MDMs transduced with HIV-1_{BaL} pseudotyped viruses appreciably expressed eGFP while both un-transduced MDMs and MDMs transduced with

the control ΔEnv vector showed background eGFP signal. Substantial variation was observed between donors but, on average, more than 10 % of MDMs were positive at the 72 h and 96 h time-points. Despite a trend towards increased eGFP expression by the NL4.3-Vpr^{+} transduced MDMs when compared to NL4.3-ΔVpr transduced MDMs, particularly at 48 h, there was no significant difference ($p > 0.05$) at any of the time-points measured. Overall, these data confirmed successful transduction of MDMs with HIV-1_{BaL} pseudotyped viruses and demonstrate that HIV-1 Vpr is not required for transduction of primary MDMs.

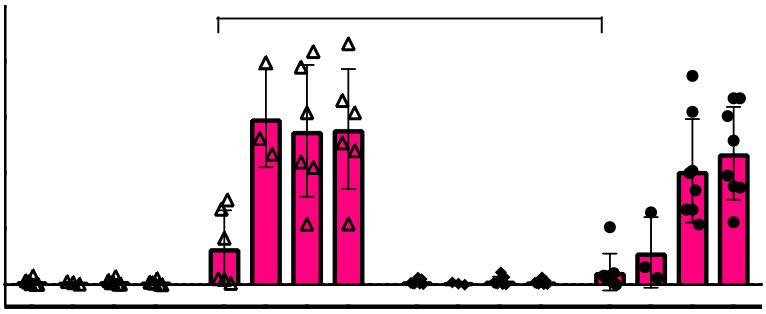


Figure 20: Efficiency of MDM transductions with HIV-1_{BaL} Env/HIV-1-NL4.3 pseudotyped virus

MDMs were transduced with HIV-1_{BaL} Env/HIV-1 NL4.3 pseudotyped viruses and ΔEnv/HIV-1 NL4.3 pseudotyped viruses at a multiplicity of infection of 0.25, or cultured in cX-Vivo$_{15}$ only for the 'no vector' condition. Transduction efficiencies were determined by flow cytometry measurement of eGFP expression at 24, 48, 72 and 96 h post transduction. The dataset was assessed using the Shapiro-Wilk normality testing

and the effect of HIV-1 Vpr expression on transduction efficiency was statistically analysed by the Mann-Whitney method. Error bars represent mean ± S.D. for 8 independent donors per transduction condition for the NL4.3-Vpr$^+$ pseudotyped viruses and 6 independent donors per transduction condition for the NL4.3-ΔVpr pseudotyped viruses. n.s. denotes p>0.05 (not significant).

4.3.3 Wide-scale analysis of 72 h MDM responses to transduction with HIV-1$_{BaL}$ Env/HIV-1-NL4.3 pseudotyped viruses

To evaluate the effect of NL4.3-eGFP transduction only, I first assessed HIV-1$_{BaL}$ Env/NL4.3 vs ∆Env/NL4.3-eGFP fold changes in analyte concentration irrespective of HIV-1 Vpr expression in the pseudotyped virus by pooling data from transductions with NL4.3-ΔVpr and NL4.3-Vpr$^+$. Heat maps generated from analyses of MDM supernatants 72 h post transduction highlight that the expression profiles of interleukins (Figure 21 A), immune modulators (Figure 21 B), chemokines (Figure 21 C) and growth factors and colony stimulating factors (Figure 21 D) varied greatly between donors. Corresponding HIV-1$_{BaL}$ Env/NL4.3 vs ∆Env/NL4.3-eGFP fold change analyses (summarised in Table 18) revealed modest responses to NL4.3eGFP transduction with only a subset of the total 102 factors investigated being differentially expressed 72 h post-transduction.

Of the 6 transductions profiled, at least 3 donors showed differential expression (fold change ≥2) for CD30, IL-12 p70, TNF-α, CCL2/MCP-1, CCL3/CCL4, CCL7/MCP-3, CXCL9/MIG, CXCL10/IP-10, CCL17/TARC, lipocalin-2, IGFB-2, IGFB-3 and vitamin D BP (Table 18). CXCL10/IP-10 was strikingly upregulated (fold change ≥ 30) in 4 of the 6 donors investigated. While MIF, CXCL4/PF4, IL-6 and CXCL12/SDF1 were not downregulated across

any of the 6 transductions analysed, expression of these analytes over the control condition was modest (1 < fold change < 2).

Wilcoxon signed-rank gene enrichment analyses of each proteome profiler dataset using the Consensus Path DB database identified activation of JaK-STAT, MAPK, PI3K-Akt and TLR signalling pathways (summarised in Table 19 and Table 20). More broadly, significant enrichment of pathways relevant to G-protein coupled receptor (GPCR), chemokine signalling, cytokine and interleukin signalling was also identified.

Together these data highlight the large extent of donor-to-donor variability at the protein level for responses to either HIV_{BaL}/HIV-1 NL4.3 transduction ± HIV-1 Vpr expression. Similar inter-donor variation has been previously reported in transcriptional studies [10] and is presumably due to differences in the expression or activity of host cell sensing machinery between the different donors. These data also show that HIV-1 induces the upregulation of a subset of pro-inflammatory factors including chemokines and mediators of immune signalling. My analyses also show that HIV-1 transduction induces a striking CXCL10/IP-10 response independent of HIV-1 Vpr expression.

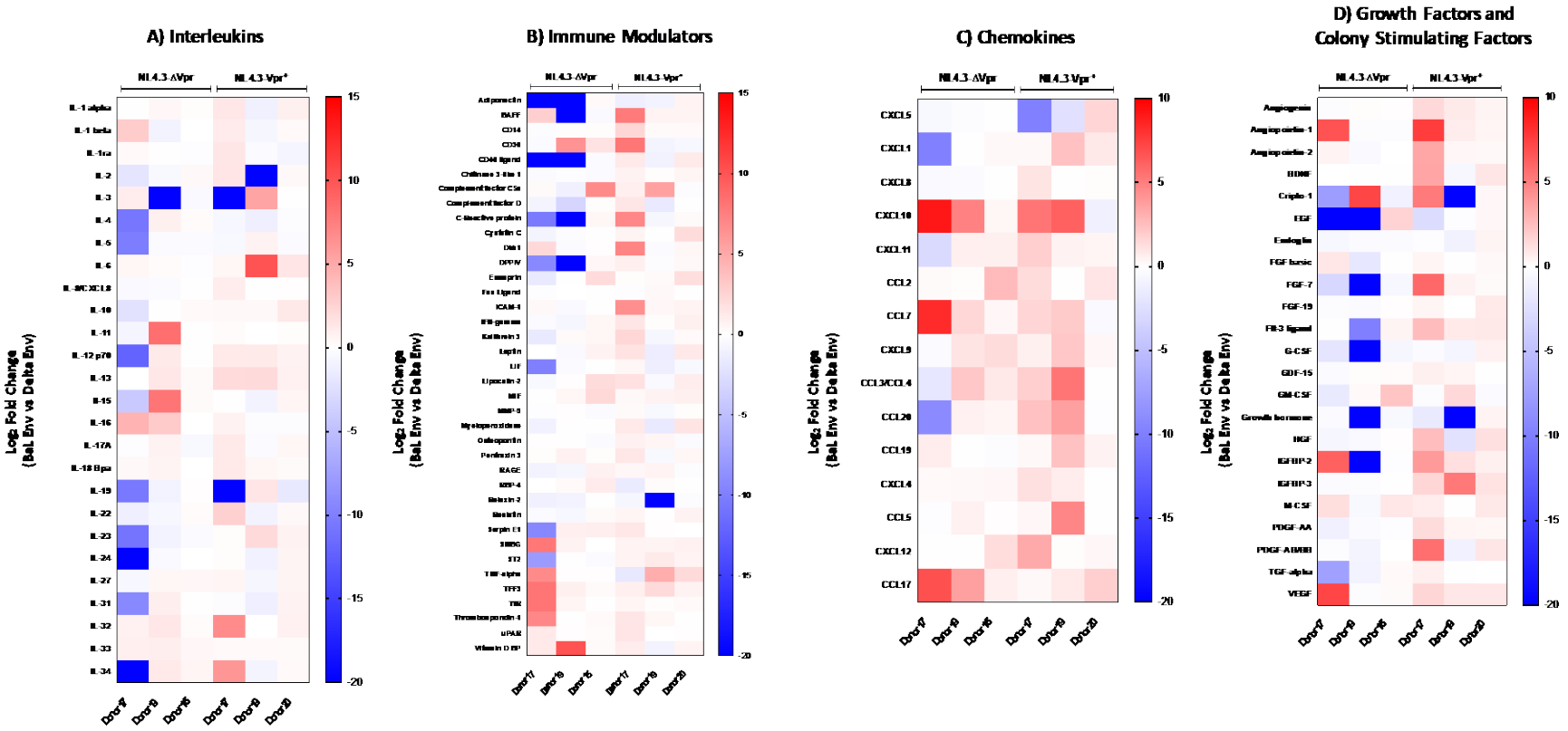


Figure 21: Proteome Profiler analysis of the MDM secreted proteome 72 h post-transduction with HIV-1_{BaL} Env/HIV-1 NL4.3-ΔVpr and HIV-1_{BaL} Env/HIV-1 NL4.3-Vpr^{+} pseudotyped viruses

Figure 21: Proteome Profiler analysis of the MDM secreted proteome 72 h post-transduction with HIV-1_{BaL} Env/HIV-1 NL4.3-ΔVpr and HIV-1_{BaL} Env/HIV-1 NL4.3-Vpr^{+} pseudotyped viruses

Cleared supernatants were harvested from MDM cultures 72 h post-transduction with either HIV-1_{BaL} Env/HIV-1 NL4.3-ΔVpr pseudotyped virus or HIV-1_{BaL} Env/HIV-1 NL4.3P-Vpr^{+} pseudotyped virus and proteome profiler arrays were used to analyse the expression of a total of 102 inflammatory factors. Expression data for the soluble factors are represented in functional groups of (A) interleukins (B) immune modulators, (C) chemokines and, (D) growth factors and colony stimulating factors. The level of each analyte present in the supernatants was semi-quantitatively detected as pixel density values. The heat maps represent log_2 -fold change of the expression levels for analytes produced by HIV-1_{BaL} Env/HIV-1 NL4.3-ΔVpr transductions versus analyte expression levels for the Delta Env/HIV-1 NL4.3-ΔVpr transductions. Data represents 2 technical replicates for each pixel density reading and 4 independent donors were analysed.

4.3.4 Pilot analysis of 24 h MDM responses to transduction using HIV-1_{BaL} Env/HIV-1-NL4.3-ΔVpr pseudotyped virus

To probe whether the magnitude and profile of inflammatory factor expression would be different at an earlier time-point of HIV-1 transduction, I conducted an additional analysis of supernatant harvested from MDMs 24 h post-transduction with HIV_{BaL}/HIV-1 NL4.3-ΔVpr pseudotyped virus.

As with the 72 h time-point analyses, heat maps generated from Proteome Profiler analyses of MDM supernatants 24 h post transduction show that the expression profiles of

interleukins (Figure 22 A), immune modulators (Figure 22 B), chemokines (Figure 22 C), and growth factors and colony stimulating factors (Figure 22 D) varied substantially between Donor 15, 17 and 19. The striking induction of CXCL10/IP-10 that I observed with previous transductions was not apparent at 24 h as the fold changes of CXCL10/IP-10 expression for Donor 15, Donor 17 and Donor 19 were 1.5, 1.4 and 1.36 respectively. The results of fold change analyses in Table 21 show that no factor was differentially expressed (fold change $\geq$ 2) across all three donors. However, fold change $\geq$ 2 was observed across two of the three donors analysed for CXCL5/ENA-78, emmprin, IL-13, IL-15, IL-16, IL-18 Bpa, CCL3/CCL4, CCL7/MCP-3 and SHBG. Otherwise, expression fold change $\geq$ 1.5 was observed across at least two donors for lipocalin-2, CCL7/MCP-3, CXCL4/PF4, Fas-ligand, growth hormone, ICAM-1, IL-3, IL-10, IL-12 p70, IL-17, M-CSF, Serpin E1, ST2, uPAR, TfR and vitamin D BP.

On the whole, HIV-1 induction of inflammatory factors was more modest at 24 h than observed at 72 h, in accord with the borderline level of pseudotyped virus transduction. Furthermore, the characteristic HIV-1-induced upregulation of CXCL10/IP-10 was not observed at this early time-point. Similarly, to the 72 h time-point, ConsensusPath DB analyses of the 24 h dataset indicated enrichment of pathways relevant to cytokine, interleukin and chemokine signalling and activation of the JaK-STAT signalling pathway (Table 22).

Given these initial observations, as well as the time and cost constraints of this study, I did not carry out additional Proteome Profiler analyses of the 24 h time-point for HIV_{BaL}/HIV-1 NL4.3-Vpr^{+} transduced MDMs. It was decided that future analyses of HIV-1-induced soluble

factor production and gene expression in MDMs would be focussed on samples harvested at the 72 h time-point.

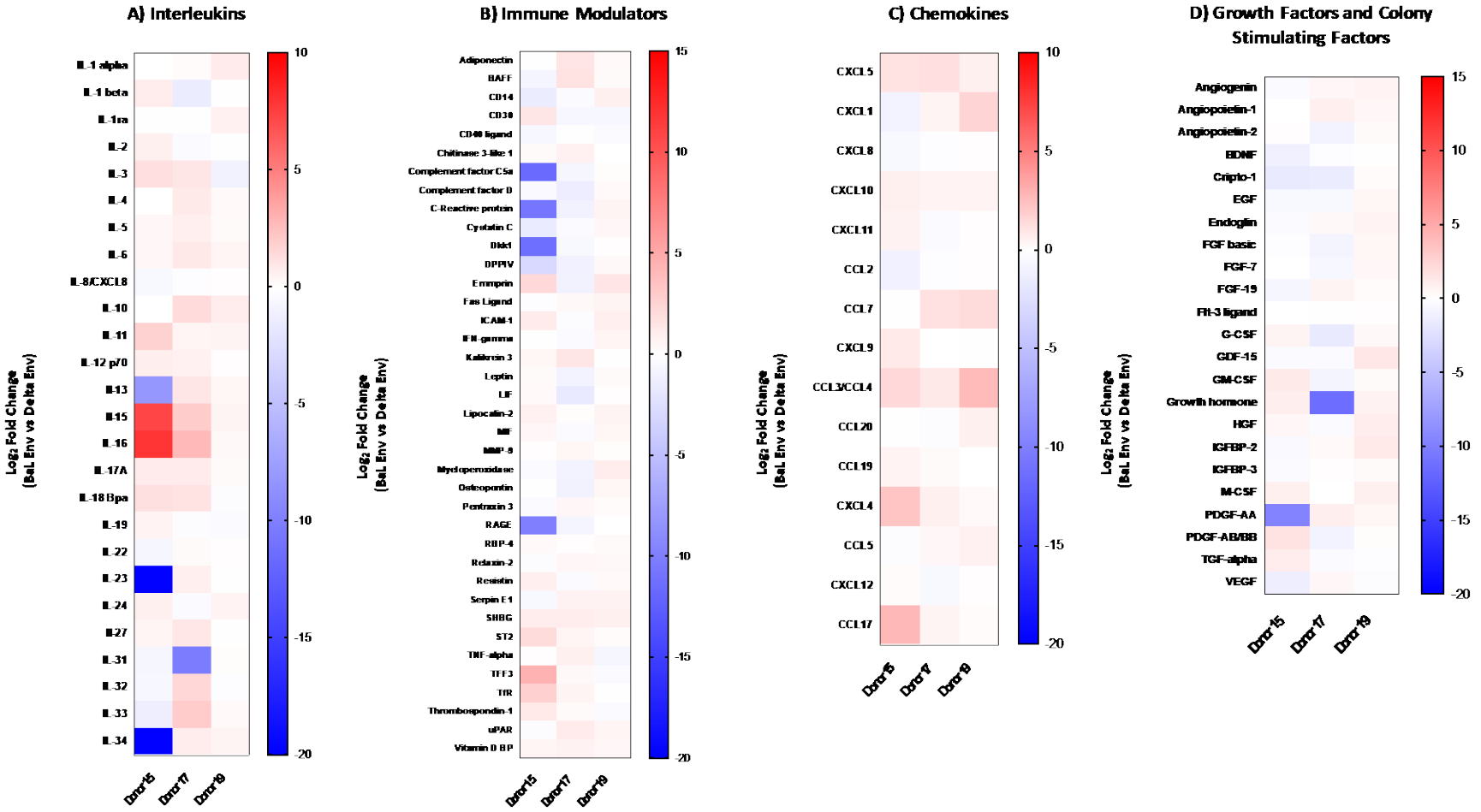


Figure 22: Proteome Profiler analysis of the MDM secreted proteome 24 h post-transduction with HIV-1_{BaL} Env/HIV-1 NL4.3-ΔVpr pseudotyped virus

Figure 22: Proteome Profiler analysis of the MDM secreted proteome 24 h post-transduction with HIV-1_{BaL} Env/HIV-1 NL4.3-ΔVpr pseudotyped virus

Cleared supernatants were harvested from MDM cultures 24 h post-transduction with HIV-1_{BaL} Env/HIV-1 NL4.3-ΔVpr pseudotyped virus and proteome profiler arrays were used to analyse the expression of a total of 102 inflammatory factors. Expression data for the soluble factors are represented in functional groups of (A) interleukins (B) immune modulators, (C) chemokines and, (D) growth factors and colony stimulating factors. The level of each analyte present in the supernatants was semi-quantitatively detected as pixel density values. The heat maps represent log_2- fold change of the expression levels for analytes produced by HIV-1_{BaL} Env/HIV-1 NL4.3-ΔVpr transductions versus analyte expression levels for the Delta Env/HIV-1 NL4.3-ΔVpr transductions. Data represents 2 technical replicates for each pixel density reading and 3 independent donors were analysed

4.3.5 Investigating the effect of HIV-1 Vpr expression on pathways relevant to MDM immune regulation

I next interrogated whether HIV-1 Vpr expression modulated biological pathways of relevance to the immune response by comparing fold changes in expression of interleukins, immune mediators, chemokines as well as growth factors and colony stimulating factors expressed by NL4.3-eGFP-Vpr^+ transduced MDMs against the fold changes in analyte expression for NL4.3-eGFP-ΔVpr transduced MDMs. As shown in Supplementary Figures 55 – 58, statistical analyses by Mann-Whitney testing did not highlight significant differences between the profile of analytes expressed by NL4.3-eGFP-Vpr^+ transduced MDMs versus NL4.3-eGFP-ΔVpr transduced MDMs. Therefore, I invetsigated differential enrichment of pathways by comparing fold changes in expression from NL4.3-eGFP-Vpr^+ transduced

MDMs against NL4.3-eGFP-ΔVpr transduced MDMs using the ConsensusPath DB tool. This approach statistically assessed differences between the two datasets using the Wilcoxon signed-rank method which evaluates the differences in the joint expression of whole predefined gene sets rather than individual genes. This approach was selected as it is reported to be useful for detecting low-levels of pathway modulation. Analyses indicate that HIV-1 Vpr significantly altered the expression of genes involved in cytokine-mediated signaling and pathways relevant to the immune response including the JAK-STAT, NF-kappa B and Toll-like receptor signaling pathways (Table 11).

Table 11: Gene set enrichment analysis of differentially expressed soluble factors for HIV-1_{BaL} Env/HIV-1 NL4.3-Vpr^+ versus HIV-1_{BaL} Env/HIV-1 NL4.3-ΔVpr transductions

	Annotation database	Term	Overlap	p-value	q-value
Donor 17	Reactome	Immune System	53/1840	0.000008	0.00197
		Cytokine signalling in immune system	39/458	0.000343	0.0381
		Signalling by interleukins	31/254	0.000831	0.0381
		Neutrophil degranulation	21/490	0.000977	0.0381
		Innate immune system	16/1077	0.00131	0.0381
	KEGG	Cytokine-cytokine receptor interaction	54/294	0.000761	0.0381
		Pathways in cancer	25/526	0.001155	0.0381
		JAK-STAT signalling pathway	23/162	0.00242	0.0621
	Wikipathways	Lung fibrosis	24/64	0.00107	0.0381
	PID	AP-1 transcription factor network	10/70	0.00391	0.0621
	INOH	GPCR signalling	33/262	0.00428	0.0621
Donor 19	KEGG	NFκB signalling pathway	10/95	0.00195	0.123
		Amoebiasis	10/96	0.00195	0.123
		Toll-like receptor signalling pathway	13/104	0.00265	0.123
		Human cytomegalovirus infection	11/255	0.00667	0.181
		Kaposi sarcoma associated herpesvirus infection	9/186	0.00781	0.181
		African trypanosomiasis	8/35	0.00781	0.181
	Wikipathways	Toll-like receptor signalling pathway	13/102	0.00265	0.123

		Regulation of toll-like receptor signalling pathway	13/143	0.0265	0.123
		Interleukin-10 signalling	20/38	0.00607	0.181
		Lung fibrosis	24/64	0.00755	0.181

Cleared supernatants were harvested from MDM cultures 72 h post-transduction with HIV-1_{BaL}/HIV-1 NL4.3-ΔVpr and Delta Env/HIV-1 NL4.3-ΔVpr pseudotyped virus, and proteome profiler arrays were used to quantify the expression levels of a total of 102 inflammatory factors. For each analyte, fold change of expression values was calculated for HIV-1_{BaL}/HIV-1 NL4.3-ΔVpr versus ⊿Env/HIV-1 NL4.3-ΔVpr transductions and for HIV-1_{BaL}/HIV-1 NL4.3-Vpr^+ versus ⊿Env/HIV-1 NL4.3-Vpr^+ transductions. The effect of HIV-1 Vpr expression on gene set pathway enrichment was analysed by paired Wilcoxon signed-rank testing using the ConsensusPath DB tool. Proteome profiler data from 2 independent donors were used for the comparative analysis of the fold change in analyte expression of Vpr^+ versus ⊿Vpr transduced MDMs. 'Overlap' denotes the number of genes that were determined to be differentially expressed in proportion to the total number of genes defined by the annotated gene set. p-values corrected for multiple testing using the false discovery rate method are represented as q-values. KEGG, Kyoto Encyclopedia of Genes and Genomes; PID, Protein Interaction Database; INOH, Integrating Network Objects with Hierarchies.

4.3.6 Quantification of inflammatory factors differentially modulated by HIV-1 Vpr expression

I next validated the Proteome Profiler dataset using a quantitative multiplex bead immunoassay (as described in Section 2.19). Analytes were selected for inclusion in the panel if Proteome Profiler analyses indicated that they had been differentially expressed (fold change $\geq$ 2) for at least three of the independent donors analysed. Analytes whose expression are known to be IFN-I-inducible were also included in the Luminex panel. Validation was carried out on the same 72 h supernatants that were analysed by Proteome Profiler.

As shown in Figure 23, CCL3/MIP-1α, CCL4/MIP-1β and MIF were found to be constitutively produced by MDMs as they were expressed at detectable levels for transductions with either control ΔEnv/HIV-1 NL4.3 pseudotyped virus or in the un-transduced condition. In contrast, levels of IL-1β and the IFN-inducible chemokines CXCL9/MIG, CXCL10/IP-10 and CXCL11/I-TAC were enhanced in response to HIV-1_{BaL} Env/HIV-1 NL4.3 transduction. I observed a trend of decreased CXCL9/MIG, CXCL10/IP-10, CXCL11/I-TAC, CCL7/MCP-3, IL-1β and MIF expression by MDMs transduced with BaL Env/NL4.3eGFP-Vpr^{+} pseudotyped virus. However, statistical analyses show that only CCL4/MIP-1β and IL-1β production were significantly downregulated by HIV-1 Vpr expression.

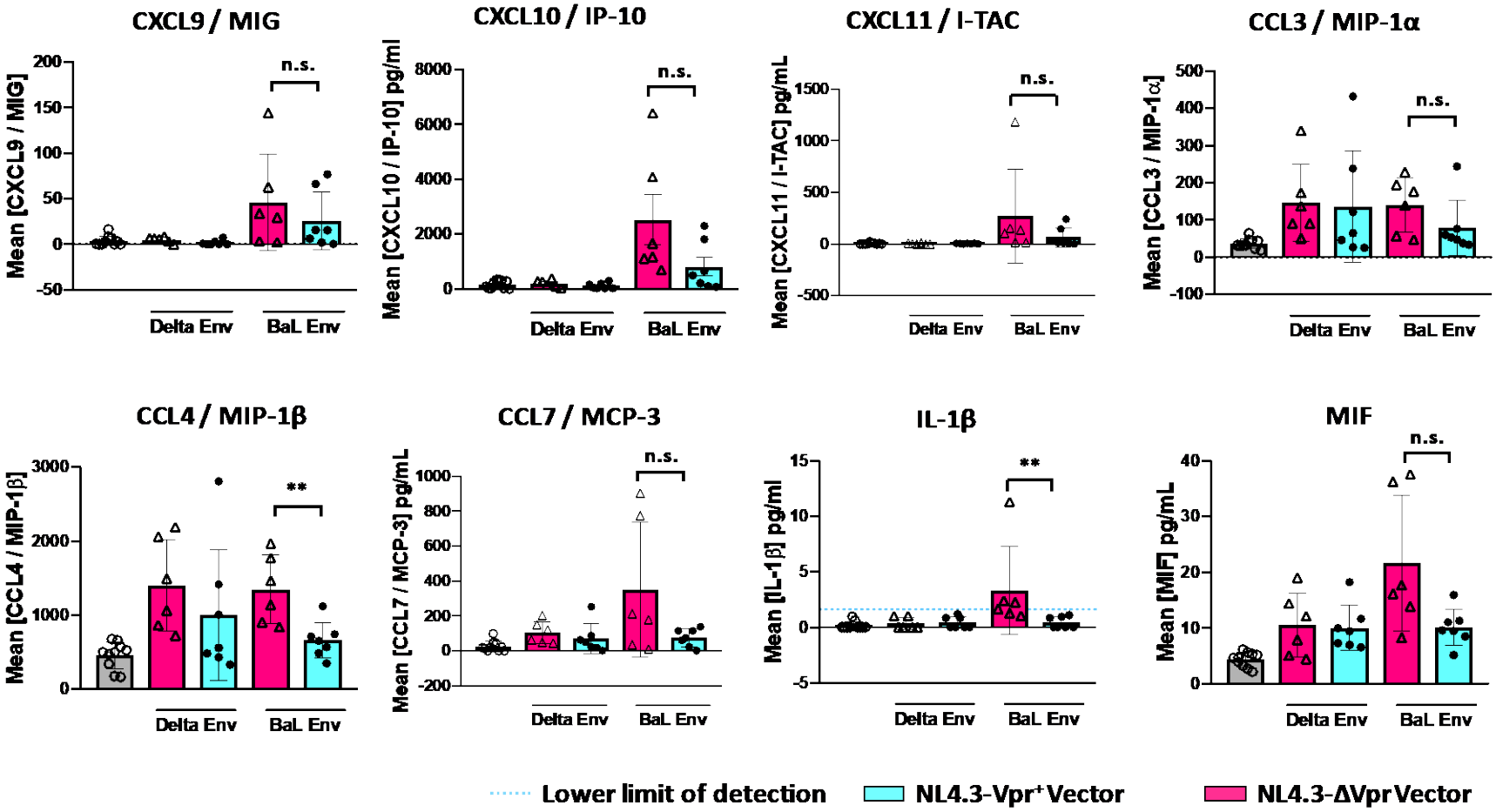


Figure 23: Quantification of differentially expressed inflammatory factors 72 h post-transduction with HIV-1_{BaL} Env/HIV-1-NL4.3-eGFP-Vpr$^+$ vector and HIV-1_{BaL} Env/HIV-1-NL4.3-eGFP-ΔVpr vectors

Figure 23: Quantification of differentially expressed inflammatory factors 72 h post-transduction with HIV-1_{BaL} Env/HIV-1-NL4.3-eGFP-Vpr^+ vector and HIV-1_{BaL} Env/HIV-1-NL4.3-eGFP-ΔVpr vectors

Cleared supernatants were harvested 72 h post-transduction and the concentration of CXCL9/MIG, CXCL11/ITAC, CCL3/MIP-1α, CCL4/MIP-1β, CCL7/MCP-3, IL-1β and MIF present in the supernatants of blood MDMs 72 h post-transduction with either HIV-1 NL4.3-Vpr^+ or HIV-1 NL4.3-ΔVpr vectors was quantified using a multiplex bead-based immunoassay. The concentration of CXCL10/IP-10 was measured by ELISA. The dataset was assessed using the Shapiro-Wilk normality testing and the effect of HIV-1 Vpr expression on cytokine and chemokine production was statistically analysed by the Mann-Whitney test. *p<0.05, **p<0.01 and n.s. denotes p>0.05 (not significant). Error bars indicate mean ± S.D. of 7 independent donors for HIV-1-NL4.3-Vpr+ transductions and 6 independent donors for HIV-1 NL4.3-ΔVpr transductions.

4.3.7 Investigating the effect of HIV-1 Vpr on IFN-I expression by HIV-1-transduced macrophages

Production of IFN-I is a hallmark of innate responses to viral infection [253-255]. Additionally, transcriptional studies by Zahoor et al have shown that HIV-1 Vpr expression using an adenoviral system enhances IFN-I signatures in MDMs [10] and myeloid-derived DCs [8]. I therefore sought to determine the effect of HIV-1 Vpr expression on the IFN-I production by HIV-1-transduced MDMs. To investigate this, I first validated a HEK293-IFN-I-stimulated response element reporter cell line (HEK293-ISRE-fLuc), which expresses firefly luciferase under the control of the ISRE promoter in response to stimulation by IFN-I and is not stimulated by other classes of IFN. Quantification of fLuc

activity in the lysate of stimulated HEK293-ISRE-fLuc cells therefore provides an accurate estimation of the levels of IFN-I to which the reporter cells have been exposed. This cell line was kindly gifted by Jan Rehwinkel and has been previously described by Hertzog et al [263].

As shown in Figure 24, fLuc expression by the reporter cell line increased as the IFN-2α and IFN-β used to stimulate the cells increased in concentration from -0.16 to 3.2 $\log_{10}$ U/mL (0.68 to 1.5 x 10^3 U/mL). Increasing IFN-2α or IFN-β concentrations beyond 3.2 $\log_{10}$ U/mL (1.5 x 10^3 U/mL) appeared to decrease the IFN-I reporter cell line's responses to stimulation. There was also no significant difference in the fLuc activity when responses to IFN-2α and IFN-β were compared, confirming that the cell line was capable of expressing fLuc in response to stimulation by different isoforms of IFN-I.

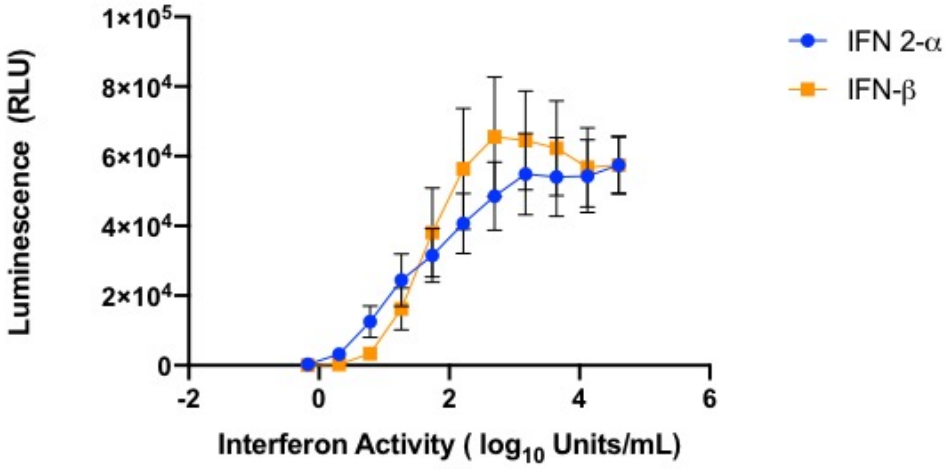


Figure 24: Validation of the HEK293-3C11-ISRE-fLuc IFN reporter cell line

A HEK293-derived reporter cell line (HEK293-3C11-ISRE-fLuc) that expresses firefly luciferase under the control of the interferon stimulated response element (ISRE) was validated by measuring responses to recombinant IFN-α and IFN-β; two prototypical IFN-I forms. HEK293-3C11-ISRE-fLuc cells were separately treated with three-fold serial dilutions of IFN-α and IFN-β for a final IFN-activity range of 6.77 x 10-1 – 4.0 x 104 U/mL (-1.69 x 10-1 - 4.6 log10 U/mL). After 24 h incubation, the treated HEK293-3C11-ISRE-fLuc cells were lysed and luminescence was measured as a read-out of IFN-induced luciferase activity.

Having validated the IFN-I reporter cell line, I quantified IFN-I activity in 24 h, 48 h, 72 h and 96 h supernatants from MDMs transduced with NL4.3-Vpr$^+$ or NL4.3-ΔVpr pseudotyped virus. As summarized in Figure 25, IFN-I activity was detectable at low levels at 24 h post-transduction across all conditions except for the un-transduced MDMs. This suggests that an early wave of IFN-I production occurred in response to the transduction process itself. However, by 48 h post-transduction, this generalized spike in IFN-I activity had resolved to levels that were not significantly enhanced over the IFN-I levels expressed by un-transduced MDMs. Markedly lower levels of IFN-I activity were detected for MDMs transduced with the NL4.3-Vpr$^+$ pseudotyped virus when compared to MDMs transduced with NL4.3-ΔVpr vector pseudotyped virus. This trend was statistically significant at 72 h ($p = 0.02$) and 96 h post-transduction ($p = 0.04$), but not at 24 h ($p = 0.84$) or 48 h ($p = 0.1$) post-transduction.

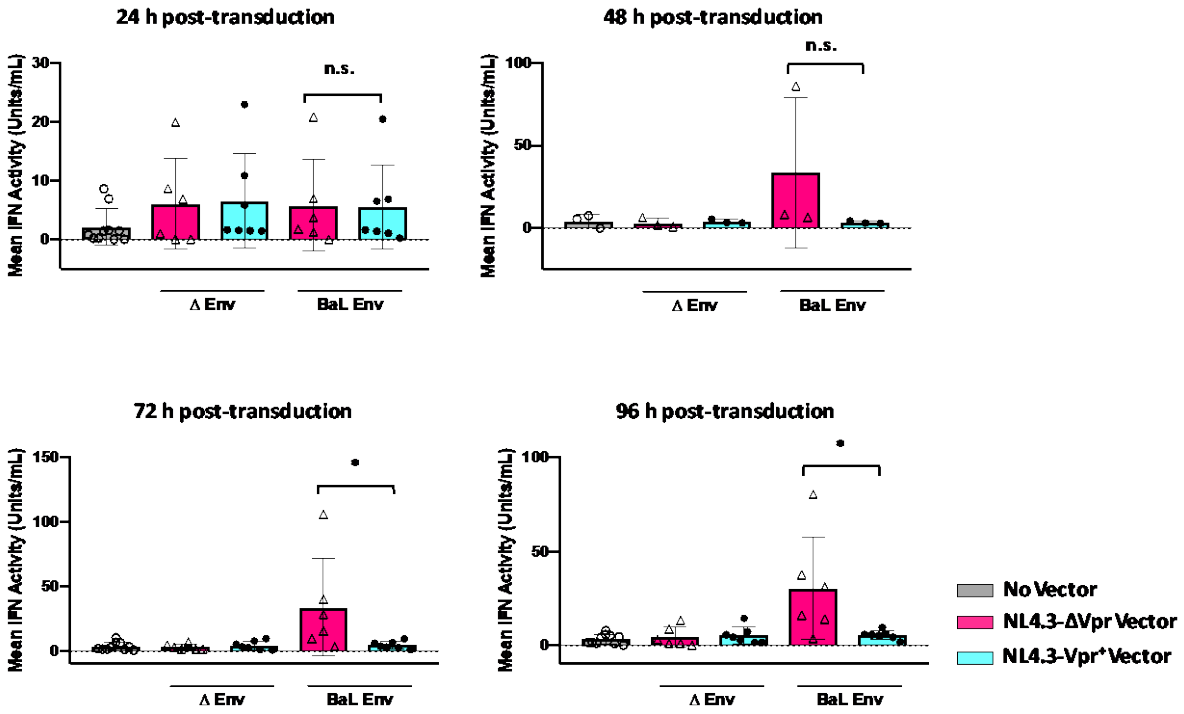


Figure 25: Time-course analysis of IFN-I activity in supernatants of HIV-1 NL4.3 transduced macrophages

Cells of the HEK293-ISRE-fLuc reporter line were incubated for 24 h with cleared supernatants harvested from blood MDM cultures 24, 48, 72 and 96 h post-transduction with HIV-1 NL4.3-ΔVpr and HIV-1 NL4.3-Vpr$^+$ vectors. IFN-I activity in the supernatants was quantified by measuring supernatant-induced fLuc expression by the reporter cell line. The dataset was assessed using the Shapiro-Wilk normality testing and differential fLuc expression was statistically analysed by the Mann-Whitney test. *p<0.05 and n.s. denotes p>0.05 (not significant). Error bars indicate mean ± S.D. of 7 independent donors for HIV-1-NL4.3-Vpr$^+$ transductions and 6 independent donors for HIV-1-NL4.3-ΔVpr transductions.

To confirm this observation and determine the type of IFN released, I used a multiplex bead-based immunoassay to measure the concentrations IFN-α (a prototypical IFN-I) and IFN-γ (IFN-II) that were produced by MDMs 72 h post-transduction. As shown in Figure 26, a mean of 8.9 pg/mL IFN-α was detected in the supernatants of MDMs transduced with HIV-1_{BaL}/NL4.3-ΔVpr pseudotyped virus, whereas supernatant from HIV-1_{BaL}/NL4.3-Vpr^{+} pseudotyped virus-transduced MDM gave a signal not significantly above background IFN-I production levels. Additionally, IFN-γ production was not detected in response to transduction with either pseudotyped virus. Together, the luminex and reporter cell line analyses suggest that the MDM response to HIV-1-transduction is IFN-I specific and confirm that HIV-1 Vpr expression significantly downregulates IFN-I production by HIV-1-transduced MDMs.

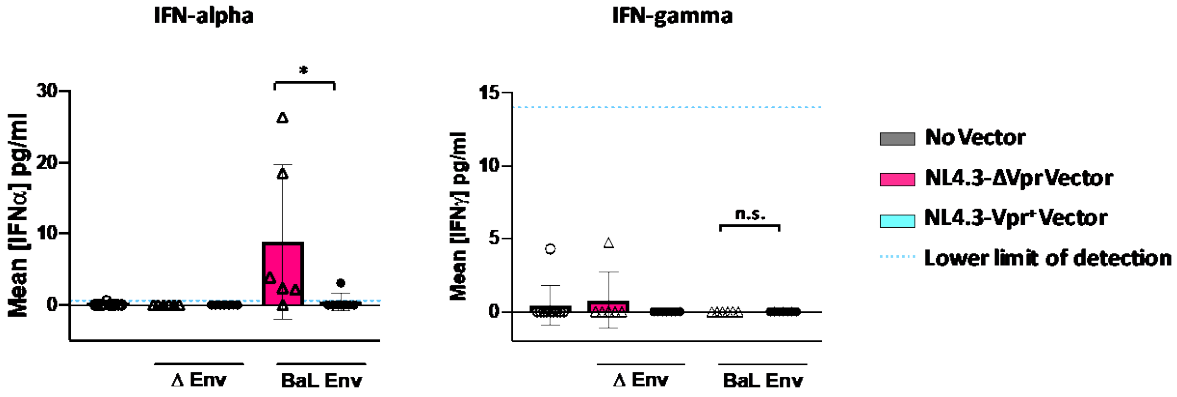


Figure 26: Luminex quantification of IFN-α and IFN-γ responses by macrophages transduced with HIV-1_{BaL} Env/HIV-1-NL4.3-eGFP pseudotyped virus

To characterise the IFN responses of blood MDM to transduction with the HIV-NL4.3eGFP vectors, a multiplex bead-based immunoassay was used to measure the concentrations of IFN-γ and a prototypical type-I interferon (IFN-α) in the supernatants of macrophages 72 h post-transduction with either HIV-1

NL4.3-Vpr+ vectors or HIV-1 NL4.3-ΔVpr vectors. The dataset was assessed using the Shapiro-Wilk normality testing and the effect of HIV-1 Vpr expression on IFN production was statistically analysed by the Mann-Whitney test. *p<0.05 and n.s. denotes p>0.05 (not significant). Error bars indicate mean with S.D. of 7 independent donors for NL4.3-Vpr+ transductions and 6 independent donors for NL4.3-ΔVpr transductions.

4.3.8 Investigating the effect of HIV-1 Vpr on ISG expression

In contrast to my analyses, previous studies have investigated the effects of HIV-1 Vpr at the transcriptomic level. Therefore, I next investigated whether HIV-1 Vpr would also influence ISG expression in transduced MDMs both for the purpose of comparing my findings to the existing body of literature and also to validate whether my observation of downregulated HIV-1-induced IFN-I expression in MDMs. For this purpose, I extracted RNA from lysates of MDMs 72 h post-transduction and measured the expression of CXCL10/IP-10, DDX58/RIG-I, ISG15, IFIH1, IFIT1 and IFI44L by qRT-PCR. Multiple ISGs are important sensors and/or restriction factors of HIV-1 infection [264], and these ISGs were selected for qRT-PCR analyses as they are commonly reported to be involved in macrophage responses to HIV-1 infection [10,265-268].

The qRT-PCR analyses shown in Figure 27 revealed enhanced ISG expression by HIV-1-transduced MDMs when compared to the respective control ΔEnv/HIV-1 NL4.3 pseudotyped virus transductions or the un-transduced condition. Differences in the magnitude of the response were selective for the ISG investigated as IFIH1 and DDX58/RIG-I were both induced to a lesser extent than ISG15, IFIT1 and MX2. Interestingly, despite

reduced IFN-I expression in the presence of HIV-1 Vpr, ISG transcription was less obviously impacted by Vpr expression. Nevertheless, DDX58, IFIT1 and MX2 showed a trend towards reduced transcription in the presence of Vpr expression, suggesting a potential correlation with biological IFN-I induction.

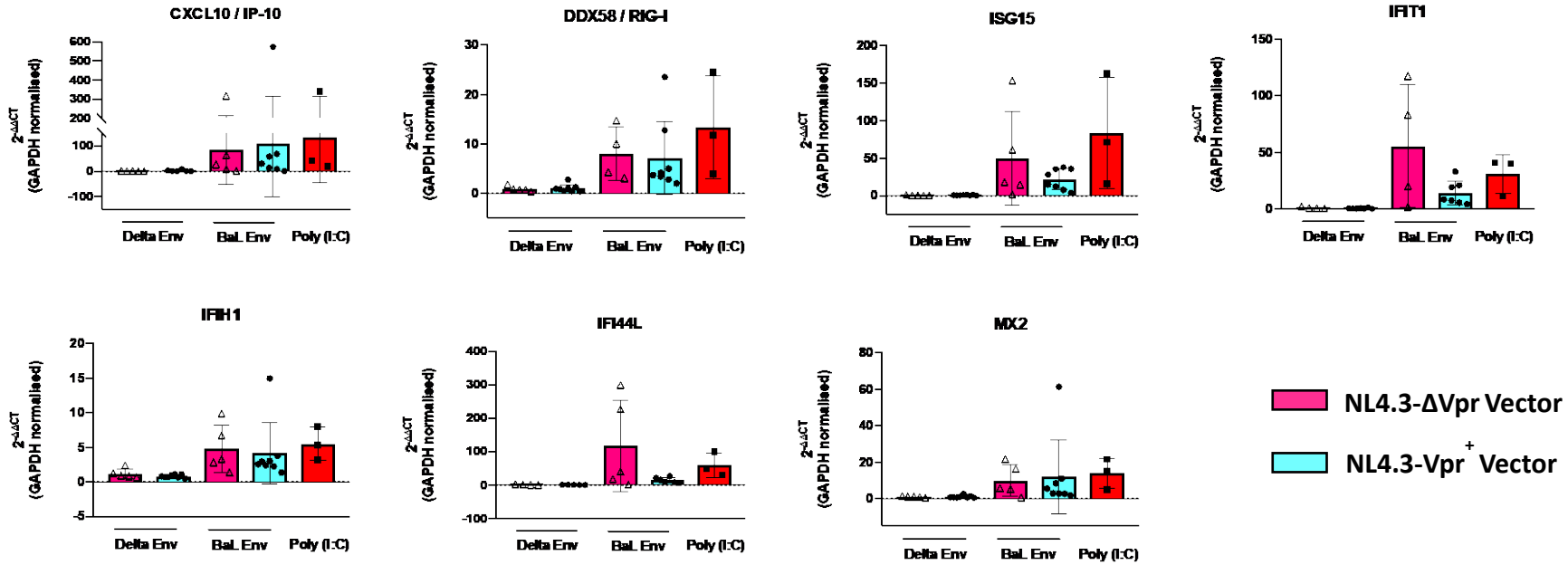


Figure 27: Quantification of ISG expression 72 h post-transduction with HIV-1-NL4.3-Vpr$^+$ and HIV-1-NL4.3-ΔVpr vectors

Total RNA was extracted from MDM lysates harvested 72 h post-transduction or after 18 h stimulation with 1µ g/mL poly(I:C). The mRNA expression of the ISGs CXCL10/IP-10, DDX58/RIG-I, ISG15, IFIH1, IFIT1, IFI44L, and MX2 was measured by real-time quantitative reverse transcription-polymerase chain reaction (qRT-PCR). Samples were analysed in triplicate and all data were normalized using GAPDH mRNA expression as an internal control. Fold changes were calculated by the $2^{-\Delta\Delta CT}$ method using either mRNA expression from the Delta Env-NL4.3 transductions or from un-transduced MDM as the reference control. The dataset was assessed using the Shapiro-Wilk normality testing and the effect of HIV-1 Vpr expression on differential ISG expression was statistically analysed by two-way ANOVA with Sidak's post-test multiple comparison. **p<0.005 and n.s. denotes p>0.05 (not significant). Error bars indicate mean with S.E.M. of 4 independent donors for HIV-1 NL4.3-Vpr$^+$ transductions and 3 independent donors for HIV-1 NL4.3-ΔVpr transductions.

4.3.9 Generation of HIV-1 NL4.3 Vpr-mutated plasmids by site-directed mutagenesis

Together my analyses confirm that HIV-1 Vpr downregulates IFN-I production by HIV-1-transduced MDMs. The results presented in the previous sections of this chapter also suggest that HIV-1 Vpr downregulates expression of a subset of pro-inflammatory cytokines and chemokines. HIV-Vpr has been reported to downregulate IFN-dependent responses to HIV-1 in STING expressing TZM-bl cells [269], HeLa cells [5], primary MDMs [6], as well as PBMCs and Jurkat T-cells [260]. Although the exact mechanism by which HIV-1 Vpr exerts these effects is controversial, most reports agree that interactions between HIV-1 Vpr and the host cell DCAF1/DDB1/CUL4 E3 ubiquitin ligase complex via DCAF1 (also referred to as Vpr Binding Protein) is involved [4,245,270]. Most recently, Greenwood et al used a mass spectrometry-based approach to demonstrate that HIV-1 Vpr's interactions with the DCAF1/DDB1/CUL4 E3 ubiquitin ligase complex mediates degradation of cellular proteins and induces systems-level changes to the proteome of HIV-1 infected CEM T-cells [7].

To facilitate further investigation of the mechanism by which HIV-1 Vpr exerted the effects observed in my study, I used site-directed mutagenesis to mutate the HIV-1 NL4.3-Vpr^+ plasmid at residues critical for interaction with the DCAF1/DDB1/CUL4 E3 ubiquitin ligase complex. Additionally, to address the technical challenges that I encountered in my initial attempts to generate isogeneic HIV-1 NL4.3- Vpr^+ and HIV-1 NL4.3-ΔVpr plasmids, I used site-directed mutagenesis to introduce stop codons into the *vpr* ORF of the HIV-1

NL4.3-Vpr$^+$ plasmid. The Q5 mutagenesis approach used in these experiments utilises a pair of non-complementary primers, one of which bears the desired mutation site.

I first attempted to generate a substitution of histidine to arginine at residue 71 (H71R) in the HIV-1 *vpr* ORF as this mutation has been reported to disrupt HIV-1 Vpr functions mediated by the DCAF1/DDB1/CUL4 E3 ligase complex [271]. Having designed the mutagenesis primers (Table 8) in-house, it was necessary to determine the optimal conditions for each mutagenesis PCR. Therefore, I carried out the PCR at T_A of 60°C, 65°C and 70°C. Additionally, at each T_A I set up reactions with 5, 10 or 100 ng of template HIV-1 NL4.3-Vpr$^+$ plasmid. As shown in Figure 28 A, PCR product bands $\geq$ 10 kbp were observed across all conditions indicating that all input amounts of template plasmid DNA was sufficient for efficient amplification using the H71R primers. Faint bands were observed when 5 or 10 ng of template HIV-1 NL4.3-Vpr$^+$ plasmid were amplified at T_A of 60°C and 65°C. However, intense bands were visualised across all conditions at T_A of 70°C, suggesting that the H71R mutagenesis was most efficient at T_A of 70°C. Therefore, in order to minimise the amount of parental methylated DNA carried over into the DpnI digestion reaction, I used PCR product from the 5ng / 70°C reaction for subsequent mutagenesis steps. Representative results of Sanger sequencing of plasmid DNA derived from AmpR transformants shown in Figure 28 C confirmed the presence of the H71R mutation.

A mutation that disrupts HIV-1 Vpr binding to DCAF1 is the substitution of glutamine to arginine at residue 65 (Q65R) [9]. Having successfully generated the H71R mutation, I next attempted to generate the Q65R substitution, double Q65R/H71R substitutions and stop codons at K27 and S28 in the HIV-1 *vpr* ORF. For these reactions, 5 ng of template HIV-1

NL4.3-eGFP-Vpr^{+} plasmid were amplified at T_A of 60°C, 65°C and 70°C using the Q5 site-directed mutagenesis approach. However, these attempts were not successful as PCR products were not observed for any of reaction conditions (Figure 28B).

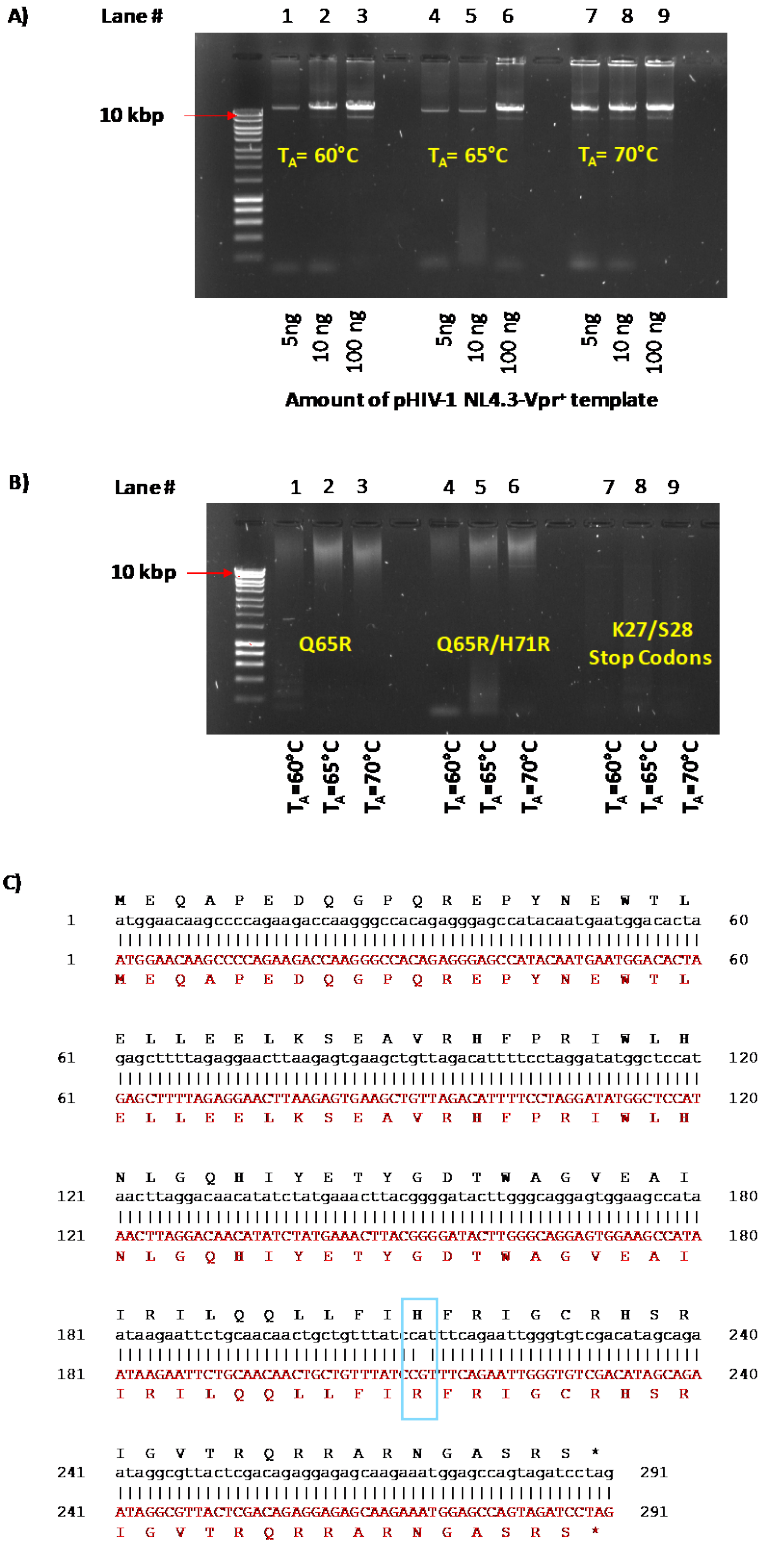


Figure 28: Site directed mutagenesis of the HIV-1 NL4.3-eGFP-Vpr+ plasmid *vpr* ORF using the NEB Q5 method

Figure 28: Site directed mutagenesis of the HIV-1 NL4.3-eGFP-Vpr$^+$ plasmid vpr ORF using the NEB Q5 method

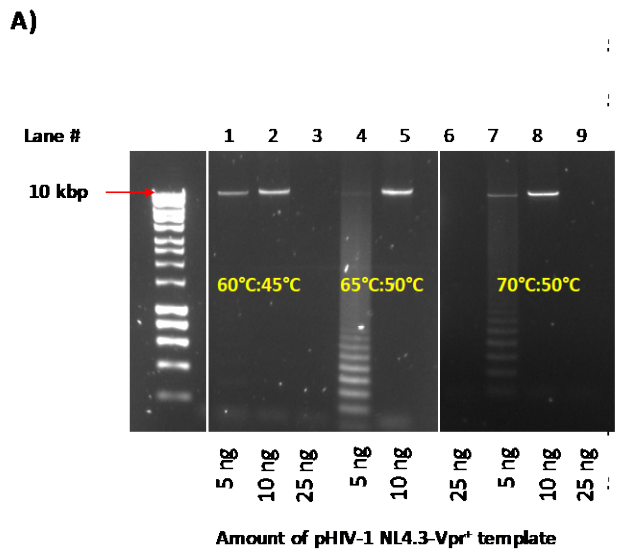
PCR was carried out according to the NEB Q5 mutagenesis method and products were visualised by electrophoresis on a 1 % agarose gel for A) H71R mutagenesis reactions carried out at annealing temperatures ranging from 60 – 70°C with 5 - 100 ng of pHIV-1 NL4.3-eGFP-Vpr$^+$ template B) Q65R mutagenesis, Q65R/H71R mutagenesis and K27/S28 stop codon substitution reactions carried out at annealing temperatures ranging from 60 – 70°C with 5 ng of pHIV-1 NL4.3-eGFP-Vpr$^+$. After PCR cycles were completed, methylated parental DNA in the PCR product was digested using DpnI. The digest product was used to transform competent E. coli. Amp^R colonies from successful transformations were expanded, plasmid DNA was extracted from the culture, and the presence of the mutation was verified using Sanger Sequencing. C) Representative alignment of the reference sequence for the HIV-1 vpr ORF (in black) and the sequence of the H71R mutated HIV-1 ORF (in red) determined by Sanger sequencing.

Low PCR amplification efficiency is a common technical challenge in SDM experiments. To address this limitation, Liu and Naismith [194] developed a modified approach to SDM primer design in which the mutagenesis primer pair contains non-overlapping sequences at their 3' end, primer-primer complementary (overlapping) sequences at their 5' end and the desired mutation site located within the overlapping region. This modified primer design facilitates exponential PCR amplification as newly synthesized PCR products can be used as the templates in subsequent PCR amplification cycles.

I re-designed mutagenesis primers for the Q65R substitution and for introducing stop codons at K27, S28 and K27/S28 according to the Liu and Naismith guidelines (Table 8). Using the re-designed primers, 5 - 25 ng of template HIV-1 NL4.3-eGFP-Vpr$^+$ plasmid were

amplified at three separate Tm_{no} - 5°C : Tm_{pp} - 5°C combinations; 60°C : 45°C, 65°C : 50°C and 70°C : 50°C ('Tm_{pp}' denotes the melting temperature calculated from the primer-primer overlap sequence and 'Tm_{no}' denotes the melting temperature calculated from the non-overlapping primer sequences). Figure 29A shows that amplification using the K27 primers was successful at all annealing temperatures when 10 ng of template HIV-1 NL4.3-eGFP-Vpr^+ plasmid was used, but use of 5 ng template often generated multiple non-specific PCR products, and amplification was not successful with 25 ng template. Similarly, Figure 30A shows that amplification using the S28 primers was successful for the 60°C : 45°C and 70°C : 50°C reactions when 10 ng of template plasmid was used, but use of 5 ng template often generated multiple non-specific PCR products, and amplification was not successful with 25 ng template was used. Lastly, Figure 31A shows that amplification using the K27/S28 primers was successful at all temperature combinations when 10 ng of template plasmid was used. However, K27/S28 amplification was not successful when either 5 ng or 25 ng of template was used.

Therefore, for each of the K27, S28 and K27/S28 reactions, PCR product from the 10 ng / 70°C : 50°C condition was used for subsequent mutagenesis steps. Representative results of Sanger sequencing of plasmid DNA derived from Amp^R transformants shown in Figure 29B, Figure 30B and Figure 31B confirmed the presence of the K27, S28 and K27/S28 mutations respectively. Unfortunately, due to the time constraints of this study, I was not able to generate the Q65R-mutated HIV-NL4.3 plasmid using the re-designed primer pair.



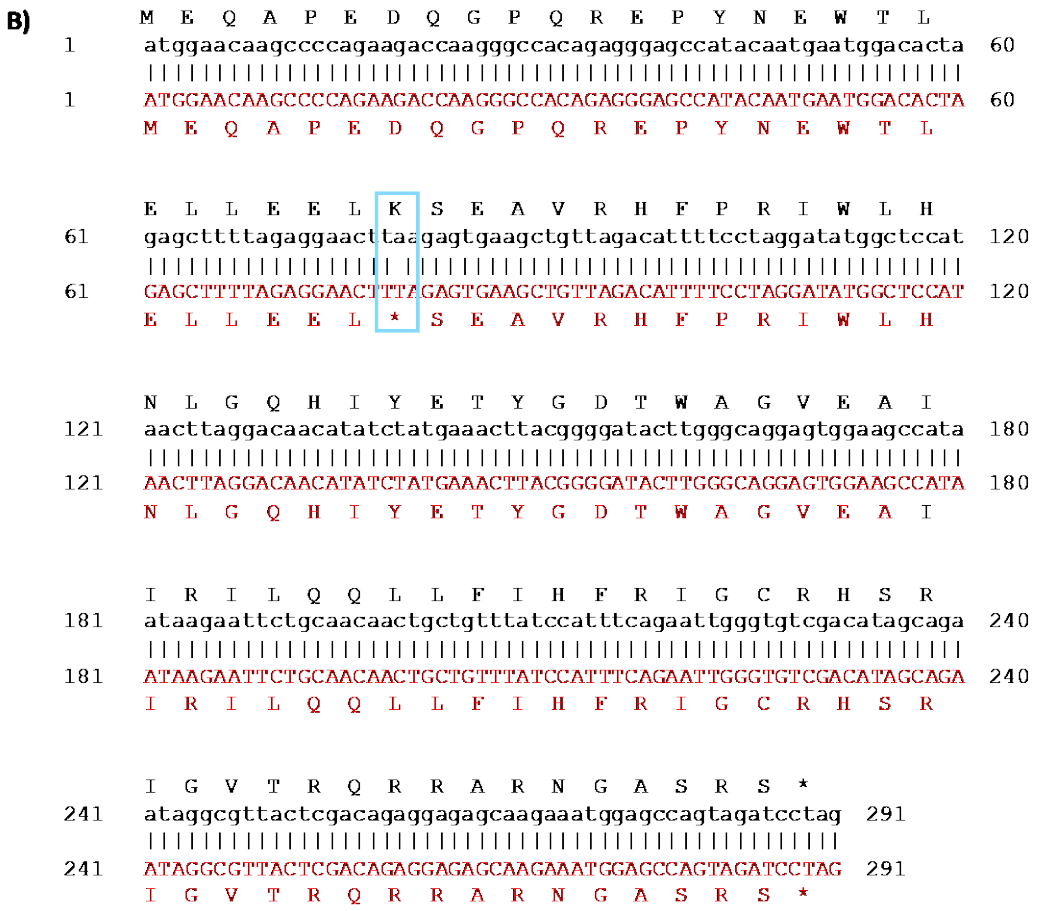


Figure 29: Site-directed mutagenesis of the HIV-1 NL4.3-Vpr+ plasmid to introduce a stop codon mutation at position K27 in the HIV-1 *vpr* ORF

Figure 29: Site-directed mutagenesis of the HIV-1 NL4.3-Vpr$^+$ plasmid to introduce a stop codon mutation at position K27 in the HIV-1 vpr ORF

A) PCR reactions for K27 stop codon mutagenesis were carried out according to the Liu and Naismith protocol with two separate annealing steps (represented as Tm_{no} - 5°C : Tm_{pp} - 5°C). 'Tm_{pp}' denotes the melting temperature calculated from the primer-primer overlap sequence and 'Tm_{no}' denotes the melting temperature calculated from the non-overlapping primer sequences. For the K27 mutagenesis reactions, Tm_{no} - 5°C ranged from 60 – 70°C while Tm_{pp} - 5°C ranged from 45 – 50°C. 5 - 25 ng of pHIV-1 NL4.3-eGFP-Vpr$^+$ template were used for each Tm_{no} - 5°C : Tm_{pp} - 5°C combination. PCR products were visualized by electrophoresis on a 1 % agarose gel and methylated parental DNA in the PCR product was digested using DpnI. The digest product was used to transform competent E. coli. The presence of the stop codon mutation was verified using Sanger Sequencing of plasmid DNA extracted from cultures of transformed E. coli. B) Representative alignment of the reference sequence for the HIV-1 vpr ORF (in black) and the sequence of the mutated HIV-1 ORF (in red) determined by Sanger sequencing. The asterisk (*) denotes a stop codon.

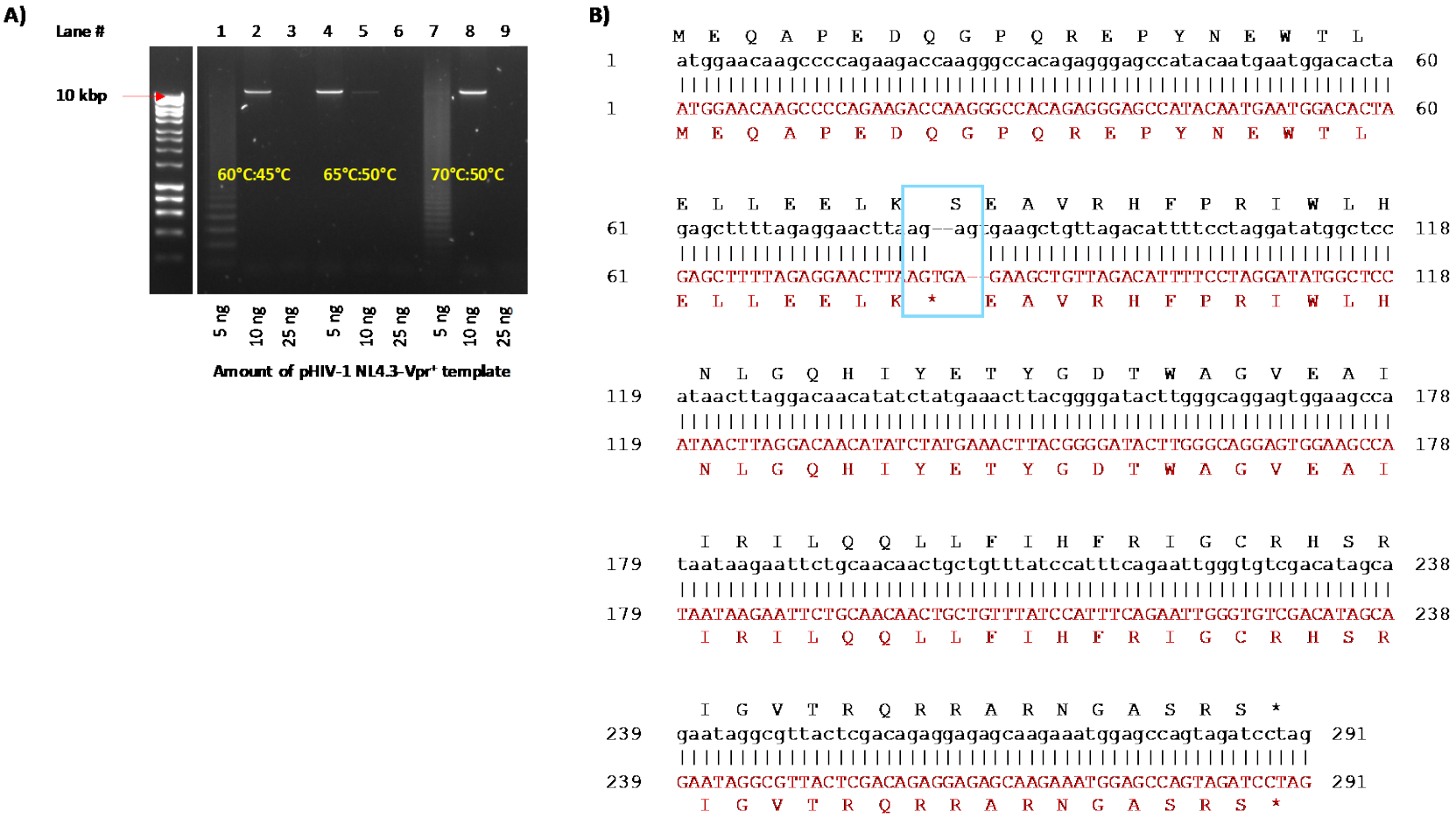


Figure 30: Site-directed mutagenesis of the HIV-1 NL4.3-Vpr$^+$ plasmid to introduce a stop codon mutation at position S28 in the HIV-1 *vpr* ORF

Figure 30: Site-directed mutagenesis of the HIV-1 NL4.3-Vpr$^+$ plasmid to introduce a stop codon mutation at position S28 in the HIV-1 vpr ORF

A) PCR reactions for S28 stop codon mutagenesis were carried out according to the Liu and Naismith protocol with two separate annealing steps (represented as Tm_{no} - 5°C : Tm_{pp} - 5°C). 'Tm_{pp}' denotes the melting temperature calculated from the primer-primer overlap sequence and 'Tm_{no}' denotes the melting temperature calculated from the non-overlapping primer sequences. For the S28 mutagenesis reactions, Tm_{no} - 5°C ranged from 60 – 70°C while Tm_{pp} - 5°C ranged from 45 – 50°C. 5 - 25 ng of pHIV-1 NL4.3-eGFP-Vpr$^+$ template were used at each Tm_{no} - 5°C : Tm_{pp} - 5°C combination. PCR products were visualized by electrophoresis on a 1 % agarose gel and methylated parental DNA in the PCR product was digested using DpnI. The digest product was used to transform competent E. coli. The presence of the stop codon mutation was verified using Sanger Sequencing of plasmid DNA extracted from cultures of transformed E. coli. B) Representative alignment of the reference sequence for the HIV-1 vpr ORF (in black) and the sequence of the mutated HIV-1 ORF (in red) determined by Sanger sequencing. The asterisk (*) denotes a stop codon.

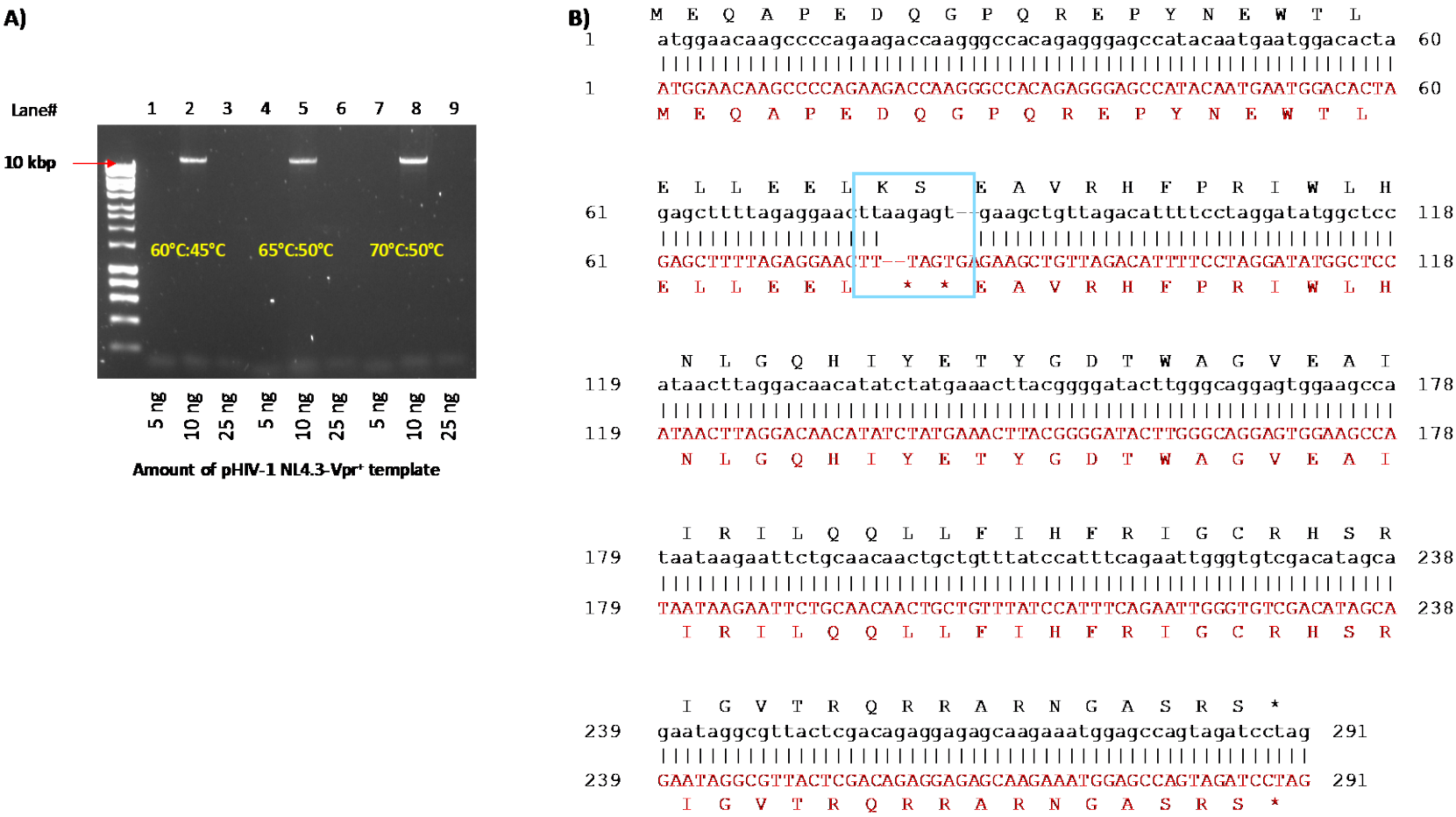


Figure 31: Site-directed mutagenesis of the HIV-1 NL4.3-Vpr$^+$ plasmid to introduce stop codon mutations at position K27 and S28 in the HIV-1 *vpr* ORF

Figure 31: Site-directed mutagenesis of the HIV-1 NL4.3-Vpr$^+$ plasmid to introduce stop codon mutations at position K27 and S28 in the HIV-1 vpr ORF

A) PCR reactions for the K27/S28 stop codon mutagenesis were carried out according to the Liu and Naismith protocol with two separate annealing steps (represented as Tm_{no} - 5°C : Tm_{pp} - 5°C). 'Tm$_{pp}$' denotes the melting temperature calculated from the primer-primer overlap sequence and 'Tm$_{no}$' denotes the melting temperature calculated from the non-overlapping primer sequences. For the K27/S28 mutagenesis reactions, Tm_{no} - 5°C ranged from 60 – 70°C while Tm_{pp} - 5°C ranged from 45 – 50°C. 5 - 25 ng of pHIV-1 NL4.3-eGFP-Vpr$^+$ template were at each Tm_{no} - 5°C : Tm_{pp} - 5°C combination. PCR products were visualized by electrophoresis on a 1 % agarose gel and methylated parental DNA in the PCR product was digested using DpnI. The digest product was used to transform competent E. coli. The presence of the stop codon mutations was verified using Sanger Sequencing of plasmid DNA extracted from cultures of transformed E. coli. B) Representative alignment of the reference sequence for the HIV-1 vpr ORF (in black) and the sequence of the mutated HIV-1 ORF (in red) determined by Sanger sequencing. The asterisk (*) denotes a stop codon.

4.4 Discussion

For the transduction experiments detailed in this chapter, I employed a single-cycle vector system to minimize potential confounding factors that arise during multiple rounds of infection, such as autocrine feedback loops. I also reduced the complexity of the transduction protocol to limit artefacts potentially associated with spinoculation and use of poly-cationic agents that enhance transduction. Under these conditions, I demonstrate that Vpr modulates the immunoproteome with particular inhibitory impact upon IFN-I and a set of proinflammatory cytokines and chemokines. Since HIV-1 infection of macrophages has been described to be reduced in M1-type differentiated cells [272], it would make sense for the virus to reduce macrophage differentiation in this type of cytokine environment. Vpr expression may therefore allow macrophages to maintain a more undifferentiated HIV-1-permissive state.

Of particular interest, Vpr downregulated IFN-I and appeared to downregulate selected ISGs including HIV-1-specific restriction factors such as MX2, which would further act to reduce a spreading HIV-1 infection in macrophages [273]. Indeed, in studies in which replication-competent ΔVpr virus has been used to infect macrophages, replication was limited compared to its Vpr^+ counterparts [6,249,250]. The use of single-cycle pseudotyped virus in this study avoids this effect, allowing equivalent transduction efficiencies with both ΔVpr and Vpr^+ vectors.

The magnitude of HIV-1 induced IFN-I-dependent immune responses in macrophages remains a topic of debate. Various authors have concluded that sensing of HIV-1 nucleic acids and reverse transcripts in macrophages is mediated by pattern recognition receptors

(PRRs) such as RIG-I [274], cGAS [108] and Toll-like receptors [275] leading to downstream induction of IFN-I signalling [276]. In contrast, other studies show that HIV-1 is a weak inducer of innate immunity in macrophages [209,210], and either circumvents the triggering of IFN-I-mediated responses by cloaking viral PAMPs within the viral capsid until entry into the nucleus [277] or expresses virulence factors which counteract host cell viral restriction and sensing [261,267]. In this study, HIV-1_{BaL} Env/HIV-1 NL4.3-ΔVpr pseudotyped virus transduction of MDMs led to readily detectable levels of IFN-α induction and IFN-I bioactivity in MDM supernatants, whereas Vpr^+ vectors produced borderline or undetectable levels, consistent with a role of Vpr in dampening these responses in macrophages.

The host cell restriction factor SAMHD1 has been shown to limit viral induction of IFN-I production [265]. SIV Vpx was used to facilitate efficient MDM transduction in my study and is known to downregulate SAMHD1 activity. Therefore, the possibility exists that SIV Vpx supplementation may have enhanced IFN responses of MDMs. While all transductions were carried out in the presence of minimal SIV Vpx VLP supplementation, it is clear that IFN-α induction and IFN-I bioactivity were specifically and markedly enhanced in response to transduction with HIV-1_{BaL} Env/HIV-1 NL4.3-ΔVpr pseudotyped virus. Nonetheless, I cannot rule out that SIV Vpx VLP treatment may have influenced the IFN-I responses of HIV-1-transduced MDMs in my study.

Previous studies have investigated the effect of HIV-1 Vpr on mRNA expression in MDMs [10], MDDCs [8], $CD4^+$ T-cells [9] or on cytokine expression in a STING-reconstituted TZM-bl cell line [269]. However, this study represents the first wide-scale investigation of the

effect of HIV-1 Vpr on soluble mediators of inflammation in primary MDMs. I found that HIV-1 induced significant upregulation of a subset of cytokines/chemokines and that this effect was enhanced in the absence of HIV-1 Vpr expression. Due to time constraints, this study did not extend to investigating underlying molecular mechanisms of these observations. However, my findings are in line with Trotard et. al's observation that HIV-1-induced cytokine mRNA expression in a STING-reconstituted TZM-bl cell line is significantly enhanced in the absence of HIV-1 Vpr expression [269]. Although Trotard et. al. did not find that enhanced mRNA expression translated to upregulated cytokine or IFN-I secretion, in my study expression of IFN- α, IL-1β and CCL4/MIP-1β were significantly downregulated by HIV-1 Vpr. Additionally, levels of CXCL9/MIG, CXCL10/IP-10, CXCL11/ITAC and MIF were decreased in the presence of HIV-1 Vpr expression although these trends were not statistically significant. The discrepancy in cytokine expression between my study and Trotard et. al's is possibly due to the TZM-bl cell line's inability to completely recapitulate all of the HIV-1 recognition events that occur in MDMs. Nonetheless, this observation is notable as investigations into the effect of Vpr on MDM expression of genes relevant to the innate immune response have implicated interferon regulatory factor 3 (IRF3), a protein which is activated downstream of HIV-1 sensing by cGAS-STING and regulates the transcription of IFN-I, as a target of Vpr. Together, these results suggest that HIV-1 Vpr antagonisation of MDM responses to infection may involve manipulation of the cGAS-STING pathway and downstream effectors of IFN-I signalling.

I observed a striking upregulation of CXCL10/IP-10 expression by transduced MDMs for the majority of donors investigated in our study. The strong induction of CXCL10/IP-10 mirrors

the findings of clinical studies that have report elevated levels of the chemokine in the plasma of HIV-1-infected individuals [278-280]. Although CXCL10/IP-10 is strongly associated with HIV-1 infection [281], and is primarily induced by IFN-γ downstream of STAT, NFκB, PI3K or MAPK signaling, I detected negligible IFN-γ expression in the supernatants of transduced macrophages. However, given that IFN-I activity was readily detectable in the supernatants of MDMs in my study, it is possible that CXCL10/IP-10 expression was induced in an IFN-I dependent manner downstream of TLR7/9 sensing of HIV-1 as reported previously by Simmons et al with monocytes [282].

The exact mechanism by which HIV-1 Vpr downregulates IFN responses in MDMs remains elusive. It is well established that HIV-1 Vpr engages with the DCAF1-DDB1-Cullin4 E3 ubiquitin-ligase complex through its interaction with DCAF1/Vpr binding protein [5,283] and thereby mediates multiple changes to the host cell proteome [7]. In order to facilitate further study of the mechanisms by which HIV-1 Vpr downregulated IFN-I responses in this study, I generated HIV-1 NL4.3-eGFP mutants that are either defective for HIV-1 Vpr expression or are defective for interactions with the Vpr binding protein of the E3 ubiquitin-ligase complex. Unfortunately, due to the significant time required to overcome the technical challenges of the site-directed mutagenesis approach, time limitations precluded further investigations using these Vpr mutants. However, in the context of IFN signaling, other authors have proposed that Vpr recruits IRF3 for ubiquitination and degradation by DCAF1-DDB1-CUL4-E3-ligase complex and thereby antagonises IFN responses to HIV-1 [260]. In contrast, Harman et. al demonstrate that HIV-1 Vpr does not target IRF3 for degradation but instead propose that HIV-1 Vpr directly interacts with the

kinase TBK1 thereby disrupting its activation and subsequent IRF3 phosphorylation, nuclear translocation, and induction of IFN gene expression [261]. While either of these mechanisms would account for the Vpr-dependent downregulation of IFN-α observed in my study, these findings and proposed mechanisms contradict previous investigations that suggest that HIV-1 Vpr potentiates IFN-I responses in $CD4^+$ T-cells [9] and upregulates ISG expression in MDDCs [8]. Therefore, the question of whether the molecular mechanisms underlying HIV-1 Vpr's modulation of immune responses may be cell-type dependent warrants further study.

A limitation of my study's experimental approach was the use of SIV-2 Vpx to downregulate SAMHD1 restriction and facilitate HIV-1 NL4.3 transduction of MDMs. It is contested that in the absence of factors such as SIV-2 Vpx which increase the host cell's ability to sense viral PAMPs, macrophages do not produce an innate response to HIV-1 infection [209]. My experimental approach emphasized the use of a low MOI, moderate transduction protocol and a CCR5-trophic HIV-1-derived Env for vector pseudotyping. Under these conditions, it was not possible to efficiently transduce MDMs without SIV-2 Vpx supplementation. However, I have corrected for any possible SIV-2 Vpx induced MDM activation by representing all fold-changes with respect to the relevant ΔEnv/HIV-1 NL4.3 control transduction in which MDMs were exposed to an equivalent dosage of SIV-2 Vpx. Additionally, extensive optimisation of my experimental protocol was carried out to ensure that a minimal amount of SIV-2 Vpx was used for MDM transductions. However, I cannot rule out the possibility that inoculating MDMs in the presence of SIV-2 Vpx enhanced MDM recognition of viral PAMPs.

Lastly, the power of statistical analyses in this study was limited by the considerable inter-donor variation in MDM responses to HIV-1 transduction and HIV-1 Vpr expression. Similar inter-donor variation has been previously reported in transcriptional studies [10] and is presumably due to differences in the expression or activity of host cell sensing machinery between the different donors. While all MDMs were transduced at a MOI of 0.25 and there was no significant difference in the net efficiency of NL4.3-ΔVpr versus NL4.3-Vpr^{+} MDM transductions, the efficiency of transduction did vary between individual donors. This suggests that donor-dependent differences in viral permissivity or expression of host antiviral factors may also contribute to the variability in the magnitude of responses to HIV-1.

4.5 Conclusion

This work presented in this chapter represents a wide-scale investigation of the effect of HIV-1 Vpr on soluble mediators of inflammation and activation of pathways relevant to the innate immune response in HIV-1 transduced primary MDMs.

Using an HIV-1 transduction system optimised for maximum biological relevance, primary MDMs were transduced with single-round HIV-1 pseudotyped viruses encoding, or deleted for, *vpr*. Contrary to previous reports, I demonstrate that HIV-1 Vpr expression does not alter the efficiency of MDM transduction.

To avoid limitations of transcriptomic approaches I measured secreted proteins of relevance to immune responses using complementary immunoassays and cell-based assays of IFN-I activity. Using these approaches, I show that HIV-1 induces a modest pro-inflammatory response in MDMs and that HIV-1 Vpr downregulates a small subset of inflammatory factors (IFN- α, IL-1β and CCL4/MIP-1β). My results are consistent with the conclusion HIV-1 Vpr downregulates the type-I IFN response in terms of type-I IFN production. However, in contrast to previous studies I do not find that CXCL10/IP-10 is modulated in a Vpr-dependent manner. HIV-1 Vpr therefore likely promotes HIV-1 replication in vivo by reduction of anti-viral innate immune responses.

Chapter 5:

Investigating primary monocyte migration towards supernatants of HIV-1-transduced MDMs and recombinant HIV-1 Env

5.1 Introduction

Chemotaxis refers to the directional migration of cells along a concentration gradient of chemical stimulus (chemoattractant) [284] and is essential to embryonic development, tissue repair, wound healing and the defence mechanisms of the immune system. The extracellular chemical stimuli necessary to direct chemotaxis are often provided by chemokines, a diverse group of small, secreted cytokines that bind to and signal through seven-transmembrane G protein-coupled chemokine receptors (GPCRs) [285].

Monocytes are a subset of circulating leucocytes known for their enhanced trafficking in response to inflammatory signals, from the bone marrow and peripheral circulation to distinct tissue sites [286]. These inflammatory monocytes can differentiate into a range of infiltrating macrophages or DCs and mediate host antimicrobial defences [287] at their target tissues. Work with murine models has shown that infiltrating monocytes also contribute to anti-tumour activity [288]. Monocyte trafficking is essential to their roles in immune defence and maintaining tissue homeostasis. Moreover, dysregulated monocyte trafficking is implicated as a central aspect of the pathophysiology of many inflammatory disorders including HIV-1-associated CVD [132] and neurocognitive disorders [135,166].

Of particular relevance to studies of the effect of HIV-1 infection on monocyte trafficking is the HIV-1 envelope glycoprotein, Env. Env is present on the virus surface as trimers of gp120/gp41 heterodimers in which the external gp120 domain is non-covalently associated with gp41, the transmembrane domain. Initial engagement of the primary HIV-1 receptor CD4 by gp120 induces a conformational change that exposes the V3 loop and CD4-induced region of gp120 for subsequent binding to the co-receptor CCR5. CCR5 engagement by

gp120 then triggers structural rearrangement of the trimer, activating gp41 and leading to exposure of its fusogenic domain. Fusion of the target cell and viral membranes enable viral entry and infection [19].

Notably, HIV-1 gp120 is readily shed from the surface of HIV-1 and is detectable in conditioned media from infected cells, and in the serum [289,290] and tissues [291] of HIV-1 positive individuals. The HIV-1 co-receptor CCR5 is a seven-transmembrane G protein-coupled chemokine receptor, and gp120 binding to CD4 and CCR5 has been reported to induce chemotaxis of T-cells [172,173,292] and immature DCs [170,171]. Furthermore, although productive HIV-1 infection is restricted in blood monocytes, they express CD4 and CCR5. Chemokine mimicry by HIV-1 gp120 therefore provides a potential mechanism by which HIV-1 infection may contribute to enhanced monocyte activation and trafficking in HIV-1-associated inflammation. Although gp120-mediated induction of T-cell and DC migration is well reported, the effects of Env on $hCD14^{+}$ blood monocyte migration warrants further study.

Numerous methods have been developed to study mechanisms of leucocyte migration and identify physiological chemoattractants important for immune function and the pathophysiology of inflammatory disorders. The Zigmond, Dunn and Boyden chambers are key examples of early approaches to studying cell migration. The Zigmond chamber [293] consists of a plastic or glass slide engraved with two troughs separated by a raised bridge Figure 32A. A concentration gradient is formed across the bridge by filling one trough with chemoattractant and the other with control media. A coverslip coated with adherent cells

is then inverted over the troughs and the migration of cells across the bridge in response to the gradient is monitored by microscopy.

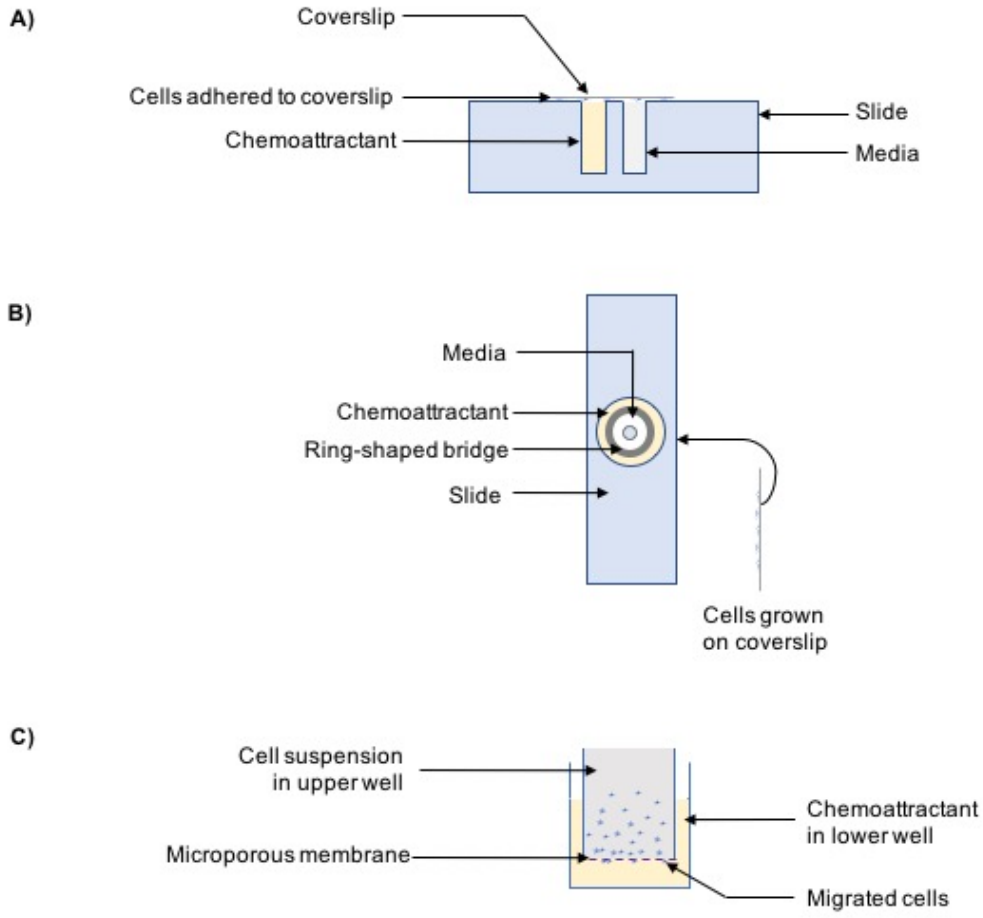


Figure 32: Schematic representation of cell migration assays

The Dunn chamber [294] is a modification of the Zigmond chamber in which a glass slide is engraved with two concentric circular wells separated by a central ring-shaped bridge (Figure 32B). One well is filled with chemoattractant and the other with control media, thereby forming a concentration gradient over the bridge. A coverslip coated with adherent cells is inverted over the concentric wells and the migration of cells across the

bridge is observed by microscopy. By enclosing the concentric wells with a coverslip, Dunn's modification reduced evaporation of the experimental set-up and improved the stability of the chemoattractant concentration gradient.

The Boyden chamber [295] features two chambers of wells separated by microporous membrane. Cells in suspension are loaded into the upper wells above the filter, while chemoattractant is loaded into the bottom wells, below the filter (Figure 32C). At the end of the assay, the number of cells that have migrated through the pores and adhered to the underside of the membrane or migrated through the pores into the lower wells, is determined by microscopy or DNA quantification. Presently, most commercially available methods for studying cell migration are based on the Boyden chamber design.

Limitations of early migration assay design include the difficulty in maintaining stable agonist concentration gradients, the need for pre-assay labelling of cells, which may alter their gene expression and subsequent performance in the migration assay, or the need for post-assay labelling which may lead to inconsistent data because of differences in intra-assay labelling efficiency. Additionally, accurate cell counting by microscopy is difficult when the density of cells adhered to trans-well membranes is high and microscopy-based quantification of migrated cells can be prone to user bias. Lastly, traditional migration assays do not provide insight into the kinetics of cell migration as they are based on a single end-point for data collection.

More recent assays have attempted to address these limitations by applying microfluidics [296,297], image-based TAXIScan technology [298], 3-D collagen gels [299], agarose gels

[300], electrical cell impedance technology [301,302], or a combination of the latter two [303] to improve upon the traditional methods of measuring cell migration.

One electrical cell impedance-based platform for measuring cell migration is the xCELLigence real-time cell analyser - dual purpose (RTCA-DP) system [304]. xCELLigence RTCA-DP migration assays are carried out using a 16-well cell invasion and migration (CIM-16) plate depicted in Figure 33. The CIM-16 plate is a modified Boyden chamber that consists of an upper well with a microporous membrane underside (yellow dotted line) that is integrated with microelectronic sensors (Figure 33A)**.** When chemoattractant is present in wells of the lower chamber (Figure 33B), cells loaded into the upper chamber migrate through the 8.0 µm pores of the CIM-16 membrane towards chemoattractant in the bottom chamber (Figure 33 C). Migrated cells adhere to the underside of the electrode (Figure 33 D) and produce a signal of electrical impedance.

Signals of electrical impedance are interpreted as the dimensionless parameter, Cell Index (CI) that is derived as follows:

$$CI = Max_N \frac{R_{cell}}{R_b} - 1 \qquad [305]$$

where N= the number of points on the membrane where impedance was measured, R_b = background resistance measured without cells and R_{cell} = resistance measured across the electrode when cells are present. Therefore, the magnitude of cell impedance increases as the surface area of the electrode covered with cells increases. In comparison to traditional migration assays, the xCELLigence RTCA-DP platform allows for real-time measurement of adherent cell migration without the need for pre- or post-assay labelling, generates kinetic

data for cell migration, and eliminates any potential bias introduced by user-quantification of migrated cells by microscopy.

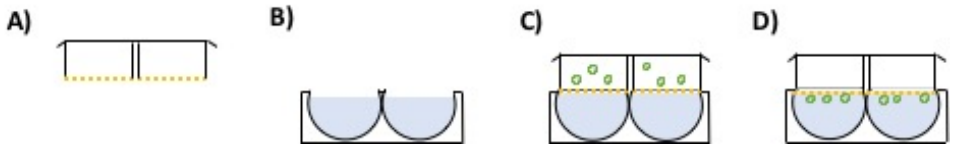


Figure 33: Schematic representation of the xCELLigence RTCA-DP cell invasion and migration assay

Schematic of the xCELLigence RTCA-DP cell invasion and migration (CIM-16) assay. The CIM-16 plate is a modified Boyden chamber that consists of A) an upper well with a microporous membrane underside (yellow dotted line) that is integrated with an electrode and B) a lower chamber into which agonist is loaded. C) Cells loaded into the upper chamber migrate through the microporous membrane towards chemoattractant in the bottom chamber. D) Migrated cells adhere to the underside of the electrode, producing a measure of electrical impedance that is output as Cell Index, CI.

5.2 Chapter Rationale

I hypothesised that I) chemokine mimicry by HIV-1 Env soluble components and II) chemotactic factors produced by HIV-1-infected macrophages provide a potential mechanism by which HIV-1 infection contributes to enhanced monocyte activation and trafficking during HIV-1-associated inflammation. Although HIV-1 Env-mediated induction of T cell and DC migration is well reported, the effects of Env and its components on $hCD14^{+}$ blood monocyte migration warrants study, particularly as this cell type is implicated as a mediator of HIV-1-associated inflammatory conditions. Additionally, my

analyses of the soluble proteome of HIV-1-transduced MDMs reveal chemokines among a subset of inflammatory factors that are upregulated in response to HIV-1.

Since traditional assays for investigating leucocyte migration are limited by the need for pre- or post-assay labelling of cells, unstable concentration gradients and a reliance on microscopy-based quantification of migrated cells, which can be prone to user bias, I developed an xCELLigence RTCA-DP CIM-16 migration assay to address these limitations.

Therefore, through the work I present in this chapter I aimed to:

I. Optimise the xCELLigence RTCA-DP electrical cell impedance-based assay to measure the migration of negatively isolated human $CD14^+$ monocytes
II. Validate the ability of the xCELLigence RTCA-DP system to measure chemotaxis of freshly isolated $hCD14^+$ monocytes towards a range of CC and non-CC chemokines
III. Apply the assay to investigate of chemokine mimicry by soluble HIV-1 Env components and migration towards supernatants of HIV-1-transduced MDMs

5.3 Results

5.3.1 Characterisation of cell surface marker and chemokine receptor expression by CD14$^+$ blood monocytes

As shown in Figure 34B flow cytometry analysis of negatively selected CD14$^+$ monocytes confirmed an average of 95.1% purity across the 5 donors analysed. The hCD14$^+$ monocytes were isolated from PBMCs, therefore the small population of contaminating cells were probably a mixture of lymphocytes (T cells, B cells and NK cells) and DC. The level of expression of each surface marker differed substantially between donors. hCD14$^+$ monocytes significantly expressed the HIV-1 receptor CD4 ($p = 0.008$) and co-receptor CCR5 ($p = 0.007$), as well as the chemoattractant receptor CCR2 ($p = 0.008$) when compared to isotype-stained cells, labelling carried out in the presence of Fc receptor block. While signals were detected for CXCR4 ($p = 0.06$) and C5aR ($p = 0.06$) expression, signal above the isotype stained condition was not statistically significant. Additionally, analyses show that expression of FPR1 ($p = 0.4$) was low to absent. There was no significant difference in MFI between the isotype and unstained conditions for any of the markers investigated.

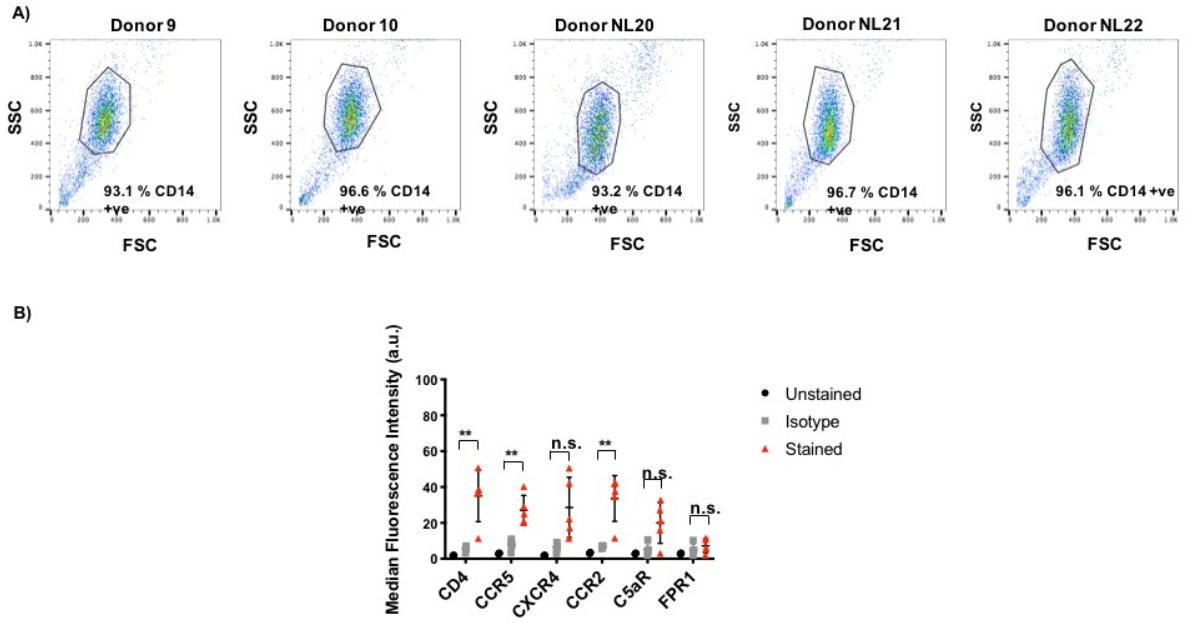


Figure 34: Analysis of cell surface maker and chemokine receptor expression by primary CD14⁺ monocytes

Negatively isolated CD14⁺ monocytes were analyzed by flow cytometry. A) Gating shows live cells with forward scatter (FSC) represented on the x-axis and side scatter (SSC represented on the y-axis). B) hCD14⁺ monocyte expression of CD4 and the chemokine receptors CCR2, CCR5, C5aR, and CXCR4 was measured by flow cytometry. Error bars represent mean with S.D. for 5 different donors. ** p<0.01 and n.s. denotes 'not significant' when MFI of the stained cells was compared to the respective isotype condition by the Holm-Sidak test.

5.3.2 Optimisation of human CD14⁺ monocyte density for xCELLigence migration assay

I sought to determine the minimal density of cells required to detect hCD14⁺ monocyte migration using the CIM-16 plate and the xCELLigence RTCA-DP system. To this end,

hCD14^{+} monocytes negatively selected from 3 individual donors were loaded into the upper wells of the CIM-16 plate at cell densities ranging from 1 x 10^5 – 8 x 10^5 cells per well and were allowed to migrate towards either vehicle (X-vivo media only) or 5 nM CCL2 / MCP-1. CCL2 / MCP-1 was used as a chemoattractant in these initial experiments as its function as a potent monocyte chemoattractant has been widely reported.

Measurement of monocyte migration in real-time generated curves of *Delta Cell Index vs Time* which I analysed using both area under curve (AUC) and $Max_{\Delta Cell\ Index}$ - $Min_{\Delta Cell\ Index}$ as indices of hCD14^{+} migration. Monocyte migration in the absence of chemoattractant (vehicle condition) generated measurable signals of electrical cell impedance and these cell index values increased with increasing cell density, indicating that non-directed hCD14^{+} monocyte migration contributes to the net magnitude of cell index measurements. However, it is unlikely that non-directed migration confounds cell index measurement to a large extent since cell index values generated by hCD14^{+} monocyte migration towards CCL2 / MCP-1 were consistently greater than those measured for the respective vehicle condition across all cell densities. Nonetheless, to account for any contribution of non-directed migration to estimates of chemotaxis, the vehicle condition was included in all reported assays and used for baseline correction of analyses.

Traces of cell index generated by monocyte migration towards CCL2/MCP-1 (Figure 35 A) highlight the inter-donor variation in both the magnitude and kinetics of hCD14^{+} monocyte response to chemoattractants. AUC analyses show that, in comparison to the vehicle condition, significant cell impedance signals were generated in response to CCL2/MCP-1 when either 4 x 10^5 monocytes ($p = 0.03$) or 8 x 10^5 monocytes ($p < 0.0001$) were loaded

per well, but not for 1 x 10^5 or 2 x 10^5 cells (Figure 35 B). $Max_{\Delta Cell\ Index}$ - $Min_{\Delta Cell\ Index}$ analysis of the migration curves reported a significant difference in the cell index signals generated using a density of 8 x 10^5 monocytes per well only ($p < 0.0001$).

I selected a working density of 4 x 10^5 $hCD14^+$ monocytes per well for future assays as this cell load was sufficient to generate a measurable increase in cell index response to the positive control chemokine (CCL2/MCP-1) and has been previously used to measure $hCD14^+$ monocyte chemotaxis with CIM-16 plates [306]. Furthermore, when compared to greater cell densities, using a working density of 4 x 10^5 cells per well generated less non-directed background migration and required a smaller, more practical scale of monocyte isolation per experiment.

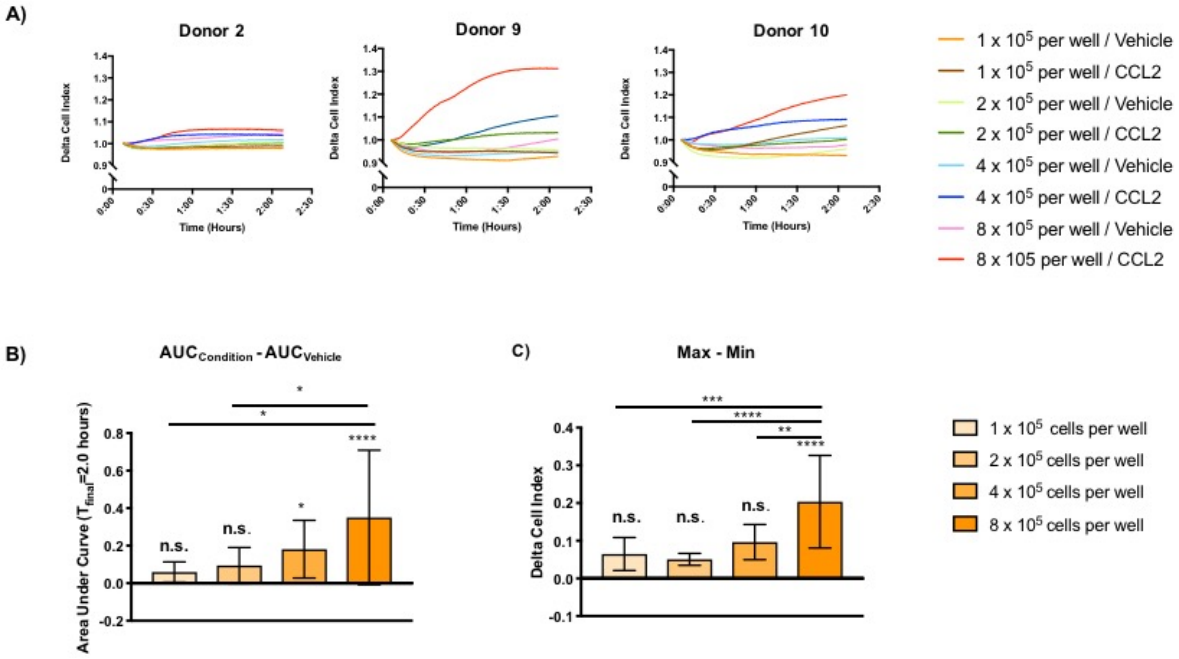


Figure 35: Optimisation of $hCD14^+$ monocyte density for xCELLigence migration assay

A) Traces of the xCELLigence RTCA-DP delta cell index values measured due to the migration of $hCD14^+$ blood monocytes isolated from 3 separate donors. B) Area under curve and C) Max-Min analysis of cell

index signals generated by CD14⁺ blood monocyte migration towards 5 nM CCL2. The vehicle condition (X-Vivo$_{10}$) was used for baseline correction of all AUC values. Error bars represent S.D. for 3 individual donors with 3 replicate wells per condition. The dataset was assessed by Shapiro-Wilk normality testing and *p<0.05, **p < 0.01, ***p < 0.001, ****p<0.0001 and n.s. denotes 'not significant' for one-way ANOVA with Holm-Sidak's post-test comparisons.

5.3.3 Validation of hCD14⁺ monocyte migration and adherence to the underside of the CIM-16 membrane in response to chemoattractant

Scanning electron microscopy images of the CIM-16 plate confirmed that hCD14⁺ monocytes adhere to the underside of the membrane after moving across the 8 µM pores towards chemoattractant in the bottom chamber. The density of monocytes adhered to the membrane was increased in response to 5 nM CCL2/MCP-1 in the bottom (Figure 36 A) wells compared to when vehicle was present in the bottom wells (Figure 36 B). Monocyte adherence to the membrane in (Figure 36 A) represents random migration across the membrane.

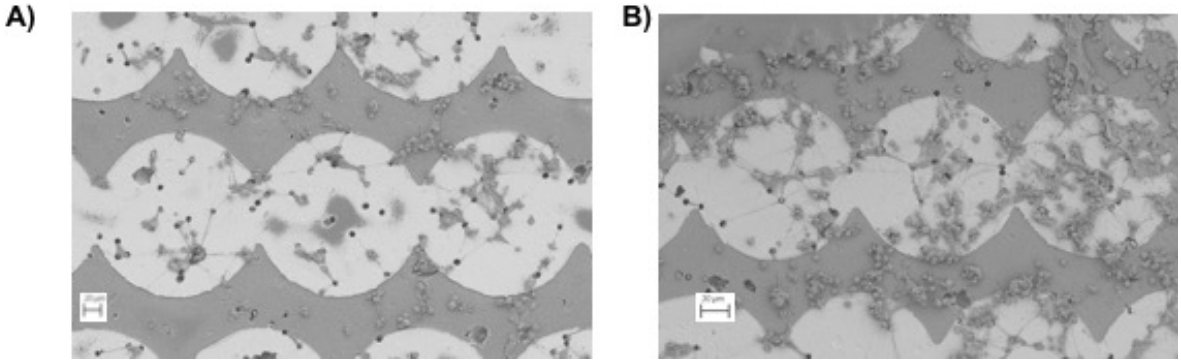


Figure 36: SEM validation of hCD14$^+$ monocyte migration

Representative SEM images of hCD14$^+$ monocytes adhered to the underside of the CIM-16 membrane after migrating through 8 µM pores in the presence of A) vehicle vs B) 5 nM CCL2/MCP-1. Pores appear as black dots on the image and light grey regions are the areas of the membrane that are integrated with the electrode.

5.3.4 Optimisation of chemokine concentration for human CD14$^+$ monocyte migration assays

To identify chemoattractants that could be used as reliable positive controls for hCD14$^+$ migration assays using the xCELLigence system, I investigated hCD14$^+$ monocyte responses to the CC chemoattractants CCL2/MCP-1 and CCL5/RANTES, as well as the non-CC chemoattractants C5a and fMLP. hCD14$^+$ monocyte responses to the chemoattractants were investigated using negatively selected CD14$^+$ monocytes from 5 individual donors. I confirmed hCD14$^+$ monocyte purity (Figure 34 A) and expression of CD4, CCR5 and CXCR4,

and the chemoattractant receptors CCR2 and C5aR1 (Figure 34 B). However, $hCD14^+$ monocyte expression of FPR1 was low across all donors (Figure 34 B).

For these experiments, $hCD14^+$ monocytes were loaded into the upper wells of the CIM-16 plate at a density of 4×10^5 cells per well and allowed to migrate towards the chemoattractant of interest. Curves of *Delta Cell Index vs Time* were analysed using both AUC and $Max_{\Delta Cell\ Index}$ - $Min_{\Delta Cell\ Index}$ as indices of cell migration.

Unlike traditional end-point cell migration assays, the xCELLigence system provides the advantage of continuous measurement of cell migration over time and thereby allows for comparison of kinetic responses to different chemoattractants and between different biological replicates. As expected due to the variability in chemoattractant receptor expression between biological replicates, the magnitude of migration to each chemokine differed between donors.

5.3.4.1 CCL2 / MCP-1

Traces of delta cell index values generated by monocyte responses to 1.25 nM – 10 nM CCL2 / MCP-1 are illustrated in Figure 37 A**.** Using $Max_{\Delta Cell\ Index}$ - $Min_{\Delta Cell\ Index}$ as an index reveals that only 2.5 nM ($p = 0.0009$) and 5.0 nM ($p = 0.0001$) CCL2 / MCP-1 induced significant $hCD14^+$ monocyte migration versus the vehicle condition. However, AUC analyses in Figure 37 B indicate that 1.25 nM ($p = 0.0005$), 2.5 nM ($p < 0.0001$), 5.0 nM ($p < 0.0001$) and 10 nM ($p = 0.02$) of CCL2 / MCP-1 induced migration of $hCD14^+$ monocytes versus the vehicle condition. Using AUC as an index, migration appeared to increase with increasing CCL2 / MCP-1 concentration up to 5 nM but increasing the concentration of

CCL2 / MCP-1 in the bottom chamber from 5 nM to 10 nM decreased the net migration of $hCD14^+$ monocytes. However, statistical analyses showed no significant effect in response to increased chemoattractant concentration from 1.25 nM – 5 nM. The negative effect of increasing CCL2/MCP-1 concentration from 5 nM to 10 nM may have been due to equilibration of this high concentration of chemoattractant into the top chamber, thereby eliminating the gradient. Alternatively, the decrease in monocyte migration and resulting bell-shape of the dose response curves may have been due to homologous desensitisation of monocyte expressed CCR2. In this desensitisation process, CCL2 binding to CCR2 initiates phosphorylation of the CCR2 cytoplasmic tail by G-protein kinases. In turn, the phosphorylation event targets CCR2 for internalisation and uncouples the G protein from the heterotrimeric CCR2 complex, thereby preventing further activation of the chemokine receptor [307].

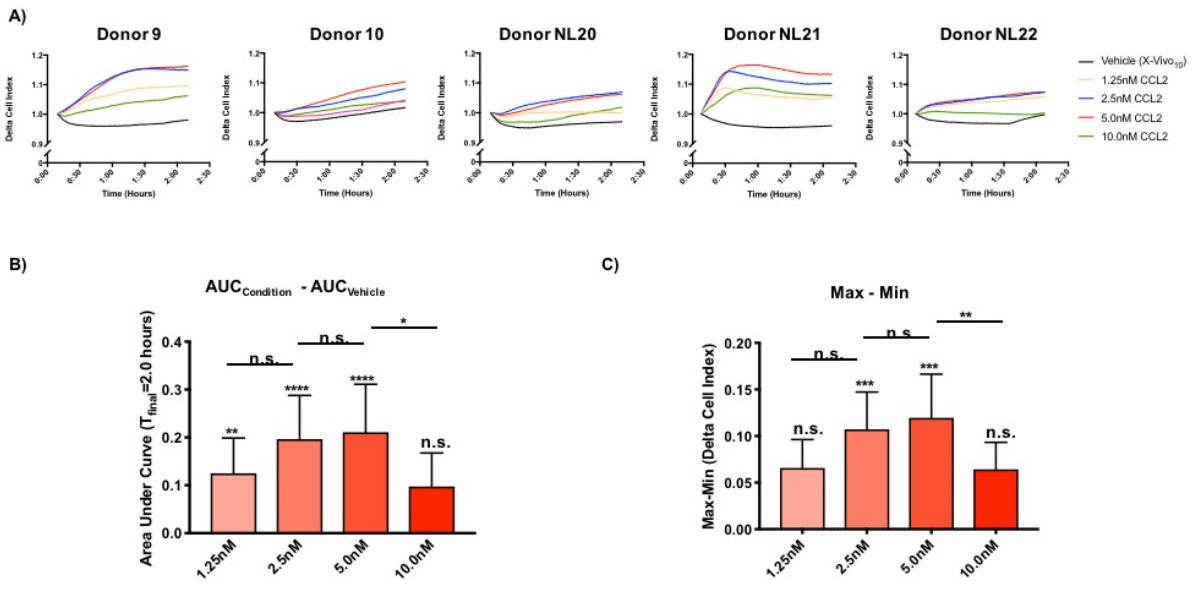


Figure 37: Optimisation of CCL2/MCP-1 concentration for the xCELLigence migration assay

A) Traces of the xCELLigence RTCA-DP delta cell index values generated by CD14+ blood monocyte migration towards CCL2/MCP-1. B) Area under curve and C) Max-Min analysis of cell index signals generated by CD14+ blood monocyte migration towards 1.25 nM – 10 nM CCL2/MCP-1. The vehicle condition (X-Vivo10) was used for baseline correction of all AUC values. Error bars represent mean with S.D. for 5 individual donors with 3 replicate wells per condition. The dataset was assessed by Shapiro-Wilk normality testing and *p<0.05, **p < 0.01, ***p < 0.001, ****p<0.0001 and n.s. denotes 'not significant' for Kruskal-Wallis testing with Dunn's post-test comparisons.

5.3.4.2 CCL5 / RANTES

Traces of delta cell index values generated by monocyte responses to 1.25 nM – 10 nM CCL5 / RANTES are illustrated in Figure 38 A. AUC analyses in Figure 38 B indicate that in comparison to the vehicle condition, 2.5 nM (0.003), 5.0 nM (p < 0.0001) and 10 nM (p =

0.009) of CCL5 / RANTES induced migration of hCD14^{+} monocytes while 1.25 nM (p = 0.9) was insufficient to induce migration. AUC analyses (Figure 38 B), show that increasing CCL5 / RANTES concentration to 5 nM had no significant effect on increasing the net migration of monocytes, and suggest that increasing the concentration of CCL5 / RANTES in the bottom chamber to 10 nM decreased the net migration of hCD14^{+} monocytes. $Max_{\Delta Cell\ Index}$ - $Min_{\Delta Cell\ Index}$ analysis indicated no difference in migration for any concentration of CCL5 / RANTES compared to the vehicle condition.

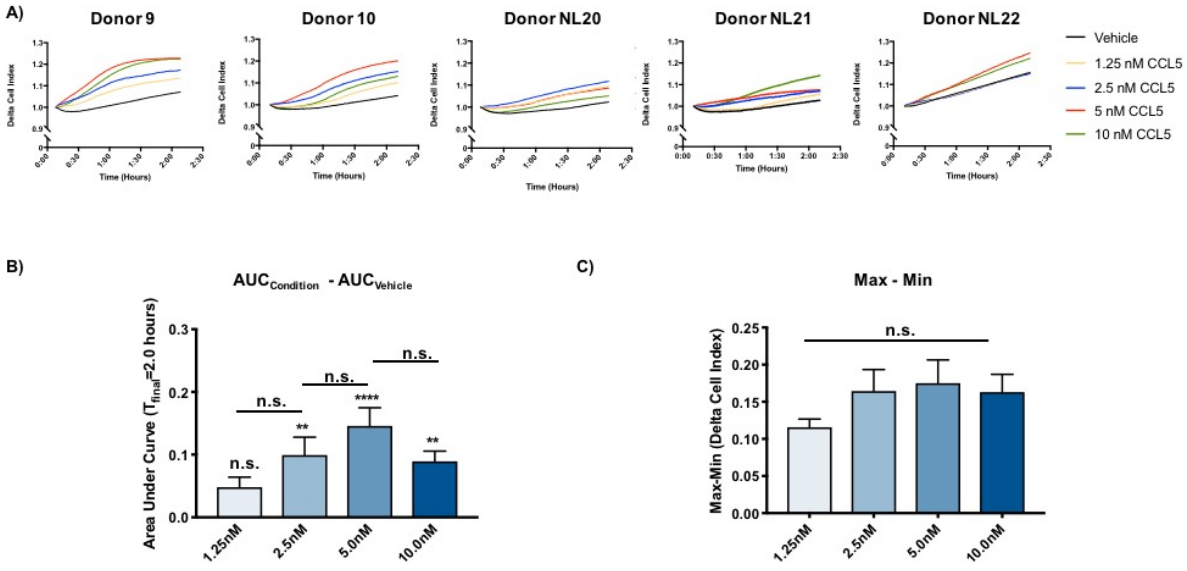


Figure 38: Optimisation of CCL5/RANTES concentration for the xCELLigence migration assay

A) Traces of the xCELLigence RTCA-DP delta cell index values generated by CD14^{+} blood monocyte migration towards CCL5/RANTES. n= 5 individual donors. B) Area under curve and C) Max-Min analysis of cell index signals generated by CD14^{+} blood monocyte migration towards 1.25 nM – 10 nM CCL5/RANTES. The vehicle condition (X-Vivo$_{10}$) was used for baseline correction of all AUC values. Error bars represent mean with S.D. for 5 individual donors with 3 replicate wells per condition. The dataset was assessed by Shapiro-Wilk

normality testing and *p<0.05, **p < 0.01, ***p < 0.001, ****p<0.0001 and n.s. denotes 'not significant' for Kruskal-Wallis testing with Dunn's post-test comparisons.

5.3.4.3 Complement component 5a (C5a)

Traces of delta cell index values generated by monocyte responses to 0.3125 nM – 40 nM C5a are illustrated in Figure 39 A**.** AUC analyses in Figure 39 B indicate that all concentrations of C5a were capable of inducing significant hCD14^{+} monocyte migration in comparison to the vehicle condition. Analysis of AUC (Figure 39 B) suggests a concentration-dependent increase in monocyte migration from 0.3125 nM – 2.5 nM C5a, while increasing C5a concentration beyond 2.5 nM appears to have had a negative effect on the net migration of hCD14^{+} monocytes. However, neither of these observations were statistically significant. $Max_{\Delta Cell\ Index}$ - $Min_{\Delta Cell\ Index}$ analysis indicated significant migration towards only 10 nM (p = 0.008) C5a when compared to the vehicle condition.

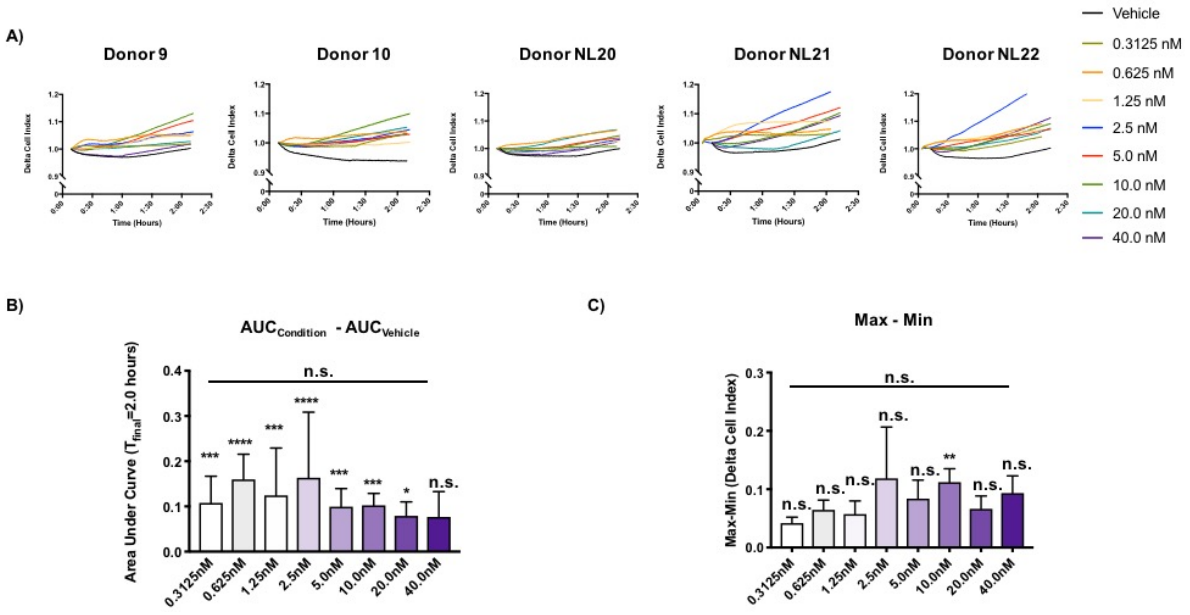


Figure 39: Optimisation of Complement component (C5a) for the xCELLigence migration assay

A) Traces of the xCELLigence RTCA-DP delta cell index values generated by CD14^{+} blood monocyte migration towards C5a. n= 5 individual donors. B) Area under curve and C) Max-Min analysis of cell index signals generated by CD14^{+} blood monocyte migration towards 0.3125 nM – 40 nM C5a. The vehicle condition (X-Vivo$_{10}$) was used for baseline correction of all AUC values. Error bars represent S.D. for 5 individual donors with 3 replicate wells per condition. The dataset was assessed by Shapiro-Wilk normality testing and *p<0.05, **p < 0.01, ***p < 0.001, ****p<0.0001 and n.s. denotes 'not significant' for Kruskal-Wallis testing with Dunn's post-test comparisons.

5.3.4.4 N-formyl-met-leu-phe (fMLP)

Traces of delta cell index values generated by monocyte responses to 0.3125 nM – 40 nM fMLP are illustrated in Figure 40 A. AUC analyses in Figure 40 B indicate that all concentrations of fMLP except 0.3125 nM ($p > 0.9$), 1.25 nM ($p > 0.9$) and 2.5 nM ($p = 0.2$) were capable of inducing significant hCD14^{+} monocyte migration versus the vehicle condition. Analysis of AUC Figure 40 B, suggests a concentration-dependent increase in net monocyte migration from 5 nM – 40 nM fMLP. However, this trend did not approach statistical significance. Using $Max_{\Delta Cell\ Index}$ - $Min_{\Delta Cell\ Index}$ as an index of migration did not reveal significant migration for any of the condition investigated.

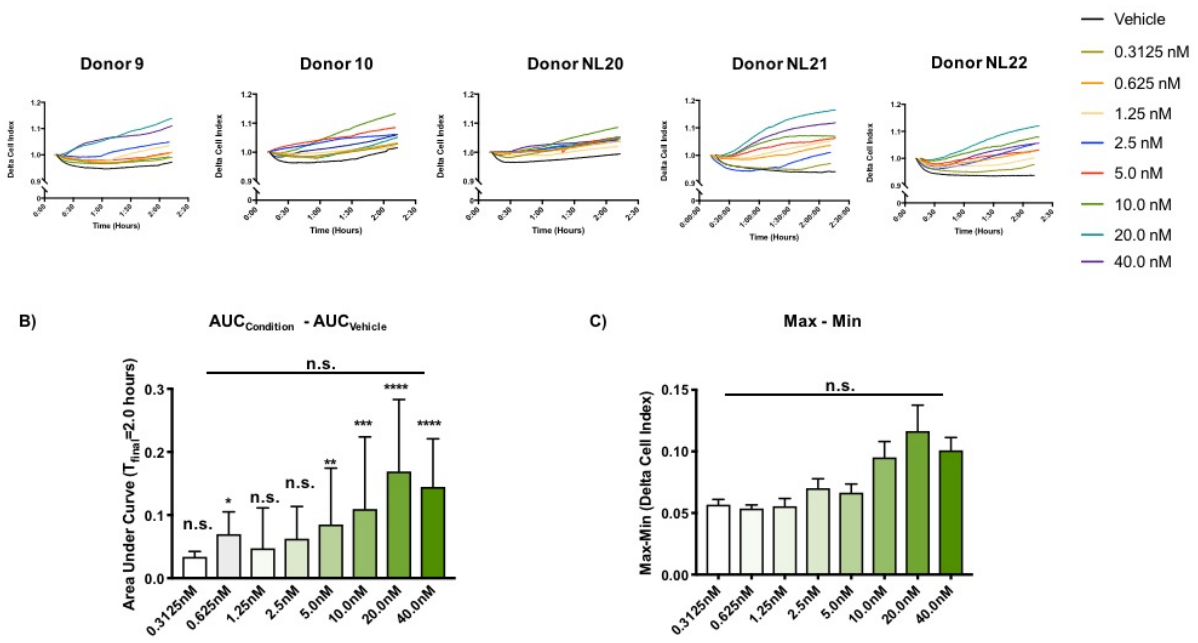


Figure 40: Optimisation N-formyl-met-leu-phe (fMLP) concentration for the xCELLigence migration assay

A) Traces of the xCELLigence RTCA-DP delta cell index values generated by CD14⁺ blood monocyte migration towards fMLP. n= 5 individual donors. B) Area under curve and C) Max-Min analysis of cell index signals generated by CD14⁺ blood monocyte migration towards 0.3125 nM – 40 nM fMLP. The vehicle condition (X-Vivo$_{10}$) was used for baseline correction of all AUC values. Error bars represent S.D. for 5 individual donors with 3 replicate wells per condition. The dataset was assessed by Shapiro-Wilk normality testing and *p < 0.05, **p < 0.01, ***p < 0.001 and ****p < 0.0001 for Kruskal-Wallis testing with Dunn's post-test comparison.

Overall, of the chemoattractants investigated, CCL2/MCP-1 and CCL5/RANTES induced the most reliable increases in hCD14⁺ monocyte migration. For each of these chemokines, a concentration of 5.0 nM increased monocyte migration significantly over the vehicle condition. Furthermore, increasing CCL2/MCP-1 and CCL5/RANTES concentrations beyond

5.0 nM resulted in less robust increases in hCD14^{+} monocyte migration. Therefore, I selected 5.0nM CCL2/MCP-1 and 5.0 nM CCL5/RANTES as optimal positive control conditions for future migration assays.

5.3.5 Validation of xCELLigence assay measurement of directed migration

In establishing the real-time chemotaxis assay, it was important to distinguish between cell index signals generated due to non-directional migration of hCD14^{+} monocytes (chemokinesis) versus the directional migration of hCD14^{+} monocytes along a concentration gradient towards the source of chemoattractant (chemotaxis). In order to validate whether the xCELLigence assay could detect directional hCD14^{+} monocyte migration in response to a difference in agonist concentration between the top and bottom chambers of the CIM-16 plate I investigated monocyte migration towards CCL2 / MCP-1 using the classical 'checkerboard' set-up of the CIM-16 plate (Figure 41 A).

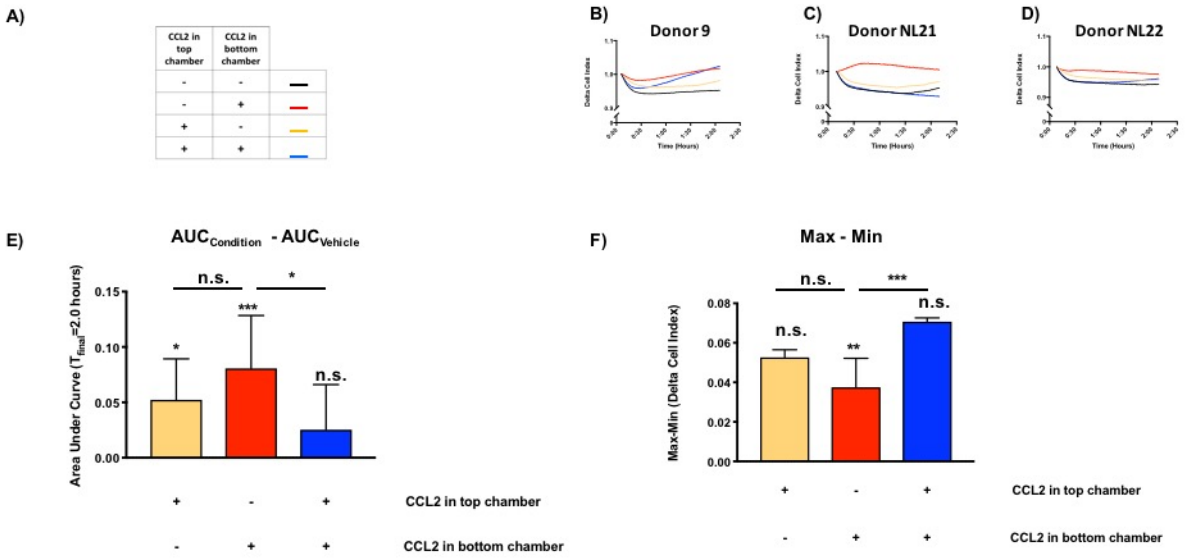


Figure 41: 'Checkerboard' validation of the xCELLigence migration assay

A) Schematic of the 'checkerboard' arrangement of the CIM-16 plate for validation of the xCELLigence migration assay. B-D) Traces of the xCELLigence RTCA-DP delta cell index values generated by CD14⁺ blood monocyte migration towards 5 nM CCL2/MCP-1. E) Area under curve and F) Max-Min analysis of cell index signals generated by CD14⁺ blood monocyte migration towards 5 nM CCL2/MCP-1. The vehicle condition (X-Vivo$_{10}$) was used for baseline correction of all AUC values. Error bars represent S.D. of 3 individual donors with 3 replicate wells per condition.

Non-directional migration refers to the random movement of cells in the absence of stimuli [284]. Across all donors, there was no significant increase in cell index values over time when vehicle (X-vivo media only) was present in both the top or bottom well indicating that little non-directional hCD14⁺ migration occurred in the absence of CCL2/MCP-1 Figure 41 B – D.

Chemokinesis refers to a change in the magnitude of non-directed cell migration in response to a chemical stimulus [284]. To test for this mode of migration, I loaded CCL2/MCP-1 into both the top and bottom chambers of the CIM-16 plate. In this way, $hCD14^+$ monocytes were exposed to the chemoattractant in the absence of a concentration gradient. Similar to the vehicle condition, traces of delta cell index generated by donor NL21 and donor NL22 $hCD14^+$ monocyte migration show little increase in cell index values for the chemokinesis test condition (Figure 41 C-D). However, donor 9 cell index values gradually increased over time to the magnitude observed for the chemotaxis test condition (Figure 41 B). It is unclear whether this increase in donor 9 cell index values was due to true $hCD14^+$ monocyte migration or spreading of $hCD14^+$ monocytes adhered to the underside of the CIM-16 membrane.

Chemotaxis refers to the directional migration of cells along a concentration gradient towards the source of chemical stimulus [284]. To test for this mode of migration and establish a concentration gradient within each test well, I loaded CCL2/MCP-1 into only the bottom chambers of the CIM-16 plate and vehicle only into the top chambers. I also established a CCL2/MCP-1 concentration gradient in the reverse orientation, with vehicle loaded in the bottom chamber only and with $hCD14^+$ monocytes re-suspended in CCL2/MCP-1 in the top chamber. For the reversed concentration gradient, cell index values increased over the vehicle condition, but were not greater than the chemotaxis test condition (Figure 41 B-D). Both AUC and Max-Min analysis confirm monocyte migration for the chemotaxis test condition (Figure 41 E and Figure 41F). As with the chemokinesis test, exposing monocytes to the chemoattractant in the reversed concentration gradient

condition may have lead to an increased number of cells migrating through the microporous membrane in a non-directional manner and adhering to the underside of the CIM-16 membrane, and may also have modulated cell spreading on the membrane. Importantly, increases in cell index values generated by monocyte migration were greatest for the chemotaxis test condition in which the CCL2/MCP-1 concentration gradient directed monocyte migration towards the bottom chamber (Figure 41 B-D). AUC analyses also indicate that the greatest increase in cell migration occurred for the chemotaxis test condition in which the concentration gradient directed monocyte migration towards the bottom chamber (Figure 41 F). Overall, these data show that the xCELLigence platform allows for real-time measurement of $hCD14^{+}$ chemotaxis towards a chemoattractant source in the bottom chamber of the CIM-16 plate. Interestingly, the Max-Min analysis failed to show significant differences between conditions, suggesting that this was not a reliable index of directed chemotactic migration.

5.3.6 ELISA analysis of chemokine diffusion across the xCELLigence CIM-16 membrane

Having confirmed that the xCELLigence system measures directed $hCD14^{+}$ migration, I next wanted to examine whether the chemoattractant gradient between the top and bottom chambers of the CIM-16 plate was maintained over the time-course of a typical chemotaxis assay. After loading 5 nM of CCL2 / MCP-1 (Figure 42 A) and CCL5 / RANTES (Figure 42 B) into the lower wells, the concentration of chemokine present in the upper wells via diffusion across the pores was quantified by ELISA over a 2 h time course.

In both cases, a slow increase in the concentration of each chemokine in the upper wells was observed over the 2 h time-course consistent with chemokine diffusion across the xCELLigence CIM-16 membrane. At the end of the time-course CCL2 / MCP-1 was present in the top chamber at a concentration of 0.49 nM while CCL5 / RANTES was present at 0.16 nM. Both of these values were well below the original 5.0 nM CCL2 / MCP-1 or 5.0 nM CCL5 / RANTES that was initially loaded into wells of the bottom chamber. These results confirm that the difference in concentration of chemokine between the top and bottom chamber of the CIM-16 plate is maintained over the time course of a typical chemotaxis assay.

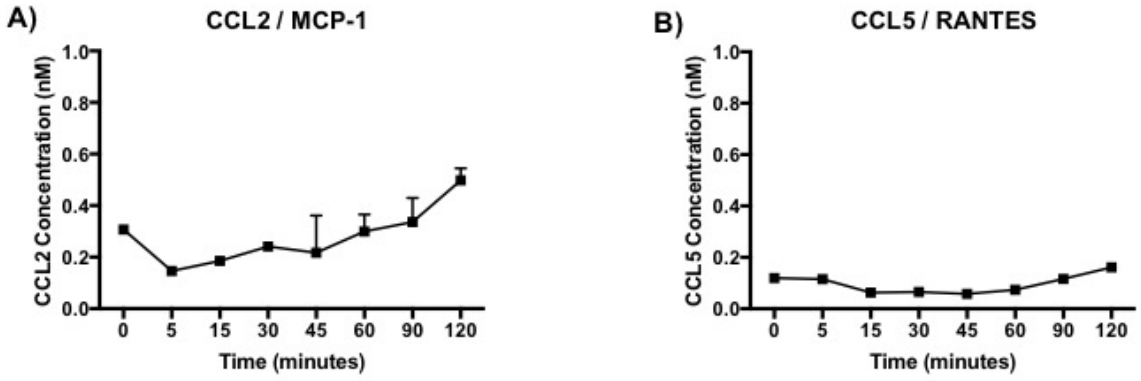


Figure 42: ELISA validation of concentration gradient across the CIM-16 membrane

ELISA analysis of the concentration of A) CCL2 / MCP-1 and B) CCL5 / RANTES in wells of the upper chamber of the CIM-16 plate over the time-course of a typical chemotaxis assay. At the start of the time course, the CIM-16 plates were set up with 5 nM CCL2 / MCP-1 (A) or 5 nM CCL5 / RANTES (B) in the bottom chamber and vehicle only (X-vivo$_{10}$) in the upper chambers. Error bars represent SD of 1 experiment with 2 replicate wells per time-point.

5.3.7 Validation of the xCELLigence migration assay using inhibitors of $G_{\alpha i}$PCR signalling and actin polymerisation

Chemoattractant detection and induction of cell signalling pathways downstream of chemokine receptor engagement are essential events that underpin chemotaxis. Likewise, rearrangement and polymerisation of the actin cytoskeleton are key steps for cell polarisation and pseudopod formation, and occur downstream of G-protein coupled chemokine receptor induced signalling [308]. Together, these events are necessary for chemotaxis.

Pharmacologic agents can be used to inhibit the $G_{\alpha i}$ Protein Coupled Receptor ($G_{\alpha i}$PCR) signalling and actin remodelling that is required for directed cell migration. Cytochalasin D, Latrunculin and Jasplakinolide inhibit G-actin polymerisation and actin filament (F-actin) elongation by different mechanisms. Cytochalasin D binds to the growing ends of actin microfilaments and prevents the addition of monomers at sites of G-actin polymerisation [309]. Latrunculin A binds to and sequesters G-actin monomers leading to a net depolymerization of F-actin [310]. Jasplakinolide increases the rate of actin-filament nucleation site formation and thereby induces the formation of aggregates of G-actin monomers that contribute to the formation of dysfunctional F-actin filaments [311]. Pertussis toxin inhibits migration via a mechanism that is distinct from the other inhibitors used in the experiments that I report. Briefly, the S1 subunit of pertussis toxin ADP-ribosylates the α subunit of heterotrimeric $G_{\alpha i}$PCRs, thereby uncoupling the $G_{\alpha i}$ protein from its receptor [312]. This uncoupling event inhibits signal transduction downstream of ligand binding to $G_{\alpha i}$PCRs. Since chemokines signal through cell surface GPCRs, pertussis

toxin inhibits the transduction of cell signalling events that occur downstream of chemokine receptor engagement and which are necessary to induce directional cell migration.

To further validate the xCELLigence system's ability to measure chemotaxis, I exposed $hCD14^+$ monocytes to inhibitors of $G_{\alpha i}$PCR signalling and actin polymerisation, and investigated the effect of inhibitor treatment on the cell index values generated during migration assays. For these experiments, I suspended $hCD14^+$ monocytes in either 0.1 – 2.5 µg/mL pertussis toxin, 1.0 – 25 µg/mL cytochalasin D, 0.04 – 1.0 µg/mL jasplakinolide or 0.2 – 5.0 µg/mL latrunculin. I then added the monocyte suspension to the upper wells of the CIM-16 plate and measured the resultant monocyte migration towards 5.0 nM CCL2 / MCP-1. I selected these conditions to reflect the range concentrations of each inhibitor previously reported to have effects on myeloid cell migration (detailed in Table 12).

Table 12: Active concentrations of inhibitors used to validate xCELLigence migration assay

Inhibitor	**Concentration**
Ctyochalasin D	1.0 – 2.0 µg/mL [313], 25.4 µg/mL [314], 0.1 – 1.0 µg/mL [315], 0.1 µg/mL [306], 5.0 µg/mL[316], 0.01 µg/mL [317], 1.0 µg/mL [318]
Latrunculin	2.1 µg/mL [313], 0.17-0.42 µg/mL [315]
Jasplakinolide	0.071 µg/mL[313], 0.36 µg/mL [319], 0.36 µg/mL [314], 0.071 - 0.71 µg/mL [320], 0.2 ng/mL – 0.71 µg/mL [315]
Pertussis toxin	0.1 µg/mL[321], 0.01 -1.0 µg/mL[322], 0.1 µg/mL[323], 0.25 -2.0 µg/mL [324] , 0.2 µg/mL [306], 0.2 µg/mL [325], 0.2 µg/mL [326]

AUC analyses confirmed that untreated hCD14^{+} monocytes migrated directionally towards 5 nM CCL2 / MCP-1 hCD14^{+} and that monocytes treated with inhibitors of $G_{\alpha i}$PCR signalling and actin polymerisation migrated towards CCL2 / MCP-1 to a lesser extent than the un-treated hCD14^{+} monocytes.

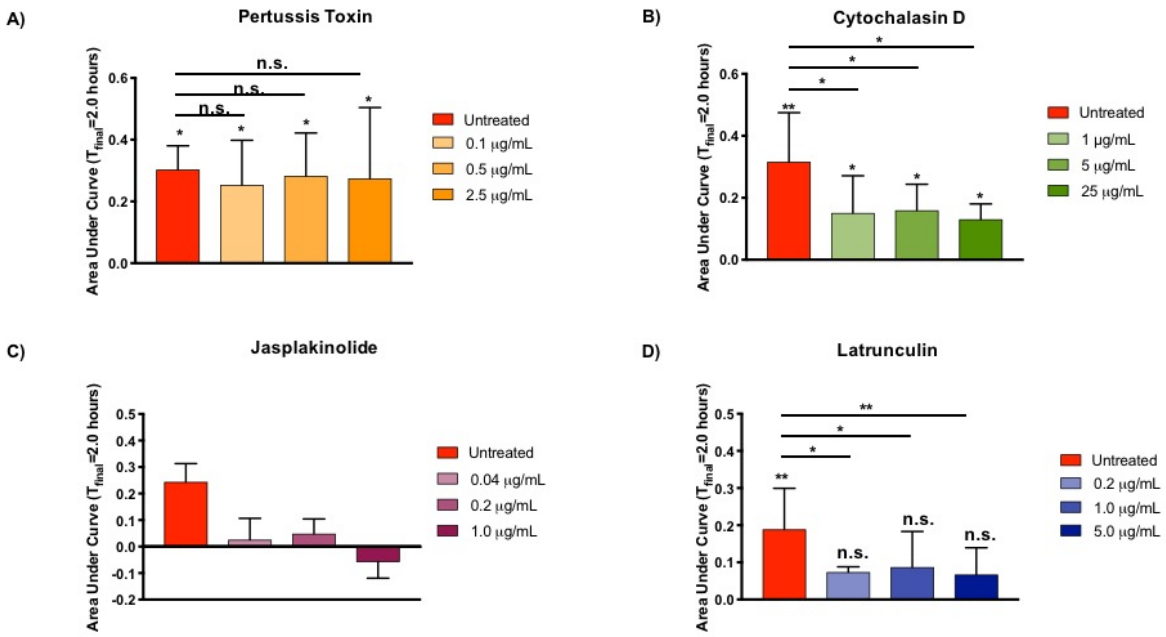


Figure 43: Validation of the xCELLigence migration assay using inhibitors of $G_{\alpha i}$PCR signalling and actin polymerisation

Area under curve analysis of the effect of inhibitors of actin polymerisation and $G_{\alpha i}$PCR signalling on CD14^{+} blood monocyte migration measurements using the xCELLigence system. Monocytes were suspended in vehicle (untreated) or the respective concentration of: A) pertussis toxin, a $G_{\alpha i}$PCR signalling inhibitor or inhibitors of actin polymerisation; B) cytochalasin D; C) jasplakinolide; or D) latrunculin. Monocytes were then allowed to migrate towards 5 nM CCL2/MCP-1. The vehicle condition (X-Vivo$_{10}$) was used for baseline correction of all AUC values. Error bars represent S.D. of 2 individual donors with 3 replicate wells per condition. The dataset was assessed by Shapiro-Wilk normality testing and *p < 0.05, **p < 0.01 and ****p < 0.0001 for one way ANOVA with Holm-Sidak's post-test comparison to either the vehicle or untreated condition.

In comparison to the vehicle condition, AUC analyses revealed significant migration towards CCL2 / MCP-1 for both untreated monocytes and monocytes treated with 0.1 ng/mL – 2.5 ng/mL of pertussis toxin. These results indicate that pertussis toxin did not inhibit monocyte migration. Additionally, there was no difference in the net migration of pertussis toxin treated monocytes when compared to the untreated condition (Figure 43 A). In contrast, significantly decreased monocyte migration was observed with cytochalasin D treatment of 1.0 μg/mL ($p = 0.04$), 5 μg/mL ($p = 0.04$) and 25 μg/mL ($p = 0.02$) when compared to the untreated condition (Figure 43 B). However, cytochalasin D treatment also did not completely inhibit migration towards CCL2/MCP-1. Exposure to jasplakinolide had a marked negative effect on monocyte migration as AUC analyses indicate that the net migration of 0.04 μg/mL ($p = 0.8$), 0.2 μg/mL ($p = 0.7$) and 1.0 μg/mL ($p = 0.7$) jasplakinolide treated monocytes (Figure 43 C) decreased to levels that were not significantly different from the vehicle condition. Furthermore, migration towards CCL2 / MCP-1 was significantly decreased for jasplakinolide treated monocytes when compared to the untreated condition. Latrunculin also had a marked negative effect on monocyte migration as 0.1 μg/mL ($p = 0.8$), 0.5 μg/mL ($p = 0.8$) and 2.5 μg/mL ($p = 0.8$) latrunculin treated monocyte migration towards CCL2/MCP-1 was not significantly different to the migration observed for the vehicle condition (Figure 43 D). Additionally, migration towards CCL2 / MCP-1 was significantly decreased for latrunculin treated monocytes when compared to the untreated condition ($p < 0.001$ for all conditions). Overall, jasplakinolide and latrunculin completely inhibited monocyte migration towards CCL2/MCP-1 whereas cytochalasin D incompletely inhibited migration. Pertussis toxin also failed to reduce chemotaxis below the untreated

condition, but there is no clear explanation for this observation as the concentrations used in the assay fell within the range of active concentrations reported in the literature (Table 12).

Along with the checkerboard validation detailed in Figure 41, the decreases in cell index values observed with jasplakinolide, latrunculin and cytochalasin D treatment confirm that signals of electrical cell impedance are generated by directional migration of $hCD14^+$ monocytes.

5.3.8 Assessing the effect of inhibitors of $G_{\alpha i}$PCR signalling and actin polymerisation on $hCD14^+$ monocyte viability

Treatment with inhibitors of $G_{\alpha i}$PCR signalling and actin polymerisation decreased $hCD14^+$ monocyte migration towards CCL2/MCP-1. To determine whether this observation was due to toxic effects of the inhibitors on the monocytes, I investigated the effect of inhibitor treatment on monocyte viability.

$hCD14^+$ monocytes were suspended in either 0.1 – 2.5 µg/mL pertussis toxin, 1.0 – 25 µg/mL cytochalasin D, 0.04 – 1.0 µg/mL jasplakinolide or 0.2 – 5.0 µg/mL latrunculin and incubated in the presence of the CellTiter 96 AQueous One Solution assay reagent which contains a tetrazolium compound in a stable solution with an electron coupling reagent. NADPH or NADH produced by dehydrogenase enzymes in metabolically active cells reduce the CellTiter 96 reagent to form a soluble coloured formazan product. The quantity of formazan product formed was determined by measuring absorbance of the culture media at 490nm (Abs_{490nm}) and is directly proportional to the number of viable cells. To account

for possible background Abs_{490nm} by cell culture media, measurements were corrected with the Abs_{490nm} readings obtained when wells were loaded with the respective inhibitor and CellTiter 96 reagent only (i.e. in the absence of cells).

I determined the fold change of Abs_{490nm} relative to the untreated condition as an index of monocyte viability. The small number of donors tested (n = 2) precluded statistical analyses. However, in comparison to the untreated condition, incubation with jasplakinolide (Figure 44 A) and latrunculin (Figure 44 B) appeared to decrease $hCD14^+$ metabolic activity across all inhibitor concentrations investigated. As shown in Figure 43 C and Figure 43 D respectively, jasplakinolide and latrunculin treatment effectively inhibited monocyte migration. However, given the possible toxic effect of these inhibitors on monocyte metabolic activity, the observed decreases in cell index could reflect an overall decrease in cell viability after inhibitor treatment as opposed to true inhibition of cytoskeletal rearrangement and subsequent migration. For cytochalasin D, treatment with 1 - 5 μg/mL did not have a large effect on the viability of monocytes from donor 8 while all concentrations appeared to decrease viability for monocytes from donor 9 (Figure 44 C). These observations highlight a donor-dependent susceptibility to the inhibitory effect of these reagents. Pertussis toxin treatment did not appear to be substantially toxic to monocytes across the concentrations investigated (Figure 44 D).

As previously discussed, treatment with either or cytochalasin D, jasplakinolide or latrunculin decreased $hCD14^+$ monocyte migration towards CCL2/MCP-1 (Figure 43 A and Figure 43). However, of the chemotaxis inhibitors investigated, pertussis toxin and cytochalasin D were the least toxic to $hCD14^+$ monocytes exposed to the inhibitors over the

time course of a typical chemotaxis assay. Therefore, Cytochalasin D is therefore a useful agent to study the mechanisms underlying hCD14^{+} monocyte chemotaxis.

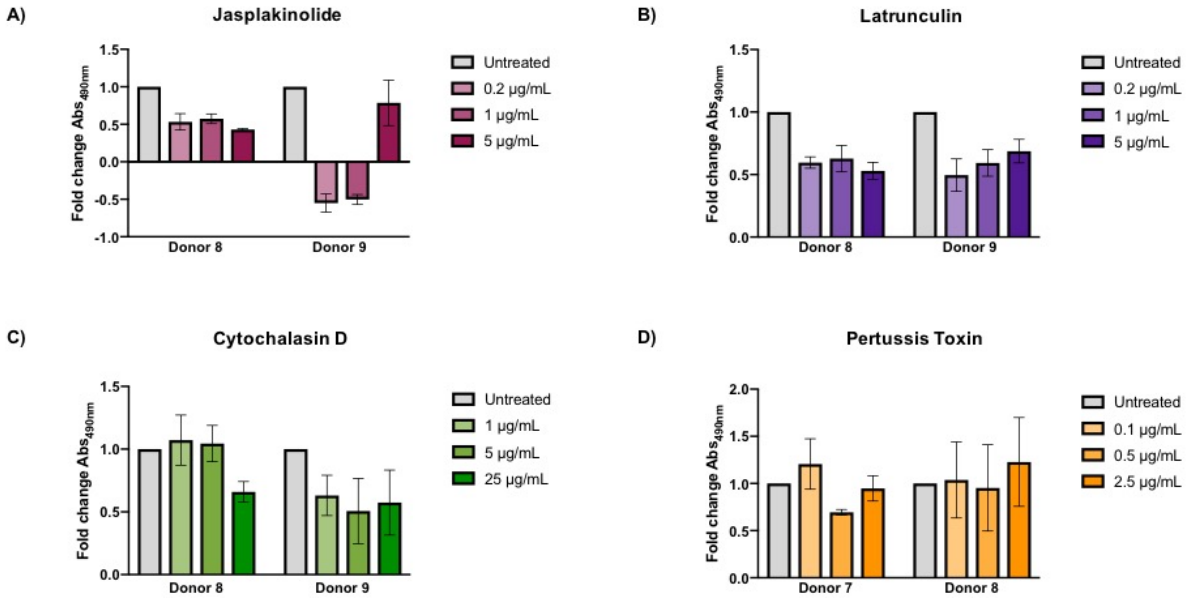


Figure 44: Assay of hCD14^{+} monocyte viability post-treatment with inhibitors of actin polymerisation or $G_{\alpha i}$PCR signaling

The effect of 2 h treatment with the inhibitors of actin polymerization or $G_{\alpha i}$PCR signaling on the viability of CD14^{+} monocytes was assessed versus the un-treated (media only) condition. CD14^{+} monocytes were suspended in the respective concentrations of inhibitors of actin polymerisation A) jasplakinolide, B) latrunculin and C) cytochalasin, or D) pertussis toxin which is an inhibitor of $G_{\alpha i}$PCR signaling. All reported Abs_{490nm} values were corrected with the Abs_{490nm} readings obtained in the absence of cells (wells were loaded with the respective inhibitor and CellTiter 96 reagent only). Error bars represent mean with S.D. of 2 replicate wells per condition for each independent donor.

5.3.9 Investigation of THP-1 cells as an alternative myeloid cell line for investigating migration using the xCELLigence platform

The most physiologically relevant system for investigating monocyte migration utilises ex-vivo negatively selected primary cells as previously described. However, when hCD14^{+} monocytes were used in migration assays I observed substantial variability in expression of chemoattractant receptors, response to chemoattractants and the time taken to achieve maximum cell index during the course of the migration assays. Under some conditions it is helpful to be able to assay cell lines, as these may give greater reproducibility and are easier to manipulate genetically.

The THP-1 cell line is derived from the peripheral blood of a paediatric acute monocytic leukaemia patient and is morphologically similar to primary human blood monocytes [327]. Compared to primary human monocytes, THP-1 cells are phenotypically similar and have a homogenous genetic background [328]. Additionally, my analyses confirmed high CD14 and CCR2 expression by THP-1 cells (Figure 45). Therefore, I hypothesised that the cell line could be a useful tool for reducing the biological variability encountered when primary human monocytes from multiple donors are used in experiments.

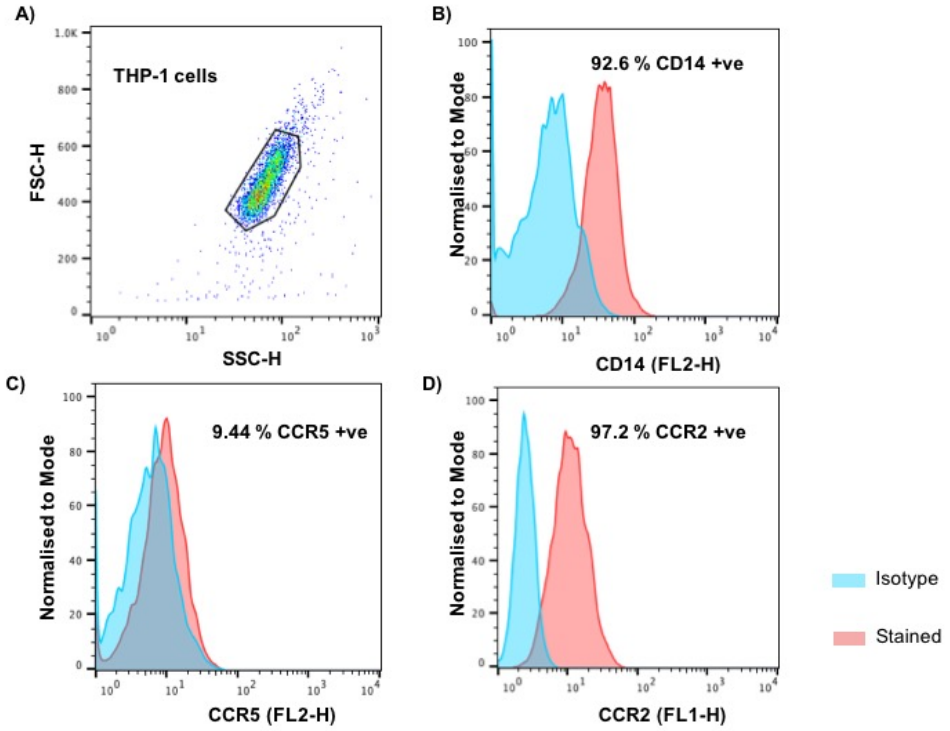


Figure 45: Characterisation of THP-1 cell surface marker and chemokine receptor expression

Representative FACS plot and histograms for flow cytometry analyses of THP-1 expression of B) the myeloid marker CD14, and the chemokine receptors C) CCR2 and D) CCR5.

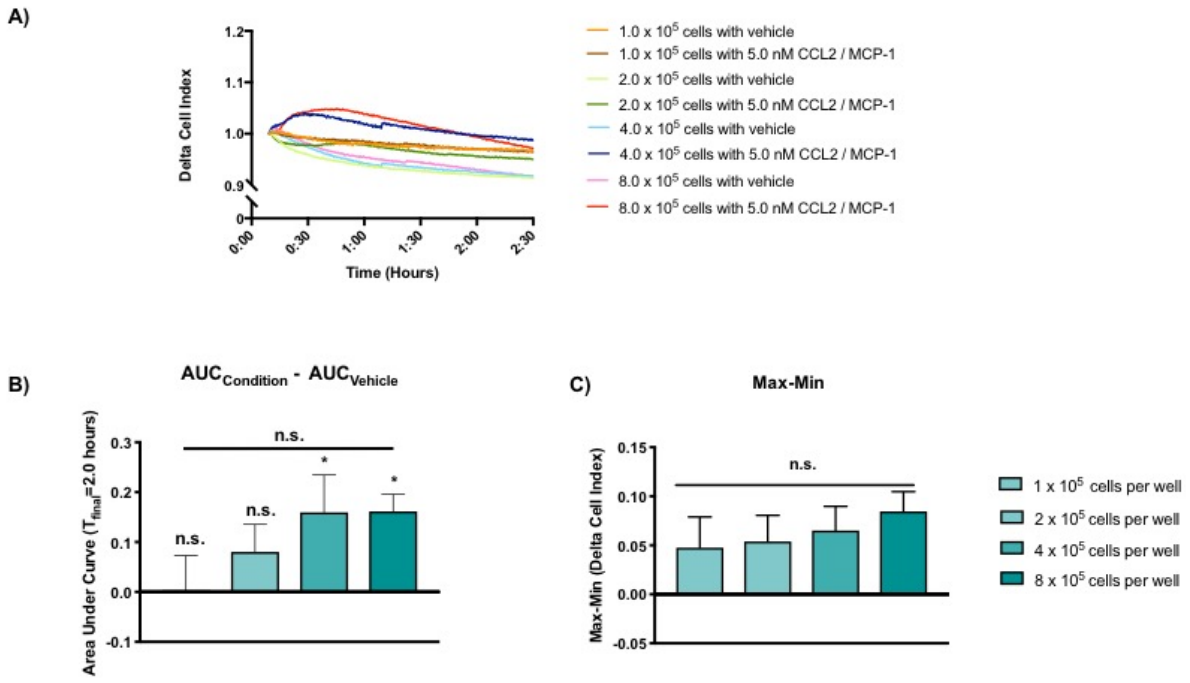


Figure 46: Optimisation of THP-1 monocyte cell density for xCELLigence assay

Representative trace of the delta cell index values generated by the xCELLigence RTCA-DP due to THP-1 monocytic cell line migration. B) Area under curve and C) $Max_{\Delta Cell\ Index}$ - $Min_{\Delta Cell\ Index}$ analysis of cell index signals generated by THP-1 migration towards 5 nM CCL2. The vehicle condition (X-$Vivo_{10}$) was used for baseline correction of all AUC values. Error bars represent mean with S.D. of 1 experiment with 3 replicate wells per condition. The dataset was analysed for normality by the Shapiro-Wilk method and n.s. denotes non-significant, *p < 0.05, ** p < 0.01 and *** p < 0.001 for one-way ANOVA with Holm-Sidak's post-test multiple comparisons.

I attempted to establish the xCELLigence migration assay using THP-1. Firstly, to determine the optimal cell density of THP-1 monocytes needed for the real-time migration assays, I loaded 1 x 10^5 – 8 x 10^5 THP-1 cells per well in the upper chamber and measured their migration towards 5 nM CCL2/MCP-1 or vehicle (X-$vivo_{10}$). An input of 1 x 10^5 1 x 10^5 cells

per well did not generate appreciable signals of cell impedance when compared to the corresponding vehicle condition (Figure 46 A). However, densities of 2 x 10^5, 4 x 10^5 and 8 x 10^5 cells per well generated measurable responses to CCL2 / MCP-1. Cell impedance was more prolonged over time using 8 x 10^5 cells per well compared to 4 x 10^5 cells per well, and the maximum cell impedance was measured using 8 x 10^5 cells per well. AUC analyses (Figure 46 B) confirm that, in comparison to the vehicle condition, migration towards CCL2 / MCP-1 generated significant increases in CI when 4 x 10^5 cells ($p = 0.008$) and 8 x 10^5 cells ($p = 0.008$) were used per well. However, there was no significant effect on the CI signal detected in response to increasing cell density from 1 x 10^5 – 8 x 10^5. In contrast, no difference in THP-1 responses to 5.0 nM CCL2 / MCP-1 was detected for any of the cell densities when $Max_{\Delta Cell\ Index}$ - $Min_{\Delta Cell\ Index}$ was used as an index of migration (Figure 46 C) for comparison to the respective vehicle conditions.

Given that I observed no difference in migration between the 4 x 10^5 and 8 x 10^5 cells per well conditions using AUC as an index of migration, I opted to use 4 x 10^5 THP-1 cells per well for future assays as this cell density allowed for a more practical scale of THP-1 culture and harvesting than would be needed if greater densities were used in the migration assay.

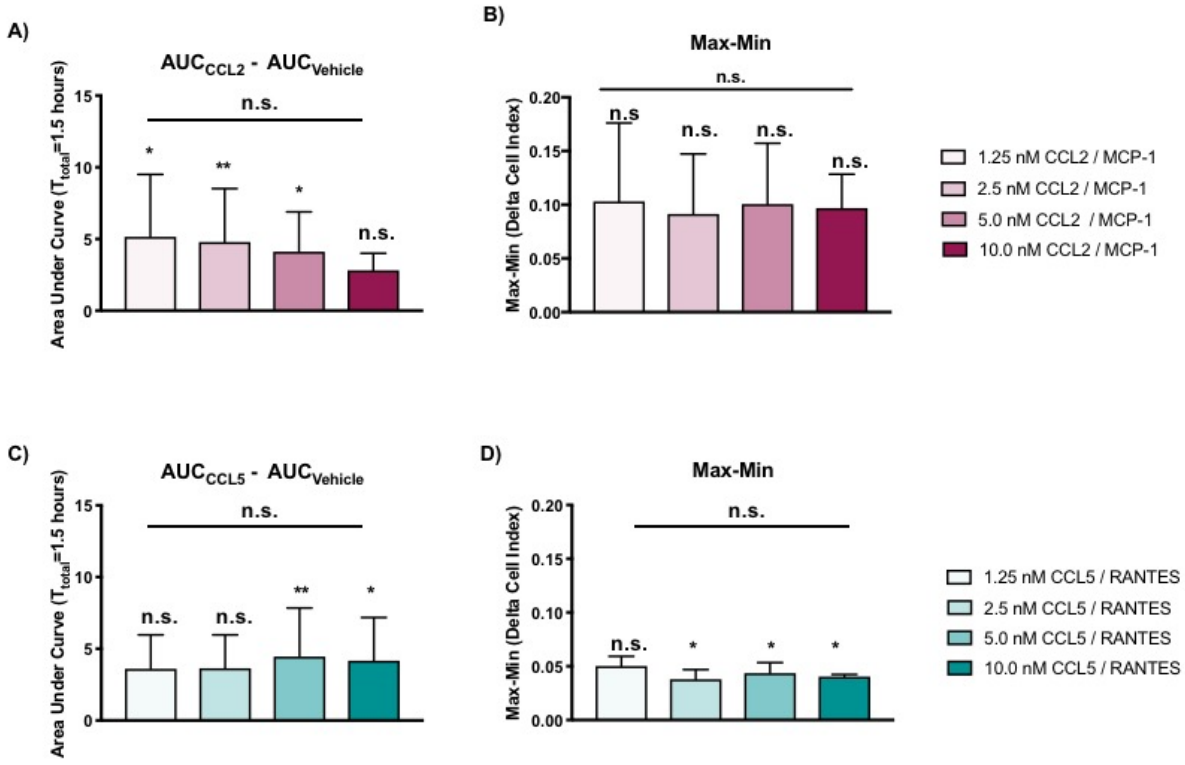


Figure 47: Optimisation of CCL2/MCP-1 and CCL5/RANTES concentration for THP-1 migration assays

Area under curve and Max$_{\Delta Cell\ Index}$ - Min$_{\Delta Cell\ Index}$ analysis of cell index signals generated after 4 x 10^5 THP-1 cells were loaded in each of the upper wells and allowed to migrate towards 1.25 nM – 10.0 nM CCL2 / MCP-1 (Figure 47 A and Figure 47 B) or 1.25 nM – 10.0 nM CCL5 / RANTES (Figure 47 C and Figure 47 D). The vehicle condition (X-Vivo$_{10}$) was used for baseline correction of all AUC values. The dataset was analysed by Shapiro-Wilk normality testing and statistical analyses were performed using Kruskal-Wallis method with Dunn's post-test multiple comparisons. Error bars represent mean with S.D. of 2 experiments with 3 replicate wells per condition, n.s. denotes 'non-significant'.

I next investigated responses of the THP-1 cell line to CCL2 / MCP-1 and CCL5 / RANTES because of the demonstrated ability of these chemokines to induce migration of primary

hCD14^{+} monocytes (Figure 37 and Figure 38). For these experiments, 4 x 10^5 THP-1 cells were loaded per well and allowed to migrate towards either 1.25 – 10 nM CCL2 / MCP-1 (Figure 47 and Figure 47 B) or 1.25 – 10 nM CCL5 / RANTES (Figure 47 C and Figure 47 D). CCL2 / MCP-1 induced THP-1 cell migration at 1.25 nM ($p = 0.01$), 2.5 nM ($p = 0.009$) and 5 nM ($p = 0.01$) relative to the vehicle condition. In contrast, no significant difference in migration was detected between the vehicle condition and any concentration of CCL2 / MCP-1 when $Max_{\Delta Cell\ Index}$ - $Min_{\Delta Cell\ Index}$ was used as an index of migration (Figure 47 C). For CCL5 / RANTES, AUC analysis showed that concentrations of 5 nM ($p = 0.002$) and 10 nM ($p = 0.01$) induced significant THP-1 cell migration relative to the vehicle condition. Additionally, analysis of $Max_{\Delta Cell\ Index}$ - $Min_{\Delta Cell\ Index}$ (Figure 47 D) indicate that 2.5 nM ($p = 0.01$), 5 nM ($p = 0.1$) and 10 nM ($p = 0.01$) CCL5 / RANTES concentrations induced significant migration relative to the vehicle. While THP-1 migration was significantly induced in response to CCL2/MCP-1 or CCL5/RANTES when compared to the vehicle condition, there was no net effect on migration in response to increasing the concentration of either chemokine from 1.25 nM – 10 nM.

5.3.10 Characterisation of HIV-1 Env integrity and purity

Previous studies have reported directed migration of DCs and CD4^{+} T cells towards HIV-1 Env components, particularly via gp120 engagement of CD4 and either CXCR4 or CCR5 (Table 13). Although monocytes express CD4 and CCR5, the effect of HIV-1 Env on monocyte migration has not been reported. Therefore, I hypothesised that HIV-1 gp120 or soluble trimeric gp140 could function as a chemoattractant for human monocytes and that

chemokine mimicry by HIV-1 gp120 or gp140 could provide a potential mechanism by which HIV-1 infection contributes to enhanced monocyte trafficking.

Table 13: Reported effects of HIV-1 Env on cell migration

HIV-1 protein	Cell type	Effect	Proposed mechanism
• Monomeric gp120 • HIV-1 JR-FL pseudotyped virus [173]	$CD4^+$ T-cells	Induced Ca^{2+} signalling and migration	CD4 and CCR5 engagement
• M-tropic gp160 [172]	$CD4^+$ T cells	Induced Ca^{2+}signalling and migration	CD4 and CCR5 engagement
• Conditioned medium from infected T-cells • HIV-IIIB gp120 [292]	PHA/IL-2 activated PBMCs	Induced migration and Ca^{2+} signalling	CXCR4 engagement
• Conditioned medium from HIV-BaL infected T-cells • Recombinant HIV-BaL and HIV-ADA gp120 [170]	Immature DC	Induced migration and Ca^{2+} signalling	CD4 and CCR5 engagement
• Monomeric and trimeric HIV-1 gp120 [171]	Immature DC	Induced migration and Ca^{2+} signalling	CCR5 engagement

To investigate this hypothesis I obtained three variants of HIV-1 Env; monomeric wild-type gp120 from the BG505 Clade A virus, a monomeric BG505 gp120 mutated in the CD4 binding site (CD4 bs) to prevent CD4 binding, and a soluble gp140 BG505 trimer [191] that

closely resembles the conformation in which native HIV-1 Env spikes bind to the CD4 receptor. I first sought to verify the integrity of the recombinant proteins by SDS-PAGE. The presence of distinct gp120 and gp140 bands on the SDS-PAGE Bis-Tris gel (Figure 48) confirmed that all three recombinant proteins were structurally intact and revealed only minor contamination by an oligomeric species. The gp120 and gp140 bands on the gel resolved at a lower molecular weight than expected. This is possibly due to the inability of the carbohydrate moieties of glycoproteins to bind to SDS. In this way, decreased SDS binding may have increased the migration through the gel by reducing the mass and frictional drag of the protein-SDS complex. As a result of this phenomenon, the gp120 and gp140 samples appear to resolve at a lower molecular weight than expected.

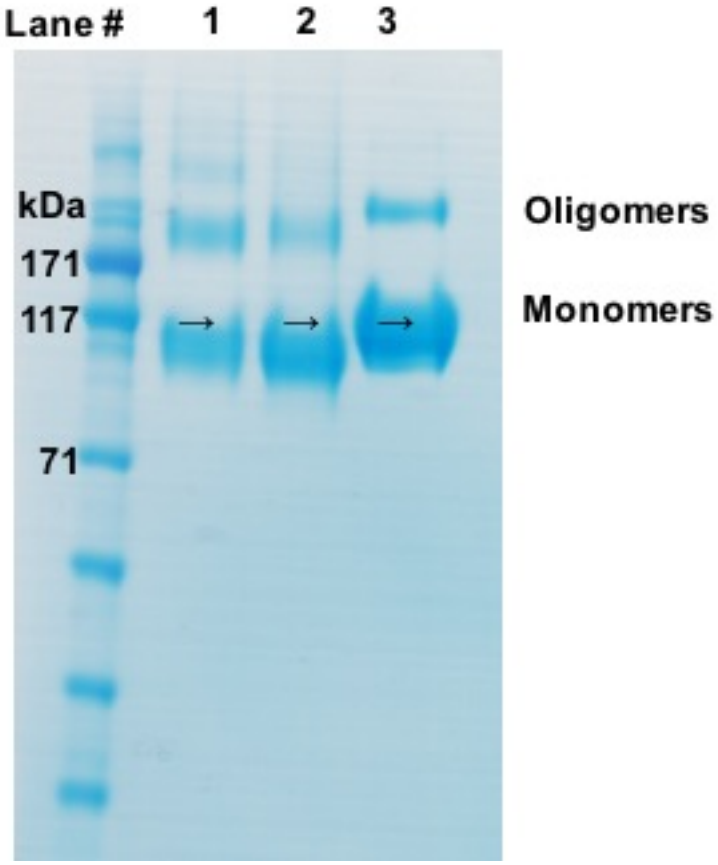


Figure 48: SDS-PAGE analysis of recombinant HIV-1 proteins

Analysis of soluble recombinant monomeric WT gp120 (lane 1), monomeric gp120 CD4 binding site mutant (lane 2) and trimeric gp140 (lane 3) by reducing SDS-PAGE. Arrows represent the expected molecular weights of gp120 and gp140.

Recombinant proteins can become contaminated with immunologically active factors such as endotoxin during their production, and such contamination may influence leukocyte behaviour including chemotaxis. It was therefore necessary to evaluate endotoxin levels in the recombinant protein preparations that would be used in subsequent chemotaxis assays using appropriate reporter cell lines. Therefore, I next investigated the endotoxin levels of each HIV-1 Env variant using THP1-XBlue-CD14 cells. This cell line has been stably transfected to express the NF-κB/AP-1-inducible secreted embryonic alkaline phosphatase (SEAP) reporter gene. TLR stimulation of the cell line induces the activation of NF-κB/AP-1 and the subsequent release of SEAP into the cell culture medium. Incubation of the THP1-XBlue-CD14 cell conditioned medium with the QUANTI-Blue colorimetric reagent results in the formation of a coloured product that is quantified by measuring absorbance at 625nm. Therefore, the amount of SEAP produced is directly proportional to the level of NF-κB/AP-1 activation induced by contaminating TLR ligands in the protein preparations. Initial analysis revealed the WT gp120 preparation was highly contaminated with NF-κB/AP-1 activation inducing factors (Figure 49 A) as NFκB/AP-1 induced signalling was greater than observed with 1 μg/mL LPS standard. The gp120 CD4 bsm preparation induced relatively lower levels of NF-κB/AP-1 activation similar to that observed for

treatment with endotoxin-free H_2O and 0.1 ng/mL LPS. I did not test the trimer gp140 Env preparation as this was certified endotoxin-free by the providers.

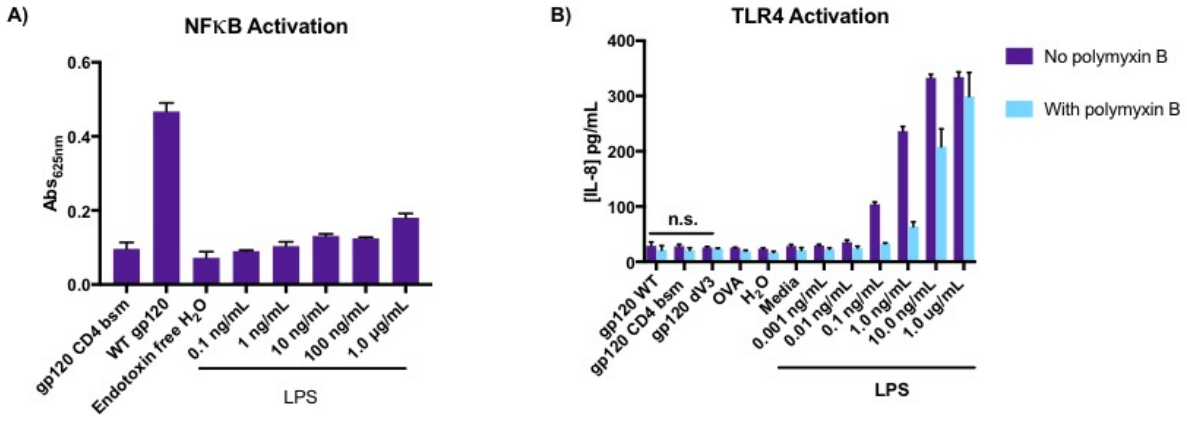


Figure 49: Analysis of recombinant HIV-1 protein purity

A) Analysis of endotoxin contamination of HIV-1 Env variants in comparison to the signals obtained from standard titrations of LPS using an NFKB/AP-1 activation reporter cell line. Error bars represent mean with S.D. for 1 experiment with 3 technical replicates per condition. B) Analysis of endotoxin contamination of HIV-1 Env variants using a TLR4-activation reporter cell line. ELISA analysis of IL-8 produced by the reporter cell line upon TLR4 activation was quantified by ELISA with 2 technical replicates for each stimulation. Error bars represent mean with SD for 1 experiment, and n.s. denotes 'not significant for two-way ANOVA with Sidak's multiple post-test comparison.

Given the high level of endotoxin contamination in the recombinant gp120 that I had obtained as a gift and used for the initial testing with the THP-1 reporter cell line, I produced new batches of recombinant HIV-1 Env in-house via transient transfection of HEK 293F cells. Included in these was a BG505 gp120 lacking the V3 loop (gp120 ΔV3), a construct obtained from the same source that cannot engage the CCR5 coreceptor. I then

subjected these recombinant gp120 preparations to multiple rounds of purification to ensure minimal endotoxin content. First, the protein preparations were purified by 2 rounds of dialysis against 1X endotoxin free PBS for a total of 24 h, then the dialysed protein preparations were filter sterilised under aseptic conditions and finally, subjected to a third round of dialysis against 1X endotoxin free PBS.

I investigated the endotoxin levels of the newly produced recombinant gp120s using the TLR4 sensitive HEK293-Dual-mTLR4 (NF/IL8) reporter cell line. This cell line is stably transfected to express the mouse TLR4 (mTLR4)-MD2-CD14 complex to which LPS binds and initiates TLR4 induced signalling. The HEK293-Dual-mTLR4 (NF/IL8) reporter cell line is specifically activated by TLR4 agonists and, as a result of TLR4 activation, expresses soluble IL-8 which is quantifiable by ELISA. Therefore, the amount of IL-8 produced is directly proportional to the level of TLR4 activation induced by contaminating factors in the protein preparations.

The reporter cell line was stimulated with a panel of agonists in the presence or absence of polymyxin B, an antimicrobial agent that binds to the lipid A portion of bacterial LPS, thereby sequestering LPS and decreasing LPS-induced TLR4 signalling by the reporter cell line. IL-8 production increased with increasing concentration of the LPS standards used to stimulate the reporter cells. Furthermore, Polymyxin B treatment decreased LPS-induced IL-8 expression at 0.1 - 1 µg/mL LPS ($p < 0.0001$), confirming that LPS binding to the mTLR4-MD2-CD14 complex was sufficient to induce TLR4 signalling (Figure 49 B). However, treatment with polymyxin B had no significant effect ($p > 0.05$) on IL-8 production in the presence of 10 ng/mL - 1 µg/mL of LPS, likely because polymyxin B's LPS-binding capacity

was saturated at these high concentrations of LPS (Figure 49 B). Treatment with polymyxin B also had no significant effect on IL-8 production ($p > 0.05$) in the presence of 0.001 ng/mL – 0.01 µg/mL of LPS, likely because such low concentrations of LPS were not sufficient to induce appreciable IL-8 production by the reporter cell line (Figure 49 B). The levels of IL-8 produced in response to treatment of the HEK293-Dual-mTLR4 reporter cell line with either WT gp120, gp120 CD4 bsm or gp120 ΔV3 was not greater than observed for the control stimulation conditions (endotoxin-free H_2O and endotoxin-free OVA) and was alos less than the level of IL-8 production observed for stimulation with 0.1 ng/mL LPS. Together, these results indicate that the new batch of HIV Env variants contained less than 0.1 ng/mL endotoxin content.

5.3.11 Characterisation of HIV-1 Env integrity and antigenicity

Having confirmed that the recombinant gp120s were structurally intact and of low endotoxin content ($\leq$ 0.1 ng/mL endotoxin), I next characterised their integrity and antigenicity present on the SDS-PAGE gel (Figure 49) by measuring their ability to bind to two monoclonal antibodies**;** 2G12 and VRC01.

2G12 is a broadly neutralizing human monoclonal antibody that recognises and binds to a cluster of oligomannose residues on the surface of HIV-1 gp120 [329]. Binding of the monomeric WT HIV-1 gp120, CD4bs mutant gp120 and trimeric HIV-1 gp140 to the anti-gp120 glycan specific mAb, 2G12 was detected by ELISA (Figure 50) thereby confirming the integrity of the gp120 moieties of each recombinant protein.

The antigenicity of the WT gp120 and gp140 trimer proteins was confirmed by ELISA analysis of the HIV-1 Env variant binding to VRC01, a CD4bs-specific mAb. VRC01 binding to the gp120 CD4bs partially mimics gp120 binding to CD4 [330]. Therefore, ELISA measurement of VRC01 binding to the HIV-1 Env variants provides a useful measure of the antigenicity of the recombinant proteins. Binding to VRC01 was confirmed for the WT gp120 and gp140 trimer proteins as these variants possess unmodified CD4 binding sites (Figure 50B). However, binding to VRC01 was not detected for the gp120 CD4bs mutant (Figure 50B). This was expected as the CD4bs mutant contains a mutation of the aspartic acid residue to an arginine residue at position 368 in its CD4-binding region which ablates its ability to bind to CD4 binding site (this mutation is denoted as D368R) [330].

Overall, I confirmed the integrity and antigenicity of the HIV-1 Env variants to be used in subsequent chemotaxis assays using ELISA analysis of binding to the anti-gp120 glycan specific mAb, 2G12 and a mAb against the CD4 binding region, VRC01.

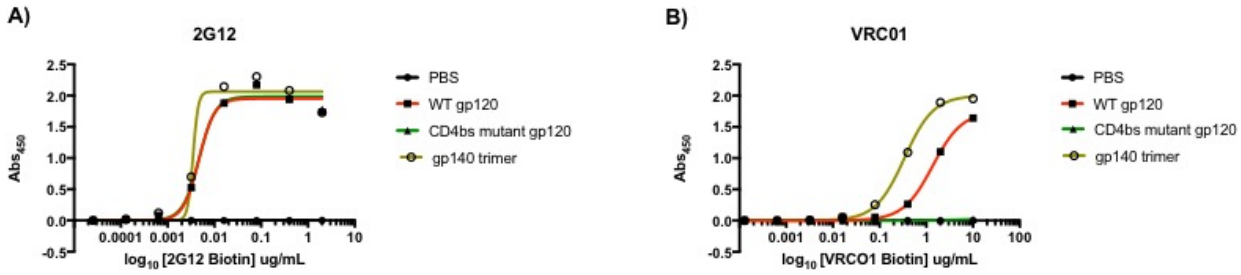


Figure 50: Characterisation of recombinant HIV-1 Env protein integrity and antigenicity

ELISA measurement of soluble Env binding to: A) anti-gp120 glycan specific mAb 2G12; B) CD4bs-specific mAb VRC01.

5.3.12 Characterisation of HIV-1 Env binding to soluble and cell surface expressed CD4

Engagement of CD4 by gp120 induces a crucial conformational change that exposes the gp120 V3 loop and CD4-induced region for subsequent binding to the co-receptor CCR5 or CXCR4. This sequence is proposed to be the mechanism by which HIV-1 Env induces migration of immature DC and $CD4^+$ T-cells. Therefore, before using the HIV-1 Env variants in assays to investigate the effect of Env on monocyte chemotaxis, it was necessary to confirm that the recombinant Env variants were capable of engaging CD4. I investigated this by ELISA analysis of Env variant binding to both soluble CD4 (sCD4) and CEM T-cell expressed CD4. I developed a flow cytometry based assay to investigate HIV-1 Env binding to CEM T-cell surface expressed CD4 as represented in Figure 51B.

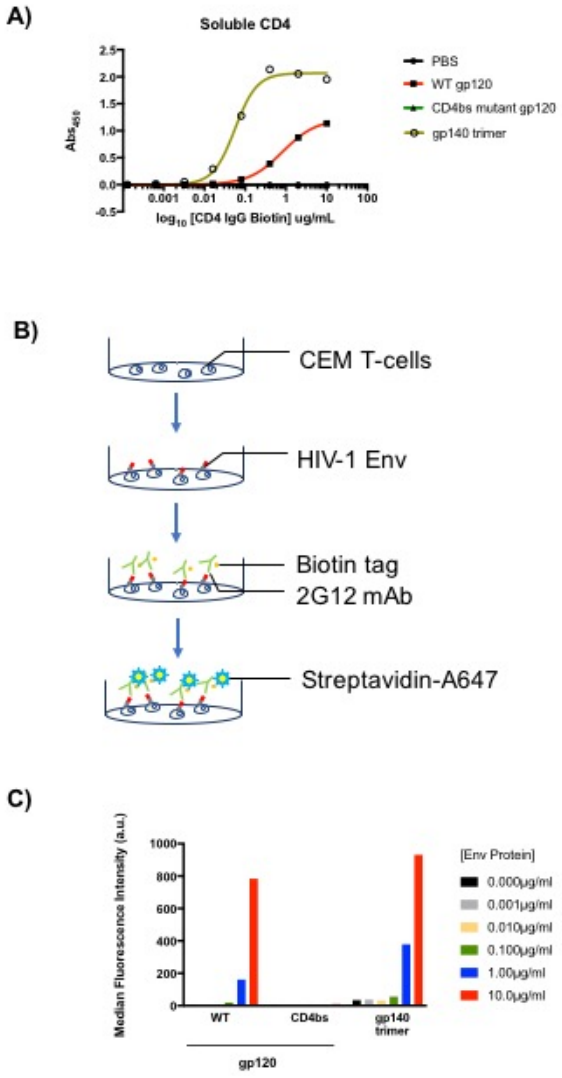


Figure 51: Characterisation of HIV-1 Env binding to soluble and cell surface expressed CD4

A) ELISA analysis of HIV-1 binding to sCD4. B) Schematic of the CEM T-cell based assay for measuring HIV-1 Env binding to cell surface expressed CD4. CEM T-cells were incubated with the envelope proteins prior to tagging with a biotinylated anti-gp120 mAb (2G12). The CD4-recombinant protein complexes were then labelled with an AlexaFluor647-streptavidin conjugate. C) The CEM CD4-Env-2G12-biotin complexes were labelled with an AlexaFluor647-streptavidin conjugate and analysed by flow cytometry. a.u.= arbitrary units.

Both WT gp120 and gp140 trimer possess functionally intact CD4 binding sites and ELISA and FACS analysis confirmed that these variants bound both sCD4 (Figure 51 B) and CD4 expressed on the CEM human T-cell line (Figure 51 C), respectively. Conversely, the CD4bs mutated gp120 bound neither sCD4 (Figure 51 A) or CEM T-cell expressed CD4 (Figure 51 C). Having confirmed the CD4bs mutant gp120's inability to bind to soluble and cell expressed CD4, I decided to include this variant in subsequent chemotaxis assays as a negative control.

5.3.13 Investigation of THP-1 and hCD14$^+$ chemotaxis towards chemokines and soluble Env

As reviewed by Klasse and Moore (2004), there is no consensus on the concentration of HIV-1 Env that is physiologically relevant and which should be used to inform in-vitro experiments [331]. Therefore, I aimed to investigate monocyte responses over a range of soluble Env concentrations (1 ng/mL – 10 µg/mL).

When using primary hCD14$^+$ monocytes in migration assays, multiple donors need to be investigated to account for donor-to-donor variability in responses to chemoattractants. However, one factor that limits the number of experiments that can be performed with the xCELLigence RTCA-DP instrument is the high cost of the CIM-16 plates required for the migration assay. As previously described, cells of the THP-1 monocyte-like line are phenotypically similar, of a homogenous background and can be a useful tool for reducing the biological variability in experiments when used as an alternative to hCD14$^+$ monocytes.

Therefore, to reduce the scale of my experimental set-up, I used THP-1 cells for initial investigation of the effect of HIV-1 Env on cell migration.

Having previously confirmed binding of WT gp120 to sCD4 (Figure 51 A) and T-cell expressed CD4 (Figure 51 B), I investigated THP-1 responses towards 1 ng/mL – 10 µg/mL of this gp120 variant. Since gp120 engagement of CD4 is a pre-requisite to gp120 V3 loop binding to CCR5, I also included the CD4bs mutant gp120 variant in the migration assay in order to determine whether any Env-induced migration observed was specifically mediated through CD4 and CCR5 engagement. 5 nM CCL2/MCP-1 and 5 nM CCL5/RANTES were included as positive control chemoattractants in these migration assays as I previously confirmed the ability of these chemoattractants to induce THP-1 cell line migration (Figure 47).

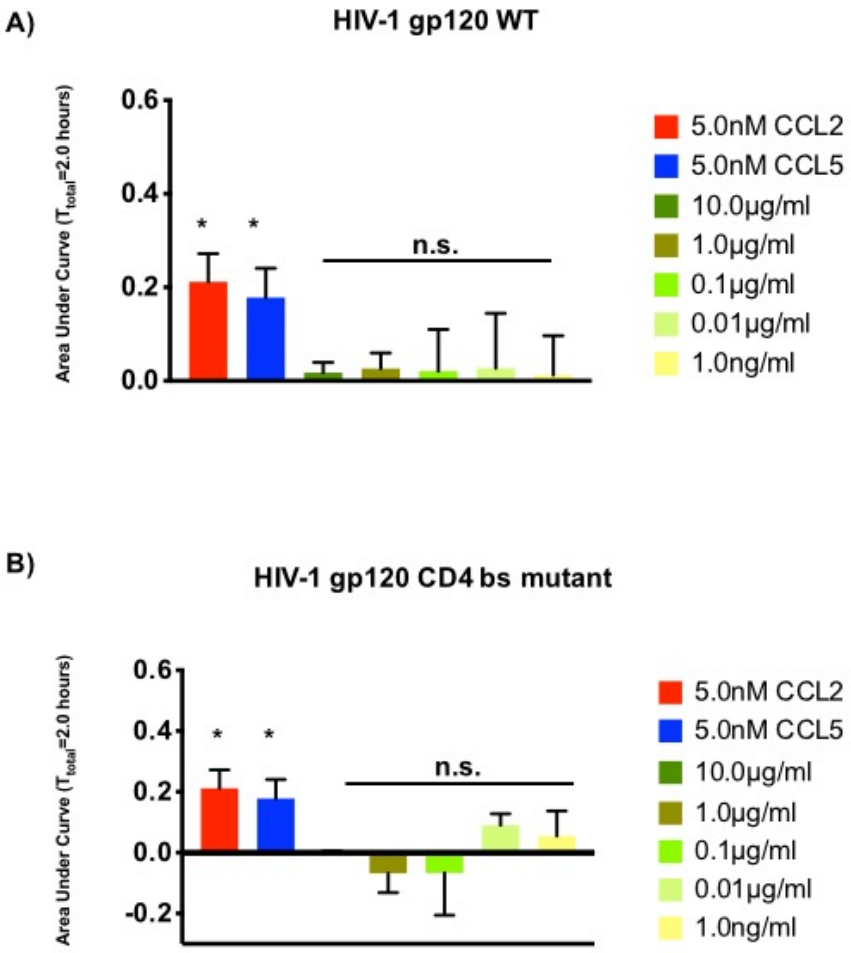


Figure 52: THP-1 cell migration towards recombinant HIV-1 Env proteins

AUC analyses of THP-1 cell line migration towards: A) WT gp120 and B) gp120 CD4bs mutant. 5 nM CCL2 / MCP-1 and 5 nM CCL5 / RANTES were included as positive controls. Bars represent mean with S.D. for 2 experiments, each with 3 technical replicates per condition. Statistical analysis was performed using one-way ANOVA with Holm-Sidak's multiple comparison post-test (*indicates p<0.05 relative to the vehicle condition).

Both 5 nM CCL2/MCP-1 and 5 nM CCL5/RANTES induced significant migration of THP-1 cells in comparison to the vehicle condition. However, the THP-1 cell line failed to show migration towards WT gp120 (Figure 52A). As expected, the CD4bs mutant gp120 did not induce THP-1 cell migration at any of the concentrations investigated (Figure 52B). It was surprising that the WT gp120 did not have an effect on THP-1 migration given that binding of the recombinant WT gp120 to both sCD4 and CEM T-cell expressed CD4 was confirmed and THP-1 cells migrated in response to the CCR5 ligand, CCL5/RANTES. While monocmeric gp120 did not induce migration of THP-1s, it would also be worthwhile investigating migration towards the gp140 trimer as its structure more closely resembles the conformation in which HIV-1 Env on virus particles engages CD4 and CCR5. However, due to time and cost constraints, I did not investigate this aspect of THP-1 migration towards HIV-1 Env.

Earlier work towards establishing the xCELLigence RTCA-DP assay for THP-1 monocytes suggested differences between $hCD14^+$ (Figure 38) and THP-1 (Figure 47 C and Figure 47 D) responses to CCR5 ligand. Therefore, to rule out the possibility that the lack of migration towards HIV-1 Env was THP-1 specific, I next investigated the responses of $hCD14^+$ monocytes to HIV-1 Env.

For these experiments, I measured migration towards 5 nM CCL2/MCP-1, 5 nM CCL5/RANTES, 10 µg/mL WT gp120 and 10 µg/mL gp120 CD4bs mutant using $hCD14^+$ monocytes isolated from 3 different donors. As shown in Figure 53, both 5 nM CCL2/MCP-1 and 5 nM CCL5/RANTES induced significant migration of $hCD14^+$ monocytes in comparison to the vehicle condition, confirming that the $hCD14^+$ monocytes were capable of migrating

and generating signals of CI in response to chemoattractant. In particular, these results confirm that the hCD14^{+} monocytes migrate in response to a CCR5 ligand, CCL5/RANTES. However, as with the THP-1 cell line, hCD14^{+} monocytes failed to show migration towards WT gp120 (Figure 53). As expected, the CD4bs mutant gp120 did not induce hCD14^{+} monocyte migration.

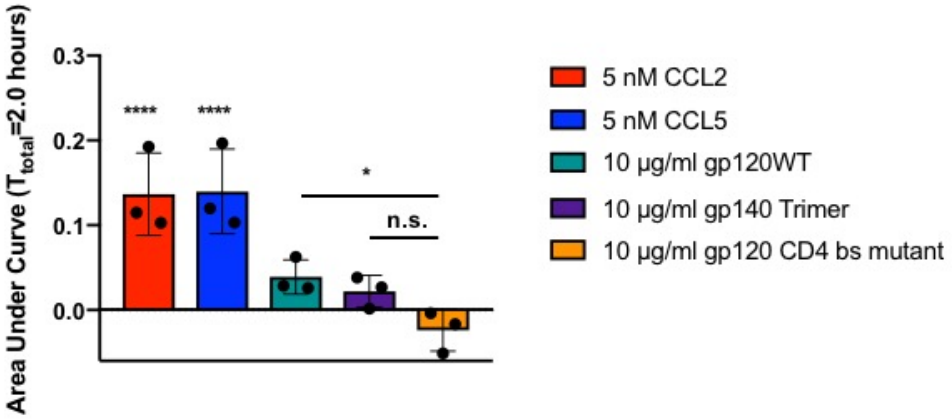


Figure 53: hCD14^{+} monocyte migration towards soluble Env

AUC analyses of hCD14^{+}monocyte migration towards WT gp120, gp120 CD4bs mutant and gp140 trimer. Error bars represent S.D. of 3 biological replicates, each with 3 technical replicates per condition. 5 nM CCL2/MCP-1 and CCL5/RANTES were included as positive controls. The dataset was statistically analysed by Shapiro-Wilk normality testing and *p< 0.05, **** p < 0.0001 for one-way ANOVA with Holm-Sidak's multiple comparison post-test

THP-1 monocyte-like cells and hCD14^{+} monocytes express CD4 and CCR5, the receptors through which HIV-1 Env is proposed to mediate migration of T-cells and immature DC. However, my investigations fail to show any effects of HIV-1 Env on THP-1 monocyte-like cells and hCD14^{+} monocytes. I hypothesised that in comparison to previous studies, my

strict control for endotoxin contamination of recombinant protein preparations is a likely reason for the lack of directed migration observed in the experiments that I report. Exposure to immunologically active factors such as LPS can influence the activation status of myeloid cells leading to altered migration and adhesion. However, except for one case [292], control for endotoxin contamination has not been reported in previous studies of the effect of HIV-1 Env on leukocyte migration. To test this hypothesis, the low endotoxin preparations of recombinant HIV-1 Env could be spiked with increasing concentrations of LPS to determine whether the presence of LPS in the protein preparations induces migration of THP-1 monocyte-like cells or hCD14^{+} monocytes.

5.3.14 Investigation of hCD14^{+} chemotaxis towards supernatants of HIV-1 transduced MDMs

As previously discussed in chapter 2, HIV-1 transduction induced a cytokine response in MDM, which included the expression of the chemokines CXCL9/MIG, CXCL10/IP-10, CXCL11/I-TAC and CCL7/MCP-3 (Table 18). Among these, CXCL10/IP-10 was markedly upregulated regardless of HIV-1 Vpr expression. Additionally, gene enrichment analysis of the Proteome Profiler dataset highlighted signalling pathways relevant to chemokine-receptor interactions and downstream GPCR signalling (Table 19 and Table 20). Therefore, I hypothesised that chemokines produced as part of the inflammatory milieu of HIV-1 infection provide stimuli to induce the migration of uninfected peripheral monocytes to sites of ongoing infection. To test this hypothesis, I investigated the migration of negatively

isolated hCD14^{+} monocytes towards cleared supernatants harvested from autologous HIV-1 transduced MDMs.

I measured migration towards cleared supernatants from MDMs transduced with NL4.3-ΔVpr and NL4.3-Vpr^{+} pseudotyped viruses using hCD14^{+} monocytes isolated from autologous donors. As shown in Figure 54, the positive control of 5 nM CCL2/MCP-1 induced significant migration of hCD14^{+} monocytes in comparison to the vehicle condition, confirming that the monocytes were capable of migrating in response to chemoattractant. Some monocyte migration was detected for supernatants from monocytes exposed to the control ΔEnv, probably because MDMs constitutively express low levels of chemotactic factors in the absence of activation by HIV-1. However, migration towards supernatants from the ΔEnv transductions was not significantly enhanced compared to the vehicle condition. In comparison to the vehicle condition, hCD14^{+} monocytes showed significant migration towards supernatants from both HIV-1_{BaL} Env/NL4.3-ΔVpr ($p = 0.007$) transductions and HIV-1_{BaL} Env/NL4.3-Vpr^{+} ($p = 0.001$) transductions. My analyses also reveal no difference between the net migration towards supernatants from HIV-1_{BaL} Env/NL4.3-ΔVpr transductions versus that of HIV-1_{BaL} Env/NL4.3-Vpr^{+} transductions. These results suggest that while HIV-1 transduction enhances the expression of chemotactic factors by MDMs, HIV-1 Vpr expression does not have an obvious differential effect on the expression of these chemotactic factors. These initial findings should be interpreted with caution as this aspect of my study was limited by i) the small number of donors included in these analyses, ii) the observed inter-donor variation in MDM responses to HIV-1 transduction and iii) the observed inter-donor variation in hCD14^{+} monocyte chemokine

receptor expression and migration towards chemoattractants. Therefore, future work should involve replicate experiments to improve the statistical power of my analyses and to draw concrete conclusions on whether HIV-1 Vpr modulates the production of chemotactic cytokines/chemokines.

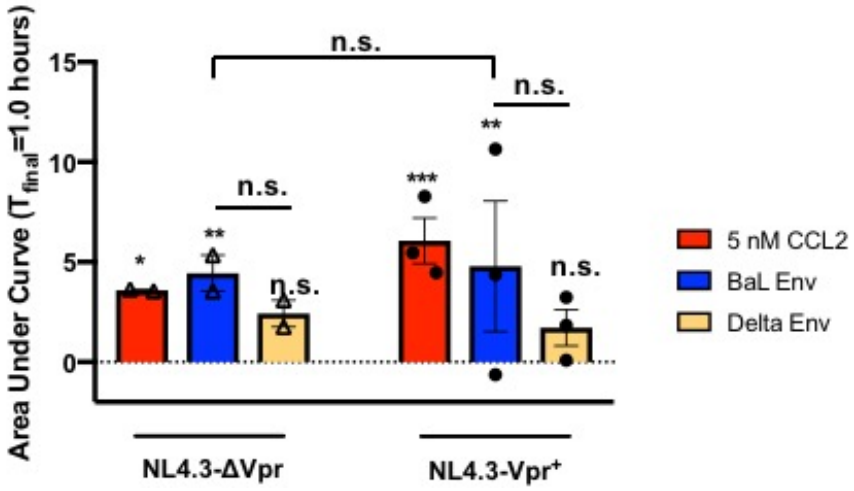


Figure 54: hCD14^{+} monocyte migration towards supernatants of HIV-1 transduced MDMs

Area under delta cell index curves generated after 4x10^{5} blood monocytes were loaded in each of the upper wells and allowed to migrate towards supernatants harvested from autologous, HIV-1 transduced MDMs. Error bars represent mean with S.D. of 3 biological replicates for NL4.3-Vpr^{+} transductions and 2 biological replicates for NL4.3-ΔVpr transductions, each with 3 technical replicates per condition.

5.4 Discussion

One aim of the work presented in this chapter was to optimise the xCELLigence RTCA-DP assay to measure migration of $hCD14^+$ monocytes. In comparison to the previously published investigations using the xCELLigence system, I found that several modifications were required to assess $hCD14^+$ monocyte chemotaxis. Firstly, the kinetic data generated by the xCELLigence system highlights that maximal $hCD14^+$ monocyte migration towards potent chemoattractants such as CCL2/MCP-1 and CCL5/RANTES occurs within the first 30 – 60 min of the assays. Given the rapid speed at which $hCD14^+$ monocytes responded to these chemoattractants, the 30 min incubation time recommended by ACEA Biosciences for sedimentation of other cell types prior to starting each migration assay was reduced to 5 min in my protocol. Without this modification, the majority of monocyte migration would be achieved during the sedimentation period, during which cell index measurements are not recorded.

In my hands, 4 x 10^5 THP-1 monocyte-like cells or $hCD14^+$ monocytes were required per well to generate measurable responses to chemoattractants. These results differ from previous reports in which lower $hCD14^+$ monocyte densities were sufficient to generate marked responses to the chemoattractants C5a or CCL2. In these reports, Taylor et al [332] incubated positively selected monocytes for 45 min at 37°C prior to adding 1 x 10^5 cells per well to the CIM-16 plate and Iqbal et al [333] incubated positively selected monocytes for 60 min at 37°C prior to adding 2 x 10^5 cells per well to the CIM-16 plate. However, for the experiments I detail, $hCD14^+$ monocytes were isolated by negative magnetic selection and immediately used in migration assays. It is possible that Taylor et al and Iqbal et al's

migration assays require lower cell densities because their hCD14$^+$ monocytes were more responsive to the chemoattractants in the lower chamber or adhered more easily to the CIM-16 membrane, either because of increased expression of chemokine receptors or adhesion molecules respectively as a result of the positive selection process. However, I have not confirmed whether such effects on monocyte phenotype can result from the differences in hCD14$^+$ monocyte isolation and handling between the protocol I have used and the previously published methods.

Throughout this chapter, AUC and Max-Min analysis values were compared for data interpretation and I found AUC to give the most reliable interpretation of cell impedance-based measurements of cell migration. Other authors have argued that slope analysis is a more appropriate index of migration than AUC as it best reflects the maximal CI and migratory speed of cells in the assay, and is not confounded by increases in CI due to the spreading of cells that have already adhered to the membrane [306,334]. However, I consider that AUC is a more appropriate index for interpreting cell migration, since although AUC represents increases in cell index due to both directed migration throughout the entire time-course of the assay and cell spreading at later time-points, my work highlights that the time taken for hCD14$^+$ monocytes to achieve maximal CI (30-60 min) occurs far more rapidly than for other cell types such as neutrophils (60-90 min) [334] or murine macrophages (160-120 min) [306,334]. I consider that cell spread is unlikely to contribute significantly to increasing CI values at such early time-points. Furthermore, the slope values determined by the xCELLigence software are extrapolated using the formula $y=mx + c$, where 'm' represents the slope as a linear function. Using slope as an index of

migration therefore assumes a completely linear relationship between the increase in cell index and time. However, the results of my hCD14$^+$ monocyte migration assays show that some donors produce trace curves of *delta cell index vs time* that are distinctly non-linear, even within the first 30-60 min of cell migration. In such cases, it would not be appropriate to assume that a linear relationship exists between the increase in cell index over time or to use of slope as an index of migration.

Another aim of the work presented in this chapter was to apply the real-time migration assay to investigating chemokine mimicry by soluble components of HIV-1 Env. Although THP-1 monocyte-like cells and hCD14$^+$ monocytes express both CD4 and CCR5, the receptors through which chemokine mimicry by Env is mediated, my findings suggest that soluble Env does not induce the migration of either of these cell types. These observations contrast with previous reports of gp120-induced migration of DC [170,171] and T cells [172,173,292]. Notably, in contrast to previous studies [170-173], I have subjected all recombinant Env preparations used in my experiments to multiple rounds of purification and ensured <0.1 ng/mL endotoxin content for my experiments. Apart from a single case [292], control for endotoxin contamination was not reported in previous studies. Since endotoxin exerts potent biological effects on myeloid cells and can influence their activation status leading to altered migration and adhesion, contamination of recombinant protein preparations may explain previous reports of leucocyte migration.

I also applied the real-time migration assay to investigate whether HIV-1 transduction of MDMs upregulates the expression of chemotactic factors that are sufficient to induce hCD14$^+$ monocyte migration. HIV-1 transduction induced a cytokine response in MDM,

which included the expression of the chemokines CXCL9/MIG, CXCL10/IP-10, CXCL11/I-TAC and CCL7/MCP-3. Of these chemokines, CXCL10/IP-10 was the most markedly enhanced (1.25 to 550 fold increase) irrespective of HIV-1 Vpr expression. This finding corroborates with previous studies which have demonstrated strong CXCL10/IP-10 induction by HIV-1, likely in response to TLR7/9 mediated sensing of viral PAMPS, and indicates that HIV-1 does not completely evade innate immune sensing mechanisms in MDMs [282,335].

My preliminary xCELLigence analyses suggest that HIV-1_{BaL} Env transduction does induce the production of chemotactic factors which enhances the migration of monocytes, and that HIV-1 Vpr does not modulate the activity of these factors. While my study did not identify the specific chemokines that may have influenced $hCD14^{+}$ monocyte migration, previous authors have demonstrated that the levels of CXCL9/MIG, CXCL10/IP-10 and CXCL11/I-TAC produced by HIV-1 infected macrophages is sufficient to mediate the recruitment of uninfected T cells in a transwell system [64] or towards HIV-1-infected lymph nodes, macrophages, and dendritic cells [335]. In this way, *in vivo* macrophage production of these chemokines during HIV-1 infection may facilitate the spread of infection to target cells and/or drive infiltration of immune cells to tissue sites. My observation of enhanced CXCL10/IP-10 expression by HIV-1-transduced MDMs is particularly relevant to the pathogenesis of HIV-1 associated inflammation and immune activation as clinical studies have implicated elevated CXCL10/IP-10 production in the progression of HIV-1 infection [336], active tuberculosis co-infection [337] and the progression of HIV-1 associated inflammatory conditions [160,338].

I also observed elevated levels of CCL3/MIP-1α, CCL4/MIP-1β and CCL7/MCP-3 expression in response to ΔEnv control transductions, as well as a non-significant trend of migration towards supernatants from ΔEnv control transductions. Therefore, these findings should be interpreted with caution as it is possible that the process of transduction itself contributed to the upregulation of chemotactic factors. Additionally, my analyses reveal that HIV-1 transduction also induced MDM expression of migration inhibitory factor (MIF) which is known to reduce the migration of leukocytes [339]. Thus, the picture of HIV-1 induction of chemokines and the mechanisms of HIV-1-induced monocyte migration that emerges is complex.

This study was limited by substantial donor-to-donor variation in $hCD14^+$ monocyte responses to MDM supernatants and HIV-1 Env, and additional investigations will be required to improve the statistical power. However, I have not pursued further investigations of HIV-1-induced migration on either THP-1 monocyte-like cells or $hCD14^+$ monocytes because of time-constraints and limitations due to the cost of CIM-16 plates. However, there are outstanding questions relevant to my original hypothesis that warrant future study. For example, the scale of the $hCD14^+$ monocyte migration assays I report was limited by the need to investigate the responses of $hCD14^+$ monocytes from multiple donors. However, it would be useful to investigate $hCD14^+$ monocyte migration towards a wider range of HIV-1 Env concentrations.

It would also be useful to attempt to replicate the findings of previous studies by measuring leukocyte migration towards Env including of immature DC and $CD4^+$ T-cells as positive controls and by measuring the migration of these cell types towards my low

endotoxin (≤ 0.1 ng/mL endotoxin content) preparations of HIV-1 Env using the xCELLigence migration assay. However, one limitation of the xCELLigence migration assay is that it requires the use of adherent cell types that are capable of adhering to the underside of the CIM-16 membrane after migrating through the pores of the membrane, and thereby generating changes in CI. While it would be technically feasible to replicate studies of immature DC migration with the xCELLigence system as these cells are adherent, attempting to replicate previous studies of the effect of HIV-Env on T-cell migration presents a greater technical challenge as these cells are non-adherent. However, Caro et al (2016) report successful modification the CIM-16 plate for measurement of non-adherent neutrophil migration by coating the underside of the membrane with agents that improve cell adhesion such as fibronectin or poly-L-lysine [334]. Applying similar modifications to CIM-16 plates could be a useful approach to measuring $CD4^+$ T-cell responses to my low endotoxin preparations of HIV-1 Env using the xCELLigence system.

5.5 Conclusion

I established a real-time electrical cell impedance based assay to measure the migration of primary human $CD14^+$ monocytes in response to a range of chemokines and chemoattractant signalling molecules. I show that the system measures primary human monocyte migration in real-time without the need for pre- or post-assay labelling of cells and eliminates potential bias introduced by user-quantification of migrated cells by microscopy. Monocyte chemotaxis produced increases in electrical cell impedance and monocytes displayed distinct donor-dependent migration profiles.

The xCELLigence system was used for pilot investigation of chemokine mimicry by HIV-1 envelope glycoproteins and of monocyte migration towards supernatants from HIV-1 transduced MDMs. These experiments suggest that HIV-1 enhances MDM expression of chemotactic factors but failed to confirm previously described chemotactic activity of HIV-1 Env. I carefully controlled for endotoxin contamination in my experiments by subjecting HIV-1 envelope glycoproteins to multiple rounds of purification, and to TLR4 activation testing. Except for one case, such controls have not been reported in previous studies. Therefore, it is possible that insufficient control for immunologically active contaminants contributed to leucocyte activation in previous studies and thereby confounded investigation of chemokine mimicry by soluble HIV-1 Env.

Chapter 6:Discussion

6.1 Summary

Routine use of cART in HIV/AIDS treatment has resulted in a significant a decline in AIDS-related opportunistic infections, increased life expectancy of HIV-infected individuals and decreased risk of HIV transmission. As a result, the epidemiology of the HIV-1 epidemic is undergoing a shift to that of a chronic and manageable infection in which the major cause of morbidity among HIV-1-infected individuals are non-AIDS defining illnesses [33,340]. Despite these gains in patient outcomes, cART only partially restores immune function and does not result in complete, long-term control of HIV-1 replication or eradication of viral reservoirs ([341] and reviewed in Table 1). Furthermore, HIV-1-infected individuals continue to be at increased risk for developing illnesses including cardiovascular disease, kidney disease, cancer, neurocognitive disorders and liver disease [33,35]. The most common of these conditions are i) HAND which affect at least 20% of HIV-1-infected individuals, and ii) HIV-1-associated CVD for which HIV-1-infected individuals bear a 1.5 – 2 times increased risk. Numerous clinical studies have demonstrated that monocyte/macrophage-associated biomarkers of immune activation, coagulopathy and inflammation are elevated in HIV-1 infection and correlate with the progression of HIV-1-associated CVD and HAND (reviewed in Table 2 and Table 3). Furthermore, monocytes/macrophages are implicated in inflammatory disease pathogenesis because they are targets of HIV-1 infection, mediators of pro-inflammatory innate immune responses and form part of the HIV-1 viral reservoir in tissues (Table 1). Therefore, the central hypotheses addressed in this thesis are that i) MDM cytosolic sensing of HIV-1 PAMPs during viral replication induces the production of pro-inflammatory immune

mediators by MDMs and ii) chemokines produced by HIV-1 infected MDMs and/or chemokine mimicry by HIV-1 Env enhance chemotaxis of uninfected monocytes.

6.2 Conclusions

To test these hypotheses, I established and optimised a panel of single-cycle HIV pseudotyped viruses for macrophage transduction and conducted a wide-scale analysis of the immune mediators produced by HIV-1-transduced MDMs. Given evidence in the literature that the HIV-1 accessory protein Vpr modulates IFN-I and pro-inflammatory cytokine/chemokine expression at the mRNA level, I investigated whether HIV-1 Vpr expression influences the profile of soluble immune mediators produced by HIV-1-transduced MDMs. Lastly, I investigated monocyte migration towards supernatants of HIV-1-transduced MDMs and towards HIV-1 Env variants which are ligands for monocyte-expressed chemokine receptors. Through these investigations, I conclude that:

1. HIV-1 induces a potent CXCL10/IP-10 response in MDMs regardless of HIV-1 Vpr expression
2. HIV-1 Vpr downregulates IFN-α, IL-1β and CCL4/MIP-1β production by MDMs
3. HIV-1 Vpr downregulates the IFN-I antiviral response in MDMs at the protein level, but does not significantly influence ISG expression by MDMs
4. Recombinant HIV-1 Env variants do not induce migration of peripheral monocytes
5. Preliminary results suggest that HIV-1 transduction of MDMs induces the expression of chemokines that are capable of enhancing autologous monocyte migration

6.3 Contributions to the field

An overarching aim of my study was to characterise HIV-1 induction of macrophage-expressed mediators of inflammation. To this end, I established a panel of single-cycle HIV pseudotyped viruses and optimised them for transduction of MDM and hPSC-DMs. Previous studies have utilised high MOI, VSV-G-pseudotyped HIV-1 particles, polybrene treatment or spinoculation to facilitate HIV-1 transduction [205-207,220,233]. However, I show that both MDMs and hPSC-DMs can be efficiently transduced using HIV-1_{BaL} pseudotyped virus at a low MOI without the assistance of polybrene treatment or spinoculation. These modifications were facilitated by minimal SIV-Vpx VLP supplementation and by differentiating macrophages in the presence of FCS which induces CDK1-mediated phosphorylation and downregulation of SAMHD1 antiviral activity, and thereby enhances transduction efficiency [208]. Therefore, my work extends the findings of Mlcochova et al by demonstrating that, in addition to MDMs, HS/FCS-differentiation enhances HIV-1 transduction efficiency in an hPSC-DM model. While cell-cycle analyses of HS/FCS-differentiated hPSC-DMs were outside the scope of my thesis, this would be worthwhile area to investigate in future work to elucidate whether HS/FCS differentiation enhances the permissivity of MDMs and hPSC-DMs by the same mechanisms. Cell cycle analyses of HS/FCS differentiated hPSC-DMs would also bear implications for the hPSC-DM model of tissue-resident macrophages since i) Mlcochova et al demonstrate expression of the G1-associated MCM2 protein in 5 - 20% of murine embryo-derived microglia cells, and ii) hPSC-DMs recapitulate the ontogeny of embryo-derived macrophages including microglia [214]. Therefore, if cell-cycle analyses confirm that HS/FCS differentiation

mediates transition to a G1-like phase in hPSC-DMs, it would be interesting to consider whether HS/FCS-differentiated hPSC-DMs more fully recapitulate tissue-resident macrophage biology in comparison to traditional M-CSF-derived hPSC-DMs.

Having established MDM differentiation and transduction protocols, I next addressed questions on the extent to which HIV-1 induces the expression of immune mediators by MDMs. One existing question is whether or not HIV-1 completely evades innate immune sensing and downstream induction of IFN-signalling pathways. RIG-I [274], cGAS [108] and Toll-like receptors [275] have been shown to detect HIV-1 PAMPS, and induce downstream IFN-I signalling as a result [276]. However, other studies have argued that HIV-1 either i) largely evades triggering innate sensing and signalling pathways in macrophages [209,210], by cloaking viral nucleic acids within the capsid [277] or ii) expresses virulence factors which counteract host cell viral restriction and sensing [261,267]. Another unanswered question in this debate is whether the HIV-1 accessory protein Vpr plays a role in modulating MDM responses to HIV-1 as it has been shown to both potentiate [8-10] and dampen [5,11,260] the IFN response in HIV-1 target cells. To address these questions, I transduced MDMs with a panel of Vpr^{+} and ΔVpr pseudotyped viruses and investigated the effects of i) HIV-1 transduction and ii) HIV-1 Vpr expression, on MDM expression of soluble mediators of inflammation and activation of pathways relevant to the innate immune response.

Previous studies have investigated the effect of HIV-1 Vpr at the mRNA level in MDMs, DCs and T cells [8-10], or on cytokine expression in a STING-reconstituted TZM-bl cell line [269]. Therefore, my study has expanded knowledge in this field as an unbiased, wide-scale

investigation of the effect of HIV-1 Vpr on the expression of soluble mediators of inflammation by primary MDMs in response to HIV-1. I have shown that HIV-1 induces a modest pro-inflammatory response in MDMs by upregulating CD30, IL-12 p70, TNF-α, CCL2/MCP-1, CCL3/CCL4, CCL7/MCP-3, CXCL9/MIG, CXCL10/IP-10, CCL17/TARC, lipocalin-2, IGFB-2, IGFB-3 and vitamin D BP expression in multiple donors. Among these, I have identified CXCL10/IP-10 as the immune mediator that is most potently and reproducibly upregulated in response to HIV-1. Simmons et al [282] report that CXCL10/IP-10 expression by MDMs is induced downstream of HIV-1 sensing by TLR7/9 in an IFN-dependent mechanism. Therefore, the CXCL10/IP-10 response observed in my study might provide further evidence that HIV-1 does not completely evade innate sensing in MDMs. Notably, both FCS and VLP-expressed SIV Vpx downregulate SAMHD1 activity, and were used to enhance macrophage permissivity to infection in my study. Therefore, the possibility that either factor may have enhanced macrophage responsiveness to HIV-1 PAMPS is a limitation that must be taken into account when interpreting these findings.

To further probe the immune mediators induced by HIV-1 and the effect of HIV-1 Vpr on their expression profile, I also conducted complementary analyses of the MDM IFN response using immunoassays, an IFN-reporter cell line and qPCR measurement of ISG expression. Both my immunoassay and IFN-reporter cell line analyses confirm that HIV-1 Vpr expression downregulates IFN-I production by MDMs. These findings support studies that demonstrate HIV-1 Vpr downregulation of IFN responses in MDMs [5,11,260], and may explain why previous authors have reported weak IFN-dependent responses in MDMs that were infected or transduced with wild-type HIV-1. In light of this finding, it was

surprising that my qRT-PCT analyses did not reveal HIV-1 Vpr modulation of ISG expression at 72 h post-transduction in contrast to previous reports of Vpr-enhanced ISG expression in MDMs [10], DCs [8] and T cells [9]. Since my HEK3C11 IFN reporter cell line analyses demonstrated that IFN-I production by transduced MDMs was short-lived, it would be worthwhile to determine if any effects of Vpr on ISG expression are also time-dependent. To investigate this, I would conduct additional qRT-PCR analyses of ISG expression using the RNA extracted from MDMs at 24 h, 48 h and 96 h post-transduction with NL4.3-Vpr^{+} and NL4.3-ΔVpr pseudotyped viruses.

In addition to IFN-α, HIV-1 Vpr also downregulated IL-1β and CCL4/MIP-1β expression by MDMs. Apart from a previous investigation into HIV-1 induced responses in STING-reconstituted TZM-bls, my study is the first to measure the effect of HIV-1 Vpr expression on MDM production of soluble cytokines/chemokines. Given that TZM-bls do not completely recapitulate all of the HIV-1 recognition events that occur in MDMs, my findings provide a more relevant picture of HIV-1 Vpr's effects on cytokine/chemokine expression in MDMs.

Most reports agree that interactions between HIV-1 Vpr and the host cell DCAF1/DDB1/CUL4 E3 ubiquitin ligase complex via its DCAF1/VprBP domain mediate the phenotypic effects of HIV-1 Vpr expression [4,7,245,270]. Therefore, I generated NL4.3-Vpr+ plasmids deficient for interaction with the E3 ubiquitin ligase complex for investigations into the effect of HIV-1 Vpr expression on activation, phosphorylation and degradation of the IRFs. Unfortunately, due to time-constraints, I was not able to complete these studies. However, these experiments would have been useful for addressing research

questions on whether Vpr downregulates IFN-I induction in MDMs by i) directly targeting IRFs for proteasomal degradation via the DCAF1/DDB1/CUL4 E3 ubiquitin ligase complex or ii) directly interacting with the kinase TBK1 thereby disrupting its activation, and inhibiting subsequent phosphorylation and nuclear translocation of IRFs. The findings of such investigations would be useful for clarifying ongoing debate into the mechanism by which HIV-1 Vpr downregulates IFN-I induction, and should be the focus of future work.

There is mounting clinical evidence that, in addition to pro-inflammatory activation of macrophages, enhanced monocyte trafficking drives the pathogenesis of HIV-1-associated inflammatory disorders. Therefore, I investigated two possible mechanisms of HIV-1-enhanced monocyte trafficking: i) chemokine mimicry by HIV-1 Env which is a ligand for monocyte-expressed CCR5 and ii) migration towards chemotactic factors released by HIV-1 transduced MDMs. My investigations did not provide evidence for $hCD14^{+}$ monocyte migration in response to either monomeric or trimeric versions of HIV-1 Env. These findings contradict previous reports of Env induced chemotaxis in T cells [172,173,292] and immature DCs [170,171], and suggest that this mechanism of chemokine mimicry may be more pronounced in T cells and DCs than for monocytes, possibly because of differences in CCR5 expression. Additionally, my in-house HIV-1 Env preparations were subjected to multiple rounds of dialysis, filtration and quality control for LPS contamination. In contrast, except for one case [292], such measures have not been reported in previous studies. Therefore, my findings also highlight the possibility that early studies of HIV-1 Env induced leukocyte migration may have been confounded by insufficient control for immunologically active contaminants in recombinant Env preparations.

As previously discussed, wide-scale analysis of the MDM response to HIV-1 transduction revealed upregulated (fold change $\geq$ 2) CCL2/MCP-1, CCL3/CCL4, CCL7/MCP-3, CXCL9/MIG, CXCL10/IP-10, CCL17/TARC expression by multiple donors. Among these chemokines, CXCL10/IP-10 was markedly upregulated. Furthermore, preliminary analyses revealed a trend of enhanced $hCD14^{+}$ monocyte migration towards supernatants of HIV-1-transduced MDMs. However, these preliminary findings are in line with those of previous studies which show that HIV-1 infected macrophages produce sufficient levels of chemokines to mediate the recruitment of uninfected leukocytes [64,335]. The conclusions that can be drawn from these migration experiments are limited as they were carried out on a small number of donors and would be improved by additional replicates.

In summary, this thesis details a wide-scale analysis of the immune mediators expressed by MDMs in response to HIV-1. I find that HIV-1 is able to induce a modest pro-inflammatory response in MDMs. Importantly, HIV-1 causes potent induction of CXCL10/IP-10, a chemokine which has been implicated in the enhanced migration of leukocytes towards HIV-1 infected MDMs and tissues as well as the progression of HIV-1-associated inflammation. I also show that HIV-1 Vpr markedly downregulates MDM IFN-I responses to HIV-1. Together, the findings presented in this thesis provide evidence to suggest that while HIV-1 does not completely evade innate sensing, HIV-1 Vpr may promote viral replication *in vivo* by counteracting anti-viral innate IFN-I responses.

Chapter 7:Appendix

7.1 Supplementary Figures

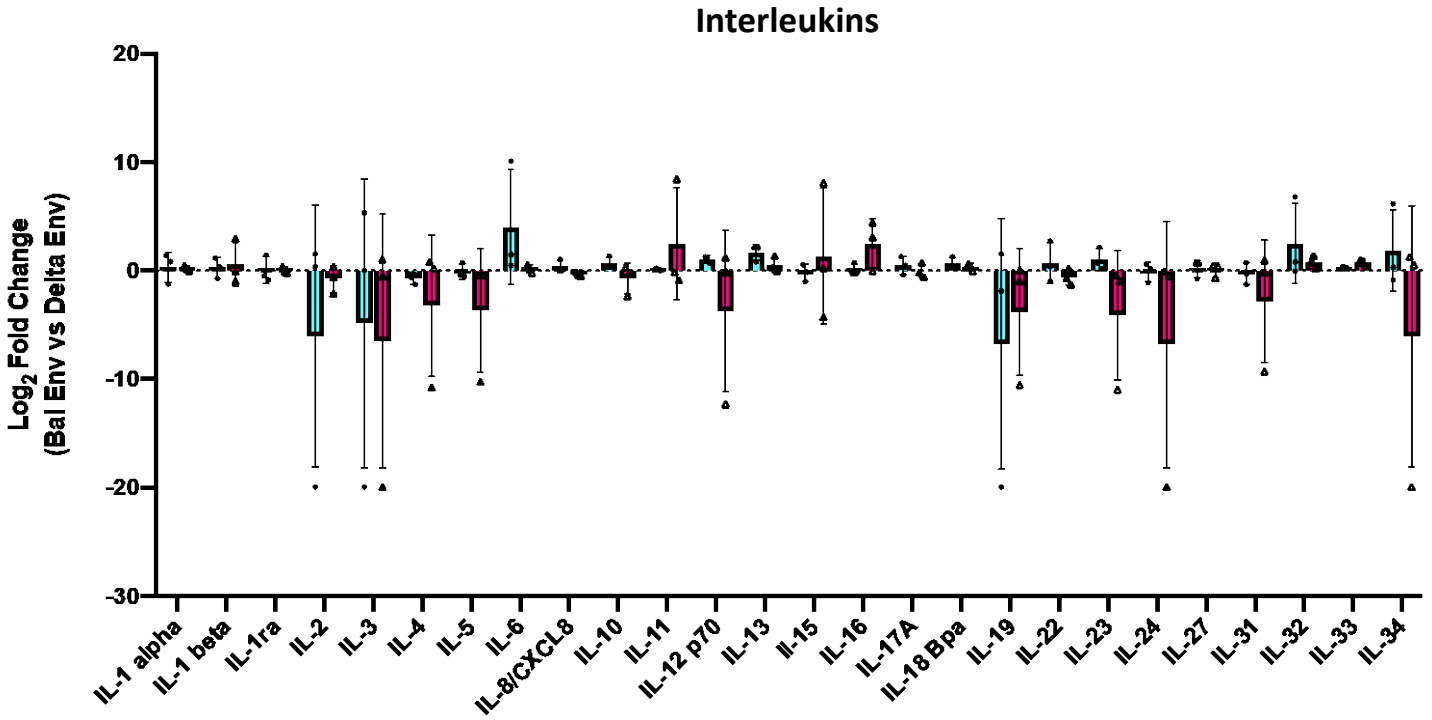


Figure 55: ***Cleared supernatants were harvested from MDM cultures 72 h post-transduction with either ΔVpr versions or Vpr$^+$ versions of the pseudotyped virus and proteome profiler arrays were used to analyse the expression of a total of 102 inflammatory factors. Expression data for the interleukins are represented as log_2 -fold change of the expression levels for analytes produced by HIV-1_{BaL} Env/HIV-1 NL4.3-ΔVpr transductions versus analyte expression levels for the Delta Env/HIV-1 NL4.3-ΔVpr transductions. Data represents 2 technical replicates for each pixel density reading and 3 independent donors were analysed per transduction. Statistical analyses were carried out by Mann-Whitney testing.***

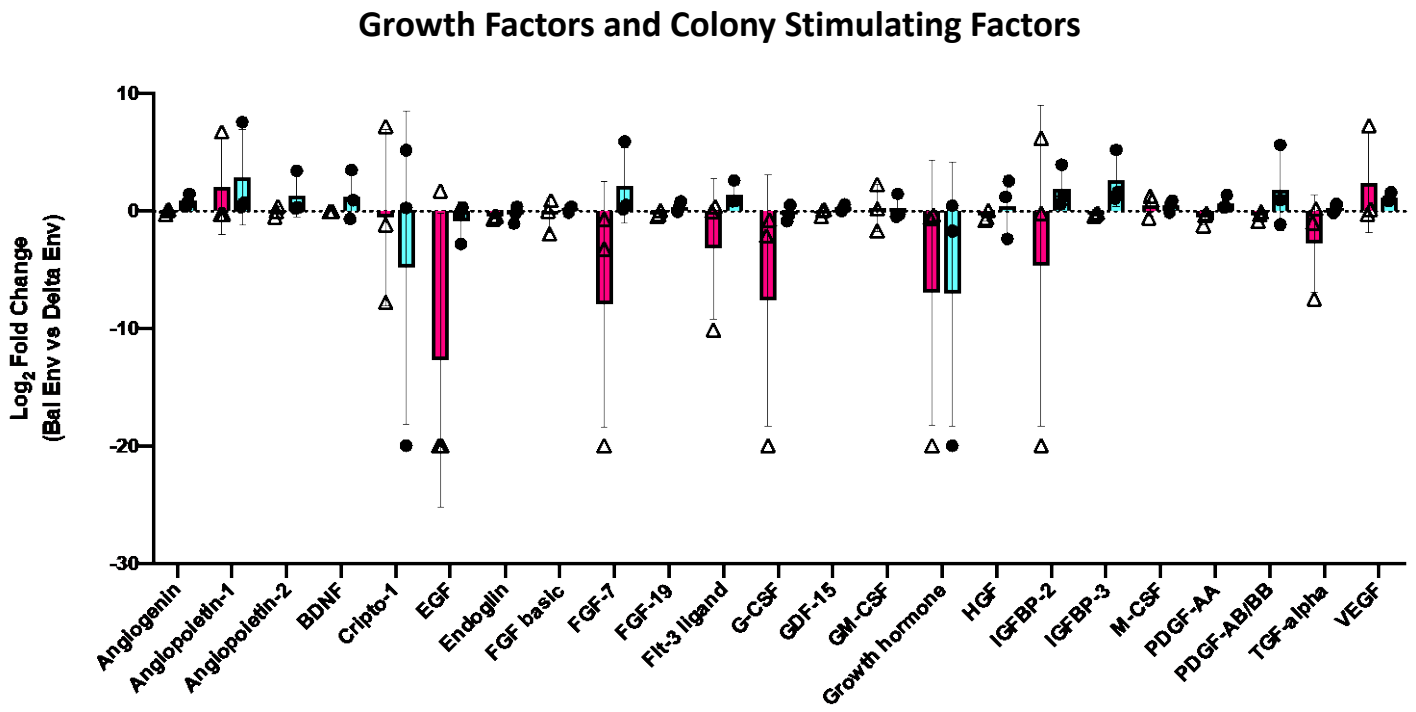


Figure 56: ***Cleared supernatants were harvested from MDM cultures 72 h post-transduction with either ΔVpr versions or Vpr^{+} versions of the pseudotyped virus and proteome profiler arrays were used to analyse the expression of a total of 102 inflammatory factors. Expression data for the growth factors and colony stimulating factors are represented as log_2 -fold change of the expression levels for analytes produced by HIV-1_{BaL} Env/HIV-1 NL4.3-ΔVpr transductions versus analyte expression levels for the Delta Env/HIV-1 NL4.3-ΔVpr transductions. Data represents 2 technical replicates for each pixel density reading and 3 independent donors were analysed per transduction. Statistical analyses were carried out by Mann-Whitney testing.***

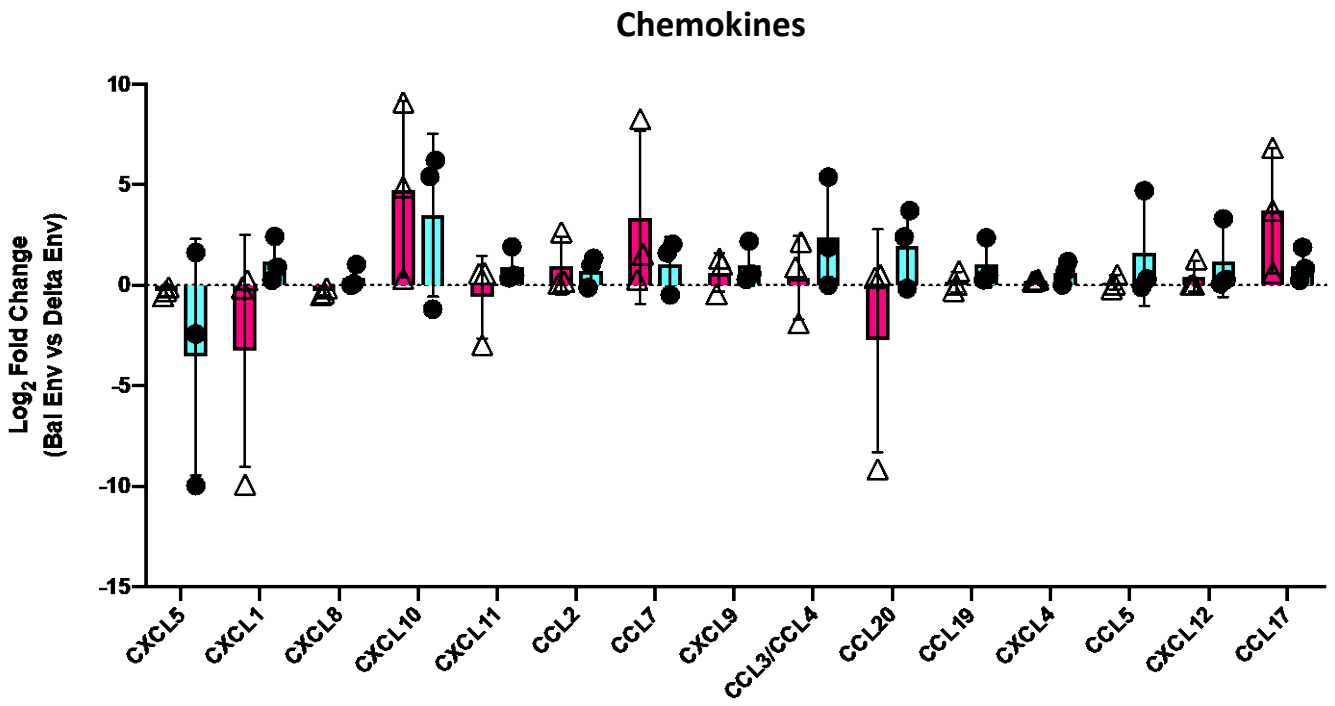


Figure 57: ***Cleared supernatants were harvested from MDM cultures 72 h post-transduction with either ΔVpr versions or Vpr$^+$ versions of the pseudotyped virus and proteome profiler arrays were used to analyse the expression of a total of 102 inflammatory factors. Expression data for the chemokines are represented as log_2 -fold change of the expression levels for analytes produced by HIV-1_{BaL} Env/HIV-1 NL4.3-ΔVpr transductions versus analyte expression levels for the Delta Env/HIV-1 NL4.3-ΔVpr transductions. Data represents 2 technical replicates for each pixel density reading and 3 independent donors were analysed per transduction. Statistical analyses were carried out by Mann-Whitney testing.***

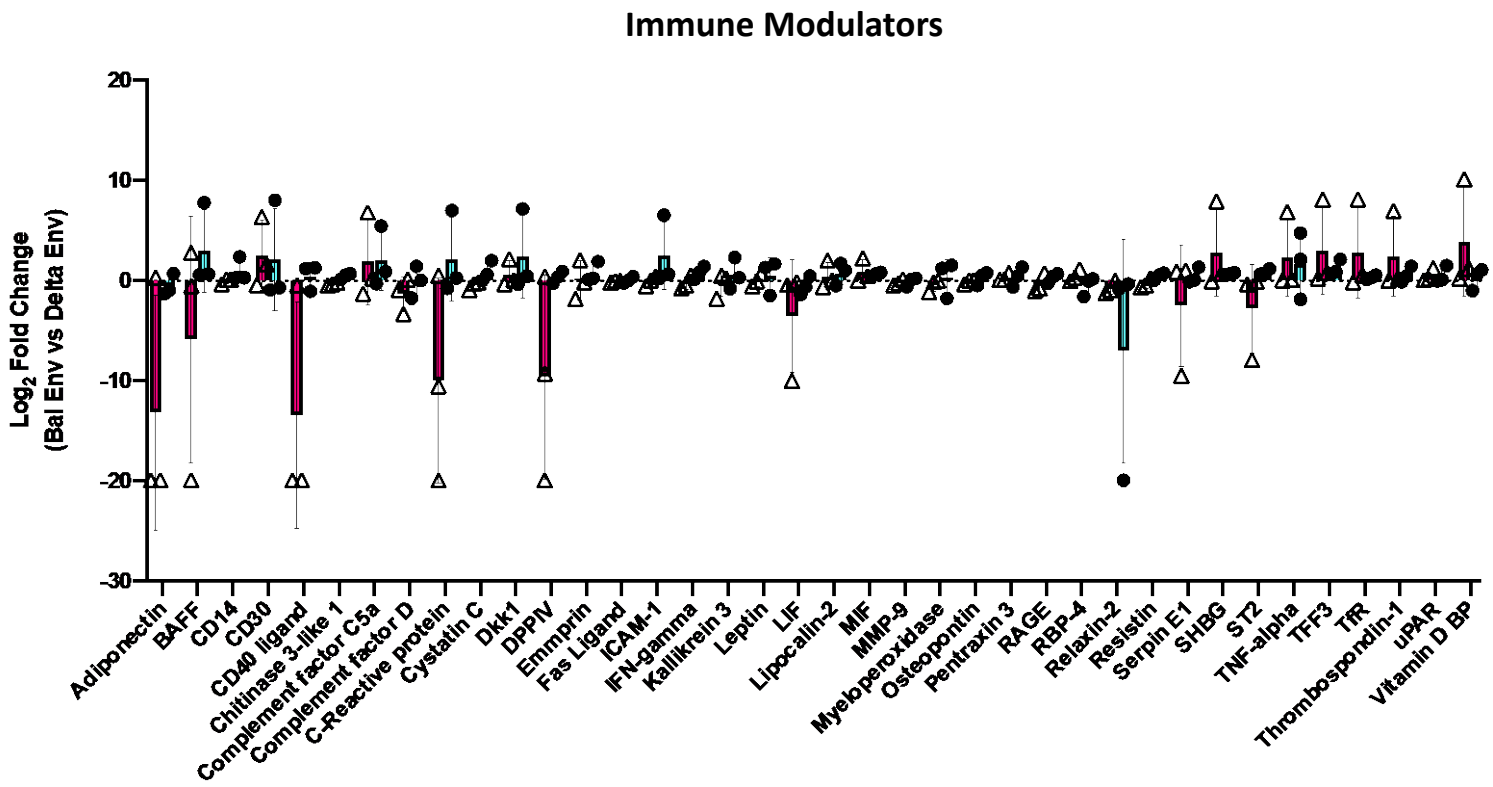


Figure 58: ***Cleared supernatants were harvested from MDM cultures 72 h post-transduction with either ΔVpr versions or Vpr$^+$ versions of the pseudotyped virus and proteome profiler arrays were used to analyse the expression of a total of 102 inflammatory factors. Expression data for the immune modulators are represented as log_2 -fold change of the expression levels for analytes produced by HIV-1_{BaL} Env/HIV-1 NL4.3-ΔVpr transductions versus analyte expression levels for the Delta Env/HIV-1 NL4.3-ΔVpr transductions. Data represents 2 technical replicates for each pixel density reading and 3 independent donors were analysed per transduction. Statistical analyses were carried out by Mann-Whitney testing.***

7.2 Supplemenatry Tables

Table 14: eGFP expression by VSV-G/HIV-1 NL4.3 transduced MDMs

	24 h			72 h			96 h		
Donor ID	No Vector	Delta Env-NL4.3	VSV-G-NL4.3	No Vector	Delta Env-NL4.3	VSV-G-NL4.3	No Vector	Delta Env-NL4.3	VSV-G-NL4.3
15	0	0.013	2.5	0.019	0.038	5.37	0.013	0	8.22
17	0	0.023	0.61	0.013	0.03	4.47	0.012	0.079	9.45
19	0.054	0.78	5.77	0.078	0.16	8.66	0.033	0.085	8.19

Table 15: 72 h Proteome Profiler analysis of differentially expressed soluble factors for VSV-G / NL4.3-ΔVpr versus Delta Env-NL4.3-ΔVpr transduced macrophages

		Mean Fold Change (VSV-G vs Delta Env)		
		HIV-1 NL4.3-ΔVpr		
Analyte	Entrez Gene ID	**Donor 15**	**Donor 17**	**Donor 19**
Adiponectin	9370	1.58	1.72	6.21
Angiogenin	283	0.67	0.15	0.69
Angiopoietin-1	284	0.71	42.40	0.00
Angiopoietin-2	285	1.14	0.78	0.54
BAFF	10673	0.68	3.64	0.00
BDNF	627	0.90	0.92	0.41
Complement Component C5/C5a	727	0.76	0.43	0.00
CD14	929	0.77	0.69	0.00

		Mean Fold Change (VSV-G vs Delta Env)		
		HIV-1 NL4.3-ΔVpr		
Analyte	Entrez Gene ID	**Donor 15**	**Donor 17**	**Donor 19**
CD30	943	1.35	0.72	0.00
CD40 ligand	959	1.26	2.18	0.00
Chitinase 3-like 1	1116	0.65	0.51	0.65
Complement Factor D	1675	0.58	0.33	0.07
C-Reactive Protein	1401	0.97	0.54	0.20
Cripto-1	6997	0.96	14.50	0.00
Cystatin C	1471	0.45	0.71	0.22
Dkk-1	22943	1.21	11.20	0.41
DPPIV	1803	0.76	1.17	0.00
EGF	1950	1.16	0.00	0.00
Emmprin	682	1.62	0.55	0.18
CXCL5/ENA-78	6374	0.37	0.38	0.12
Endoglin	2022	0.90	0.64	0.34
Fas Ligand	356	0.66	0.40	0.36
FGF basic	2247	0.82	1.25	0.35
FGF-7	2252	1.07	0.30	0.00
FGF-19	9965	0.68	0.80	0.38
Flt-3 Ligand	2323	0.78	0.46	0.31
G-CSF	1440	0.79	0.51	0.46
GDF-15	9518	0.61	0.70	0.26
GM-CSF	1437	1.55	0.54	0.39
CXCL1/GROα	2919	0.29	0.11	0.37

		Mean Fold Change (VSV-G vs Delta Env)		
		HIV-1 NL4.3-ΔVpr		
Analyte	Entrez Gene ID	**Donor 15**	**Donor 17**	**Donor 19**
Growth Hormone	2688	1.20	0.22	1.15
HGF	3082	0.76	0.67	0.27
ICAM-1	3383	1.12	2.27	0.00
IFN-γ	3458	1.46	0.68	0.20
IGFBP-2	3485	0.64	4.11	0.00
IGFBP-3	3486	0.86	1.45	0.00
IL-1α	3552	1.17	0.96	0.68
IL-1β	3553	0.83	9.50	0.94
IL-1ra	3557	1.11	0.85	0.86
IL-2	3558	0.70	0.79	0.40
IL-3	3562	0.83	9.60	6.00
IL-4	3565	0.66	0.53	0.00
IL-5	3567	0.89	0.00	0.23
IL-6	3569	0.49	2.60	0.19
CXCL8/IL-8	3576	0.72	0.29	0.40
IL-10	3586	0.68	0.50	0.32
IL-11	3589	0.85	0.19	0.00
IL-12 p70	3593	0.94	0.39	0.49
IL-13	3596	0.66	0.98	2.25
IL-15	3600	0.76	0.16	0.00
IL-16	3603	1.05	9.75	0.00
IL-17A	3605	0.90	1.18	0.44

		Mean Fold Change (VSV-G vs Delta Env)		
		HIV-1 NL4.3-ΔVpr		
Analyte	Entrez Gene ID	**Donor 15**	**Donor 17**	**Donor 19**
IL-18 Bpa	10068	0.92	1.33	0.32
IL-19	29949	0.64	0.45	0.25
IL-22	50616	0.74	0.49	0.46
IL-23	51561	0.86	0.53	0.25
IL-24	11009	0.86	0.00	0.28
IL-27	246778	0.82	0.21	0.21
IL-31	386653	1.08	96.43	0.44
IL-32	9235	1.26	0.55	0.00
IL-33	90865	0.79	0.63	0.12
IL-34	146433	0.84	42.50	0.00
CXCL10/IP-10	3627	35.87	15.88	36.74
CXCL11/I-TAC	6373	1.48	0.12	0.55
Kallikrein 3	354	1.42	1.13	0.37
Leptin	3952	0.65	0.18	0.33
LIF	3976	0.75	0.00	0.43
Lipocalin-2	3934	0.88	0.97	0.35
CCL2/MCP-1	6347	3.00	0.45	0.55
CCL7/MCP-3	6354	0.60	211.00	0.33
M-CSF	1435	0.95	1.52	0.34
MIF	4282	4.17	1.66	2.53
CXCL9/MIG	4283	1.81	0.46	1.63
CCL3/MIP-1α	6348	0.16	0.01	0.33

		Mean Fold Change (VSV-G vs Delta Env)		
		HIV-1 NL4.3-ΔVpr		
Analyte	Entrez Gene ID	**Donor 15**	**Donor 17**	**Donor 19**
CCL4/MIP-1β	6351	0.16	0.01	0.33
CCL20/MIP-3α	6364	0.94	6.73	0.43
CCL19/MIP-3β	6363	1.10	2.17	0.43
MMP-9	4318	0.87	0.86	0.95
Myeloperoxidase	4353	1.39	1.31	0.56
Osteopontin	6696	0.79	0.34	0.72
PDGF-AA	5154	0.40	0.02	0.45
PDGF-AB	5154	0.44	0.00	0.20
PDGF-BB	5155	0.44	0.00	0.20
Pentraxin 3	5806	1.01	0.87	0.57
CXCL4/PF4	5196	0.90	3.14	1.00
RAGE	177	0.93	0.63	0.21
CCL5/RANTES	6352	0.80	0.79	0.26
RBP-4	5950	0.88	1.10	1.36
Relaxin-2	6019	1.53	0.46	0.07
Resistin	56729	0.88	1.28	0.28
CXCL12/SDF-1α	6387	0.89	0.87	0.00
Serpin E1	5054	0.53	1.11	0.07
SHBG	6462	3.24	177.00	0.00
ST2	9173	0.59	169.00	0.38
CCL17/TARC	6361	0.76	240.50	2.48
TFF3	7033	1.13	274.50	0.52

		Mean Fold Change (VSV-G vs Delta Env)		
		HIV-1 NL4.3-ΔVpr		
Analyte	Entrez Gene ID	**Donor 15**	**Donor 17**	**Donor 19**
TfR	7037	1.38	485.50	0.52
TGF-α	7039	0.65	0.50	0.19
Thrombospondin-1	7057	1.08	299.50	0.31
TNF-α	7124	0.47	31.00	0.22
uPAR	5329	0.83	0.75	0.98
VEGF	7422	0.66	41.00	0.20
Vitamin D BP	2638	1.01	1.75	823.00

Proteome profiler arrays were used to analyse the expression of a total of 102 inflammatory factors produced by macrophages 72 h post-transduction with NL4.3eGFP-ΔVpr pseudotyped virus. Levels of each analyte present in the supernatant were semi-quantitatively expressed as pixel density values and fold change of expression levels of analyte produced by VSV-G/NL4.3eGFP-ΔVpr transduced macrophages was determined in comparison to the respective expression levels for VSV-G/NL4.3eGFP-ΔVpr transduced macrophages. Data represents analyses of 3 independent donors.

Table 16: eGFP expression by HIV-1_{BaL} Env/HIV-1 NL4.3-ΔVpr transduced MDMs

	24 h post-transduction			48 h post-transduction			72 h post-transduction			96 h post transduction		
Donor ID	**No Vector**	**Delta Env-NL4.3**	**BaL Env-NL4.3**	**No Vector**	**Delta Env-NL4.3**	**BaL Env-NL4.3**	**No Vector**	**Delta Env-NL4.3**	**BaL Env-NL4.3**	**No Vector**	**Delta Env-NL4.3**	**BaL Env-NL4.3**
15	0	0.013	0.093	n/a	n/a	n/a	0.019	0.038	5.42	0.013	0	5.44
17	0	0.023	0.49	n/a	n/a	n/a	0.013	0.03	11	0.12	0.079	12
19	0.054	0.78	4.15	n/a	n/a	n/a	0.078	0.16	10.5	0.033	0.085	12.7
23	0.2	0.082	0.53	0	0.026	13.1	0.56	0.72	15.4	0.27	0.22	16.5
24	0.68	0.34	7.59	0.25	0.26	19.9	0.14	0.18	19.5	0.35	0.53	21.6
25	0.8	0.24	6.77	0.44	0.16	11.7	0.55	0.37	20.9	0.54	0.18	15.4

Table 17: eGFP expression by HIV-1_{BaL} Env/HIV-1 NL4.3-Vpr^+ transduced MDMs

	24 h post-transduction			48 h post-transduction			72 h post-transduction			96 h post transduction		
Donor ID	**No Vector**	**Delta Env-NL4.3**	**BaL Env-NL4.3**	**No Vector**	**Delta Env-NL4.3**	**BaL Env-NL4.3**	**No Vector**	**Delta Env-NL4.3**	**BaL Env-NL4.3**	**No Vector**	**Delta Env-NL4.3**	**BaL Env-NL4.3**
17	0.12	0.25	0.25	n/a	n/a	n/a	0.01	0.03	15.5	0	0.06	9.77
18	0.11	0.15	0	n/a	n/a	n/a	0.066	0.02	8.44	0.085	0.13	16.7
19	0.046	0.089	0.39	n/a	n/a	n/a	0.1	0.17	10.2	0.1	0.036	5.6
20	0.26	0.61	0.8	n/a	n/a	n/a	0.13	1.1	18.7	0.28	0.16	15.1
21	0.18	0.042	1.02	n/a	n/a	n/a	0.2	0.12	10	0.12	0.043	8.24
23	0.2	0.096	5.15	0	0	0.6	0.56	0.38	5.39	0.27	0.2	8.69
24	0.68	0.49	0.8	0.25	0.077	6.48	0.14	0.092	6.71	0.35	0.34	8.82
25	0.8	0.088	0.62	0.44	0.2	1.57	0.55	0.66	6.71	0.54	0.65	12.9

Table 18: 72 h Proteome Profiler analysis of differentially expressed soluble factors between HIV-1_{BaL} Env-NL4.3 vs Delta Env-NL4.3 transduced macrophages

		Mean Fold Change (BaL Env vs Delta Env)					
		HIV-1 NL4.3-ΔVpr			HIV-1 NL4.3-Vpr^+		
Analyte	**Entrez Gene ID**	**Donor 15**	**Donor 17**	**Donor 19**	**Donor 17**	**Donor 19**	**Donor 20**
Adiponectin	9370	1.27	0.00	0.00	0.40	0.52	1.62
Angiogenin	283	1.04	0.82	1.08	2.78	1.74	1.34
Angiopoietin-1	284	0.81	107.80	0.84	193.71	1.63	1.29
Angiopoietin-2	285	0.99	1.35	0.71	10.83	1.22	1.19
BAFF	10673	0.71	6.98	0.00	221.86	1.60	1.51
BDNF	627	1.00	0.97	1.01	11.37	0.63	1.95
Complement Component C5/C5a	727	1.19	0.42	114.37	1.91	44.66	0.82
CD14	929	1.09	0.81	1.10	5.26	1.20	1.23
CD30	943	3.12	0.75	82.95	265.05	0.53	0.63
CD40 ligand	959	0.75	0.00	0.00	2.43	0.48	2.33
Chitinase 3-like 1	1116	0.73	0.80	0.88	1.65	1.11	1.48
Complement Factor D	1675	1.12	0.53	0.10	2.74	0.30	1.03
C-Reactive Protein	1401	1.44	0.00	0.00	128.69	0.60	1.21
Cripto-1	6997	0.46	0.00	149.63	36.41	0.00	1.23
Cystatin C	1471	0.92	0.54	0.81	1.53	1.01	4.07
Dkk-1	22943	1.05	4.59	0.80	146.50	0.79	1.39

		Mean Fold Change (BaL Env vs Delta Env)					
		HIV-1 NL4.3-ΔVpr			HIV-1 NL4.3-Vpr$^+$		
Analyte	**Entrez Gene ID**	**Donor 15**	**Donor 17**	**Donor 19**	**Donor 17**	**Donor 19**	**Donor 20**
DPPIV	1803	1.34	0.00	0.00	1.91	0.85	1.31
EGF	1950	3.30	0.00	0.00	0.14	0.88	1.24
Emmprin	682	4.23	0.29	0.90	1.09	1.19	3.80
CXCL5/ENA-78	6374	0.94	0.68	0.83	0.00	0.19	3.10
Endoglin	2022	0.75	0.64	0.74	0.89	0.48	1.32
Fas Ligand	356	1.01	0.88	1.00	0.87	1.32	1.03
FGF basic	2247	1.01	1.91	0.26	1.31	0.92	1.20
FGF-7	2252	0.63	0.11	0.00	60.55	1.42	1.12
FGF-19	9965	1.04	0.82	0.74	1.29	0.98	1.77
Flt-3 Ligand	2323	1.01	0.00	1.32	6.09	1.82	1.86
G-CSF	1440	0.60	0.23	0.00	0.78	0.56	1.43
GDF-15	9518	1.09	0.73	1.07	1.48	1.28	1.02
GM-CSF	1437	4.83	0.32	1.16	0.83	2.76	0.72
CXCL1/GROα	2919	1.19	0.00	0.92	1.19	5.37	1.87
Growth Hormone	2688	0.67	0.79	0.00	0.31	0.00	1.38
HGF	3082	1.05	0.58	0.68	5.95	0.20	2.32
ICAM-1	3383	1.04	1.31	0.70	93.91	1.39	1.57
IFN-γ	3458	1.44	0.72	0.59	2.68	1.10	1.82
IGFBP-2	3485	0.88	72.17	0.00	15.43	2.38	1.48
IGFBP-3	3486	0.91	0.77	0.84	3.04	37.35	2.12
IL-1α	3552	1.10	1.00	1.38	2.64	0.42	1.78

		Mean Fold Change (BaL Env vs Delta Env)					
		HIV-1 NL4.3-ΔVpr			HIV-1 NL4.3-Vpr^{+}		
Analyte	**Entrez Gene ID**	**Donor 15**	**Donor 17**	**Donor 19**	**Donor 17**	**Donor 19**	**Donor 20**
IL-1β	3553	0.97	7.78	0.52	2.25	0.60	1.28
IL-1ra	3557	0.88	1.27	0.94	2.72	0.72	0.56
IL-2	3558	1.30	0.24	0.65	2.87	0.00	1.28
IL-3	3562	0.70	2.08	0.00	0.00	40.23	1.02
IL-4	3565	1.16	0.00	1.79	0.65	0.41	0.82
IL-5	3567	0.76	0.00	0.76	0.68	1.67	0.75
IL-6	3569	0.88	1.44	1.17	1.39	1084.99	2.84
CXCL8/IL-8	3576	0.91	0.71	0.77	2.06	1.01	1.06
IL-10	3586	1.25	0.20	0.93	1.30	1.30	2.55
IL-11	3589	0.92	0.56	349.00	1.15	0.99	1.10
IL-12 p70	3593	0.94	0.00	2.31	2.44	2.32	1.65
IL-13	3596	1.21	0.98	2.57	4.24	4.36	1.74
IL-15	3600	1.18	0.05	271.74	0.90	0.50	1.46
IL-16	3603	0.98	21.86	8.38	1.65	0.83	0.83
IL-17A	3605	0.67	0.90	1.66	2.43	0.77	1.41
IL-18 Bpa	10068	0.98	1.31	1.55	2.45	1.39	1.19
IL-19	29949	1.05	0.00	0.52	0.00	2.89	0.27
IL-22	50616	1.13	0.41	0.63	6.71	0.52	1.29
IL-23	51561	0.76	0.00	0.52	1.12	4.45	1.67
IL-24	11009	0.96	0.00	0.72	1.11	0.46	1.54
IL-27	246778	1.34	0.62	1.39	1.50	0.60	1.53

		Mean Fold Change (BaL Env vs Delta Env)					
		HIV-1 NL4.3-ΔVpr			HIV-1 NL4.3-Vpr$^+$		
Analyte	**Entrez Gene ID**	**Donor 15**	**Donor 17**	**Donor 19**	**Donor 17**	**Donor 19**	**Donor 20**
IL-31	386653	0.91	0.00	1.96	0.82	0.42	1.68
IL-32	9235	1.13	1.77	2.61	112.25	0.97	1.75
IL-33	90865	1.34	1.90	1.97	1.25	1.26	1.19
IL-34	146433	1.44	0.00	2.41	71.45	0.55	1.26
CXCL10/IP-10	3627	1.25	550.24	29.92	42.31	74.93	0.44
CXCL11/I-TAC	6373	1.49	0.13	1.51	3.75	1.41	1.29
Kallikrein 3	354	1.43	0.29	1.22	5.06	0.58	1.25
Leptin	3952	1.66	0.98	0.70	3.22	0.36	2.53
LIF	3976	0.93	0.00	0.77	1.39	0.39	0.66
Lipocalin-2	3934	4.10	0.65	1.07	3.31	0.72	2.04
CCL2/MCP-1	6347	6.22	1.13	1.06	2.55	0.92	1.98
CCL7/MCP-3	6354	1.21	310.64	2.93	3.05	4.11	0.72
M-CSF	1435	2.44	0.67	1.92	1.64	0.92	1.86
MIF	4282	1.02	1.40	4.76	1.29	1.64	1.78
CXCL9/MIG	4283	2.53	0.73	2.07	1.47	4.56	1.22
CCL3/MIP-1α	6348	1.86	0.27	4.52	3.70	41.80	1.01
CCL4/MIP-1β	6351	1.86	0.27	4.52	3.70	41.80	1.01
CCL20/MIP-3α	6364	1.30	0.00	1.42	5.32	13.22	0.89
CCL19/MIP-3β	6363	0.83	1.63	1.01	1.20	5.17	1.41
MMP-9	4318	0.75	0.86	1.08	1.20	0.66	1.10
Myeloperoxidase	4353	0.94	0.45	1.00	2.37	0.30	2.92

		Mean Fold Change (BaL Env vs Delta Env)					
		HIV-1 NL4.3-ΔVpr			HIV-1 NL4.3-Vpr$^+$		
Analyte	**Entrez Gene ID**	**Donor 15**	**Donor 17**	**Donor 19**	**Donor 17**	**Donor 19**	**Donor 20**
Osteopontin	6696	0.80	1.07	1.03	1.73	1.46	0.73
PDGF-AA	5154	0.89	0.43	0.78	2.57	1.28	1.27
PDGF-AB	5154	0.97	0.83	0.54	49.90	0.46	1.94
PDGF-BB	5155	0.97	0.83	0.54	49.90	0.46	1.94
Pentraxin 3	5806	1.09	1.12	1.73	2.56	0.65	1.39
CXCL4/PF4	5196	1.23	1.15	1.18	2.27	1.61	1.01
RAGE	177	1.70	0.51	0.59	1.34	1.62	0.84
CCL5/RANTES	6352	1.04	0.89	1.44	1.24	26.30	0.93
RBP-4	5950	2.22	1.00	1.27	0.33	1.14	1.00
Relaxin-2	6019	1.01	0.43	0.51	0.58	0.00	0.81
Resistin	56729	1.21	0.73	0.64	1.47	1.04	1.68
CXCL12/SDF-1α	6387	2.47	1.02	1.01	9.94	1.06	1.22
Serpin E1	5054	2.00	0.00	1.91	2.57	1.07	0.96
SHBG	6462	0.96	251.91	1.64	1.61	1.50	1.76
ST2	9173	0.78	0.00	0.94	1.58	2.27	1.61
CCL17/TARC	6361	1.53	113.74	13.14	1.19	1.78	3.70
TFF3	7033	1.19	278.50	1.80	1.86	4.44	1.66
TfR	7037	0.91	283.66	1.49	1.49	1.11	1.23
TGF-α	7039	1.15	0.01	0.52	1.51	0.90	1.00
Thrombospondin-1	7057	1.24	128.17	1.02	2.72	1.39	0.93
TNF-α	7124	1.08	116.57	1.04	0.28	27.72	4.42

		Mean Fold Change (BaL Env vs Delta Env)					
		HIV-1 NL4.3-ΔVpr			HIV-1 NL4.3-Vpr^{+}		
Analyte	**Entrez Gene ID**	**Donor 15**	**Donor 17**	**Donor 19**	**Donor 17**	**Donor 19**	**Donor 20**
uPAR	5329	1.13	2.42	1.07	2.86	0.99	1.08
VEGF	7422	1.12	155.12	0.84	3.04	1.91	1.91
Vitamin D BP	2638	1.19	2.36	1118.39	2.11	0.51	1.62

Proteome profiler arrays were used to analyse the expression of a total of 102 inflammatory factors produced by macrophages 72 h post-transduction with HIV-1$_{BaL}$ Env/NL4.3-eGFP-ΔVpr and HIV-1$_{BaL}$ Env/NL4.3-eGFP-Vpr^{+} pseudotyped viruses. Levels of each analyte present in the supernatant were semi-quantitatively expressed as pixel density values and fold change of expression levels of analyte produced by BaL Env/NL4.3-eGFPr transduced macrophages was determined in comparison to the expression levels for the respective Delta Env/NL4.3eGFP-ΔVpr transduced macrophages. Data represents analyses of 4 independent donors.

Table 19: Gene set enrichment analysis of soluble factors expressed 72 h post HIV-1_{BaL} Env/NL4.3-ΔVpr transductions

	Annotation database	Term	Overlap	p-value	q-value
Donor 15	Reactome	Peptide ligand-binding receptors	13/194	0.00122	0.0334
		Rhodopsin-like receptors	13/330	0.00122	0.0334
		GPCR ligand binding	13/466	0.00122	0.0334
		GPCR signalling	20/1175	0.00199	0.0334
	KEGG	Chemokine signalling pathway	15/185	0.00248	0.0348
		Cytokine-cytokine receptor interaction	15/270	0.00929	0.071
	Wikipathways	Interleukin-10 signalling	20/38	0.00607	0.0566
Donor 17	KEGG	JaK-STAT signalling pathway	21/162	0.00137	0.29
Donor 19	Wikipathways	Chemokine signalling pathway	13/165	0.00415	0.00415

Cleared supernatants were harvested from MDM cultures 72 h post-transduction with HIV-1_{BaL}/NL4.3eGFP-ΔVpr and Delta Env/NL4.3eGFP-ΔVpr vectors, and proteome profiler arrays were used to quantify the expression levels of a total of 102 inflammatory factors. Gene set pathway enrichment was carried out by paired Wilcoxon signed-rank testing using the ConsensusPath DB tool. Expression values from Delta Env/NL4.3eGFP-ΔVpr transduced MDMs were used as the control dataset for gene set enrichment analysis. Proteome profiler data from 3 independent donors were analysed. 'Overlap' denotes the number of genes that were determined to be differentially expressed in proportion to the total number of genes defined by the annotated gene set. p-values corrected for multiple testing using the false discovery rate method are

represented as q-values. KEGG, Kyoto Encyclopedia of Genes and Genomes; INOH, Integrating Network Objects with Hierarchies.

Table 20: Gene set enrichment analysis of soluble factors 72 h post HIV-1_{BaL} Env/NL4.3-Vpr^{+} transductions

	Annotation database	Term	Overlap	p-value	q-value
Donor 17	Reactome	Immune system	53/1840	0.00003	0.00336
		Metabolism of proteins	12/2008	0.00049	0.0269
		Neutrophil degranulation	12/490	0.00049	0.0269
Donor 19	KEGG	Chemokine signalling pathway	16/185	0.00842	0.227
	Wikipathways	Toll-like receptor signalling pathway	13/102	0.00516	0.227
Donor 20	KEGG	MAPK signalling pathway	19/295	<0.00001	0.00093
		Pathways in cancer	25/526	0.00004	0.00093
		Rheumatoid arthritis	23/90	0.00005	0.00109
		Cytokine-cytokine receptor interactions	51/270	0.00006	0.00128
		Ras signalling pathway	15/232	0.000122	0.00224
		PI3K-Akt signalling pathway	23/352	0.000253	0.00398
	INOH	GPCR signalling	33/262	0.00004	0.00009
	Wikipathways	IL-4 and IL-13 signalling	17/98	0.00029	0.00403
		MAPK signalling pathway	12/246	0.00049	0.00537
		Cytokines and inflammatory response	19/29	0.000965	0.00934

Cleared supernatants were harvested from MDM cultures 72 h post-transduction with HIV-1_{BaL}/NL4.3eGFP-Vpr^{+} and Delta Env/NL4.3eGFP-Vpr^{+} vectors, and proteome profiler arrays were used to quantify the expression levels of a total of 102 inflammatory factors. Gene set pathway enrichment was carried out by paired Wilcoxon signed-rank testing using the ConsensusPath DB tool. Expression values from Delta

Env/NL4.3eGFP-Vpr^{+} transduced MDMs were used as the control dataset for gene set enrichment analysis. Proteome profiler data from 3 independent donors were analysed. 'Overlap' denotes the number of genes that were determined to be differentially expressed in proportion to the total number of genes defined by the annotated gene set. p-values corrected for multiple testing using the false discovery rate method are represented as q-values. KEGG, Kyoto Encyclopedia of Genes and Genomes; INOH, Integrating Network Objects with Hierarchies.

Table 21: 24 h Proteome Profiler analysis of differentially expressed soluble factors between HIV-1_{BaL} Env-NL4.3-ΔVpr versus Delta Env-NL4.3-ΔVpr transduced macrophages

		Mean Fold Change (BaL Env vs Delta Env)		
		HIV-1 NL4.3-ΔVpr		
Analyte	**Entrez Gene ID**	**Donor 15**	**Donor 17**	**Donor 19**
Adiponectin	9370	1.29	2.85	1.25
Angiogenin	283	0.75	1.34	1.61
Angiopoietin-1	284	1.00	2.42	1.36
Angiopoietin-2	285	1.08	0.52	1.19
BAFF	10673	0.58	3.25	1.21
BDNF	627	0.44	0.88	1.00
Complement Component C5/C5a	727	0.04	0.61	1.13
CD14	929	0.48	0.79	1.78
CD30	943	2.72	0.62	0.62
CD40 ligand	959	0.82	1.02	0.79
Chitinase 3-like 1	1116	1.21	1.73	1.00
Complement Factor D	1675	0.76	0.37	1.24
C-Reactive Protein	1401	0.15	0.48	1.50
Cripto-1	6997	0.34	0.35	1.14
Cystatin C	1471	0.36	0.74	1.35
Dkk-1	22943	0.07	0.68	1.08
DPPIV	1803	0.13	0.45	1.31
EGF	1950	0.68	0.68	1.42

		Mean Fold Change (BaL Env vs Delta Env)		
		HIV-1 NL4.3-ΔVpr		
Analyte	**Entrez Gene ID**	**Donor 15**	**Donor 17**	**Donor 19**
Emmprin	682	4.70	0.49	2.82
CXCL5/ENA-78	6374	2.22	2.42	1.49
Endoglin	2022	0.73	1.31	1.61
Fas Ligand	356	0.88	1.54	1.56
FGF basic	2247	0.90	0.56	1.43
FGF-7	2252	1.17	0.64	1.37
FGF-19	9965	0.62	1.54	1.17
Flt-3 Ligand	2323	1.29	0.95	1.08
G-CSF	1440	1.55	0.32	1.29
GDF-15	9518	0.77	0.79	2.59
GM-CSF	1437	2.35	0.54	1.22
CXCL1/GROα	2919	0.50	1.33	3.18
Growth Hormone	2688	1.96	0.06	1.65
HGF	3082	1.38	0.76	2.17
ICAM-1	3383	2.23	0.85	1.86
IFN-γ	3458	1.02	0.81	1.45
IGFBP-2	3485	0.71	1.30	2.42
IGFBP-3	3486	0.80	1.07	1.22
IL-1α	3552	0.98	1.11	1.68
IL-1β	3553	1.71	0.35	1.02
IL-1ra	3557	0.91	0.92	1.43
IL-2	3558	1.48	0.78	1.02

		Mean Fold Change (BaL Env vs Delta Env)		
		HIV-1 NL4.3-ΔVpr		
Analyte	**Entrez Gene ID**	**Donor 15**	**Donor 17**	**Donor 19**
IL-3	3562	2.37	1.95	0.49
IL-4	3565	1.00	1.74	1.16
IL-5	3567	1.22	1.53	1.14
IL-6	3569	1.24	1.90	1.35
CXCL8/IL-8	3576	0.66	0.88	1.03
IL-10	3586	1.01	2.67	1.59
IL-11	3589	3.32	1.42	1.32
IL-12 p70	3593	1.55	1.50	1.04
IL-13	3596	5.50	2.00	1.25
IL-15	3600	153.50	3.97	1.31
IL-16	3603	270.50	6.71	1.20
IL-17A	3605	1.71	1.68	1.14
IL-18 Bpa	10068	2.31	2.17	0.83
IL-19	29949	1.47	0.85	0.74
IL-22	50616	0.65	1.14	1.05
IL-23	51561	0.00	1.56	1.00
IL-24	11009	1.49	0.82	1.35
IL-27	246778	1.29	1.93	1.01
IL-31	386653	0.98	0.32	1.06
IL-32	9235	0.73	2.92	0.87
IL-33	90865	0.38	4.21	1.16
IL-34	146433	0.00	1.72	1.35

		Mean Fold Change (BaL Env vs Delta Env)		
		HIV-1 NL4.3-ΔVpr		
Analyte	**Entrez Gene ID**	**Donor 15**	**Donor 17**	**Donor 19**
CXCL10/IP-10	3627	1.50	1.40	1.36
CXCL11/I-TAC	6373	1.41	0.80	1.05
Kallikrein 3	354	1.44	2.71	0.90
Leptin	3952	1.21	0.52	1.19
LIF	3976	1.35	0.37	1.07
Lipocalin-2	3934	1.71	1.11	1.53
CCL2/MCP-1	6347	0.46	0.88	1.05
CCL7/MCP-3	6354	1.03	2.26	2.55
M-CSF	1435	1.85	0.98	1.82
MIF	4282	1.36	0.75	1.42
CXCL9/MIG	4283	1.98	0.99	0.92
CCL3/MIP-1α	6348	2.80	1.84	6.39
CCL4/MIP-1β	6351	2.80	1.84	6.39
CCL20/MIP-3α	6364	0.94	0.85	1.47
CCL19/MIP-3β	6363	1.36	1.13	0.97
MMP-9	4318	1.06	1.42	1.12
Myeloperoxidase	4353	0.79	0.51	2.11
Osteopontin	6696	0.90	0.48	1.39
PDGF-AA	5154	0.69	2.05	1.43
PDGF-AB	5154	3.37	0.52	1.12
PDGF-BB	5155	3.37	0.52	1.12
Pentraxin 3	5806	0.80	1.36	1.17

		Mean Fold Change (BaL Env vs Delta Env)		
		HIV-1 NL4.3-ΔVpr		
Analyte	**Entrez Gene ID**	**Donor 15**	**Donor 17**	**Donor 19**
CXCL4/PF4	5196	5.07	1.49	1.16
RAGE	177	0.49	0.59	0.99
CCL5/RANTES	6352	0.82	1.43	1.43
RBP-4	5950	1.27	1.08	1.19
Relaxin-2	6019	0.85	1.33	1.32
Resistin	56729	2.10	0.78	1.27
CXCL12/SDF-1α	6387	1.11	0.67	1.03
Serpin E1	5054	0.68	1.66	1.68
SHBG	6462	2.03	2.14	1.82
ST2	9173	4.06	1.47	1.15
CCL17/TARC	6361	6.84	1.33	1.10
TFF3	7033	22.62	1.34	0.80
TfR	7037	6.71	1.51	0.93
TGF-α	7039	2.10	0.76	0.89
Thrombospondin-1	7057	2.39	1.21	0.79
TNF-α	7124	1.07	1.81	0.59
uPAR	5329	0.81	2.26	1.47
VEGF	7422	0.39	1.37	0.83
Vitamin D BP	2638	1.48	1.69	1.33

Proteome profiler arrays were used to analyse the expression of a total of 102 inflammatory factors produced by macrophages 24 h post-transduction with either NL4.3eGFP-ΔVpr pseudotyped virus. Levels of each analyte present in the supernatant were semi-quantitatively expressed as pixel density values and

fold change of expression levels of analyte produced by BaL Env transduced macrophages was determined in comparison to the respective expression levels for Delta Env transduced macrophages. Data represents analyses of 3 independent donors.

Table 22: Gene set enrichment analysis of soluble factors expressed 24 h post HIV-1_{BaL} Env/NL4.3-ΔVpr transductions

	Annotation database	Term	Overlap	p-value	q-value
Donor 15	Reactome	Cytokine signalling in immune system	39/458	0.00118	0.0969
		Signalling by interleukins	31/254	0.00125	0.0969
	KEGG	JaK-STAT signalling pathway	23/162	0.00345	0.165
		Cytokine-cytokine receptor interaction	54/294	0.00361	0.165
		Cytokines and inflammatory response	19/29	0.00533	0.177
	Wikipathways	Chemokine signalling pathway	13/165	0.0079	0.183
Donor 17	*No significant pathway enrichment*				
Donor 19	KEGG	Cytokine-cytokine receptor interaction	54/294	<0.00001	0.0007
		Rheumatoid arthritis	23/90	0.00028	0.0058
		IL-17 signalling pathway	20/90	0.000553	0.00987
		JaK-STAT signalling pathway	23/162	0.000738	0.0114
		Ras signalling pathway	15/232	0.00116	0.0134
		Chemokine signalling pathway	16/189	0.00123	0.0134
	Reactome	Innate immune system	16/1077	0.00015	0.00393
		Signalling by interleukins	31/254	0.00834	0.0114
		Neutrophil degranulation	12/490	0.000834	0.0114

Cleared supernatants were harvested from MDM cultures 24 h post-transduction with HIV-1_{BaL}/NL4.3eGFP-ΔVpr and Delta Env/NL4.3eGFP-ΔVpr vectors, and proteome profiler arrays were used to quantify the expression levels of a total of 102 inflammatory factors. Gene set pathway enrichment was carried out by paired Wilcoxon signed-rank testing using the ConsensusPath DB tool. Expression values from Delta Env/NL4.3eGFP-ΔVpr transduced MDMs were used as the control dataset for gene set enrichment analysis. Proteome profiler data from 3 independent donors were analysed. 'Overlap' denotes the number of genes that were determined to be differentially expressed in proportion to the total number of genes defined by the annotated gene set. p-values corrected for multiple testing using the false discovery rate method are represented as q-values. KEGG, Kyoto Encyclopedia of Genes and Genomes; INOH, Integrating Network Objects with Hierarchies.

7.3 Conferences, symposiums and publications

I. **Dacon C**, Russell RA and Sattentau Q. (2019). **HIV-1 Vpr modulates innate immune responses to HIV-1 in primary human macrophages.** Lightning talk presented at the 2019 Blizard Institute Symposium on HIV, UK.

II. **Dacon C**, Russell RA and Sattentau Q. (2019). **HIV-1 Vpr accessory protein modulates macrophage pro-inflammatory responses to HIV-1.** Poster session presented at the 2019 Keystone Symposium on Myeloid Cells, USA.

III. **Dacon C**, Greaves D, Moore MD, Russell RA and Sattentau Q. (2018). **Myeloid cell activation and trafficking during HIV-1 infection.** Poster session presented at the 2018 Oxford Immunology Symposium, UK.

IV. Thanh LT, Phan TH, Rattanavong S, Nguyen TM, Duong AV, **Dacon C**, Hoang TN, Nguyen LPH, Tran CTH, Davong V, Nguyen CVV, Thwaites GE, Boni M, Dance D, Ashton PM, Day JN. (2018). **Multilocus sequence typing of Cryptococcus neoformans var. grubii from Laos in a regional and global context.** *Med Mycol*.

References

1. German Advisory Committee Blood SAoPTbB: **Human Immunodeficiency Virus (HIV)**. *Transfus Med Hemother* 2016, **43**:203-222.
2. Neil SJ, Zang T, Bieniasz PD: **Tetherin inhibits retrovirus release and is antagonized by HIV-1 Vpu**. *Nature* 2008, **451**:425-430.
3. Cullen BR: **Role and mechanism of action of the APOBEC3 family of antiretroviral resistance factors**. *J Virol* 2006, **80**:1067-1076.
4. Le Rouzic E, Belaidouni N, Estrabaud E, Morel M, Rain JC, Transy C, Margottin-Goguet F: **HIV1 Vpr arrests the cell cycle by recruiting DCAF1/VprBP, a receptor of the Cul4-DDB1 ubiquitin ligase**. *Cell Cycle* 2007, **6**:182-188.
5. Laguette N, Bregnard C, Hue P, Basbous J, Yatim A, Larroque M, Kirchhoff F, Constantinou A, Sobhian B, Benkirane M: **Premature activation of the SLX4 complex by Vpr promotes G2/M arrest and escape from innate immune sensing.** *Cell* 2014, **156**:134 - 145.
6. Mashiba M, Collins DR, Terry VH, Collins KL: **Vpr Overcomes Macrophage-Specific Restriction of HIV-1 Env Expression and Virion Production**. *Cell Host Microbe* 2015, **17**:414.
7. Greenwood EJD, Williamson JC, Sienkiewicz A, Naamati A, Matheson NJ, Lehner PJ: **Promiscuous Targeting of Cellular Proteins by Vpr Drives Systems-Level Proteomic Remodeling in HIV-1 Infection**. *Cell Rep* 2019, **27**:1579-1596 e1577.
8. Zahoor MA, Xue G, Sato H, Aida Y: **Genome-wide transcriptional profiling reveals that HIV-1 Vpr differentially regulates interferon-stimulated genes in human monocyte-derived dendritic cells**. *Virus Res* 2015, **208**:156-163.
9. Vermeire J, Roesch F, Sauter D, Rua R, Hotter D, Van Nuffel A, Vanderstraeten H, Naessens E, Iannucci V, Landi A, et al.: **HIV Triggers a cGAS-Dependent, Vpu- and Vpr-Regulated Type I Interferon Response in CD4(+) T Cells**. *Cell Rep* 2016, **17**:413-424.
10. Zahoor MA, Xue G, Sato H, Murakami T, Takeshima SN, Aida Y: **HIV-1 Vpr induces interferon-stimulated genes in human monocyte-derived macrophages**. *PLoS One* 2014, **9**:e106418.
11. Deoehle BP, Hladik F, McNevin JP, McElrath MJ, Gale MJ: **Human immunodeficiency virus type 1 mediates global disruption of innate antiviral signaling and immune defences within infected cells.** *J. Virol.* 2008, **83**:10395 - 10405.
12. Steckbeck JD, Kuhlmann AS, Montelaro RC: **C-terminal tail of human immunodeficiency virus gp41: functionally rich and structurally enigmatic**. *J Gen Virol* 2013, **94**:1-19.
13. Faria NR, Rambaut A, Suchard MA, Baele G, Bedford T, Ward MJ, Tatem AJ, Sousa JD, Arinaminpathy N, Pepin J, et al.: **HIV epidemiology. The early spread and epidemic ignition of HIV-1 in human populations**. *Science* 2014, **346**:56-61.
14. Barre-Sinoussi F, Chermann JC, Rey F, Nugeyre MT, Chamaret S, Gruest J, Dauguet C, Axler-Blin C, Vezinet-Brun F, Rouzioux C, et al.: **Isolation of a T-lymphotropic retrovirus from a patient at risk for acquired immune deficiency syndrome (AIDS)**. *Science* 1983, **220**:868-871.
15. Levy JA, Hoffman AD, Kramer SM, Landis JA, Shimabukuro JM, Oshiro LS: **Isolation of lymphocytopathic retroviruses from San Francisco patients with AIDS**. *Science* 1984, **225**:840-842.
16. Popovic M, Sarngadharan MG, Read E, Gallo RC: **Detection, isolation, and continuous production of cytopathic retroviruses (HTLV-III) from patients with AIDS and pre-AIDS**. *Science* 1984, **224**:497-500.
17. UNAIDS: **Fact Sheet - Global AIDS Update 2019.** . *https://www.unaids.org/sites/default/files/media_asset/UNAIDS_FactSheet_en.pdf.* Accessed September 28th 2019.
18. Hemelaar J, Gouws E, Ghys PD, Osmanov S, Isolation W-UNfH, Characterisation: **Global trends in molecular epidemiology of HIV-1 during 2000-2007**. *AIDS* 2011, **25**:679-689.
19. Blumenthal R, Durell S, Viard M: **HIV entry and envelope glycoprotein-mediated fusion**. *J Biol Chem* 2012, **287**:40841-40849.
20. Carter GC, Bernstone L, Sangani D, Bee JW, Harder T, James W: **HIV entry in macrophages is dependent on intact lipid rafts**. *Virology* 2009, **386**:192-202.

21. Carter GC, Bernstone L, Baskaran D, James W: **HIV-1 infects macrophages by exploiting an endocytic route dependent on dynamin, Rac1 and Pak1**. *Virology* 2011, **409**:234-250.
22. Arhel N: **Revisiting HIV-1 uncoating**. *Retrovirology* 2010, **7**:96.
23. Ganser-Pornillos BK, Yeager M, Pornillos O: **Assembly and architecture of HIV**. *Adv Exp Med Biol* 2012, **726**:441-465.
24. Galluzzi L, Bravo-San Pedro JM, Vitale I, Aaronson SA, Abrams JM, Adam D, Alnemri ES, Altucci L, Andrews D, Annicchiarico-Petruzzelli M, et al.: **Essential versus accessory aspects of cell death: recommendations of the NCCD 2015**. *Cell Death Differ* 2015, **22**:58-73.
25. Monroe KM, Yang Z, Johnson JR, Geng X, Doitsh G, Krogan NJ, Greene WC: **IFI16 DNA sensor is required for death of lymphoid CD4 T cells abortively infected with HIV**. *Science* 2014, **343**:428-432.
26. Doitsh G, Cavrois M, Lassen KG, Zepeda O, Yang Z, Santiago ML, Hebbeler AM, Greene WC: **Abortive HIV infection mediates CD4 T cell depletion and inflammation in human lymphoid tissue**. *Cell* 2010, **143**:789-801.
27. Doitsh G, Galloway NL, Geng X, Yang Z, Monroe KM, Zepeda O, Hunt PW, Hatano H, Sowinski S, Munoz-Arias I, et al.: **Cell death by pyroptosis drives CD4 T-cell depletion in HIV-1 infection**. *Nature* 2014, **505**:509-514.
28. Collini P, Noursadeghi M, Sabroe I, Miller RF, Dockrell DH: **Monocyte and macrophage dysfunction as a cause of HIV-1 induced dysfunction of innate immunity**. *Curr Mol Med* 2010, **10**:727-740.
29. Gottlieb MS, Schroff R, Schanker HM, Weisman JD, Fan PT, Wolf RA, Saxon A: **Pneumocystis carinii pneumonia and mucosal candidiasis in previously healthy homosexual men: evidence of a new acquired cellular immunodeficiency**. *N Engl J Med* 1981, **305**:1425-1431.
30. An P, Winkler CA: **Host genes associated with HIV/AIDS: advances in gene discovery**. *Trends Genet* 2010, **26**:119-131.
31. Nielsen MH, Pedersen FS, Kjems J: **Molecular strategies to inhibit HIV-1 replication**. *Retrovirology* 2005, **2**:10.
32. Teeraananchai S, Kerr SJ, Amin J, Ruxrungtham K, Law MG: **Life expectancy of HIV-positive people after starting combination antiretroviral therapy: a meta-analysis**. *HIV Med* 2017, **18**:256-266.
33. Hsu DC, Sereti I: **Serious Non-AIDS Events: Therapeutic Targets of Immune Activation and Chronic Inflammation in HIV Infection**. *Drugs* 2016, **76**:533-549.
34. McGettrick P, Barco EA, Mallon PWG: **Ageing with HIV**. *Healthcare (Basel)* 2018, **6**.
35. Deeks SG, Phillips AN: **HIV infection, antiretroviral treatment, ageing, and non-AIDS related morbidity**. *BMJ* 2009, **338**:a3172.
36. Kaplan RC, Sinclair E, Landay AL, Lurain N, Sharrett AR, Gange SJ, Xue X, Hunt P, Karim R, Kern DM, et al.: **T cell activation and senescence predict subclinical carotid artery disease in HIV-infected women**. *J Infect Dis* 2011, **203**:452-463.
37. Tenorio AR, Zheng Y, Bosch RJ, Krishnan S, Rodriguez B, Hunt PW, Plants J, Seth A, Wilson CC, Deeks SG, et al.: **Soluble markers of inflammation and coagulation but not T-cell activation predict non-AIDS-defining morbid events during suppressive antiretroviral treatment**. *J Infect Dis* 2014, **210**:1248-1259.
38. Grimm MC, Pullman WE, Bennett GM, Sullivan PJ, Pavli P, Doe WF: **Direct evidence of monocyte recruitment to inflammatory bowel disease mucosa**. *J Gastroenterol Hepatol* 1995, **10**:387-395.
39. Platt AM, Bain CC, Bordon Y, Sester DP, Mowat AM: **An independent subset of TLR expressing CCR2-dependent macrophages promotes colonic inflammation**. *J Immunol* 2010, **184**:6843-6854.
40. Roszer T: **Understanding the Biology of Self-Renewing Macrophages**. *Cells* 2018, **7**.
41. Haldar M, Murphy KM: **Origin, development, and homeostasis of tissue-resident macrophages**. *Immunol Rev* 2014, **262**:25-35.
42. Gomez Perdiguero E, Klapproth K, Schulz C, Busch K, Azzoni E, Crozet L, Garner H, Trouillet C, de Bruijn MF, Geissmann F, et al.: **Tissue-resident macrophages originate from yolk-sac-derived erythro-myeloid progenitors**. *Nature* 2015, **518**:547-551.
43. Hashimoto D, Chow A, Noizat C, Teo P, Beasley MB, Leboeuf M, Becker CD, See P, Price J, Lucas D, et al.: **Tissue-resident macrophages self-maintain locally throughout adult life with minimal contribution from circulating monocytes**. *Immunity* 2013, **38**:792-804.

44. Bain CC, Bravo-Blas A, Scott CL, Perdiguero EG, Geissmann F, Henri S, Malissen B, Osborne LC, Artis D, Mowat AM: **Constant replenishment from circulating monocytes maintains the macrophage pool in the intestine of adult mice**. *Nat Immunol* 2014, **15**:929-937.
45. Hoeffel G, Chen J, Lavin Y, Low D, Almeida FF, See P, Beaudin AE, Lum J, Low I, Forsberg EC, et al.: **C-Myb(+) erythro-myeloid progenitor-derived fetal monocytes give rise to adult tissue-resident macrophages**. *Immunity* 2015, **42**:665-678.
46. Ginhoux F, Greter M, Leboeuf M, Nandi S, See P, Gokhan S, Mehler MF, Conway SJ, Ng LG, Stanley ER, et al.: **Fate mapping analysis reveals that adult microglia derive from primitive macrophages**. *Science* 2010, **330**:841-845.
47. Sieweke MH, Allen JE: **Beyond stem cells: self-renewal of differentiated macrophages**. *Science* 2013, **342**:1242974.
48. Almodovar S, Del CCM, Maldonado IM, Villafane R, Abreu S, Melendez I, Dominguez C, Cuevas W, Collins TM, Lorenzo E: **HIV-1 infection of monocytes is directly related to the success of HAART**. *Virology* 2007, **369**:35-46.
49. Neil S, Martin F, Ikeda Y, Collins M: **Postentry restriction to human immunodeficiency virus-based vector transduction in human monocytes**. *J Virol* 2001, **75**:5448-5456.
50. Sonza S, Maerz A, Deacon N, Meanger J, Mills J, Crowe S: **Human immunodeficiency virus type 1 replication is blocked prior to reverse transcription and integration in freshly isolated peripheral blood monocytes**. *J Virol* 1996, **70**:3863-3869.
51. Triques K, Stevenson M: **Characterization of restrictions to human immunodeficiency virus type 1 infection of monocytes**. *J Virol* 2004, **78**:5523-5527.
52. Spivak AM, Salgado M, Rabi SA, O'Connell KA, Blankson JN: **Circulating monocytes are not a major reservoir of HIV-1 in elite suppressors**. *J Virol* 2011, **85**:10399-10403.
53. Honeycutt JB, Wahl A, Baker C, Spagnuolo RA, Foster J, Zakharova O, Wietgrefe S, Caro-Vegas C, Madden V, Sharpe G, et al.: **Macrophages sustain HIV replication in vivo independently of T cells**. *J Clin Invest* 2016, **126**:1353-1366.
54. Wong ME, Jaworowski A, Hearps AC: **The HIV Reservoir in Monocytes and Macrophages**. *Front Immunol* 2019, **10**:1435.
55. Ballweber L, Robinson B, Kreger A, Fialkow M, Lentz G, McElrath MJ, Hladik F: **Vaginal langerhans cells nonproductively transporting HIV-1 mediate infection of T cells**. *J Virol* 2011, **85**:13443-13447.
56. Sewald X, Ladinsky MS, Uchil PD, Beloor J, Pi R, Herrmann C, Motamedi N, Murooka TT, Brehm MA, Greiner DL, et al.: **Retroviruses use CD169-mediated trans-infection of permissive lymphocytes to establish infection**. *Science* 2015, **350**:563-567.
57. Chang J, Naif HM, Li S, Sullivan JS, Randle CM, Cunningham AL: **Twin studies demonstrate a host cell genetic effect on productive human immunodeficiency virus infection of human monocytes and macrophages in vitro**. *J Virol* 1996, **70**:7792-7803.
58. Naif HM, Li S, Alali M, Sloane A, Wu L, Kelly M, Lynch G, Lloyd A, Cunningham AL: **CCR5 expression correlates with susceptibility of maturing monocytes to human immunodeficiency virus type 1 infection**. *J Virol* 1998, **72**:830-836.
59. Yukl SA, Sinclair E, Somsouk M, Hunt PW, Epling L, Killian M, Girling V, Li P, Havlir DV, Deeks SG, et al.: **A comparison of methods for measuring rectal HIV levels suggests that HIV DNA resides in cells other than CD4+ T cells, including myeloid cells**. *AIDS* 2014, **28**:439-442.
60. Lawn SD, Roberts BD, Griffin GE, Folks TM, Butera ST: **Cellular compartments of human immunodeficiency virus type 1 replication in vivo: determination by presence of virion-associated host proteins and impact of opportunistic infection**. *J Virol* 2000, **74**:139-145.
61. Musich T, Jones JC, Keele BF, Jenkins LMM, Demberg T, Uldrick TS, Yarchoan R, Robert-Guroff M: **Flow virometric sorting and analysis of HIV quasispecies from plasma**. *JCI Insight* 2017, **2**:e90626.
62. Karpel ME, Boutwell CL, Allen TM: **BLT humanized mice as a small animal model of HIV infection**. *Curr Opin Virol* 2015, **13**:75-80.
63. Le Douce V, Herbein G, Rohr O, Schwartz C: **Molecular mechanisms of HIV-1 persistence in the monocyte-macrophage lineage**. *Retrovirology* 2010, **7**:32.

64. Clayton KL, Collins DR, Lengieza J, Ghebremichael M, Dotiwala F, Lieberman J, Walker BD: **Resistance of HIV-infected macrophages to CD8(+) T lymphocyte-mediated killing drives activation of the immune system**. *Nat Immunol* 2018, **19**:475-486.
65. Lambotte O, Taoufik Y, de Goer MG, Wallon C, Goujard C, Delfraissy JF: **Detection of infectious HIV in circulating monocytes from patients on prolonged highly active antiretroviral therapy**. *J Acquir Immune Defic Syndr* 2000, **23**:114-119.
66. Calcaterra S, Cappiello G, Di Caro A, Garbuglia AR, Benedetto A: **Comparative analysis of total and integrated HIV-1 DNA in peripheral CD4 lymphocytes and monocytes after long treatment with HAART**. *J Infect* 2001, **43**:239-245.
67. Sonza S, Mutimer HP, Oelrichs R, Jardine D, Harvey K, Dunne A, Purcell DF, Birch C, Crowe SM: **Monocytes harbour replication-competent, non-latent HIV-1 in patients on highly active antiretroviral therapy**. *AIDS* 2001, **15**:17-22.
68. Zhu T, Muthui D, Holte S, Nickle D, Feng F, Brodie S, Hwangbo Y, Mullins JI, Corey L: **Evidence for human immunodeficiency virus type 1 replication in vivo in CD14(+) monocytes and its potential role as a source of virus in patients on highly active antiretroviral therapy**. *J Virol* 2002, **76**:707-716.
69. Crowe SM, Sonza S: **HIV-1 can be recovered from a variety of cells including peripheral blood monocytes of patients receiving highly active antiretroviral therapy: a further obstacle to eradication**. *J Leukoc Biol* 2000, **68**:345-350.
70. Delobel P, Sandres-Saune K, Cazabat M, L'Faqihi FE, Aquilina C, Obadia M, Pasquier C, Marchou B, Massip P, Izopet J: **Persistence of distinct HIV-1 populations in blood monocytes and naive and memory CD4 T cells during prolonged suppressive HAART**. *AIDS* 2005, **19**:1739-1750.
71. Ellery PJ, Tippett E, Chiu YL, Paukovics G, Cameron PU, Solomon A, Lewin SR, Gorry PR, Jaworowski A, Greene WC, et al.: **The CD16+ monocyte subset is more permissive to infection and preferentially harbors HIV-1 in vivo**. *J Immunol* 2007, **178**:6581-6589.
72. Gibellini D, Borderi M, De Crignis E, Cicola R, Cimatti L, Vitone F, Chiodo F, Re MC: **HIV-1 DNA load analysis in peripheral blood lymphocytes and monocytes from naive and HAART-treated individuals**. *J Infect* 2008, **56**:219-225.
73. Valcour VG, Shiramizu BT, Sithinamsuwan P, Nidhinandana S, Ratto-Kim S, Ananworanich J, Siangphoe U, Kim JH, de Souza M, Degruttola V, et al.: **HIV DNA and cognition in a Thai longitudinal HAART initiation cohort: the SEARCH 001 Cohort Study**. *Neurology* 2009, **72**:992-998.
74. Ndhlovu LC, Umaki T, Chew GM, Chow DC, Agsalda M, Kallianpur KJ, Paul R, Zhang G, Ho E, Hanks N, et al.: **Treatment intensification with maraviroc (CCR5 antagonist) leads to declines in CD16-expressing monocytes in cART-suppressed chronic HIV-infected subjects and is associated with improvements in neurocognitive test performance: implications for HIV-associated neurocognitive disease (HAND)**. *J Neurovirol* 2014, **20**:571-582.
75. Hansen EC, Ransom M, Hesselberth JR, Hosmane NN, Capoferri AA, Bruner KM, Pollack RA, Zhang H, Drummond MB, Siliciano JM, et al.: **Diverse fates of uracilated HIV-1 DNA during infection of myeloid lineage cells**. *Elife* 2016, **5**.
76. Cattin A, Wiche Salinas TR, Gosselin A, Planas D, Shacklett B, Cohen EA, Ghali MP, Routy JP, Ancuta P: **HIV-1 is rarely detected in blood and colon myeloid cells during viral-suppressive antiretroviral therapy**. *AIDS* 2019, **33**:1293-1306.
77. Deleage C, Moreau M, Rioux-Leclercq N, Ruffault A, Jegou B, Dejucq-Rainsford N: **Human immunodeficiency virus infects human seminal vesicles in vitro and in vivo**. *Am J Pathol* 2011, **179**:2397-2408.
78. Wang TH, Donaldson YK, Brettle RP, Bell JE, Simmonds P: **Identification of shared populations of human immunodeficiency virus type 1 infecting microglia and tissue macrophages outside the central nervous system**. *J Virol* 2001, **75**:11686-11699.
79. Cribbs SK, Lennox J, Caliendo AM, Brown LA, Guidot DM: **Healthy HIV-1-infected individuals on highly active antiretroviral therapy harbor HIV-1 in their alveolar macrophages**. *AIDS Res Hum Retroviruses* 2015, **31**:64-70.
80. Lamers SL, Rose R, Ndhlovu LC, Nolan DJ, Salemi M, Maidji E, Stoddart CA, McGrath MS: **The meningeal lymphatic system: a route for HIV brain migration?** *J Neurovirol* 2016, **22**:275-281.

81. Lamers SL, Fogel GB, Singer EJ, Salemi M, Nolan DJ, Huysentruyt LC, McGrath MS: **HIV-1 Nef in macrophage-mediated disease pathogenesis**. *Int Rev Immunol* 2012, **31**:432-450.
82. Rose R, Lamers SL, Nolan DJ, Maidji E, Faria NR, Pybus OG, Dollar JJ, Maruniak SA, McAvoy AC, Salemi M, et al.: **HIV Maintains an Evolving and Dispersed Population in Multiple Tissues during Suppressive Combined Antiretroviral Therapy in Individuals with Cancer**. *J Virol* 2016, **90**:8984-8993.
83. Tso FY, Kang G, Kwon EH, Julius P, Li Q, West JT, Wood C: **Brain is a potential sanctuary for subtype C HIV-1 irrespective of ART treatment outcome**. *PLoS One* 2018, **13**:e0201325.
84. Kandathil AJ, Sugawara S, Goyal A, Durand CM, Quinn J, Sachithanandham J, Cameron AM, Bailey JR, Perelson AS, Balagopal A: **No recovery of replication-competent HIV-1 from human liver macrophages**. *J Clin Invest* 2018, **128**:4501-4509.
85. Ko A, Kang G, Hattler JB, Galadima HI, Zhang J, Li Q, Kim WK: **Macrophages but not Astrocytes Harbor HIV DNA in the Brains of HIV-1-Infected Aviremic Individuals on Suppressive Antiretroviral Therapy**. *J Neuroimmune Pharmacol* 2019, **14**:110-119.
86. Ganor Y, Real F, Sennepin A, Dutertre CA, Prevedel L, Xu L, Tudor D, Charmeteau B, Couedel-Courteille A, Marion S, et al.: **HIV-1 reservoirs in urethral macrophages of patients under suppressive antiretroviral therapy**. *Nat Microbiol* 2019, **4**:633-644.
87. Baxter AE, Russell RA, Duncan CJ, Moore MD, Willberg CB, Pablos JL, Finzi A, Kaufmann DE, Ochsenbauer C, Kappes JC, et al.: **Macrophage infection via selective capture of HIV-1-infected CD4+ T cells**. *Cell Host Microbe* 2014, **16**:711-721.
88. Groot F, Welsch S, Sattentau QJ: **Efficient HIV-1 transmission from macrophages to T cells across transient virological synapses**. *Blood* 2008, **111**:4660-4663.
89. Mantovani A, Sica A, Sozzani S, Allavena P, Vecchi A, Locati M: **The chemokine system in diverse forms of macrophage activation and polarization**. *Trends Immunol* 2004, **25**:677-686.
90. Martinez FO, Gordon S: **The M1 and M2 paradigm of macrophage activation: time for reassessment**. *F1000Prime Rep* 2014, **6**:13.
91. Sattentau QJ, Stevenson M: **Macrophages and HIV-1: An Unhealthy Constellation**. *Cell Host Microbe* 2016, **19**:304-310.
92. Lamers SL, Rose R, Maidji E, Agsalda-Garcia M, Nolan DJ, Fogel GB, Salemi M, Garcia DL, Bracci P, Yong W, et al.: **HIV DNA Is Frequently Present within Pathologic Tissues Evaluated at Autopsy from Combined Antiretroviral Therapy-Treated Patients with Undetectable Viral Loads**. *J Virol* 2016, **90**:8968-8983.
93. Igarashi T, Brown CR, Endo Y, Buckler-White A, Plishka R, Bischofberger N, Hirsch V, Martin MA: **Macrophage are the principal reservoir and sustain high virus loads in rhesus macaques after the depletion of CD4+ T cells by a highly pathogenic simian immunodeficiency virus/HIV type 1 chimera (SHIV): Implications for HIV-1 infections of humans**. *Proc Natl Acad Sci U S A* 2001, **98**:658-663.
94. Stacey AR, Norris PJ, Qin L, Haygreen EA, Taylor E, Heitman J, Lebedeva M, DeCamp A, Li D, Grove D, et al.: **Induction of a striking systemic cytokine cascade prior to peak viremia in acute human immunodeficiency virus type 1 infection, in contrast to more modest and delayed responses in acute hepatitis B and C virus infections**. *J Virol* 2009, **83**:3719-3733.
95. Malherbe G, Steel HC, Cassol S, de Oliveira T, Seebregts CJ, Anderson R, Cassol E, Rossouw TM: **Circulating biomarkers of immune activation distinguish viral suppression from nonsuppression in HAART-treated patients with advanced HIV-1 subtype C infection**. *Mediators Inflamm* 2014, **2014**:198413.
96. Burdo TH, Lo J, Abbara S, Wei J, DeLelys ME, Preffer F, Rosenberg ES, Williams KC, Grinspoon S: **Soluble CD163, a novel marker of activated macrophages, is elevated and associated with noncalcified coronary plaque in HIV-infected patients**. *J Infect Dis* 2011, **204**:1227-1236.
97. Bahrami H, Budoff M, Haberlen SA, Rezaeian P, Ketlogetswe K, Tracy R, Palella F, Witt MD, McConnell MV, Kingsley L, et al.: **Inflammatory Markers Associated With Subclinical Coronary Artery Disease: The Multicenter AIDS Cohort Study**. *J Am Heart Assoc* 2016, **5**.
98. Zidar DA, Juchnowski S, Ferrari B, Clagett B, Pilch-Cooper HA, Rose S, Rodriguez B, McComsey GA, Sieg SF, Mehta NN, et al.: **Oxidized LDL Levels Are Increased in HIV Infection and May Drive Monocyte Activation**. *J Acquir Immune Defic Syndr* 2015, **69**:154-160.

99. Kamat A, Misra V, Cassol E, Ancuta P, Yan Z, Li C, Morgello S, Gabuzda D: **A plasma biomarker signature of immune activation in HIV patients on antiretroviral therapy**. *PLoS One* 2012, **7**:e30881.
100. Makhubele TG, Steel HC, Anderson R, van Dyk G, Theron AJ, Rossouw TM: **Systemic Immune Activation Profiles of HIV-1 Subtype C-Infected Children and Their Mothers**. *Mediators Inflamm* 2016, **2016**:9026573.
101. Angelovich TA, Hearps AC, Maisa A, Martin GE, Lichtfuss GF, Cheng WJ, Palmer CS, Landay AL, Crowe SM, Jaworowski A: **Viremic and Virologically Suppressed HIV Infection Increases Age-Related Changes to Monocyte Activation Equivalent to 12 and 4 Years of Aging, Respectively**. *J Acquir Immune Defic Syndr* 2015, **69**:11-17.
102. McKibben RA, Margolick JB, Grinspoon S, Li X, Palella FJ, Jr., Kingsley LA, Witt MD, George RT, Jacobson LP, Budoff M, et al.: **Elevated levels of monocyte activation markers are associated with subclinical atherosclerosis in men with and those without HIV infection**. *J Infect Dis* 2015, **211**:1219-1228.
103. Arinola OG, Adedapo KS, Kehinde AO, Olaniyi JA, Akiibinu MO: **Acute phase proteins, trace elements in asymptomatic human immunodeficiency virus infection in Nigerians**. *Afr J Med Med Sci* 2004, **33**:317-322.
104. Noursadeghi M, Miller RF: **Clinical value of C-reactive protein measurements in HIV-positive patients**. *Int J STD AIDS* 2005, **16**:438-441.
105. Triant VA, Meigs JB, Grinspoon SK: **Association of C-reactive protein and HIV infection with acute myocardial infarction**. *J Acquir Immune Defic Syndr* 2009, **51**:268-273.
106. Freiberg MS, Bebu I, Tracy R, So-Armah K, Okulicz J, Ganesan A, Armstrong A, O'Bryan T, Rimland D, Justice AC, et al.: **D-Dimer Levels before HIV Seroconversion Remain Elevated Even after Viral Suppression and Are Associated with an Increased Risk of Non-AIDS Events**. *PLoS One* 2016, **11**:e0152588.
107. Fontaine J, Poudrier J, Roger M: **Short communication: persistence of high blood levels of the chemokines CCL2, CCL19, and CCL20 during the course of HIV infection**. *AIDS Res Hum Retroviruses* 2011, **27**:655-657.
108. Gao D, Wu J, Wu YT, Du F, Aroh C, Yan N, Sun L, Chen ZJ: **Cyclic GMP-AMP synthase is an innate immune sensor of HIV and other retroviruses**. *Science* 2013, **341**:903-906.
109. Takuma Shibata MT, Shin-Ichiroh Saitoh, Yoshio Yamauchi, Yuji Motoi, Mayumi Komine, Etsuko Fujita, Ryota Sato, Hiroshi Sagara, Takeshi Ichinohe, Mimi Kawazoe, Chiharu Kato, Katsuhiro Furusho, Yusuke Murakami, Ryutaro Fukui, Mamitaro Ohtsuki, Umeharu Ohto, Toshiyuki Shimizu, Nobuaki Yoshida, Toshiaki Isobe, Kensuke Miyake: **Nucleosides drive histiocytosis in SLC29A3 disorders by activating TLR7**. *bioRxiv* 2019.
110. Iwasaki A: **Innate immune recognition of HIV-1**. *Immunity* 2012, **37**:389-398.
111. Jakobsen MR, Olagnier D, Hiscott J: **Innate immune sensing of HIV-1 infection**. *Curr Opin HIV AIDS* 2015, **10**:96-102.
112. Cai X, Chiu YH, Chen ZJ: **The cGAS-cGAMP-STING pathway of cytosolic DNA sensing and signaling**. *Mol Cell* 2014, **54**:289-296.
113. Bergantz L, Subra F, Deprez E, Delelis O, Richetta C: **Interplay between Intrinsic and Innate Immunity during HIV Infection**. *Cells* 2019, **8**.
114. Appelberg KS, Wallet MA, Taylor JP, Cash MN, Sleasman JW, Goodenow M: **HIV-1 infection primes macrophages via STAT signaling to promote enhanced inflammation and viral replication**. *AIDS Res Hum Retroviruses* 2017.
115. Ben Haij N, Planes R, Leghmari K, Serrero M, Delobel P, Izopet J, BenMohamed L, Bahraoui E: **HIV-1 Tat Protein Induces Production of Proinflammatory Cytokines by Human Dendritic Cells and Monocytes/Macrophages through Engagement of TLR4-MD2-CD14 Complex and Activation of NF-kappaB Pathway**. *PLoS One* 2015, **10**:e0129425.
116. Herbein G, Gras G, Khan KA, Abbas W: **Macrophage signaling in HIV-1 infection**. *Retrovirology* 2010, **7**:34.
117. Kanmogne GD, Schall K, Leibhart J, Knipe B, Gendelman HE, Persidsky Y: **HIV-1 gp120 compromises blood-brain barrier integrity and enhances monocyte migration across blood-brain barrier: implication for viral neuropathogenesis**. *J Cereb Blood Flow Metab* 2007, **27**:123-134.

118. Ben Haij N, Leghmari K, Planes R, Thieblemont N, Bahraoui E: **HIV-1 Tat protein binds to TLR4-MD2 and signals to induce TNF-alpha and IL-10**. *Retrovirology* 2013, **10**:123.
119. Pu H, Tian J, Flora G, Lee YW, Nath A, Hennig B, Toborek M: **HIV-1 Tat protein upregulates inflammatory mediators and induces monocyte invasion into the brain**. *Mol Cell Neurosci* 2003, **24**:224-237.
120. Dillon SM, Lee EJ, Kotter CV, Austin GL, Dong Z, Hecht DK, Gianella S, Siewe B, Smith DM, Landay AL, et al.: **An altered intestinal mucosal microbiome in HIV-1 infection is associated with mucosal and systemic immune activation and endotoxemia**. *Mucosal Immunol* 2014, **7**:983-994.
121. Sandler NG, Wand H, Roque A, Law M, Nason MC, Nixon DE, Pedersen C, Ruxrungtham K, Lewin SR, Emery S, et al.: **Plasma levels of soluble CD14 independently predict mortality in HIV infection**. *J Infect Dis* 2011, **203**:780-790.
122. Lurain NS, Hanson BA, Hotton AL, Weber KM, Cohen MH, Landay AL: **The Association of Human Cytomegalovirus with Biomarkers of Inflammation and Immune Activation in HIV-1-Infected Women**. *AIDS Res Hum Retroviruses* 2016, **32**:134-143.
123. Patel EU, Gianella S, Newell K, Tobian AA, Kirkpatrick AR, Nalugoda F, Grabowski MK, Gray RH, Serwadda D, Quinn TC, et al.: **Elevated cytomegalovirus IgG antibody levels are associated with HIV-1 disease progression and immune activation**. *AIDS* 2017.
124. Albini A, Ferrini S, Benelli R, Sforzini S, Giunciuglio D, Aluigi MG, Proudfoot AE, Alouani S, Wells TN, Mariani G, et al.: **HIV-1 Tat protein mimicry of chemokines**. *Proc Natl Acad Sci U S A* 1998, **95**:13153-13158.
125. Murphy PM: **Viral exploitation and subversion of the immune system through chemokine mimicry**. *Nat Immunol* 2001, **2**:116-122.
126. Izmailova E, Bertley FM, Huang Q, Makori N, Miller CJ, Young RA, Aldovini A: **HIV-1 Tat reprograms immature dendritic cells to express chemoattractants for activated T cells and macrophages**. *Nat Med* 2003, **9**:191-197.
127. Fiume G, Vecchio E, De Laurentiis A, Trimboli F, Palmieri C, Pisano A, Falcone C, Pontoriero M, Rossi A, Scialdone A, et al.: **Human immunodeficiency virus-1 Tat activates NF-kappaB via physical interaction with IkappaB-alpha and p65**. *Nucleic Acids Res* 2012, **40**:3548-3562.
128. Wood MP, Cole AL, Eade CR, Chen LM, Chai KX, Cole AM: **The HIV-1 gp41 ectodomain is cleaved by matriptase to produce a chemotactic peptide that acts through FPR2**. *Immunology* 2014, **142**:474-483.
129. Su SB, Gao J, Gong W, Dunlop NM, Murphy PM, Oppenheim JJ, Wang JM: **T21/DP107, A synthetic leucine zipper-like domain of the HIV-1 envelope gp41, attracts and activates human phagocytes by using G-protein-coupled formyl peptide receptors**. *J Immunol* 1999, **162**:5924-5930.
130. de Paulis A, Florio G, Prevete N, Triggiani M, Fiorentino I, Genovese A, Marone G: **HIV-1 envelope gp41 peptides promote migration of human Fc epsilon RI+ cells and inhibit IL-13 synthesis through interaction with formyl peptide receptors**. *J Immunol* 2002, **169**:4559-4567.
131. Le Y, Jiang S, Hu J, Gong W, Su S, Dunlop NM, Shen W, Li B, Ming Wang J: **N36, a synthetic N-terminal heptad repeat domain of the HIV-1 envelope protein gp41, is an activator of human phagocytes**. *Clin Immunol* 2000, **96**:236-242.
132. Nou E, Lo J, Grinspoon SK: **Inflammation, immune activation, and cardiovascular disease in HIV**. *AIDS* 2016, **30**:1495-1509.
133. Hsu DC, Ma YF, Hur S, Li D, Rupert A, Scherzer R, Kalapus SC, Deeks S, Sereti I, Hsue PY: **Plasma IL-6 levels are independently associated with atherosclerosis and mortality in HIV-infected individuals on suppressive antiretroviral therapy**. *AIDS* 2016, **30**:2065-2074.
134. Sereti I, Krebs SJ, Phanuphak N, Fletcher JL, Slike B, Pinyakorn S, O'Connell RJ, Rupert A, Chomont N, Valcour V, et al.: **Persistent, Albeit Reduced, Chronic Inflammation in Persons Starting Antiretroviral Therapy in Acute HIV Infection**. *Clin Infect Dis* 2017, **64**:124-131.
135. Williams DW, Eugenin EA, Calderon TM, Berman JW: **Monocyte maturation, HIV susceptibility, and transmigration across the blood brain barrier are critical in HIV neuropathogenesis**. *J Leukoc Biol* 2012, **91**:401-415.
136. Williams DW, Byrd D, Rubin LH, Anastos K, Morgello S, Berman JW: **CCR2 on CD14(+)CD16(+) monocytes is a biomarker of HIV-associated neurocognitive disorders**. *Neurol Neuroimmunol Neuroinflamm* 2014, **1**:e36.

137. Williams DW, Veenstra M, Gaskill PJ, Morgello S, Calderon TM, Berman JW: **Monocytes mediate HIV neuropathogenesis: mechanisms that contribute to HIV associated neurocognitive disorders**. *Curr HIV Res* 2014, **12**:85-96.
138. Sackoff JE, Hanna DB, Pfeiffer MR, Torian LV: **Causes of death among persons with AIDS in the era of highly active antiretroviral therapy: New York City**. *Ann Intern Med* 2006, **145**:397-406.
139. Grinspoon SK, Grunfeld C, Kotler DP, Currier JS, Lundgren JD, Dube MP, Lipshultz SE, Hsue PY, Squires K, Schambelan M, et al.: **State of the science conference: Initiative to decrease cardiovascular risk and increase quality of care for patients living with HIV/AIDS: executive summary**. *Circulation* 2008, **118**:198-210.
140. Kuller LH, Tracy R, Belloso W, De Wit S, Drummond F, Lane HC, Ledergerber B, Lundgren J, Neuhaus J, Nixon D, et al.: **Inflammatory and coagulation biomarkers and mortality in patients with HIV infection**. *PLoS Med* 2008, **5**:e203.
141. Kelesidis T, Kendall MA, Yang OO, Hodis HN, Currier JS: **Biomarkers of microbial translocation and macrophage activation: association with progression of subclinical atherosclerosis in HIV-1 infection**. *J Infect Dis* 2012, **206**:1558-1567.
142. Duprez DA, Neuhaus J, Kuller LH, Tracy R, Belloso W, De Wit S, Drummond F, Lane HC, Ledergerber B, Lundgren J, et al.: **Inflammation, coagulation and cardiovascular disease in HIV-infected individuals**. *PLoS One* 2012, **7**:e44454.
143. Hileman CO, Longenecker CT, Carman TL, McComsey GA: **C-reactive protein predicts 96-week carotid intima media thickness progression in HIV-infected adults naive to antiretroviral therapy**. *J Acquir Immune Defic Syndr* 2014, **65**:340-344.
144. Hileman CO, Turner R, Funderburg NT, Semba RD, McComsey GA: **Changes in oxidized lipids drive the improvement in monocyte activation and vascular disease after statin therapy in HIV**. *AIDS* 2016, **30**:65-73.
145. Lo J, Abbara S, Shturman L, Soni A, Wei J, Rocha-Filho JA, Nasir K, Grinspoon SK: **Increased prevalence of subclinical coronary atherosclerosis detected by coronary computed tomography angiography in HIV-infected men**. *AIDS* 2010, **24**:243-253.
146. Post WS, Budoff M, Kingsley L, Palella FJ, Jr., Witt MD, Li X, George RT, Brown TT, Jacobson LP: **Associations between HIV infection and subclinical coronary atherosclerosis**. *Ann Intern Med* 2014, **160**:458-467.
147. Srinivasa S, Grinspoon SK: **Metabolic and body composition effects of newer antiretrovirals in HIV-infected patients**. *Eur J Endocrinol* 2014, **170**:R185-202.
148. McArthur JC: **HIV dementia: an evolving disease**. *J Neuroimmunol* 2004, **157**:3-10.
149. Robertson KR, Smurzynski M, Parsons TD, Wu K, Bosch RJ, Wu J, McArthur JC, Collier AC, Evans SR, Ellis RJ: **The prevalence and incidence of neurocognitive impairment in the HAART era**. *AIDS* 2007, **21**:1915-1921.
150. Valcour V, Chalermchai T, Sailasuta N, Marovich M, Lerdlum S, Suttichom D, Suwanwela NC, Jagodzinski L, Michael N, Spudich S, et al.: **Central nervous system viral invasion and inflammation during acute HIV infection**. *J Infect Dis* 2012, **206**:275-282.
151. Brew BJ, Pemberton L, Cunningham P, Law MG: **Levels of human immunodeficiency virus type 1 RNA in cerebrospinal fluid correlate with AIDS dementia stage**. *J Infect Dis* 1997, **175**:963-966.
152. McArthur JC, McClernon DR, Cronin MF, Nance-Sproson TE, Saah AJ, St Clair M, Lanier ER: **Relationship between human immunodeficiency virus-associated dementia and viral load in cerebrospinal fluid and brain**. *Ann Neurol* 1997, **42**:689-698.
153. Sailasuta N, Ross W, Ananworanich J, Chalermchai T, DeGruttola V, Lerdlum S, Pothisri M, Busovaca E, Ratto-Kim S, Jagodzinski L, et al.: **Change in brain magnetic resonance spectroscopy after treatment during acute HIV infection**. *PLoS One* 2012, **7**:e49272.
154. Gelman BB, Chen T, Lisinicchia JG, Soukup VM, Carmical JR, Starkey JM, Masliah E, Commins DL, Brandt D, Grant I, et al.: **The National NeuroAIDS Tissue Consortium brain gene array: two types of HIV-associated neurocognitive impairment**. *PLoS One* 2012, **7**:e46178.
155. Roberts ES, Masliah E, Fox HS: **CD163 identifies a unique population of ramified microglia in HIV encephalitis (HIVE)**. *J Neuropathol Exp Neurol* 2004, **63**:1255-1264.

156. Burdo TH, Weiffenbach A, Woods SP, Letendre S, Ellis RJ, Williams KC: **Elevated sCD163 in plasma but not cerebrospinal fluid is a marker of neurocognitive impairment in HIV infection**. *AIDS* 2013, **27**:1387-1395.
157. Cinque P, Vago L, Mengozzi M, Torri V, Ceresa D, Vicenzi E, Transidico P, Vagani A, Sozzani S, Mantovani A, et al.: **Elevated cerebrospinal fluid levels of monocyte chemotactic protein-1 correlate with HIV-1 encephalitis and local viral replication**. *AIDS* 1998, **12**:1327-1332.
158. Letendre SL, Zheng JC, Kaul M, Yiannoutsos CT, Ellis RJ, Taylor MJ, Marquie-Beck J, Navia B, Consortium HIVN: **Chemokines in cerebrospinal fluid correlate with cerebral metabolite patterns in HIV-infected individuals**. *J Neurovirol* 2011, **17**:63-69.
159. Anderson AM, Fennema-Notestine C, Umlauf A, Taylor MJ, Clifford DB, Marra CM, Collier AC, Gelman BB, McArthur JC, McCutchan JA, et al.: **CSF biomarkers of monocyte activation and chemotaxis correlate with magnetic resonance spectroscopy metabolites during chronic HIV disease**. *J Neurovirol* 2015, **21**:559-567.
160. Cinque P, Bestetti A, Marenzi R, Sala S, Gisslen M, Hagberg L, Price RW: **Cerebrospinal fluid interferon-gamma-inducible protein 10 (IP-10, CXCL10) in HIV-1 infection**. *J Neuroimmunol* 2005, **168**:154-163.
161. Hagberg L, Cinque P, Gisslen M, Brew BJ, Spudich S, Bestetti A, Price RW, Fuchs D: **Cerebrospinal fluid neopterin: an informative biomarker of central nervous system immune activation in HIV-1 infection**. *AIDS Res Ther* 2010, **7**:15.
162. Kamat A, Lyons JL, Misra V, Uno H, Morgello S, Singer EJ, Gabuzda D: **Monocyte activation markers in cerebrospinal fluid associated with impaired neurocognitive testing in advanced HIV infection**. *J Acquir Immune Defic Syndr* 2012, **60**:234-243.
163. Brown A, Islam T, Adams R, Nerle S, Kamara M, Eger C, Marder K, Cohen B, Schifitto G, McArthur JC, et al.: **Osteopontin enhances HIV replication and is increased in the brain and cerebrospinal fluid of HIV-infected individuals**. *J Neurovirol* 2011, **17**:382-392.
164. Burdo TH, Ellis RJ, Fox HS: **Osteopontin is increased in HIV-associated dementia**. *J Infect Dis* 2008, **198**:715-722.
165. Muratori C, Mangino G, Affabris E, Federico M: **Astrocytes contacting HIV-1-infected macrophages increase the release of CCL2 in response to the HIV-1-dependent enhancement of membrane-associated TNFalpha in macrophages**. *Glia* 2010, **58**:1893-1904.
166. Eugenin EA, Osiecki K, Lopez L, Goldstein H, Calderon TM, Berman JW: **CCL2/monocyte chemoattractant protein-1 mediates enhanced transmigration of human immunodeficiency virus (HIV)-infected leukocytes across the blood-brain barrier: a potential mechanism of HIV-CNS invasion and NeuroAIDS**. *J Neurosci* 2006, **26**:1098-1106.
167. Buckner CM, Calderon TM, Willams DW, Belbin TJ, Berman JW: **Characterization of monocyte maturation/differentiation that facilitates their transmigration across the blood-brain barrier and infection by HIV: implications for NeuroAIDS**. *Cell Immunol* 2011, **267**:109-123.
168. Veenstra M, Williams DW, Calderon TM, Anastos K, Morgello S, Berman JW: **Frontline Science: CXCR7 mediates CD14(+)CD16(+) monocyte transmigration across the blood brain barrier: a potential therapeutic target for NeuroAIDS**. *J Leukoc Biol* 2017, **102**:1173-1185.
169. Swingler S, Mann A, Jacque J, Brichacek B, Sasseville VG, Williams K, Lackner AA, Janoff EN, Wang R, Fisher D, et al.: **HIV-1 Nef mediates lymphocyte chemotaxis and activation by infected macrophages**. *Nat Med* 1999, **5**:997-103.
170. Lin CL, Sewell AK, Gao GF, Whelan KT, Phillips RE, Austyn JM: **Macrophage-tropic HIV induces and exploits dendritic cell chemotaxis**. *J Exp Med* 2000, **192**:587-594.
171. Anand AR, Prasad A, Bradley RR, Deol YS, Nagaraja T, Ren X, Terwilliger EF, Ganju RK: **HIV-1 gp120-induced migration of dendritic cells is regulated by a novel kinase cascade involving Pyk2, p38 MAP kinase, and LSP1**. *Blood* 2009, **114**:3588-3600.
172. Weissman D, Rabin RL, Arthos J, Rubbert A, Dybul M, Swofford R, Venkatesan S, Farber JM, Fauci AS: **Macrophage-tropic HIV and SIV envelope proteins induce a signal through the CCR5 chemokine receptor**. *Nature* 1997, **389**:981-985.
173. Davis CB, Dikic I, Unutmaz D, Hill CM, Arthos J, Siani MA, Thompson DA, Schlessinger J, Littman DR: **Signal transduction due to HIV-1 envelope interactions with chemokine receptors CXCR4 or CCR5**. *J Exp Med* 1997, **186**:1793-1798.

174. Iyengar S, Schwartz DH, Clements JE, Hildreth JE: **CD4-independent, CCR5-dependent simian immunodeficiency virus infection and chemotaxis of human cells**. *J Virol* 2000, **74**:6720-6724.
175. Mitola S, Sozzani S, Luini W, Primo L, Borsatti A, Weich H, Bussolino F: **Tat-human immunodeficiency virus-1 induces human monocyte chemotaxis by activation of vascular endothelial growth factor receptor-1**. *Blood* 1997, **90**:1365-1372.
176. Park IW, Wang JF, Groopman JE: **HIV-1 Tat promotes monocyte chemoattractant protein-1 secretion followed by transmigration of monocytes**. *Blood* 2001, **97**:352-358.
177. Lafrenie RM, Wahl LM, Epstein JS, Hewlett IK, Yamada KM, Dhawan S: **HIV-1-Tat protein promotes chemotaxis and invasive behavior by monocytes**. *J Immunol* 1996, **157**:974-977.
178. Lafrenie RM, Wahl LM, Epstein JS, Yamada KM, Dhawan S: **Activation of monocytes by HIV-Tat treatment is mediated by cytokine expression**. *J Immunol* 1997, **159**:4077-4083.
179. Nath A, Conant K, Chen P, Scott C, Major EO: **Transient exposure to HIV-1 Tat protein results in cytokine production in macrophages and astrocytes. A hit and run phenomenon**. *J Biol Chem* 1999, **274**:17098-17102.
180. Khiati A, Chaloin O, Muller S, Tardieu M, Horellou P: **Induction of monocyte chemoattractant protein-1 (MCP-1/CCL2) gene expression by human immunodeficiency virus-1 Tat in human astrocytes is CDK9 dependent**. *J Neurovirol* 2010, **16**:150-167.
181. Funderburg NT, Zidar DA, Shive C, Lioi A, Mudd J, Musselwhite LW, Simon DI, Costa MA, Rodriguez B, Sieg SF, et al.: **Shared monocyte subset phenotypes in HIV-1 infection and in uninfected subjects with acute coronary syndrome**. *Blood* 2012, **120**:4599-4608.
182. Walker JA, Beck GA, Campbell JH, Miller AD, Burdo TH, Williams KC: **Anti-alpha4 Integrin Antibody Blocks Monocyte/Macrophage Traffic to the Heart and Decreases Cardiac Pathology in a SIV Infection Model of AIDS**. *J Am Heart Assoc* 2015, **4**.
183. Kelly KM, Tocchetti CG, Lyashkov A, Tarwater PM, Bedja D, Graham DR, Beck SE, Metcalf Pate KA, Queen SE, Adams RJ, et al.: **CCR5 inhibition prevents cardiac dysfunction in the SIV/macaque model of HIV**. *J Am Heart Assoc* 2014, **3**:e000874.
184. Rossi R, Lichtner M, De Rosa A, Sauzullo I, Mengoni F, Massetti AP, Mastroianni CM, Vullo V: **In vitro effect of anti-human immunodeficiency virus CCR5 antagonist maraviroc on chemotactic activity of monocytes, macrophages and dendritic cells**. *Clin Exp Immunol* 2011, **166**:184-190.
185. Goldstein JL, Brown MS: **The LDL receptor**. *Arterioscler Thromb Vasc Biol* 2009, **29**:431-438.
186. Mosepele M, Molefe-Baikai OJ, Grinspoon SK, Triant VA: **Benefits and Risks of Statin Therapy in the HIV-Infected Population**. *Curr Infect Dis Rep* 2018, **20**:20.
187. Yadav A, Betts MR, Collman RG: **Statin modulation of monocyte phenotype and function: implications for HIV-1-associated neurocognitive disorders**. *J Neurovirol* 2016, **22**:584-596.
188. Calza L, Colangeli V, Magistrelli E, Contadini I, Bon I, Re MC, Conti M, Mancini R, Viale P: **Significant Decrease in Plasma Levels of D-Dimer, Interleukin-8, and Interleukin-12 After a 12-Month Treatment with Rosuvastatin in HIV-Infected Patients Under Antiretroviral Therapy**. *AIDS Res Hum Retroviruses* 2017, **33**:126-132.
189. Spouge JL: **Statistical analysis of sparse infection data and its implications for retroviral treatment trials in primates**. *Proc Natl Acad Sci U S A* 1992, **89**:7581-7585.
190. Herwig R, Hardt C, Lienhard M, Kamburov A: **Analyzing and interpreting genome data at the network level with ConsensusPathDB**. *Nat Protoc* 2016, **11**:1889-1907.
191. Sanders RW, Dankers MM, Busser E, Caffrey M, Moore JP, Berkhout B: **Evolution of the HIV-1 envelope glycoproteins with a disulfide bond between gp120 and gp41**. *Retrovirology* 2004, **1**:3.
192. Gach JS, Quendler H, Tong T, Narayan KM, Du SX, Whalen RG, Binley JM, Forthal DN, Poignard P, Zwick MB: **A human antibody to the CD4 binding site of gp120 capable of highly potent but sporadic cross clade neutralization of primary HIV-1**. *PLoS One* 2013, **8**:e72054.
193. Zhang H, Zhou Y, Alcock C, Kiefer T, Monie D, Siliciano J, Li Q, Pham P, Cofrancesco J, Persaud D, et al.: **Novel single-cell-level phenotypic assay for residual drug susceptibility and reduced replication capacity of drug-resistant human immunodeficiency virus type 1**. *J Virol* 2004, **78**:1718-1729.
194. Liu H, Naismith JH: **An efficient one-step site-directed deletion, insertion, single and multiple-site plasmid mutagenesis protocol**. *BMC Biotechnol* 2008, **8**:91.

195. Yamashita M, Emerman M: **Retroviral infection of non-dividing cells: old and new perspectives**. *Virology* 2006, **344**:88-93.
196. Bhargava A, Lahaye X, Manel N: **Let me in: Control of HIV nuclear entry at the nuclear envelope**. *Cytokine Growth Factor Rev* 2018, **40**:59-67.
197. Fassati A: **HIV infection of non-dividing cells: a divisive problem**. *Retrovirology* 2006, **3**:74.
198. Stavrou S, Ross SR: **APOBEC3 Proteins in Viral Immunity**. *J Immunol* 2015, **195**:4565-4570.
199. Van Damme N, Goff D, Katsura C, Jorgenson RL, Mitchell R, Johnson MC, Stephens EB, Guatelli J: **The interferon-induced protein BST-2 restricts HIV-1 release and is downregulated from the cell surface by the viral Vpu protein**. *Cell Host Microbe* 2008, **3**:245-252.
200. Lahouassa H, Daddacha W, Hofmann H, Ayinde D, Logue EC, Dragin L, Bloch N, Maudet C, Bertrand M, Gramberg T, et al.: **SAMHD1 restricts the replication of human immunodeficiency virus type 1 by depleting the intracellular pool of deoxynucleoside triphosphates**. *Nat Immunol* 2012, **13**:223-228.
201. Laguette N, Sobhian B, Casartelli N, Ringeard M, Chable-Bessia C, Segeral E, Yatim A, Emiliani S, Schwartz O, Benkirane M: **SAMHD1 is the dendritic- and myeloid-cell-specific HIV-1 restriction factor counteracted by Vpx**. *Nature* 2011, **474**:654-657.
202. Hrecka K, Hao C, Gierszewska M, Swanson SK, Kesik-Brodacka M, Srivastava S, Florens L, Washburn MP, Skowronski J: **Vpx relieves inhibition of HIV-1 infection of macrophages mediated by the SAMHD1 protein**. *Nature* 2011, **474**:658-661.
203. Cureton DK, Massol RH, Saffarian S, Kirchhausen TL, Whelan SP: **Vesicular stomatitis virus enters cells through vesicles incompletely coated with clathrin that depend upon actin for internalization**. *PLoS Pathog* 2009, **5**:e1000394.
204. Johannsdottir HK, Mancini R, Kartenbeck J, Amato L, Helenius A: **Host cell factors and functions involved in vesicular stomatitis virus entry**. *J Virol* 2009, **83**:440-453.
205. O'Doherty U, Swiggard WJ, Malim MH: **Human immunodeficiency virus type 1 spinoculation enhances infection through virus binding**. *J Virol* 2000, **74**:10074-10080.
206. Guo J, Wang W, Yu D, Wu Y: **Spinoculation triggers dynamic actin and cofilin activity that facilitates HIV-1 infection of transformed and resting CD4 T cells**. *J Virol* 2011, **85**:9824-9833.
207. Davis HE, Morgan JR, Yarmush ML: **Polybrene increases retrovirus gene transfer efficiency by enhancing receptor-independent virus adsorption on target cell membranes**. *Biophys Chem* 2002, **97**:159-172.
208. Mlcochova P, Sutherland KA, Watters SA, Bertoli C, de Bruin RA, Rehwinkel J, Neil SJ, Lenzi GM, Kim B, Khwaja A, et al.: **A G1-like state allows HIV-1 to bypass SAMHD1 restriction in macrophages**. *EMBO J* 2017, **36**:604-616.
209. Cingoz O, Goff SP: **HIV-1 Is a Poor Inducer of Innate Immune Responses**. *MBio* 2019, **10**.
210. Tsang J, Chain BM, Miller RF, Webb BL, Barclay W, Towers GJ, Katz DR, Noursadeghi M: **HIV-1 infection of macrophages is dependent on evasion of innate immune cellular activation**. *AIDS* 2009, **23**:2255-2263.
211. Takahashi K, Yamanaka S: **Induction of pluripotent stem cells from mouse embryonic and adult fibroblast cultures by defined factors**. *Cell* 2006, **126**:663-676.
212. Park IH, Zhao R, West JA, Yabuuchi A, Huo H, Ince TA, Lerou PH, Lensch MW, Daley GQ: **Reprogramming of human somatic cells to pluripotency with defined factors**. *Nature* 2008, **451**:141-146.
213. Wernig M, Meissner A, Foreman R, Brambrink T, Ku M, Hochedlinger K, Bernstein BE, Jaenisch R: **In vitro reprogramming of fibroblasts into a pluripotent ES-cell-like state**. *Nature* 2007, **448**:318-324.
214. Buchrieser J, James W, Moore MD: **Human Induced Pluripotent Stem Cell-Derived Macrophages Share Ontogeny with MYB-Independent Tissue-Resident Macrophages**. *Stem Cell Reports* 2017, **8**:334-345.
215. Jiang Y, Cowley SA, Siler U, Melguizo D, Tilgner K, Browne C, Dewilton A, Przyborski S, Saretzki G, James WS, et al.: **Derivation and functional analysis of patient-specific induced pluripotent stem cells as an in vitro model of chronic granulomatous disease**. *Stem Cells* 2012, **30**:599-611.
216. Lang J, Cheng Y, Rolfe A, Hammack C, Vera D, Kyle K, Wang J, Meissner TB, Ren Y, Cowan C, et al.: **An hPSC-Derived Tissue-Resident Macrophage Model Reveals Differential Responses of Macrophages to ZIKV and DENV Infection**. *Stem Cell Reports* 2018, **11**:348-362.

217. Muffat J, Li Y, Omer A, Durbin A, Bosch I, Bakiasi G, Richards E, Meyer A, Gehrke L, Jaenisch R: **Human induced pluripotent stem cell-derived glial cells and neural progenitors display divergent responses to Zika and dengue infections**. *Proc Natl Acad Sci U S A* 2018, **115**:7117-7122.
218. Muffat J, Li Y, Yuan B, Mitalipova M, Omer A, Corcoran S, Bakiasi G, Tsai LH, Aubourg P, Ransohoff RM, et al.: **Efficient derivation of microglia-like cells from human pluripotent stem cells**. *Nat Med* 2016.
219. Haenseler W, Sansom SN, Buchrieser J, Newey SE, Moore CS, Nicholls FJ, Chintawar S, Schnell C, Antel JP, Allen ND, et al.: **A Highly Efficient Human Pluripotent Stem Cell Microglia Model Displays a Neuronal-Co-culture-Specific Expression Profile and Inflammatory Response**. *Stem Cell Reports* 2017, **8**:1727-1742.
220. van Wilgenburg B, Moore MD, James WS, Cowley SA: **The productive entry pathway of HIV-1 in macrophages is dependent on endocytosis through lipid rafts containing CD4**. *PLoS One* 2014, **9**:e86071.
221. Cribier A, Descours B, Valadao AL, Laguette N, Benkirane M: **Phosphorylation of SAMHD1 by cyclin A2/CDK1 regulates its restriction activity toward HIV-1**. *Cell Rep* 2013, **3**:1036-1043.
222. White TE, Brandariz-Nunez A, Valle-Casuso JC, Amie S, Nguyen LA, Kim B, Tuzova M, Diaz-Griffero F: **The retroviral restriction ability of SAMHD1, but not its deoxynucleotide triphosphohydrolase activity, is regulated by phosphorylation**. *Cell Host Microbe* 2013, **13**:441-451.
223. Durafourt BA, Moore CS, Zammit DA, Johnson TA, Zaguia F, Guiot MC, Bar-Or A, Antel JP: **Comparison of polarization properties of human adult microglia and blood-derived macrophages**. *Glia* 2012, **60**:717-727.
224. Mantovani A, Sozzani S, Locati M, Allavena P, Sica A: **Macrophage polarization: tumor-associated macrophages as a paradigm for polarized M2 mononuclear phagocytes**. *Trends Immunol* 2002, **23**:549-555.
225. Mosser DM, Edwards JP: **Exploring the full spectrum of macrophage activation**. *Nat Rev Immunol* 2008, **8**:958-969.
226. Nikolic J, Belot L, Raux H, Legrand P, Gaudin Y, A AA: **Structural basis for the recognition of LDL-receptor family members by VSV glycoprotein**. *Nat Commun* 2018, **9**:1029.
227. McClure MO, Marsh M, Weiss RA: **Human immunodeficiency virus infection of CD4-bearing cells occurs by a pH-independent mechanism**. *EMBO J* 1988, **7**:513-518.
228. Chen B: **Molecular Mechanism of HIV-1 Entry**. *Trends Microbiol* 2019.
229. Platt EJ, Wehrly K, Kuhmann SE, Chesebro B, Kabat D: **Effects of CCR5 and CD4 cell surface concentrations on infections by macrophagetropic isolates of human immunodeficiency virus type 1**. *J Virol* 1998, **72**:2855-2864.
230. Wei X, Decker JM, Liu H, Zhang Z, Arani RB, Kilby JM, Saag MS, Wu X, Shaw GM, Kappes JC: **Emergence of resistant human immunodeficiency virus type 1 in patients receiving fusion inhibitor (T-20) monotherapy**. *Antimicrob Agents Chemother* 2002, **46**:1896-1905.
231. Cronin J, Zhang XY, Reiser J: **Altering the tropism of lentiviral vectors through pseudotyping**. *Curr Gene Ther* 2005, **5**:387-398.
232. Karlsson KR, Cowley S, Martinez FO, Shaw M, Minger SL, James W: **Homogeneous monocytes and macrophages from human embryonic stem cells following coculture-free differentiation in M-CSF and IL-3**. *Exp Hematol* 2008, **36**:1167-1175.
233. van Wilgenburg B, Browne C, Vowles J, Cowley SA: **Efficient, long term production of monocyte-derived macrophages from human pluripotent stem cells under partly-defined and fully-defined conditions**. *PLoS One* 2013, **8**:e71098.
234. Xu C, Inokuma MS, Denham J, Golds K, Kundu P, Gold JD, Carpenter MK: **Feeder-free growth of undifferentiated human embryonic stem cells**. *Nat Biotechnol* 2001, **19**:971-974.
235. Pick M, Azzola L, Mossman A, Stanley EG, Elefanty AG: **Differentiation of human embryonic stem cells in serum-free medium reveals distinct roles for bone morphogenetic protein 4, vascular endothelial growth factor, stem cell factor, and fibroblast growth factor 2 in hematopoiesis**. *Stem Cells* 2007, **25**:2206-2214.
236. Garrus JE, von Schwedler UK, Pornillos OW, Morham SG, Zavitz KH, Wang HE, Wettstein DA, Stray KM, Cote M, Rich RL, et al.: **Tsg101 and the vacuolar protein sorting pathway are essential for HIV-1 budding**. *Cell* 2001, **107**:55-65.

237. Bachand F, Yao XJ, Hrimech M, Rougeau N, Cohen EA: **Incorporation of Vpr into human immunodeficiency virus type 1 requires a direct interaction with the p6 domain of the p55 gag precursor**. *J Biol Chem* 1999, **274**:9083-9091.
238. Zhu H, Jian H, Zhao LJ: **Identification of the 15FRFG domain in HIV-1 Gag p6 essential for Vpr packaging into the virion**. *Retrovirology* 2004, **1**:26.
239. Agostini I, Navarro JM, Rey F, Bouhamdan M, Spire B, Vigne R, Sire J: **The human immunodeficiency virus type 1 Vpr transactivator: cooperation with promoter-bound activator domains and binding to TFIIB**. *J Mol Biol* 1996, **261**:599-606.
240. Liu X, Guo H, Wang H, Markham R, Wei W, Yu XF: **HIV-1 Vpr suppresses the cytomegalovirus promoter in a CRL4(DCAF1) E3 ligase independent manner**. *Biochem Biophys Res Commun* 2015, **459**:214-219.
241. Logan AC, Nightingale SJ, Haas DL, Cho GJ, Pepper KA, Kohn DB: **Factors influencing the titer and infectivity of lentiviral vectors**. *Hum Gene Ther* 2004, **15**:976-988.
242. de Los Milagros Bassani Molinas M, Beer C, Hesse F, Wirth M, Wagner R: **Optimizing the transient transfection process of HEK-293 suspension cells for protein production by nucleotide ratio monitoring**. *Cytotechnology* 2014, **66**:493-514.
243. Kuroda H, Kutner RH, Bazan NG, Reiser J: **Simplified lentivirus vector production in protein-free media using polyethylenimine-mediated transfection**. *J Virol Methods* 2009, **157**:113-121.
244. Muller B, Tessmer U, Schubert U, Krausslich HG: **Human immunodeficiency virus type 1 Vpr protein is incorporated into the virion in significantly smaller amounts than gag and is phosphorylated in infected cells**. *J Virol* 2000, **74**:9727-9731.
245. Guenzel CA, Herate C, Benichou S: **HIV-1 Vpr-a still "enigmatic multitasker"**. *Front Microbiol* 2014, **5**:127.
246. Gonzalez ME: **The HIV-1 Vpr Protein: A Multifaceted Target for Therapeutic Intervention**. *Int J Mol Sci* 2017, **18**.
247. Sauter D, Kirchhoff F: **Multilayered and versatile inhibition of cellular antiviral factors by HIV and SIV accessory proteins**. *Cytokine Growth Factor Rev* 2018, **40**:3-12.
248. M AV, M S: **Host and viral factors influencing interplay between the macrophage and HIV-1**. *J. Neuroimmune Pharmacology* 2019, **14**:33 - 42.
249. Connor RI, Chen BK, Choe S, Landau NR: **Vpr is required for efficient replication of human immunodeficiency virus type-1 in mononuclear phagocytes**. *Virology* 1995, **206**:935 - 944.
250. Balotta C, Lusso P, Crowley R, Gallo RC, Francini G: **Antisense phosphorothioate oligodeoxynucleotides targeted to the vpr gene inhibit human immunodeficiency virus type 1 replication in primary human macrophages**. *J. Virol* 1993, **67**:4409 - 4414.
251. de silva S, Planelles V, Wu L: **Differential effects of Vpr on single cycle and spreading HIV-1 infections in CD4+ T cells and dendritic cells**. *Plos One* 2012, **7**:e35385.
252. Dedera D, Hu W, Vander Hayden N, Ratner L: **Viral protein R of human immunodeficiency virus types 1 and 2 is idspensible for replication and cytopathogenicity in lymphoid cells.** *J. Virol.* 1989, **63**:3205 - 3208.
253. Takeuchi O, Akira S: **Pattern recognition receptors and inflammation**. *Cell* 2010, **140**:805-820.
254. Sun L, Liu S, Chen ZJ: **SnapShot: pathways of antiviral innate immunity**. *Cell* 2010, **140**:436-436 e432.
255. Krapp C, Jonsson K, Jakobsen MR: **STING dependent sensing - Does HIV actually care?** *Cytokine Growth Factor Rev* 2018, **40**:68-76.
256. Platanias LC: **Mechanisms of type-I- and type-II-interferon-mediated signalling**. *Nat Rev Immunol* 2005, **5**:375-386.
257. Randall RE, Goodbourn S: **Interferons and viruses: an interplay between induction, signalling, antiviral responses and virus countermeasures**. *J Gen Virol* 2008, **89**:1-47.
258. Roux P, Alfieri C, Hrimech M, Cohen EA, Tanner JE: **Activation of transcription factors NFkB and NF-IL-6 by human immunodeficiency virus type 1 protein R (Vpr) induces interleukin 8 expression.** *J. Virol.* 2000, **74**:4658 - 4665.
259. Roesch F, Richard L, Rua R, Porrot F, Casartelli N, Schwartz O: **Vpr Enhances Tumor Necrosis Factor Production by HIV-1-Infected T Cells**. *J Virol* 2015, **89**:12118-12130.
260. Okumura A, Alce, T., Lubyova B, Ezelle H, Strebel K, Pitha PM: **HIV-1 accessory proteins Vpr and Vif modulate antiviral response by targeting IRF-3 for degradation.** *Virology* 2008, **373**:85 - 97.

261. Harman AN, Nasr N, Feetham A, Galoyan A, Alshehri AA, Rambukwelle D, Botting RA, Hiener BM, Diefenbach E, Diefenbach RJ, et al.: **HIV Blocks Interferon Induction in Human Dendritic Cells and Macrophages by Dysregulation of TBK1**. *J Virol* 2015, **89**:6575-6584.
262. Kamburov A, Pentchev K, Galicka H, Wierling C, Lehrach H, Herwig R: **ConsensusPathDB: toward a more complete picture of cell biology**. *Nucleic Acids Res* 2011, **39**:D712-717.
263. Hertzog J, Dias Junior AG, Rigby RE, Donald CL, Mayer A, Sezgin E, Song C, Jin B, Hublitz P, Eggeling C, et al.: **Infection with a Brazilian isolate of Zika virus generates RIG-I stimulatory RNA and the viral NS5 protein blocks type I IFN induction and signaling**. *Eur J Immunol* 2018, **48**:1120-1136.
264. Schneider WM, Chevillotte MD, Rice CM: **Interferon-stimulated genes: a complex web of host defenses**. *Annu Rev Immunol* 2014, **32**:513-545.
265. Maelfait J, Bridgeman A, Benlahrech A, Cursi C, Rehwinkel J: **Restriction by SAMHD1 Limits cGAS/STING-Dependent Innate and Adaptive Immune Responses to HIV-1**. *Cell Rep* 2016, **16**:1492-1501.
266. Wie SH, Du P, Luong TQ, Rought SE, Beliakova-Bethell N, Lozach J, Corbeil J, Kornbluth RS, Richman DD, Woelk CH: **HIV downregulates interferon-stimulated genes in primary macrophages**. *J Interferon Cytokine Res* 2013, **33**:90-95.
267. Nasr N, Maddocks S, Turville SG, Harman AN, Woolger N, Helbig KJ, Wilkinson J, Bye CR, Wright TK, Rambukwelle D, et al.: **HIV-1 infection of human macrophages directly induces viperin which inhibits viral production**. *Blood* 2012, **120**:778-788.
268. Nasr N, Alshehri AA, Wright TK, Shahid M, Heiner BM, Harman AN, Botting RA, Helbig KJ, Beard MR, Suzuki K, et al.: **Mechanism of Interferon-Stimulated Gene Induction in HIV-1-Infected Macrophages**. *J Virol* 2017, **91**.
269. Trotard M, Tsopoulidis N, Tibroni N, Willemsen J, Binder M, Ruggieri A, Fackler OT: **Sensing of HIV-1 Infection in Tzm-bl Cells with Reconstituted Expression of STING**. *J Virol* 2016, **90**:2064-2076.
270. Dehart JL, Planelles V: **Human immunodeficiency virus type 1 Vpr links proteasomal degradation and checkpoint activation**. *J Virol* 2008, **82**:1066-1072.
271. Kawano K, Doucet AJ, Ueno M, Kariya R, An W, Marzetta F, Kuroki M, Turelli P, Sukegawa S, Okada S, et al.: **HIV-1 Vpr and p21 restrict LINE-1 mobility**. *Nucleic Acids Res* 2018, **46**:8454-8470.
272. Cassol E, Cassetta L, Rizzi C, Alfano M, Poli G: **M1 and M2a polarization of human monocyte-derived macrophages inhibits HIV-1 replication by distinct mechanisms**. *J Immunol* 2009, **182**:6237-6246.
273. Goujon C, Moncorge O, Bauby H, Doyle T, Ward CC, Schaller T, Hue S, Barclay WS, Schulz R, Malim MH: **Human MX2 is an interferon-induced post-entry inhibitor of HIV-1 infection**. *Nature* 2013, **502**:559-562.
274. Berg RK, Melchjorsen J, Rintahaka J, Diget E, Soby S, Horan KA, Gorelick RJ, Matikainen S, Larsen CS, Ostergaard L, et al.: **Genomic HIV RNA induces innate immune responses through RIG-I-dependent sensing of secondary-structured RNA**. *PLoS One* 2012, **7**:e29291.
275. Meier A, Alter G, Frahm N, Sidhu H, Li B, Bagchi A, Teigen N, Streeck H, Stellbrink HJ, Hellman J, et al.: **MyD88-dependent immune activation mediated by human immunodeficiency virus type 1-encoded Toll-like receptor ligands**. *J Virol* 2007, **81**:8180-8191.
276. Decalf J, Desdouits M, Rodrigues V, Gobert FX, Gentili M, Marques-Ladeira S, Chamontin C, Mougel M, Cunha de Alencar B, Benaroch P: **Sensing of HIV-1 Entry Triggers a Type I Interferon Response in Human Primary Macrophages**. *J Virol* 2017, **91**.
277. Bejarano DA, Peng K, Laketa V, Borner K, Jost KL, Lucic B, Glass B, Lusic M, Muller B, Krausslich HG: **HIV-1 nuclear import in macrophages is regulated by CPSF6-capsid interactions at the nuclear pore complex**. *Elife* 2019, **8**.
278. Jiao Y, Zhang T, Wang R, Zhang H, Huang X, Yin J, Zhang L, Xu X, Wu H: **Plasma IP-10 is associated with rapid disease progression in early HIV-1 infection**. *Viral Immunol* 2012, **25**:333-337.
279. Wu X, Zhang LL, Yin LB, Fu YJ, Jiang YJ, Ding HB, Chu ZX, Shang H, Zhang ZN: **Deregulated MicroRNA-21 Expression in Monocytes from HIV-Infected Patients Contributes to Elevated IP-10 Secretion in HIV Infection**. *Front Immunol* 2017, **8**:1122.
280. Mhandire K, Mlambo T, Zijenah LS, Duri K, Mateveke K, Tshabalala M, Mhandire DZ, Musarurwa C, Wekare PT, Mazengera LR, et al.: **Plasma IP-10 Concentrations Correlate Positively with Viraemia and Inversely with CD4 Counts in Untreated HIV Infection**. *Open AIDS J* 2017, **11**:24-31.
281. Lei J, Yin X, Shang H, Jiang Y: **IP-10 is highly involved in HIV infection**. *Cytokine* 2019, **115**:97-103.

282. Simmons RP, Scully EP, Groden EE, Arnold KB, Chang JJ, Lane K, Lifson J, Rosenberg E, Lauffenburger DA, Altfeld M: **HIV-1 infection induces strong production of IP-10 through TLR7/9-dependent pathways**. *AIDS* 2013, **27**:2505-2517.
283. Wen X, Duus KM, Friedrich TD, de Noronha CM: **The HIV1 protein Vpr acts to promote G2 cell cycle arrest by engaging a DDB1 and Cullin4A-containing ubiquitin ligase complex using VprBP/DCAF1 as an adaptor**. *J Biol Chem* 2007, **282**:27046-27057.
284. Wilkinson PC: **Random locomotion; chemotaxis and chemokinesis. A guide to terms defining cell locomotion**. *Immunol Today* 1985, **6**:273-278.
285. Hughes CE, Nibbs RJB: **A guide to chemokines and their receptors**. *FEBS J* 2018.
286. Serbina NV, Pamer EG: **Monocyte emigration from bone marrow during bacterial infection requires signals mediated by chemokine receptor CCR2**. *Nat Immunol* 2006, **7**:311-317.
287. Auffray C, Sieweke MH, Geissmann F: **Blood monocytes: development, heterogeneity, and relationship with dendritic cells**. *Annu Rev Immunol* 2009, **27**:669-692.
288. Pommier A, Audemard A, Durand A, Lengagne R, Delpoux A, Martin B, Douguet L, Le Campion A, Kato M, Avril MF, et al.: **Inflammatory monocytes are potent antitumor effectors controlled by regulatory CD4+ T cells**. *Proc Natl Acad Sci U S A* 2013, **110**:13085-13090.
289. Rychert J, Strick D, Bazner S, Robinson J, Rosenberg E: **Detection of HIV gp120 in plasma during early HIV infection is associated with increased proinflammatory and immunoregulatory cytokines**. *AIDS Res Hum Retroviruses* 2010, **26**:1139-1145.
290. Oh SK, Cruikshank WW, Raina J, Blanchard GC, Adler WH, Walker J, Kornfeld H: **Identification of HIV-1 envelope glycoprotein in the serum of AIDS and ARC patients**. *J Acquir Immune Defic Syndr* 1992, **5**:251-256.
291. Santosuosso M, Righi E, Lindstrom V, Leblanc PR, Poznansky MC: **HIV-1 envelope protein gp120 is present at high concentrations in secondary lymphoid organs of individuals with chronic HIV-1 infection**. *J Infect Dis* 2009, **200**:1050-1053.
292. Iyengar S, Schwartz DH, Hildreth JE: **T cell-tropic HIV gp120 mediates CD4 and CD8 cell chemotaxis through CXCR4 independent of CD4: implications for HIV pathogenesis**. *J Immunol* 1999, **162**:6263-6267.
293. Zigmond SH, Hirsch JG: **Leukocyte locomotion and chemotaxis. New methods for evaluation, and demonstration of a cell-derived chemotactic factor**. *J Exp Med* 1973, **137**:387-410.
294. Zicha D, Dunn GA, Brown AF: **A new direct-viewing chemotaxis chamber**. *J Cell Sci* 1991, **99 (Pt 4)**:769-775.
295. Boyden S: **The chemotactic effect of mixtures of antibody and antigen on polymorphonuclear leucocytes**. *J Exp Med* 1962, **115**:453-466.
296. Ma Y, Pan JZ, Zhao SP, Lou Q, Zhu Y, Fang Q: **Microdroplet chain array for cell migration assays**. *Lab Chip* 2016, **16**:4658-4665.
297. Jowhar D, Wright G, Samson PC, Wikswo JP, Janetopoulos C: **Open access microfluidic device for the study of cell migration during chemotaxis**. *Integr Biol (Camb)* 2010, **2**:648-658.
298. Nitta N, Tsuchiya T, Yamauchi A, Tamatani T, Kanegasaki S: **Quantitative analysis of eosinophil chemotaxis tracked using a novel optical device -- TAXIScan**. *J Immunol Methods* 2007, **320**:155-163.
299. Martin KJ, Muessel MJ, Pullar CE, Willars GB, Wardlaw AJ: **The role of phosphoinositide 3-kinases in neutrophil migration in 3D collagen gels**. *PLoS One* 2015, **10**:e0116250.
300. Heit B, Kubes P: **Measuring chemotaxis and chemokinesis: the under-agarose cell migration assay**. *Sci STKE* 2003, **2003**:PL5.
301. Scrace S, O'Neill E, Hammond EM, Pires IM: **Use of the xCELLigence system for real-time analysis of changes in cellular motility and adhesion in physiological conditions**. *Methods Mol Biol* 2013, **1046**:295-306.
302. Kowolenko M, Keese CR, Lawrence DA, Giaever I: **Measurement of macrophage adherence and spreading with weak electric fields**. *J Immunol Methods* 1990, **127**:71-77.
303. Pietrosimone KM, Yin X, Knecht DA, Lynes MA: **Measurement of cellular chemotaxis with ECIS/Taxis**. *J Vis Exp* 2012.

304. Bird CK, S.: **Roche application note: Real-time, label-free monitoring of cellular invasion and migration with the xCELLigence system**. *Nature Methods* 2009.
305. Sun M, Fu H, Cheng H, Cao Q, Zhao Y, Mou X, Zhang X, Liu X, Ke Y: **A dynamic real-time method for monitoring epithelial barrier function in vitro**. *Anal Biochem* 2012, **425**:96-103.
306. Iqbal AJ, Regan-Komito D, Christou I, White GE, McNeill E, Kenyon A, Taylor L, Kapellos TS, Fisher EA, Channon KM, et al.: **A real time chemotaxis assay unveils unique migratory profiles amongst different primary murine macrophages**. *PLoS One* 2013, **8**:e58744.
307. Bennett LD, Fox JM, Signoret N: **Mechanisms regulating chemokine receptor activity**. *Immunology* 2011, **134**:246-256.
308. Van Haastert PJ, Devreotes PN: **Chemotaxis: signalling the way forward**. *Nat Rev Mol Cell Biol* 2004, **5**:626-634.
309. Goodman SR: *Medical cell biology* edn Third edition. Amsterdam ; London: Elsevier/Academic Press; 2008.
310. Yarmola EG, Somasundaram T, Boring TA, Spector I, Bubb MR: **Actin-latrunculin A structure and function. Differential modulation of actin-binding protein function by latrunculin A**. *J Biol Chem* 2000, **275**:28120-28127.
311. Bubb MR, Spector I, Beyer BB, Fosen KM: **Effects of jasplakinolide on the kinetics of actin polymerization. An explanation for certain in vivo observations**. *J Biol Chem* 2000, **275**:5163-5170.
312. Mangmool S, Kurose H: **G(i/o) protein-dependent and -independent actions of Pertussis Toxin (PTX)**. *Toxins (Basel)* 2011, **3**:884-899.
313. Rossol M, Gartner D, Hauschildt S: **Diverse regulation of microfilament assembly, production of TNF-alpha, and reactive oxygen intermediates by actin modulating substances and inhibitors of ADP-ribosylation in human monocytes stimulated with LPS**. *Cell Motil Cytoskeleton* 2001, **48**:96-108.
314. Kustermans G, El Benna J, Piette J, Legrand-Poels S: **Perturbation of actin dynamics induces NF-kappaB activation in myelomonocytic cells through an NADPH oxidase-dependent pathway**. *Biochem J* 2005, **387**:531-540.
315. Yonezawa A, Cavrois M, Greene WC: **Studies of ebola virus glycoprotein-mediated entry and fusion by using pseudotyped human immunodeficiency virus type 1 virions: involvement of cytoskeletal proteins and enhancement by tumor necrosis factor alpha**. *J Virol* 2005, **79**:918-926.
316. Ravetto A, Hoefer IE, den Toonder JM, Bouten CV: **A membrane-based microfluidic device for mechano-chemical cell manipulation**. *Biomed Microdevices* 2016, **18**:31.
317. Graziano F, Elia C, Laudanna C, Poli G, Alfano M: **Urokinase plasminogen activator inhibits HIV virion release from macrophage-differentiated chronically infected cells via activation of RhoA and PKCepsilon**. *PLoS One* 2011, **6**:e23674.
318. Chan JR, Hyduk SJ, Cybulsky MI: **Chemoattractants induce a rapid and transient upregulation of monocyte alpha4 integrin affinity for vascular cell adhesion molecule 1 which mediates arrest: an early step in the process of emigration**. *J Exp Med* 2001, **193**:1149-1158.
319. Trendowski M, Wong V, Zoino JN, Christen TD, Gadeberg L, Sansky M, Fondy TP: **Preferential enlargement of leukemia cells using cytoskeletal-directed agents and cell cycle growth control parameters to induce sensitivity to low frequency ultrasound**. *Cancer Lett* 2015, **360**:160-170.
320. Kusner DJ, Barton JA, Wen KK, Wang X, Rubenstein PA, Iyer SS: **Regulation of phospholipase D activity by actin. Actin exerts bidirectional modulation of Mammalian phospholipase D activity in a polymerization-dependent, isoform-specific manner**. *J Biol Chem* 2002, **277**:50683-50692.
321. Del Corno M, Liu QH, Schols D, de Clercq E, Gessani S, Freedman BD, Collman RG: **HIV-1 gp120 and chemokine activation of Pyk2 and mitogen-activated protein kinases in primary macrophages mediated by calcium-dependent, pertussis toxin-insensitive chemokine receptor signaling**. *Blood* 2001, **98**:2909-2916.
322. Kang BH, Shim YJ, Tae YK, Song JA, Choi BK, Park IS, Min BH: **Clusterin stimulates the chemotactic migration of macrophages through a pertussis toxin sensitive G-protein-coupled receptor and Gbetagamma-dependent pathways**. *Biochem Biophys Res Commun* 2014, **445**:645-650.
323. Sodhi A, Biswas SK: **Monocyte chemoattractant protein-1-induced activation of p42/44 MAPK and c-Jun in murine peritoneal macrophages: a potential pathway for macrophage activation**. *J Interferon Cytokine Res* 2002, **22**:517-526.

324. Harokopakis E, Albzreh MH, Martin MH, Hajishengallis G: **TLR2 transmodulates monocyte adhesion and transmigration via Rac1- and PI3K-mediated inside-out signaling in response to Porphyromonas gingivalis fimbriae**. *J Immunol* 2006, **176**:7645-7656.
325. Seow V, Lim J, Iyer A, Suen JY, Ariffin JK, Hohenhaus DM, Sweet MJ, Fairlie DP: **Inflammatory responses induced by lipopolysaccharide are amplified in primary human monocytes but suppressed in macrophages by complement protein C5a**. *J Immunol* 2013, **191**:4308-4316.
326. Papaspyridonos M, McNeill E, de Bono JP, Smith A, Burnand KG, Channon KM, Greaves DR: **Galectin-3 is an amplifier of inflammation in atherosclerotic plaque progression through macrophage activation and monocyte chemoattraction**. *Arterioscler Thromb Vasc Biol* 2008, **28**:433-440.
327. Tsuchiya S, Yamabe M, Yamaguchi Y, Kobayashi Y, Konno T, Tada K: **Establishment and characterization of a human acute monocytic leukemia cell line (THP-1)**. *Int J Cancer* 1980, **26**:171-176.
328. Bosshart H, Heinzelmann M: **THP-1 cells as a model for human monocytes**. *Ann Transl Med* 2016, **4**:438.
329. Sanders RW, Venturi M, Schiffner L, Kalyanaraman R, Katinger H, Lloyd KO, Kwong PD, Moore JP: **The mannose-dependent epitope for neutralizing antibody 2G12 on human immunodeficiency virus type 1 glycoprotein gp120**. *J Virol* 2002, **76**:7293-7305.
330. Li Y, Migueles SA, Welcher B, Svehla K, Phogat A, Louder MK, Wu X, Shaw GM, Connors M, Wyatt RT, et al.: **Broad HIV-1 neutralization mediated by CD4-binding site antibodies**. *Nat Med* 2007, **13**:1032-1034.
331. Klasse PJ, Moore JP: **Is there enough gp120 in the body fluids of HIV-1-infected individuals to have biologically significant effects?** *Virology* 2004, **323**:1-8.
332. Taylor L, Brodermann MH, McCaffary D, Iqbal AJ, Greaves DR: **Netrin-1 Reduces Monocyte and Macrophage Chemotaxis towards the Complement Component C5a**. *PLoS One* 2016, **11**:e0160685.
333. Iqbal AJ, Barrett TJ, Taylor L, McNeill E, Manmadhan A, Recio C, Carmineri A, Brodermann MH, White GE, Cooper D, et al.: **Acute exposure to apolipoprotein A1 inhibits macrophage chemotaxis in vitro and monocyte recruitment in vivo**. *Elife* 2016, **5**.
334. Cano PM, Vargas A, Lavoie JP: **A real-time assay for neutrophil chemotaxis**. *Biotechniques* 2016, **60**:245-251.
335. Foley JF, Yu CR, Solow R, Yacobucci M, Peden KW, Farber JM: **Roles for CXC chemokine ligands 10 and 11 in recruiting CD4+ T cells to HIV-1-infected monocyte-derived macrophages, dendritic cells, and lymph nodes**. *J Immunol* 2005, **174**:4892-4900.
336. Valverde-Villegas JM, de Medeiros RM, Ellwanger JH, Santos BR, Melo MG, Almeida SEM, Chies JAB: **High CXCL10/IP-10 levels are a hallmark in the clinical evolution of the HIV infection**. *Infect Genet Evol* 2018, **57**:51-58.
337. Wergeland I, Pullar N, Assmus J, Ueland T, Tonby K, Feruglio S, Kvale D, Damas JK, Aukrust P, Mollnes TE, et al.: **IP-10 differentiates between active and latent tuberculosis irrespective of HIV status and declines during therapy**. *J Infect* 2015, **70**:381-391.
338. Burlacu R, Umlauf A, Marcotte TD, Soontornniyomkij B, Diaconu CC, Bulacu-Talnariu A, Temereanca A, Ruta SM, Letendre S, Ene L, et al.: **Plasma CXCL10 correlates with HAND in HIV-infected women**. *J Neurovirol* 2019.
339. Nishihira J: **Macrophage migration inhibitory factor (MIF): its essential role in the immune system and cell growth**. *J Interferon Cytokine Res* 2000, **20**:751-762.
340. Deeks SG, Lewin SR, Havlir DV: **The end of AIDS: HIV infection as a chronic disease**. *Lancet* 2013, **382**:1525-1533.
341. Bruzzesi E, Sereti I: **Residual Immune Activation and Latency**. *Curr Top Microbiol Immunol* 2018, **417**:157-180.